# On the Use of a Spacetime Formalism for Thermomechanical Applications

Roula Al Nahas

Thèse
de doctorat
de l'UTT

**Roula AL NAHAS**

# On the Use of a Spacetime Formalism for Thermomechanical Applications

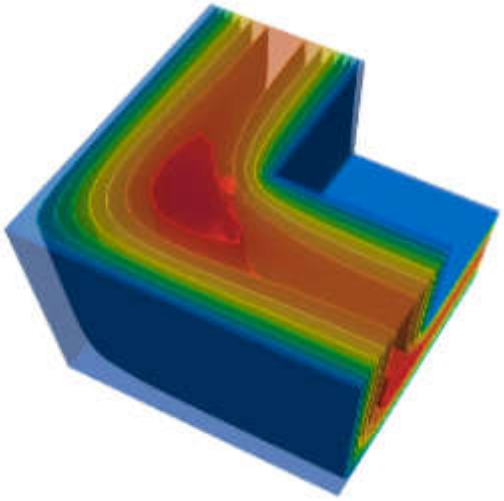

**Champ disciplinaire :**
Sciences pour l'Ingénieur

**2021TROY0001** **Année 2021**

utt
UNIVERSITÉ DE TECHNOLOGIE
TROYES

# THESE

*pour l'obtention du grade de*

# DOCTEUR
# de l'UNIVERSITE DE TECHNOLOGIE DE TROYES

# en SCIENCES POUR L'INGENIEUR

**Spécialité : MATERIAUX, MECANIQUE, OPTIQUE, NANOTECHNOLOGIE**

*présentée et soutenue par*

**Roula AL NAHAS**

*le 7 janvier 2021*

## On the Use of a Spacetime Formalism for Thermomechanical Applications

## JURY

| | | |
|---|---|---|
| M. Aziz HAMDOUNI | PROFESSEUR DES UNIVERSITES | Président |
| M. Géry DE SAXCÉ | PROFESSEUR DES UNIVERSITES | Rapporteur |
| M. Rodrigue DESMORAT | PROFESSEUR DES UNIVERSITES | Rapporteur |
| Mme Christelle COMBESCURE | MAITRE DE CONFERENCES | Examinatrice |
| M. Johann PETIT | MAITRE DE CONFERENCES | Examinateur |
| M. Arjen ROOS | DOCTEUR - HDR | Examinateur |
| M. Alexandre CHARLES | MAITRE DE CONFERENCES ASSOCIE | Directeur de thèse |
| M. Benoît PANICAUD | PROFESSEUR DES UNIVERSITES | Directeur de thèse |

# Acknowledgement

Firstly, I would like to express my sincere gratitude to my advisors Prof. Benoît PANICAUD and Dr. Alexandre CHARLES for the continuous support of my PhD study, for their patience, motivation, and immense knowledge. Their guidance helped me in all the time of research and writing of this thesis.

I would also like to thank: Prof. Géry DE SAXCE and Prof. Rodrigue DESMORAT for accepting to be in the dissertation committee and for all their valuable suggestions.

I thank the rest of the research team concerned in spacetime modeling: Prof. Emmanuelle ROUHAUD and Prof. Richard KERNER for their insightful comments. In particular, I am grateful to Dr. Israa CHOUCAIR for all the knowledge she generously shared with me. I could not have imagined having a better colleague. I am also grateful for the scientific collaboration with Dr. Johann PETIT which added an important experimental aspect to my thesis.

My sincere thanks also goes to the LASMIS laboratory members who provided me an opportunity to join their team as a PhD student and who always shared their research experience. I also thank my fellow labmates and my friends at UTT for the stimulating discussions, advises and valuables opinions. They were a scientific and moral support throughout this thesis.

I would like to thank all the contributors for the financial support. This work was supported by the European Regional Development Funds (FEDER), the region Grand Est of France and Safran Tech company.

Last but not the least, I would like to thank my family: my parents Carmel and Raymond and to my two sisters Rana and Carine for supporting me spiritually throughout this journey and in my life in general but also for offering help whenever they could. It would not be possible to conduct this research without their precious support.

## Abstract

In order to optimize the forming processes, modeling the thermomecanical behavior for large deformations is particularly interesting. Objectivity of the models is therefore questioned. The need to develop the existing models is the motivation of this work. This study investigates the spacetime approach as a mean to build thermomechanical models respecting the covariance and causality principles as well as the laws of thermodynamics. In this manuscript, spacetime models are mainly obtained using the relativization of Newtonian models method and the spacetime thermodynamical method. Several models are proposed in the spacetime framework and next compared to existing Newtonian models: heat conduction (Fourier's and Cattaneo's models) and the thermo-hyperelastic behavior are discussed. The spacetime numerical resolution is also investigated: the variational forms corresponding to thermal and thermomechanical problems are developed. The study of material behavior is possible using these forms written in the proper frame. Numerical simulations implementing these forms in the software FEniCS project are then conducted in order to validate test cases with the spacetime models. Comparison of the spacetime models with the classical Newtonian models at the non-relativistic limit shows the compatibility of their results. Applications aiming to model the heat conduction in cooling fins, the self-heating occurring during fatigue tests and the behavior of a bimetallic element show that the use of the spacetime approach enables predicting material behaviors while guaranteeing objectivity of the models. We also suggest the use of this approach to model the tube bending process, preliminary results requiring more investigation are given in the appendix. Since this approach is shown advantageous for the applications proposed, further research could cover different material behaviors e.g. plasticity.

# Résumé en français

La modélisation du comportement thermomécanique des grandes déformations est un sujet de recherche de grand intérêt. L'objectivité des modèles est mise en question. Cette étude évalue l'approche de modélisation en espace-temps (modélisation relativiste) comme un moyen de construire des modèles thermomécaniques respectant à la fois les principes de covariance et de causalité ainsi que les lois de la thermodynamique.

Dans ce manuscrit, les modèles relativistes sont principalement obtenus soit par la relativisation des modèles newtoniens, soit à partir des lois de la thermodynamique formulées en espace-temps. Plusieurs modèles sont proposés dans le cadre de l'espace-temps et ensuite comparés aux modèles existants: la conduction thermique (modèles de Fourier et Cattaneo) et le comportement thermo-hyperélastique des matériaux sont discutés.

La résolution numérique spatio-temporelle est également testée: les formes variationnelles correspondant aux problèmes thermiques et thermomécaniques ont été développées. L'étude du comportement des matériaux est possible en utilisant ces formes écrites dans le référentiel propre. Des simulations numériques faites par implémentation de ces formes dans le logiciel FEniCS project ont ensuite été réalisées afin de valider des cas tests des modèles relativistes. La comparaison des modèles relativistes avec les modèles Newtoniens classiques faite à la limite non relativiste montre la compatibilité de leurs résultats.

Des applications dans le but de la modélisation de la conduction thermique dans les ailettes de refroidissement, l'auto-échauffement survenant lors des essais de fatigue et le comportement d'un bilame montrent que l'utilisation de l'approche relativiste permet de prédire les comportements des matériaux tout en garantissant l'objectivité des modèles. Nous suggérons également l'utilisation de cette approche pour modéliser le processus de flexion des tubes, des résultats préliminaires sont donnés en annexe. Étant donné que cette approche s'avère avantageuse pour les applications proposées, il serait intéressant que des recherches supplémentaires couvrent différents comportements des matériaux, comme la plasticité à titre d'exemple.

# Contents

# Notations

## List of operators

| | |
|---|---|
| $X$ | **Scalar** |
| $\mathbf{X}$ | **Tensor** |
| $X^{ij}$, $X^{\mu\nu}$ | **Contravariant components of a Newtonian respectively spacetime tensor** |
| $X_{ij}$, $X_{\mu\nu}$ | **Covariant components of a Newtonian respectively spacetime tensor** |
| $tr(\mathbf{X})$ | **Trace of a 3D second-rank tensor** |
| $\|X\|$ | **Determinant of a second-rank tensor** |
| $\mathbf{e}_i$, $\mathbf{e}_\mu$ | **Covariant base vectors** |
| $\otimes$ | **Tensor product** |
| $\nabla_i$, $\nabla_\mu$ | **Covariant derivative** |
| $\frac{\partial}{\partial x^i}, \frac{\partial}{\partial t}$ | **Partial derivative to space respectively time** |
| $\frac{d}{dx^i}, \frac{d}{dt}$ | **Total derivative to space respectively time** |
| $\mathcal{L}_u(.)$ | **Lie derivative with respect to the velocity four-vector $u$** |
| $u^\lambda \nabla_\lambda(.)$ | **Covariant transport** |
| $LT$ | **Laplace transform** |
| $\theta_{d(av)}$ | **Average value of temperature over the time** |
| $\|\|.\|\|$ | **Norm of a quantity** |
| $< . >$ | **Arithmetic mean value over particles** |
| $\Pi^{\mu\nu}$ | **Orthogonal projector to the observer's four-velocity** |
| $\underline{(.)}$ | **Projection using the orthogonal projector $\Pi^{\mu\nu}$** |
| $\bar{(.)}$, $\bar{\bar{(.)}}$, $\bar{\bar{\bar{(.)}}}$ | **Average over respectively one, two, three directions** |
| $\hat{(.)}$ | **Variable in the proper/covariant frame** |
| $\Delta$ | **Laplace differential operator** |
| $\mathcal{S}$ | **Scalar density** |
| $\boldsymbol{\mathcal{V}}$ | **First-rank four-tensor** |
| $\boldsymbol{\mathcal{T}}$ | **Second-rank four-tensor density** |
| $D^X_{3D}$ | **Objective rate operator of $D_{ij}$** |

## List of symbols

| | |
|---|---|
| $a$ | **Diffusivity of the material** |
| $a(.,.)$ | **Left hand-side of a bilinear functional** |
| $a^{\nu}$ | **Spacetime acceleration** |
| $a_K$ | **Scalar mathematical functions** |
| $A_x$ | **Small area normal to the $x$ -direction at the abscissa $x$** |
| $A_I^{\mu\nu}$, $A_{II}^{\mu\nu}$ | **Tensorial functions** |
| $b^{ij}$, $b^{\mu\nu}$ ($\boldsymbol{b}$) | **Newtonian respectively spacetime inverse of left Cauchy-Green deformation** |
| $Bi$ | **Biot number** |
| $b_K$ | **Invariants of $b$** |
| $c$ | **Speed of light** |
| $\mathcal{C}_{mP}$ | **Specific heat coefficient at constant pressure** |
| $\mathcal{C}_{m\omega}$ | **Specific heat capacity at constant 3D volume** |
| $C^{ij}$, $C^{\mu\nu}$ ($\boldsymbol{C}$) | **Newtonian respectively spacetime right Cauchy-Green deformation** |
| $d^{ij}$, $d^{\mu\nu}$ ($\boldsymbol{d}$) | **Newtonian respectively spacetime rate of deformation tensor** |
| $d_1$ | **Intrinsic dissipation** |
| $dep_i$, $dep_{\mu}$ (**dep**) | **Newtonian respectively spacetime displacement vector** |
| $dep_i^*$, $dep_{\mu}^*$ (**dep**$^*$) | **Newtonian respectively spacetime virtual displacement vector** |
| $\partial\mathcal{D}$ | **Frontier of a hypervolume in a spacetime** |
| $\mathrm{d}H_{\Omega}$ | **Spacetime hypervolume of integration** |
| $\mathrm{d}V_{\omega}$ | **3D volume of integration** |
| $\mathrm{d}S_{\Omega}$ | **3D surface of integration** |
| $ds$ | **Interval between 2 close events** |
| $\mathcal{D}$ | **Hypervolume in a spacetime continuum** |
| $D_{ij}$, $D_{\mu\nu}$ ($\boldsymbol{D}$) | **Newtonian respectively spacetime Lagrangian rate of deformation tensor** |
| $e^{ij}$, $e^{\mu\nu}$ ($e$) | **Newtonian respectively spacetime Euler-Almansi strain tensor** |
| $e_{int}$ | **Specific internal energy** |
| $E$ | **Young's modulus** |
| $E_t$ | **Tangent elastic modulus** |
| $E^{ij}$, $E^{\mu\nu}$ ($\boldsymbol{E}$) | **Newtonian respectively spacetime Green-Lagrange strain tensor** |
| $f$ | **Volume heat source** |
| $f_a$ | **Force applied** |
| $f_M^j$ | **Mechanical body force per unit volume** |
| $f_L$ | **Frequency of cyclic loading** |
| $f_r$ | **Normalized heat source** |
| $f_{IR}$ | **Sampling frequency** |
| $f_{SC}$ | **Function representing the space boundary conditions** |
| $f_{TC}$ | **Function representing the initial time boundary conditions** |
| $F_i$ | **Generalized forces** |
| $F_j^i$, $F_{\nu}^{\mu}$ ($\boldsymbol{F}$) | **Newtonian respectively spacetime deformation gradient** |
| $F_j'^i$, $F_{\nu}'^{\mu}$ ($\boldsymbol{F'}$) | **Newtonian respectively spacetime inverse of deformation gradient** |
| $\mathcal{F}$ | **Mapping in the domain $\mathcal{D}$** |
| $g$ | **Statistical distribution of heat carriers (electrons, photons or phonons ...)** |
| $\mathcal{G}(x)$ | **Mean value of $Q$ at any point** |
| $g^{ij}$, $g^{\mu\nu}$ ($\boldsymbol{g}$) | **Newtonian respectively spacetime second-rank metric tensor** |
| $G$ | **Temperature gradient** |
| $h$ | **Coefficient of convection of the surrounding medium** |
| $H$ | **Isotropic hardening of modulus** |
| $I^{ij}$ | **3D identity tensor** |
| $\overline{I}_I$, $\overline{I}_{II}$ | **Invariants of the projected strain tensor** |
| $j^i$ | **Flux of particles through an area** |
| $J$ | **Mass density ratio** |

| | |
|---|---|
| $l^{(k)}$ | Free path of the particle $k$ |
| $l$, $L$, $L_1$ | Length at atomic, macroscopic and upper macroscopic scale |
| $L(.)$ | Right hand-side of a bilinear functional |
| $L_c$ | Characteristic length of the body |
| $L^{ij}$, $L^{\mu\nu}$ $(\boldsymbol{L})$ | Newtonian respectively spacetime velocity gradient tensor |
| $n$ | Number of particles per unit volume |
| $n_i$, $n_\mu$ $(\boldsymbol{n})$ | Outward unit normal to the 3D respectively 4D surface |
| $\mathfrak{n}_1$, $\mathfrak{n}_2$ | Exponents of the power laws of $\overline{I}_I$, $\overline{I}_{II}$ |
| $N_t$ | Step along $t$ |
| $N_x$ | Step along $x$ |
| $\mathfrak{p}$ | Hydrostatic pressure of fluid |
| $p_L$ | Laplace variable |
| $p$ | Cumulated equivalent plastic strain |
| $\mathcal{P}$ | Perimeter of the fin |
| $P$ | Total potential energy |
| $PEEQ$ | Equivalent plastic strain |
| $Q^i_j(t)$ | Orthogonal matrix depending on time |
| $Q$ | Physical quantity attached to a gas particle |
| $q^i$, $q^\mu$ $(\boldsymbol{q})$ | Newtonian respectively spacetime volume heat flux four-vector |
| $q^j_{ext}$ | Surface heat flux in the proper frame imposed on the hypersurface $\partial\Omega_q$ |
| $r$ | Bend radius |
| $r^i$ | Position vector |
| $R^2$ | Coefficient of determination |
| $s_{thc}$ | Possible thermomechanical coupling source |
| $s_{the}$ | Thermoelastic source |
| $s^{ij}$ | Newtonian respectively spacetime deviatoric part of $\sigma^{ij}$ |
| $strain^{ij}$ | Newtonian respectively spacetime generalization of strain tensor in case of small and large deformations |
| $strain^{ij}_P$ | Newtonian respectively spacetime strain due to plasticity behavior |
| $S$ | Section of the fin |
| $t$ | Time |
| $t_i$ | Initial time |
| $t_f$ | Final time |
| $T$ | Momentum acting on a group of heat carriers |
| $T^i_M$ | Stress vector at the boundary applied on $\partial\Omega_{T_M}$ |
| $T^{\mu\nu}_\sigma$ | Stress four-tensor |
| $\boldsymbol{u}$ | Spacetime velocity |
| $\mathcal{U}$ | Energy density |
| $v^i$ | Newtonian velocity |
| $r^*_\mu$ | Test function combining the virtual temperature field $\theta^*$ and the virtual displacement field $dep^*_\mu$ |
| $v_g$ | Average of mean particle speeds |
| $v_h$ | Speed of propagation of temperature in the liquid Helium |
| $W$ | Weight of tensor density |
| $X^\mu$ | Newtonian respectively spacetime coordinates |
| $x^\mu$ | Spacetime event |
| $z^i$, $z^\mu$ $(\boldsymbol{z})$ | Newtonian respectively spacetime spatial or Eulerian coordinates |
| $Z^i$, $Z^\mu$ $(\boldsymbol{Z})$ | Newtonian respectively spacetime coordinates of the particles in the reference configuration |

| | |
|---|---|
| $\alpha$ | **Thermal expansion coefficient** |
| $\alpha_s$ | **Internal state variables** |
| $\boldsymbol{\beta}$ | **Left Cauchy-Green deformation** |
| $\beta^{(k)}$ | **Inclination of the speed of the particle $k$ with respect to the $x$-direction** |
| $\beta_1$ | **Coupling for the second order terms** |
| $\gamma$ | **Lorentz factor** |
| $\delta_i$ | **Elongation in the direction $i$** |
| $\varepsilon^{ij}$, $\varepsilon^{\mu\nu}$ $(\boldsymbol{\varepsilon})$ | **Newtonian respectively spacetime elastic strain tensor for small deformations** |
| $\eta^{ij}$, $\eta^{\mu\nu}$ $(\boldsymbol{\eta})$ | **Newtonian respectively spacetime second-rank Minkovski metric tensor** |
| $\eta_c$ | **Entropy density** |
| $\theta$ | **Temperature** |
| $\theta^*$ | **Virtual temperature** |
| $\theta_f$ | **Final temperature** |
| $\theta_0$ | **Initial/Room temperature** |
| $\theta_d$ | $\theta - \theta_0$ |
| $\bar{\theta}_d$, $\bar{\bar{\theta}}_d$, $\bar{\bar{\bar{\theta}}}_d$ | **Average difference between the specimen temperature and the room temperature made over respectively one, two, three directions** |
| $\kappa$ | **Bulk modulus** |
| $\lambda$ | **Thermal conductivity** |
| $\lambda^i(t)$ | **Vector depending on time** |
| $\Lambda$, $\mu$ | **Lamé's coefficients** |
| $\nu$ | **Poisson coefficient** |
| $\xi^i, \xi^\mu$ | **Newtonian respectively spacetime coordinate system** |
| $\pi$ | **Term related to viscous pressure** |
| $\pi^{\mu\nu}$ | **Mechanical stress not taking into account stress resulting from viscous pressure** |
| $\widetilde{\rho_c}$ | **Mass density (at rest) with the specific internal energy $e_{int} = 0$ interpreted in the convective frame** |
| $\sigma_n$ | **Amplitude of cyclic loading stress** |
| $F_l$ | **Fatigue limit** |
| $\sigma_c^{ij}$, $\sigma_c^{\mu\nu}$ $(\boldsymbol{\sigma_c})$ | **Newtonian respectively spacetime Cauchy stress** |
| $\sigma_{PK2}^{ij}$, $\sigma_{PK2}^{\mu\nu}$ $(\boldsymbol{\sigma_{PK2}})$ | **Newtonian respectively spacetime Piola-Kirchhoff stress** |
| $\sigma_{TH}^{ij}$, $\sigma_{TH}^{\mu\nu}$ $(\boldsymbol{\sigma_{TH}})$ | **Newtonian respectively spacetime stress due to thermal expansion** |
| $\sigma^{ij}{}^{eq}_{elas}$ | **Elastic predictor** |
| $\sigma_0$ | **Von Mises yield condition of uniaxial strength** |
| $\tau$, $\tau_1$ | **relaxation time constants** |
| $\tau_{0D}$, $\tau_{1D}$, $\tau_{2D}$, $\tau_S$ | **Time parameters characterizing the heat transfer perpendicular to the direction of heat conduction flux** |
| $\phi^i$, $\phi^\mu$ $(\boldsymbol{\phi})$ | **Newtonian respectively spacetime specific heat flux** |
| $\Phi$ | **Dissipation** |
| $\Psi$ | **Specific free energy** |
| $\Psi_\sigma$ | **Part of $\Psi$ corresponding to the mechanical and thermomechanical phenomena** |
| $\Psi_{\theta,\sigma}$ | **Part of $\Psi$ corresponding thermomechanical phenomena** |
| $\Psi_\theta$ | **Part of $\Psi$ corresponding to the thermal phenomena** |
| $\Omega$ | **Spacetime domain of integration** |
| $\omega$ | **3D spatial domain of integration** |
| $\boldsymbol{\omega}$ | **Spin tensor** |

We assume that space and time are universal constants because that explains
how we perceive the world. But it turns out that they are not universal constants.
And that changes everything.
What we believe is the universal constant of our experience is, in fact, not constant at all.
And, instead, much of what we assume to be true and real is relative to our own perception.

MARK MANSON

# General introduction

## Scope of the research

Industrial sectors such as automotive, aeronautics, building equipment.. are in constant development. The main motivation is the economic competition which has been growing in the last decades. Despite the extensive development of these sectors (e.g. shape and material optimization of cars, performance of aircraft), particular challenges remain unsolved. The reduction of the time-to-market and the cost of development of forming processes were among the difficulties that motivated the use of numerical simulations [Ablat and Qattawi,2017, Banabic,2010, Wang,2016]. Not to mention the fast improvement of computational performance of devices which promoted them as a convenient means to alleviate the other industries problems.

On one hand, numerical simulations for small deformations are already developed and used to design mechanical systems. They are able to cover lots of applications [Banabic,2010]. On the other hand, one of the obstacles facing the use of numerical simulations is modeling material behavior for large deformations [Panicaud et al.,2015]. Several contributions in this field adopt a geometrical point of view to describe the mechanics of materials for large deformations [Yavari et al.,2006, Yavari and Marsden,2012]. This is what we also propose to do. Moreover, the standpoint adopted in the present study is to formulate physical models whose form is preserved by changing frames. It leads us to study the action of changes of frames on the physical equations/models.

In order to guarantee obtaining models independent with respect to frames changes, we are therefore applying the principle of covariance to physical laws. In physics, the principle of covariance is ensured in relativistic theories. As a consequence of the application of this principle, the theories of relativity describe the phenomena in a domain of space and time simultaneously whatever the observers are.

Furthermore, dissipative models which are necessary for the modeling of the forming processes must be compatible with the second principle of thermodynamics, which generally takes the form of the Clausius-Duhem inequality. In order to propose covariant dissipation models, it will therefore be necessary to propose a covariant formulation of this inequality as suggested in [Lamoureux-Brousse,1989] for small deformations. This starting point should systematically allow providing satisfactory models of behavior and dissipation.

## Relevance of the research

As previously mentioned, the aim of this study is to find representative models for industrial applications especially the forming processes. These processes frequently involve thermal phenomena, hence the need to take also into account thermomechanical couplings in the covariant modeling.

In the modeling of thermal phenomena, different modes of heat exchange can be considered: conduction, convection/advection, radiation [Fourier,1988]. In this manuscript, we will aim to model particularly the heat conduction phenomena: heat exchanges by convection/advection will only be taken into account via boundary conditions and those related to radiation are not taken into consideration. The three main questions to ask in order to verify the reliablity of thermal (and thermomechanical) models are: "Do they respect the laws of thermodynamics?", "Do they respect the causality principle?" and "Do they respect the covariance principle?" (section 1.6). Note that we designate by the terms "causality and covariance principles" their definitions in a relativistic framework. These questions may seem straightforward but it turns out a Newtonian Fourier's type model does not respect the causality principle because of the form of the corresponding heat equation. This will be further detailed in section 1.5. Nothing paradoxical here, but it suggests that, dealing with thermomechanics, we should assemble thermal and mechanical models that understand causality and covariance in the same way.

In order to enhance this model, many authors [Cattaneo,1958, Osborne,1950, Tavernier,1962] suggested Newtonian models by adding a relaxation term to the heat conduction equation. The problem of causality

violation of the heat models is hence resolved. However, these Newtonian models are not necessarily covariant with respect to changes of frames (section 1.6).

Other thermal models are obtained using a relativistic approach [Eckart,1940, Landau and Lifshitz,1975, Stewart,1977, Carter,1988] which can be called "spacetime approach" (the models are built in a spacetime or 3D+1D domain, further detailed in chapter 1). These models fulfill the covariance criterion and are thermodynamically compatible but not all of them respect the causality principle. This will be further detailed in section 1.8. In this manuscript, we suggest the use of a spacetime thermodynamical approach in order to develop heat conduction models respecting at the same time the notions of causality and covariance.

On another note, mechanical modeling of forming processes requires the ability to model large deformations. Hence the need to improve models of material behavior and of operating conditions of processes. This requires numerical analysis of mechanical models on the base of experimental data [Oliveira and Fernandes,2019]. These models should fulfill the conditions of covariance and compatibility with laws of thermodynamics. Limitations encountered in Newtonian modeling open the discussion on finding a new approach.

First, the non linearity of the models is encountered when modeling large deformations [Bertram,2012] or dissipative behaviors e.g. plasticity, viscosity...[Valanis,1970, Lubliner,1984, Prasolov,1997] or even a combination of these two cases. This condition requires an incremental formulation in time of the corresponding problem. The covariance is then not fulfilled using Newtonian modeling because of the incremental form of the models. This brings up the spacetime formalism as a convenient way of resolution as discussed about the thermal models. In mechanical phenomena, it corresponds classically to the invariance with respect to rigid body motion but also to the objectivity of equations of mechanical models [Rouhaud et al.,2013] especially for large deformation [Truesdell,1966, Prost-Domasky et al.,1997]. Authors propose the use of objective transports in order to ensure objectivity in hypoelastic modeling (i.e stress rate) as well as in elastic modeling (i.e velocity, deformation rate) [Frewer,2009, Jaumann,1911, Green and Naghdi,1965, Bruhns and Meyers,1998]. A geometric point of view is agreed to be able to ensure objectivity [Eringen,1962, Truesdell and Noll,2003, Marsden and Hughes,1994, Venturi,2009], which will also be used in this manuscript via the spacetime formalism.

Second, the argument of thermodynamic compatibility also holds for mechanical models [Eckart,1940, Havas,1964, Grot and Eringen,1966a, Grot and Eringen,1966b, Muller,1969, Maugin,1971a, Maugin,1971b, Maugin,1973, Bressan,1978, Vallée,1981, Israel,1987, Kijowski and Magli,1997, Yavari and Ozakin,2008, Romano and Barretta,2011, Yavari and Marsden,2012, Schellstede et al.,2014]. To sum up, the aim of this work is to model thermomechanical behavior in a relativistic framework. The use of a thermodynamical approach built in a spacetime formalism seems to be able to solve the problems of both thermal and mechanical types of models [Eckart,1940, Landau and Lifshitz,1975, Stewart,1977].

The models will have to be able to present the least possible assumptions in order to be applicable for large deformations occurring during forming processes and to be also used to model materials behaviors using large deformations such as modeling the plasticity/viscoplasticity behavior of steel or thermoplastic behavior of polymers. The use of such a formalism may add new terms to models when modeling forming processes for large deformations and when critical temperatures (very high/low temperatures) are reached during manufacturing [Rouhaud et al.,2013, Eckart,1940].

We note that our approach is based on the study of the existing Newtonian and spacetime thermal/mechanical models reviewed in parts 1 and 2 of the manuscript: some of our models are deduced by relativization of Newtonian models in the suggested spacetime framework, others are deduced from a direct application of laws of thermodynamics in spacetime.

## Thesis statement and objectives

After its development in the first half of the 20th century, continuum mechanics is now a reliable theory to describe transformations of media at macroscopic scale. Solids or fluids can be modeled through a common framework obtained either from balance laws [Truesdell,1966] or the virtual work/power principle

[Germain,1973]. However, despite the accumulated contributions to this theory, modeling of thermomechanical behaviors faces particular challenges related to geometric description and the choice of constitutive models. The goal of obtaining models that fulfill the causality principle as well as the covariance principle and respect the laws of thermodynamics, is not fully achieved yet. The innovative point of view used in this manuscript is the use of a spacetime formalism to grant covariance in the context of large deformations for modeling thermomechanical behaviors. Throughout this manuscript, we will be answering the questions: How to build thermomechanical models in this spacetime formalism? Are these models the extensions of Newtonian models for any displacement/velocity?

## The spacetime framework scope

As previously discussed, differential geometry is used in this manuscript in the description of tensors, techniques of differential calculus... It is reviewed in [Schouten,1954, Kerner,2014]. Moreover, vocabulary and notations of the spacetime formalism used to develop the thermomechanical models in this manuscript are reviewed in [Boratav,1991]. We will only introduce the concepts necessary to our study throughout the manuscript (see chapters 1 and 4). Furthermore, the principles and applications of the theory of relativity are found in [Eckart,1940, Weinberg,1972, Landau and Lifshitz,1975].

We develop our models in a similar framework. The following describes the scope of the study:

- A relativistic framework is considered where gravitation is not taken into account.
- Motion is described for continuous media.
- Models are built in this framework in order to be frame-indifferent.
- Models are written for large deformations in order to fit for forming processes during which deformations are large enough to invalidate assumptions of the infinitesimal strain theory. Instead of it, a large deformation theory is considered. In this case, initial and deformed configurations of the continuum are significantly different. Lagrangian and Eulerian point of views can be used to describe the motion 1.4.4.

## Methodology for building and validating spacetime thermomechanical models

In order to build thermomechanical models as per the requirements previously mentioned, a spacetime thermodynamic approach is suggested. The final goal is obtaining thermomechanical models which can represent as close as possible the reality of materials analysis and characterization techniques (e.g. study of self-heating occurring during fatigue test) and of forming processes (e.g. beam bending) in the spacetime domain. This is all done in order to simulate the procceses numerically by implementing the models. Steps of the modeling approach tested in this manuscript are as follows:

1. Recall of a spacetime framework guaranteeing the covariance of physical laws: spacetime geometry, kinematics, energy-momentum tensor, spacetime covariant derivatives, projectors...
2. Relativization of the laws of thermodynamics (i.e. balance of internal energy, balance of momentum and energy). This leads in particular to a covariant form of the Clausius-Duhem inequality.
3. Modeling the heat conduction phenomenon (Fourier-like and Cattaneo-like models) and the thermomechanical behavior in the spacetime formalism.
4. Formulation of the corresponding weak integral forms in order to simulate coupled multiphysics problem.
5. Numerical implementation and simulation run using FEniCS project.
6. Engineering applications, material characterization and forming processes modeling (e.g. heat conduction in a cooling fin, self-heating phenomenon, beam bending...).
7. Comparison of results obtained using Newtonian models and spacetime models in order to validate the latter at the Newtonian limit.

## Overall structure of the manuscript

This manuscript is divided into two parts: the first includes 3 chapters and is dedicated to spacetime thermal modeling, while the second which includes 2 chapters is dedicated to spacetime thermomechanical modeling. In chapter 1, we review the classical notations and definitions of physics that are used in this manuscript. We also analyze the features of the Newtonian and spacetime thermal models found in the literature. In chapter 2, we remind elements of the spacetime formalism used for thermal modeling. These are further used in developing spacetime thermal models using different methods in a thermodynamical approach. At the end of chapter 2, an engineering application is illustrated: a spacetime modeling of heat transfer in a cooling fin. Numerical simulations are done using FEniCS project. Chapter 3 holds another application: we are interested in studying the self-heating phenomenon occurring during fatigue tests using a thermal spacetime model as obtained in chapter 2 with the appropriate boundary conditions. This study is based on experimental data which provides the input of the methodology used for modeling. Numerical simulations enable the study of the model parameters. Note that, in the first part of the manuscript, we introduce some notions about mechanics which are necessary for the spacetime thermal modeling. However these notions are further extended in the second part. In chapter 4, we review the thermomechanical modeling adapted for large deformations: several Newtonian and spacetime models are discussed. We also introduce further notations of the spacetime formalism in order to add the mechanical ingredient to the spacetime thermal models obtained in chapter 2. In chapter 5, we develop spacetime thermomechanical models. We also consider the modeling of bimetallic element behavior and a tube bending process using our spacetime thermomechanical model.

# Part 1: Modeling of thermal behavior of materials

# 1 Bibliographic review on thermal modeling

## 1.1 Introduction

In this thesis the thermomechanical behavior of materials for large deformations will be modeled. For this reason, the kinematic (i.e. mechanical and thermal) variables as well as the static/dynamic elements related to this behavior will be respectively introduced all throughout the manuscript. In this first part of the manuscript, the heat conduction modeling in a spacetime domain will be specifically investigated. First, the heat equation in case of heat conduction will be reviewed in both Newtonian and relativistic approaches. Then, a model deriving from a thermodynamical approach in spacetime will be proposed. The application of the obtained spacetime heat model to a self-heating study will be done in order to show its ability to represent such a phenomenon.

At the beginning of this chapter, the definitions of quantities and the elements of kinematics used to describe a motion in continuous media are summarized. Different frames that can be used with the Lagrangian and Eulerian descriptions of the motion of a particle in continuous media are also defined. Difficulties facing thermal modeling in Newtonian and relativistic approaches are then discussed: they can be summarized as the violation of the causality and covariance principles. These difficulties emphasize the need of an innovative method to model thermal phenomena. The self-heating phenomenon is also reviewed in this chapter: studies investigating this phenomenon in the literature are discussed, in order to define the parameters necessary for its modeling.

## 1.2 Classical/Newtonian kinematics in continuum thermomechanics

We first place ourselves within the framework of continuous media using a classical three-dimensional approach (3D approach) related to the space variations of the field quantities. The term "classical" is here equivalent to the adjective "Newtonian", which is used to oppose the adjective "relativistic". In this section, we will introduce vocabulary, concepts and notations of continuum thermomechanics that will be used in this manuscript.

It is assumed in particular that the properties and characteristics of the medium are continuous and differentiable in space and in time. The material point in this medium is considered as being a *"representative elementary volume"* [Eringen,1962, Rougée,1997]. It is centered around a given position in the 3D space (supposed to be Euclidean). It is worth noting that in geometry, Euclidean space is associated to a vector product. It is, for example, the case of a three-dimensional space in which material points are designated by coordinates and the distance between two material points can be computed using a distance formula [Britannica,2011, Gray,1997, O'Neill,1966].

The position of the material point is written by the coordinates $z^i$ $(i = 1, 2, 3)$ in an orthonormal coordinate system $\xi^i$. We denote $\mathbf{e}_i$ the base unit vectors associated with this coordinate system representing the frame in which quantities are observed. Note that the Latin letters are used to designate the coordinates of the particle and the Greek letters to designate the coordinate systems.

In this manuscript Einstein's summation will be used. Latin indices ($i$, $j$, ...) ranging from 1 to 3 correspond to the spatial parts of the quantities.

In classical continuum thermomechanics, coordinate systems are generally considered as orthonormal, hence in this manuscript we will consider orthonormal 3D coordinate systems only. Consequently, the metric of the manifold in this framework is expressed by the tensor $\mathbf{g}$ of signature $(1, 1, 1)$ [Marleau,2017]. We note that the use of general curvilinear coordinates is possible and can be found in the literature also for 3D coordinate systems [Eringen,1962].

### 1.2.1 Classifications of frames in thermomechanics

In order to describe phenomena in physics (e.g. motion), the use of frames is essential. For the purpose of classifying frames, we introduce the speed of light $c$ according to which the norm of the linear 3D velocity of particles $v^i$ can be compared. Thermomechanics can therefore be divided into Newtonian thermomechanics ($||v||$ is negligible comparing to $c$) and relativistic thermomechanics ($v$ is not negligible comparing to $c$). This last category can be divided into thermomechanics description considering special relativity where gravitation is not taken into account [Knudsen and Hjorth,1995] and thermomechanics description considering general relativity where gravitation is considered.

Furthermore, privileged classes of frames are defined in thermomechanics [Landau and Lifshitz,1975]. In the following, we discuss classes of frames used in Newtonian thermomechanics. Frames in relativistic thermomechanics will be later discussed (see section 1.3).

The description of thermomechanical behaviors of materials depends of these classes. Some frames are related to the material body, others are not. Therefore, different measures of parameters (e.g. deformation) are obtained for different classes.

### 1.2.2 Frames in Newtonian thermomechanics

Note that in this manuscript, we use the adjective "Newtonian" to indicate notions defined in Newtonian thermomechanics and we define the classical 3D space as the space in which relativity is not taken into account (see section 1.2). The definition of a Newtonian frame is not trivial. We review some of the definitions found in the literature:

- A general frame is defined in [Landau and Lifshitz,1975] as being a coordinate system giving the spatial positions of particles and corresponding to a clock giving the time.
- A Newtonian frame is defined in [Wang,2016] as being the combination of "a chronology measuring the instants of time and the 3D coordinates".

We will use the following definition: A set of 3 non-collinear points associated to a chronology, that by the definition of a frame are fixed between them and one can locate a position or a motion with respect to them. Therefore, the Newtonian frame enables the description of the thermomechanics of discrete elements that can be assumed to be points for a certain scale (e.g. kinetics of gaz as well as satellite motion). Within the continuum, these discrete elements correspond to the representative elementary volumes (REV) that are assumed to be infinitely small. A frame in Newtonian thermomechanics can be defined using 3 parameters: the base vectors $\mathbf{e}_i$, the associated coordinate system $\xi^i$ and a chronology parameterized by the time $t$ (e.g. $(\mathbf{e}_i, \xi^i, t)$).

As previously mentioned, in the Newtonian thermomechanics approach, time is an external parameter to the spatial coordinate system. It is therefore necessary to associate a chronology with the 3D coordinate system allowing to locate the system and its evolution in time. Newtonian frames are (infinitely) rigid bodies that can undergo rigid body motion in the Euclidean space. Two types of Newtonian frames can be distinguished: Galilean and non Galilean frames.

Galilean frames are frames having a uniform rectilinear translation motion of velocity $v^i$ with respect to each other while one of them is predetermined to be Galilean. Practically, it is convenient at first approximation to consider the heliocentric frame as Galilean (because it can be considered roughly static to the far stars during the observation) and define/construct all other frames with respect to this one. "Galilean" frames can also be called "inertial" frames. A more abstract but equivalent definition is given in [Landau and Lifshitz,1976]: a Galilean frame is a frame according to which time is uniform and space is homogeneous and isotropic. It is an idealization of the previous definition.

The transformation from one Galilean frame ($R$) to another Galilean frame ($R'$) is defined by the Galilean transformation. As follows are examples of Galilean transformations. Let $[z^1, z^2, z^3]$ be the spatial

components of the position vector $r^i$ in $(R)$ and $t$ the time relative to $(R)$. And let $[z'^1, z'^2, z'^3]$ be the spatial components of the position $r'^i$ in $(R')$ and $t'$ the time relative to $(R')$.

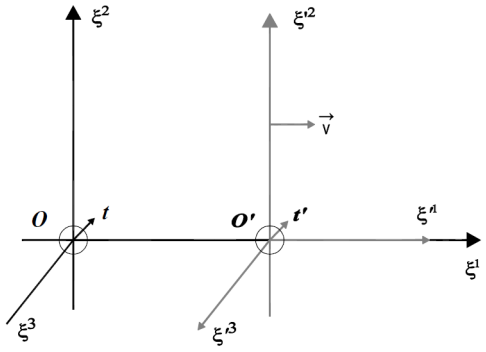


**Fig. 1:** A transformation between frames $(R)$ and $(R')$ where $v^i$ is parallel to the $z^1$-direction.

In the particular case where the axes of the frames are parallel and the direction of the relative velocity is parallel to the $z^1$-direction, the Galilean transformation is written [Truesdell,1966]:

$$\begin{cases} z'^1 = z^1 - vt \\ z'^2 = z^2 \\ z'^3 = z^3 \\ t' = t \end{cases} \tag{1.1}$$

In the case where the axes of the frames remain parallel but the direction of the relative velocity is arbitrary, the Galilean transformation is generalized to:

$$\begin{cases} r'^i = r^i - v^i t \\ t' = t \end{cases} \tag{1.2}$$

Authors like [Taillet et al.,2009] generally define non Galilean frames as being frames that do not check the conditions necessary to be Galilean. In these frames, Newton's second law of motion is only verified by adding additional forces called inertial forces which are due to the accelerated motion of the frame with respect to a Galilean (or inertial) frame of reference.

## 1.3 Relativistic kinematics in continuum thermomechanics

We place ourselves now in the relativistic framework where frames are associated with the continuum. This association enables the transition to the description of the thermomechanics of the continuum (e.g. thermomechanical behaviors of material).

In addition to that, a set of four coordinates denoted:

$$x^\mu = (x^1, x^2, x^3, x^4) = (x^i, ct) \tag{1.3}$$

is used to parameterize a point in a spacetime manifold. It is related to the spacetime coordinate system $\xi^\mu$.

A frame in spacetime thermomechanics can then be defined using 2 parameters: a set of four base vectors of spacetime $\mathbf{e}_\mu$ and the associated coordinate system $\xi^\mu$ (e.g. $(\mathbf{e}_\mu, \xi^\mu)$). Greek indices ($\mu$, $\nu$... running from 1 to 4) label the spacetime quantities.

### 1.3.1 Introduction of proper time and absolute time

In order to describe classes of frames in relativistic thermomechanics, it is important to note that time is now a coordinate parameter which have a different value between frames for the measure of the same phenomenon. As its name indicates the proper time is the time measured by a clock related to the matter (at rest). It is represented by the red clock associated to the matter frame in Fig. 2. However, the absolute time is independent of the matter frame. The matter can be in motion with respect to the clock measuring the absolute time. This is represented by the blue clock in Fig. 2. The object's red clock is in motion with respect to the the blue clock. For example, the time taken by a spacecraft to travel between two locations and measured by a fixed clock to earth is shorter than that measured by a clock related to the moving spacecraft.

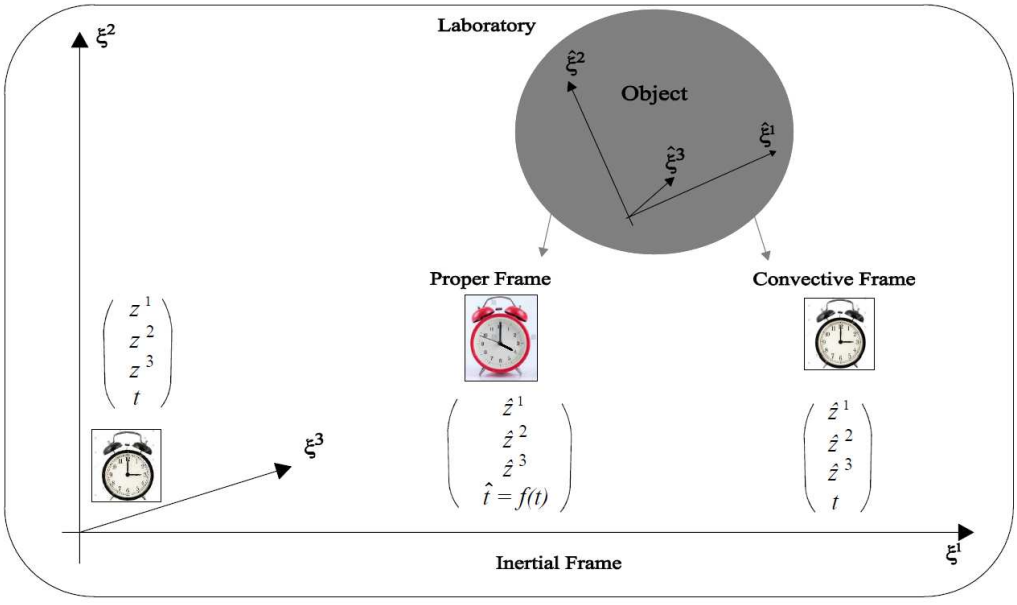


**Fig. 2:** Categorisation of time and corresponding frames. Note that the hat on the symbols denotes quantities described in the frame related to the matter (i.e. proper/convective).

As follows, we discuss classes of frames in relativistic thermomechanics: inertial, convective and proper frames.

### 1.3.2 Inertial frames in relativistic thermomechanics

It can be defined in relativistic thermomechanics generalizing the definition of "a Galilean frame" in Newtonian thermomechanics. Inertial frames are frames animated with respect to one another with a rectilinear non accelerated motion with a predefined speed $v$, whatever the value of $v$ to $c$ is (especially taking into account relativistic case). The motion is characterized by a linear 3D velocity $v^i$ having the Euclidean norm $v$. Within these frames any isolated (no external forces acting on it) or pseudo-isolated body (the resultant force acting on it is null) which is in motion at a constant speed remains at constant speed. In the particular case where $v$ is negligible with respect to $c$ this frame coincides asymptotically with Galilean frame (see section 1.2.2).

The metric in this framework is expressed either by $\boldsymbol{\eta} = (1, 1, 1, -1)$ or by $\boldsymbol{\eta} = (-1, -1, -1, 1)$. Note that this $(+, +, +, -)$ or $(-, -, -, +)$ signature is conventional and has no physical implications [Marleau,2017].

Different signatures are considered in the manuscript. In this bibliographic chapter, we will consider the signature of metric $(+,+,+,-)$. In the following chapters, since a spacetime domain is considered thus to assign positive components in the time direction, we will consider the signature of metric $(-,-,-,+)$. The transformation from one inertial frame $(R)$ to another inertial frame $(R')$ is now defined by the Lorentz transformation.

In the particular case where the axes of the frames are parallel and the direction of the relative velocity is parallel to the $z^1$-direction, the Lorentz transformation is expressed by [Bernard,2019]:

$$\begin{cases} z'^1 = \gamma z^1 - \gamma v t \\ z'^2 = z^2 \\ z'^3 = z^3 \\ t' = \gamma t + \gamma \dfrac{v}{c^2} z^1 \end{cases} \tag{1.4}$$

where $\gamma$ is the Lorentz factor defined by:

$$\gamma = \frac{1}{\sqrt{1 - \frac{v^2}{c^2}}} \tag{1.5}$$

The Lorentz transformation is valid for every 3D velocity $v^i$ ($||v|| \leq c$) [Gondran and Gondran,2014]. Moreover, the Galilean transformation is a limiting case of Lorentz transformation (at the non-relativistic limit).

### 1.3.3 Proper and convective frames in relativistic thermomechanics

The proper frame is a notion deriving from relativistic physics that is very similar to the definition of the convective frame [López-Monsalvo,2011]. Both frames are related to the evolving matter (co-moving with the matter [López-Monsalvo,2011, Louck and Galbraith,1976]). Thus, in these frames, a point of the matter is stationary. Quantities described in both frames will be systematically marked with a hat on their symbols [Wang,2016].

These frames may or may not be inertial. The difference between the two frames is that: the time in the proper frame is proper to the evolving matter (it means that an internal process can be used to define the time measuring the evolution of phenomena) while in a convective frame the time is absolute thus related to an exterior clock to the system (see 1.3.1). These two frames are introduced in details in [Rouhaud et al.,2013, Wang,2016].

In addition to these classes of frames defined above, other classes are privileged in thermomechanics for application to the general relativity [Einstein,1920] (such as the harmonic coordinate systems [Belinfante and Garrison,1962, Soffel and Langhans,2013]).

### 1.3.4 Examples of possible configurations

A material body (object) is identified using a continuous and differentiable 3D manifold. The projection of the ensemble of material points into the three-dimensional space is called a configuration [Wang,2016]. In every configuration, information about the positions of the material points at a given instant are obtainable, as presented in Fig. 3. Different configurations can be obtained when different types of frames taken into account. In Fig. 3 and table 1, we give the notation of the space coordinates and time corresponding to each frame.

An instant of reference $t_0 = \hat{t}_0 = 0$ is chosen to define the initial configuration. At this instant, we note the configuration $\Omega_0$. Note that $\Omega_0$ is identical in the inertial frame and in the convective/proper frame.

Then at an instant $t$ of the absolute time, the object is deformed. The configuration in an inertial frame noted (1) in which the frame remains the same and the object is deformed, is different of that in a convective/proper frame noted (3)/(4) in which the frame is deformed with the object.
There is also a difference between configurations if we consider the proper time instead of the absolute time. The instant $\hat{t}$ is different from the instant $t$, then the configuration in an inertial frame is (2) (different from configuration (1)) and in the object frame the configuration (4) (different from configuration (2)).

Let's consider that the object in Fig. 3 is a square whose sides have a length of $L$ and it is observed respectively at a time $t_0 = \hat{t}_0 = 0$ and after deformation at a time $t$ corresponding to the proper time $\hat{t}$ at which its sides elongations are $\delta_x$ in the $x-$direction and $\delta_y$ in the $y-$direction. Then the dimensions in the configurations and times corresponding to frames will be: (1): $(z^1, z^2, t) = (L + \delta_x, L + \delta_y, t)$, (2): $(z^1, z^2, \hat{t}) = (L + \delta_x, L + \delta_y, \hat{t})$, (3): $(\hat{z}^1, \hat{z}^2, t) = (L, L, t)$ and (4): $(\hat{z}^1, \hat{z}^2, \hat{t}) = (L, L, \hat{t})$.

This shows that configurations vary according to the frames chosen for observation. Numbers in the table correspond to the configurations in figure 3.

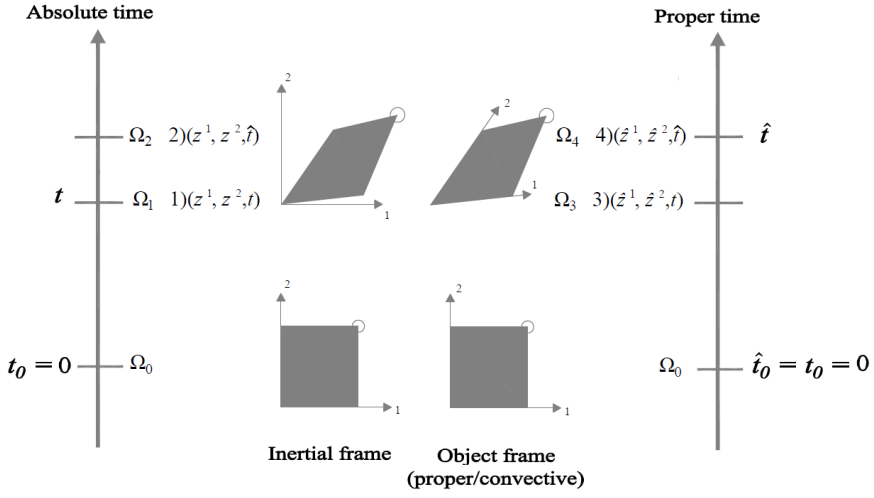


**Fig. 3:** Different configurations and times corresponding to different frames to observe the same phenomenon (see table 1)

| Frame/Time | Absolute | Proper |
|---|---|---|
| Inertial | 1 | 2 (unusual use) |
| Convective | 3 | - |
| Proper | - | 4 |

**Tab. 1:** Different frames corresponding to different configurations and times corresponding to observe the same phenomenon (see Fig. 3).

## 1.4 Additional notions for Newtonian and relativistic thermomechanics

### 1.4.1 Invariance

The notion of invariance is verified when the value of the physical quantity does not differ during a transformation on the elements of a group (e.g. change of frames) [Liu,2004]. The spacetime norm of a velocity vector in spacetime, for example, is invariant with respect to the change of frames.

Let us illustrate this notion: suppose that we dispose of an aquarium full of water and we define a Cartesian coordinate system associated with the time $t$ denoted: $\xi^\mu : [x, y, z, t]$ to identify each point in the recipient. A spacetime Cartesian frame $(\mathbf{e}_\mu, \xi^\mu)$ can be defined using this coordinate system, where $\mathbf{e}_\mu$ represents the base vectors associated to this spacetime frame. The water temperature at each point can then be described by the function $\theta(x, y, z, t)$. It is a unique value representing the temperature of each point of the space and time domain.

Let us then consider a cylindrical coordinate system associated with the time $\widetilde{t}$ denoted $\widetilde{\xi}^\mu : [r, \alpha, \widetilde{z}, \widetilde{t}]$ that can move relatively to $\xi^\mu$. The coordinates of $\widetilde{\xi}^\mu$ are functions of the coordinates of $\xi^\mu$ such that: $r(x, y, z, t)$, $\alpha(x, y, z, t), \widetilde{z}(x, y, z, t), \widetilde{t}(x, y, z, t)$. A spacetime cylindrical frame $(\widetilde{\mathbf{e}}_\mu, \widetilde{\xi}^\mu)$ can be defined using this coordinate system, where $\widetilde{\mathbf{e}}_\mu$ represents the base vectors associated to this spacetime frame.
The value of the temperature $\theta$, at a given point and at a specific time, is invariant compared to the change of frame. We can then write:

$$\theta(x, y, z, t) = \theta(r, \alpha, \widetilde{z}, \widetilde{t}) \tag{1.6}$$

This is equivalent to say that the value of $\theta$ is independent of the coordinate system chosen therefore to the change of the corresponding frames. This is related to the scalar nature of temperature, that we have assumed based on experimental observations.

### 1.4.2 Material objectivity

Material objectivity is rather a notion characterizing quantities in Newtonian thermomechanics. It postulates that the qualitative and quantitative descriptions of the phenomena remain the same when these phenomena are observed in different frames. The historical development of the term can be found in [Eringen,1962, Nemat-Nasser,2004, Truesdell and Noll,2003, Marsden and Hughes,1994, Speziale and Galbraith,1987].

In [Truesdell and Noll,2003], the principle of objectivity is defined as: *"it is a fundamental principle of classical physics that material properties are indifferent, i.e., independent of the frame of reference or observer"*. In [Nemat-Nasser,2004], it is defined by: *"Constitutive relations must remain invariant under any rigid-body rotation of the reference coordinate system. This is called objectivity or the material frame indifference."*

A Newtonian constitutive model has to verify the principle of material objectivity. The notion of objectivity actually covers two physical definitions:

- The independence with respect to the change of frames (i.e. frame-indifference [Panicaud et al.,2014]): The frame does not affect the motion of the body (the choice of frame has not consequences on the motion itself). It is a fundamental principle in classical physics. This point of view is adopted in this study. It is important in the formulation of constitutive models and the price to pay is to use differential geometry in a spacetime domain [Rouhaud et al.,2013]. This notion in spacetime refers to the covariance principle.
- The indifference with respect to the superposition of rigid body motions (i.e. material indifference [Panicaud et al.,2014]): When a body is animated by a rigid body motion, there are no constraints applied to this body [Frewer,2009]. It is the classical point of view that leads to the classical 3D Euclidean geometry [Coxeter,1961].

To sum up, the notion of objectivity covers the notion of indifference with respect to the action of the group of frame changes and the notion of indifference with respect to the action of the group of rotations of the 3D space. The two notions of objectivity merge in the classical 3D space previously defined.

*-Objectivity requirement for a 3D tensor:*
A 3D tensor is a tensor defined in the classical 3D space (see definition in section 1.2). Let us consider 2 Newtonian frames $(e_i, \xi^i, t)$ and $(\widetilde{e_i}, \widetilde{\xi^i}, \widetilde{t})$ such that:

$$\widetilde{\xi^i} = Q^i_j(t)\xi^j + \lambda^i(t) \tag{1.7}$$

where $Q^i_j(t)$ is an orthogonal matrix related to rotation and $\lambda^i(t)$ is a vector related to translation, both depending only on time.
Let us also consider a second-rank tensor observed in these 2 frames such that:

$$\tau = \tau^{ij}\mathbf{e}_i \otimes \mathbf{e}_j = \widetilde{\tau}^{ij}\widetilde{\mathbf{e}}_i \otimes \widetilde{\mathbf{e}}_j \tag{1.8}$$

where "$\otimes$" denotes the tensor product. This tensor is frame-independent in case it verifies:

$$\widetilde{\tau}^{ij} = Q^i_m(t)Q^j_n(t)\tau^{mn} \tag{1.9}$$

### 1.4.3 Covariance principle

In this manuscript, the spacetime formalism is used for purposes explained in section 1.6 and section 4.3. Briefly, this principle postulates that the form of the laws/models of physics is identical in all the frames, inertial or not. The variables of these laws/models obey the law of change of frames and the laws/models themselves conserve their form (i.e are form invariant). The notion of covariance brings to light the notion of relativity and spacetime formalism. Within the spacetime formalism, three coordinates represent the space and one coordinate represents time as presented in section 1.3 [Wang,2016]. Hence the observers are completely defined once the spacetime frame is chosen and spacetime transformations describe change of frames [Eringen,1962]. The indifference to the change of frames must apply to all spacetime tensors and to all equations and operators.

As an illustration, Einstein's theory of special relativity is based physically on the evidence that the celerity of light in a vacuum remains constant for all the frames moving between them in uniform translation with constant velocity [Einstein,1920]. Mathematically, the result of the invariance of celerity of light is expressed by building covariant models (mechanical or others) with respect to the Lorentz transformation.

Let us now consider the example taken in section 1.4.1. Let us suppose that we have measured the temperature gradient $G(x, y, z, t)$ at a given point of space at a specific time in the different spacetime frames used. The components of this spacetime vector are defined at each point by the derivatives:

$$G_x = \frac{\partial\theta}{\partial x}, G_y = \frac{\partial\theta}{\partial y}, G_z = \frac{\partial\theta}{\partial z}, G_t = \frac{\partial\theta}{\partial t} \tag{1.10}$$

where $\dfrac{\partial}{\partial x^i}$ is the partial derivative to space. Now let us consider the first cylindrical coordinate of this gradient resulting from a spacetime transformation, it is given by:

$$G_r = \frac{\partial\theta}{\partial r} \tag{1.11}$$

To compute $G_r$, it is necessary to formulate the relation between the cylindrical coordinates and the Cartesian coordinates:

$$G_r = \frac{\partial x}{\partial r}G_x + \frac{\partial y}{\partial r}G_y + \frac{\partial z}{\partial r}G_z + \frac{\partial t}{\partial r}G_r \tag{1.12}$$

Therefore :

$$G_r \neq G_x \tag{1.13}$$

In other words, the components of the temperature gradient are not individually independent of the choice of coordinate system (consequently not independent of the frame in which the quantity is expressed) although the temperature itself is. Entities like the spacetime temperature gradient $G$ should be build covariant to preserve their form by change of frames.

We thus propose to describe the large transformations of materials (including large deformations and finite temperature variations) with a spacetime covariant approach using the formalism of differential geometry [Schouten,1954]. Differential geometry also used to describe motion in Newtonian formalism [Eringen,1962, Truesdell and Noll,2003, Marsden and Hughes,1994, Venturi,2009] has found a major application in the description of physics in spacetime formalism.

In a relativistic framework (referred to as the spacetime formalism), the covariance principle is intrinsically verified with the use of four-tensors densities and four-operators that are by construction indifferent to changes of observer (i.e. covariant). We specifically consider a scalar density $\mathcal{S}$ and the components of a second-rank tensor density $\boldsymbol{\mathcal{T}}$:

Through coordinate transformations from corresponding to a material point $x^\mu$ to $\widetilde{x^\mu}$, the scalar density $\mathcal{S}$ and the components of a second-rank tensor density $\boldsymbol{\mathcal{T}}$ verify the relations:

$$\widetilde{\mathcal{S}} = \mathcal{S} \tag{1.14a}$$

$$\widetilde{\mathcal{T}}^{\mu\nu} = \frac{\partial \widetilde{x}^\mu}{\partial x^\lambda}\frac{\partial \widetilde{x}^\nu}{\partial x^\kappa}\mathcal{T}^{\lambda\kappa} \tag{1.14b}$$

$$\widetilde{\mathcal{T}}_{\mu\nu} = \frac{\partial x^\lambda}{\partial \widetilde{x}^\mu}\frac{\partial x^\kappa}{\partial \widetilde{x}^\nu}\mathcal{T}_{\lambda\kappa}, \tag{1.14c}$$

These definitions are detailed and developed in section 2.2.3.

### 1.4.4 Lagrangian and Eulerian descriptions of the motion in spacetime

Let us describe two descriptive approaches of the motion: the Lagrangian approach and the Eulerian approach [Boratav and Kerner,1991, Havas,1964].

A Lagrangian description follows the matter in its motion. The initial configuration is considered to be Lagrangian. The coordinates in this description are noted by $X^\mu$ ($\mu$ varying from 1 to 4). In other words, it is the description of the motion of a matter with respect to the initial configuration. For example, let us reconsider the case mentioned in section 1.4.1, with water particles that can move in this aquarium: the motion of a particle inside of the aquarium can be described with respect to an observer moving with the particle, this illustrates the Lagrangian description.

However, Eulerian description is the description of matter with respect to the current deformed configuration. After the deformation, the deformed configuration is defined at the time $t$ ($t \neq t_0$). The coordinates at $t$ are noted $x^\mu$. Physical quantities such as density, velocity, temperature ... can then be defined as a function of $x^\mu$ ($\rho(x^\mu)$ , $v^i(x^\mu)$, $\theta(x^\mu)$ ...).

The relation between the quantities in the two descriptions can be written:

$$x^\mu = x^\mu(X^i, t) = \begin{cases} x^i = x^i(X^k, t) \\ x^4 = ct \end{cases} \tag{1.15}$$

For example, let us reconsider the case mentioned in section 1.4.1, with water particles that can flow in and out of this aquarium: The motion of the particles inside of the aquarium can be observed at a time $t$ by an external observer, this illustrates the Eulerian description. These descriptions and the corresponding deformations are further detailed in chapter 4.

### 1.4.5 Comparison between Newtonian and spacetime notions

Notions of independence with respect to the change of frames and indifference with respect to superposition of rigid body motions are indiscernible in Newtonian thermomechanics.
On one hand, if we consider 2 frames $(e_i, \xi^i, t)$ and $(\widetilde{e_i}, \widetilde{\xi^i}, \widetilde{t})$, the equation representing the change of frame

from $\xi^i$ to $\widetilde{\xi^i}$ is given in Eq. 1.7 of section 1.4.2. On the other hand, the transformation of $\xi^i$ into $\widetilde{\xi^i}$ via a transformation of rigid body motion composed of a rotation $Q^i_j(t)$ and a translation $\lambda^i(t)$, is also written:

$$\widetilde{\xi^i} = Q^i_j(t)\xi^j + \lambda^i(t) \tag{1.16}$$

However, in a spacetime domain the two concepts are different: Eq. 1.7 and Eq. 1.16 are different because they are associated to different motions. The first corresponds to a motion in a frame $(e_i, \xi^i, t)$ written with respect to the frame $(\widetilde{e_i}, \widetilde{\xi^i}, \widetilde{t})$ while the second corresponds to a rigid body motion described in the frame $(\widetilde{e_i}, \widetilde{\xi^i}, \widetilde{t})$. Since the mapping of events in a spacetime frame includes time and the rotation and translation matrix are function of time, thus there is no mathematical difference between these two equations.

The approach discussed in this manuscript is based on the theory of relativity (without gravitation) which allows the simplification of the formulations [Rouhaud et al.,2013, Edelen,1967]. In the theory of relativity, the principle of covariance guarantees the independence with respect to the change of frames of any physical law [Landau and Lifshitz,1975]. Table 2 sets the limits of the case of relativity considered. However, if the studied systems are subjected to gravitation then a conventional treatment of gravitation can be carried out.

| **Covariance:** | **4D Riemannian space** | **4D Euclidean space** |
|---|---|---|
| Lorentz Group | - | Special relativity |
| Diffeomorphism | General relativity | The case we are considering |

**Tab. 2:** Type of relativity applied for the spacetime approach studied in the manuscript

## 1.5 Newtonian heat conduction modeling in literature

We aim in the first part of this manuscript to write the heat equation and build a heat conduction model and the associated weak integral forms in a spacetime domain. This is in order to overcome the difficulties faced when using Newtonian modeling (section 1.6) and to develop new relativistic models. In the previous paragraph, the elements of the continuum medium have been defined. The heat conduction modeling in such a domain will be discussed hereinafter.
We begin by summarizing the heat conduction models found in literature in both Newtonian and relativistic approaches. The evolution of the heat conduction models is investigated and comparison between models is established. The necessity of a more developed model is then discussed: it can be summed up by the need of a covariant model respecting both the laws of thermodynamics and the principle of causality.

According to [Battaglia,2007], the heat conduction phenomenon can be described as follows: *"When a heat source is applied to a body, the nearest atoms to the source undergo intense vibrations later transmitted to the adjacent atoms. The result of these vibrations is the production of heat inside the body and its diffusion. The intensity of the vibrations is function of the intensity of the heat source applied and it is measured by the body temperature. The discovery of the thermodynamics as well as the discovery of static and quantum physics led to the evolution of this definition especially the* $19^{th}$ *and* $20^{th}$ *centuries"*. This phenomenon is characterized by 2 useful dependent parameters: the thermal conductivity $\lambda(W.m^{-1}.K^{-1})$ and the thermal diffusivity $a(m^2.s^{-1})$ [Battaglia,2007]. They reflect the material ability to conduct heat: the material is called a conductor if it allows the flux of heat in one or more direction (e.g. metals with a conductivity superior to $10W.m^{-1}.K^{-1}$), otherwise it is called an insulator (e.g. glass wool with a conductivity inferior to $1W.m^{-1}.K^{-1}$). They also characterize the heat flux diffusion. These parameters are function of the temperature notably when approaching the phase change domain in the case of solids and fluids [Battaglia,2007]. The heat conduction phenomenon can be illustrated in the hot molding process

(i.e. gravity die casting, Figure 4) [Prucha,2003]. During this process, a melt alloy is poured into a mold in order to obtain a part having the same geometrical properties as the mold. The heat transfer between the part and the mold is ensured by conduction. The heat conduction phenomenon can also be seen in the functioning of a cooling fin (e.g. on a tubular body, Figure 4): heat is transferred by conduction from the hot body to the external surfaces of the fin. Then, it is evacuated to the surrounding environment by convection.

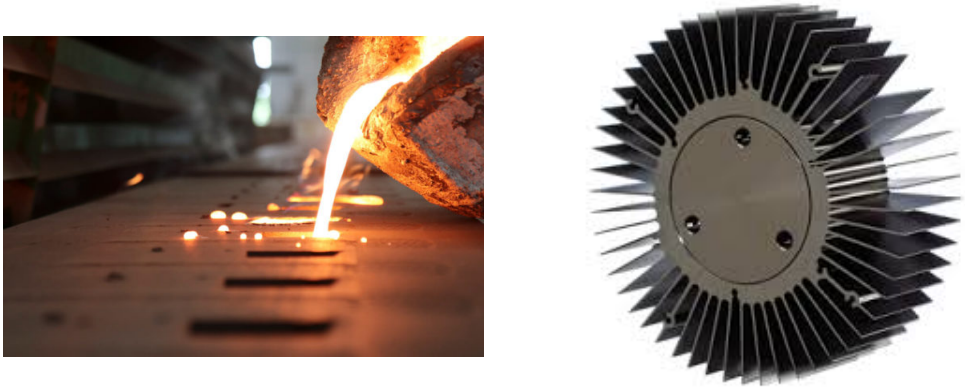

**Fig. 4:** On the left: thermal molding. On the right: cooling fin.

### 1.5.1 Summary of the Newtonian thermodynamic approach

The thermodynamic approach is one way to obtain Newtonian models of heat conduction. Heat conduction models should satisfy the heat dissipation obtained via this approach [Landau and Lifshitz,1975, Onsager,1931, Zubarev,1974, Nakagawa and Sasa,2019].

The Clausius-Duhem inequality can be derived from the first and the second laws of thermodynamics combined together in the Newtonian approach [Frémond,2006, Fer,1970, Muller,1985]. It can be written:

$$-\widetilde{\rho_c}(-\theta\frac{d\eta_c}{dt}+\frac{de_{int}}{dt})+\sigma_{ij}d^{ij}-\frac{\phi^i\nabla_i\theta}{\theta}\geq 0 \tag{1.17}$$

Where:

- $\widetilde{\rho_c}$ can be interpreted in the convective frame as the mass density (at rest) with the specific internal energy $e_{int}=0$. $(._c)$ denotes convective as in the convective frame and $\widetilde{(.)}$ is to express that this quantity is measured at rest for $e_{int}=0$.
- $\eta_c$ is the entropy density.
- $\frac{d}{dt}$ is the total derivative to time.
- $\sigma_{ij}$ is the 3D stress tensor.
- $d^{ij}$ is the 3D rate of deformation.
- $\phi^i$ is the specific heat flux.
- $\nabla_i$ is the spatial covariant derivative. $\theta$ is scalar and $x^i$ are orthogonal, thus $\nabla_i=\frac{\partial}{\partial x^i}$.

Then the heat dissipation, which represents the heat transfer occuring during an irreversible process, can be deduced from Eq. 1.17 by separating mechanical dissipation from the dissipation due to temperature gradient:

$$\forall\theta, \forall(\nabla_i\theta) \qquad -\frac{\phi^i \nabla_i \theta}{\theta} \geq 0 \tag{1.18}$$

### 1.5.2 Assumptions on Newtonian models of heat conduction in the literature

Many models of heat conduction are found in the literature [Battaglia,2007, Fourier,1988, Cattaneo,1958, Osborne,1950, Vernotte,1961, Tavernier,1962]. They are built using different approaches under certain assumptions. The Newtonian models reviewed in the next sections (1.5.3 to 1.5.6) are subject to the assumptions listed as follows.

**Assumptions**

- The model is built for a continuous media
- The model is purely thermal. Thermomechnical couplings are not taken into account.
- Heat transfer by convection and radiation are taken into account through separate modeling.
- $\forall t$, $\forall x^i$ the material coefficients are constant.
- We consider the case of a homogeneous isotropic material.
- For simplification, no volume heat source is applied to the body in the following modeling unless otherwise specified.

Slightly different assumptions describing the spacetime domain considered, will be held for the spacetime heat conduction models built in this work (see section 2.3.1).

### 1.5.3 Newtonian Fourier's model of heat conduction and corresponding heat equation

The Newtonian Fourier model derives originally from experimental results. It results from the study of heat transfer in a wire subjected to different temperatures at its 2 ends while being insulated on the other boundaries [Battaglia,2007]. The Fourier heat conduction model can be expressed by [Battaglia,2007, Fourier,1988]:

$$\phi^i = -\lambda I^{ij} \frac{\partial \theta}{\partial x^j} \tag{1.19}$$

where $\lambda$ is the material conductivity and $I^{ij}$ is the 3D second-rank identity tensor. Eq. 1.19 should also verify the inequality in Eq. 1.18 to be compatible with laws of thermodynamics. The heat equation can be deduced from the balance of internal energy [Battaglia,2007, Fourier,1988] which in case a volume heat source $f$ is imposed, it is written:

$$\mathcal{C}_{m\omega}\widetilde{\rho_c}\frac{\partial \theta}{\partial t} + \frac{\partial \phi}{\partial x^i} - f = 0 \tag{1.20}$$

where $\mathcal{C}_{m\omega}$ is the specific heat capacity ($de_{int} = \mathcal{C}_{m\omega} d\theta$ under the assumption that the state variables are independent and mechanical phenomena are not occurring).

By replacing the flux of the heat conduction model (Eq. 1.19) in Eq. 1.20, we obtain the well-known heat equation:

$$\mathcal{C}_{m\omega}\widetilde{\rho_c}\frac{\partial \theta}{\partial t} - \lambda I^{ij}\frac{\partial \theta}{\partial x^i}\frac{\partial \theta}{\partial x^j} - f = 0 \tag{1.21}$$

### 1.5.4 Motivation to find new models of heat conduction

Among the models of heat conduction proposed in the Newtonian approach, let us discuss in particular the consequences of Newtonian Fourier model of heat conduction. When this model is used, we deal with

the fundamental problem of instantaneous character of heat propagation [Straugham,2011, Auriault,2017]: according to this model the thermal signals may propagate at a velocity greater than that of the speed of light $c$ which implies a causal problem.

Let us illustrate the propagation of the heat signal for Newtonian Fourier model of heat conduction in comparison to another Newtonian model of heat conduction respecting the causality principle (Figure 5). We consider the case of a $1D$ heat model of length $L$. The initial temperature of the model is $\theta_0 = 0^oC$. We impose the following boundary conditions: $\theta(x = 0) = \theta_s$ and $\theta(x = L) = 0$, where $\theta(x)$ is the temperature at a position $x$ and $\theta_s = 100^oC$. The evolution of the temperature of a point located at a certain distance $0 < x < L$ is observed. The graph representing this evolution in a Fourier model of heat conduction (red line) shows an instantaneous change of temperature of the point at $x$ at a certain time $t$. While the graph (blue dots) representing the propagation of heat at a finite speed shows a gradual evolution of the temperature through the time. It corresponds to a "Cattaneo-like" model of heat conduction further detailed (see sections 1.5.5 and 1.5.6).

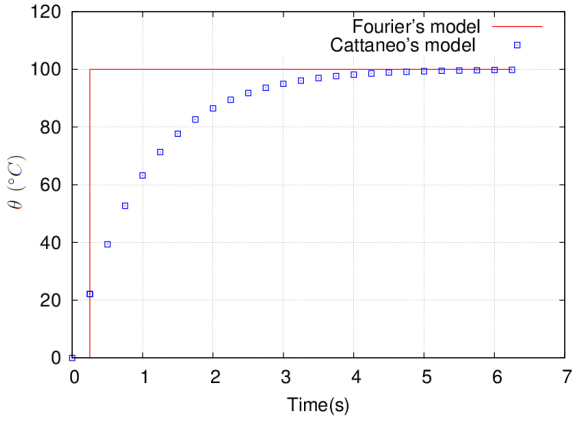


**Fig. 5:** Illustration of the causality problem. The figure shows the variation of the temperature of a spatial point located at a certain distance $x$ from a heat source in 2 cases: the propagation of heat at an infinite speed (red line) and the propagation of heat at a finite speed (blue dots).

The previous example shows that the heat transfer is instantaneous according to Fourier's model, therefore violating causality. In order to solve this conflict and to obtain a heat transfer rate bounded by the speed of light to respect the causality principle, different authors add a relaxation term to Fourier's equation [Cattaneo,1958, Christov,2009, Osborne,1950, Vernotte,1961, Tavernier,1962, Chapman and Cowling,1970].

### 1.5.5 Newtonian Cattaneo's model of heat conduction and corresponding heat equation

This heat conduction model introduces a relaxation time to the Fourier heat conduction model.

Cattaneo's model [Cattaneo,1958] is developed based on the kinetic gas theory and by taking into account some delay on the collisions leading to heat transmission [Stewart,1977, Israel and Stewart,1979a, Israel and Stewart,1979b, Murdoch,1983]. One-dimensional case is considered (propagation in the $x$-direction).

Let $Q$ be a random physical quantity attached to a gas particle and let $\mathcal{G}(x) =< Q >$ be its arithmetic mean value over gas particles at any point. $< . >$ denotes the arithmetic mean value over particles. Let us then consider a small area $A_x$ normal to the $x$ -direction at the abscissa $x$. This area is crossed in both directions by particles of different speeds. $Q$ is supposed to be the quantity of gas particle crossing $A_x$ at the

instant $t$. Let M be the point where the particle undergoes the last collision with other particles and $l^{(k)}$ the free path of the particle $k$ between M and $A_x$. Let $\beta^{(k)}$ be the inclination of the speed of the particle $k$ with respect to the $x$-direction. Let $j^l(x)$ be the total algebraic flux of the quantity $Q$ through $A_x$. The average value $\mathcal{G}(x)$ of the quantity $Q$ attached to gas particle is then calculated at M of abscissa $x - l^{(k)}cos\beta^{(k)}$.

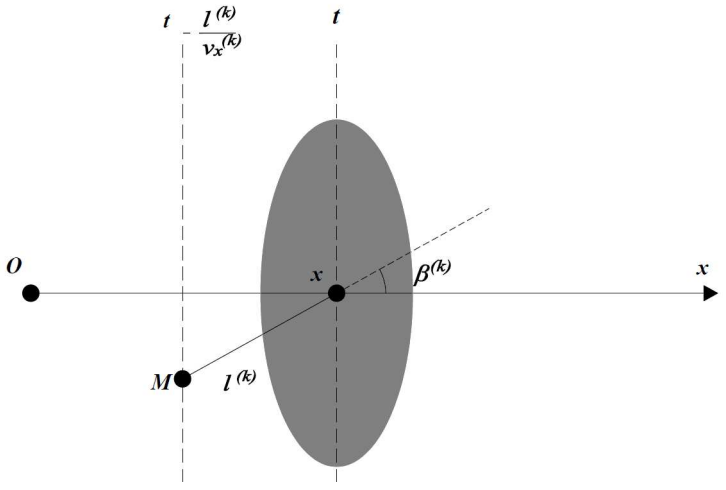


**Fig. 6:** The geometric description of Cattaneo's hypothesis

To compute the flux $j^l(x)$ through $A_x$, we need to compute the variation of the quantity $\mathcal{G}$ between the points M at abscissa 0 and that of abscissa $x$ [Papon and Leblond,2005]. This last position is the position of collision with $A_x$. We set $\tau$ the time interval between two collisions:

$$\tau = \frac{l^{(k)}}{< v^{(k)} >} \tag{1.22}$$

where $l^{(k)}$ is the free path of the particles having a speed $v^{(k)}$, $v^{(k)}$ is the speed of particles $k$ having the same speed and $< v^{(k)} >$ is the mean value over gas particles of $v^{(k)}$.
The variation of $\mathcal{G}(x)$ in the $x$-direction will be:

$$(d\mathcal{G}(x))^i = \frac{\partial \mathcal{G}(x)}{\partial x^i} < v_x^{(k)} > \tau \tag{1.23}$$

where $v_x^{(k)}$ is the speed of particles $k$ having the same speed in the $x$-direction. In the $x$-direction, the flux of $n$ particles (per unit volume) is equal to $n < v_x^{(k)} >$. Consequently, using Eq. 1.23, $j^l(x)$ can be written:

$$j^l(x) = -I^{lm} n < v_x^{(k)} >^2 \tau \frac{\partial \mathcal{G}(x)}{\partial x^m} \tag{1.24}$$

Taking the equal energy hypothesis into account and by introducing the mean free path in $j^l$, it can be expressed by:

$$j^l(x) = -I^{lm} \frac{n < v^{(k)} >< l^{(k)} >}{3} \frac{\partial \mathcal{G}(x)}{\partial x^m} \tag{1.25}$$

Where $< v_x^{(k)} >^2 = \dfrac{< v^{(k)} >^2}{3}$ and $< l^{(k)} > = < v^{(k)} > \tau$.

In the particular case where $Q$ (whose algebraic flow is $j^l(x)$) is identified with the kinetic energy of the particles, $\mathcal{G}(x)$ is then identified to the absolute temperature $\theta$ of the gas and $j^l(x)$ is identified to $\phi^i$ by a factor $\alpha$ (constant)[Cattaneo,1958]. In this case, we obtain:

$$\lambda = \frac{1}{3} n < v^{(k)} l^{(k)} > \alpha \tag{1.26}$$

where $< v^{(k)} l^{(k)} >$ is the mean value over gas particles of $v^{(k)} l^{(k)}$. We also assume that the last collision happens at $t - \frac{l}{k}$.
Cattaneo shows that the Taylor expansion on $\phi^i$ to a suitable order at least in the case of a quasi-stationary regime leads to:

$$\zeta \frac{\partial \phi^i}{\partial t} = -\lambda \phi^i - \lambda^2 I^{ij} \frac{\partial \theta}{\partial x^j} \tag{1.27}$$

Where we define: $\zeta = \frac{1}{2} n \alpha < l^2 >$.
$< l^2 >$ is the mean quadratic value of the mean free path.
By substituting $\phi^i$ we obtain a hyperbolic differential heat equation.

$$\frac{\partial^2 \theta}{\partial t^2} - \frac{\lambda^2}{\zeta \mathcal{C}_{m\omega} \widetilde{\rho_c}} I^{ij} \frac{\partial}{\partial x^i} \frac{\partial \theta}{\partial x^j} + \frac{\lambda}{\zeta} \frac{\partial \theta}{\partial t} = 0 \tag{1.28}$$

The same form of equation is obtained in function of $\phi^i$ by substituting $\theta$.

$$\frac{\partial^2 \phi^i}{\partial t^2} - \frac{\lambda^2}{\zeta \mathcal{C}_{m\omega} \widetilde{\rho_c}} I^{ij} \frac{\partial \phi^k}{\partial x^l} \frac{\partial \phi^l}{\partial x^k} + \frac{\lambda}{\zeta} \frac{\partial \phi^i}{\partial t} = 0 \tag{1.29}$$

The parabolic heat equation corresponding to the classical Fourier's model of heat diffusion (Eq. 1.21) is thus replaced by a hyperbolic heat equation (Eq. 1.28) corresponding to a model of heat propagation.

The heat waves propagate at a group speed and the propagation speed depends on the average of mean particle speeds [Cattaneo,1958] can be deduced from Eqs. 1.28 or 1.29:

$$v_g = \sqrt{\frac{\lambda^2}{\zeta \mathcal{C}_{m\omega} \widetilde{\rho_c}}} = \frac{1}{\sqrt{3}} \frac{< v^{(k)} l^{(k)} >}{< l^2 >} \tag{1.30}$$

### 1.5.6 Other arguments justifying Newtonian Cattaneo-like heat conduction models and corresponding heat equations

Several arguments ending to Cattaneo-like models of heat conduction that respect the causality principle are found in the literature.

Osborne [Osborne,1950] built a heat conduction model with relaxation terms using the analogy with the transmission lines of Maxwell's electrodynamics [Narasimhan,1999, Ekoue et al.,2013] to obtain the heat equation expressing the propagation of heat for liquid Helium by conduction.

$$\frac{\partial^2 \theta}{\partial t^2} - v_h^2 I^{ij} \frac{\partial}{\partial x^i} \frac{\partial \theta}{\partial x^j} + \frac{1}{\tau} \frac{\partial \theta}{\partial t} = 0 \tag{1.31}$$

Where: $\tau$ is the relaxation time introduced in Eq. 1.22.
$v_h$ represents the speed of propagation of temperature in the liquid Helium.

Vernotte [Vernotte,1961] added a term of production of internal energy $e_{int}$ in a Cattaneo type model. The heat equation in this case can be expressed by:

$$\frac{\partial}{\partial x^i} \frac{\partial \theta}{\partial x^j} I^{ij} + \frac{1}{\lambda} \left[ e_{int}(x,t) + \tau \frac{\partial e_{int}(x,t)}{\partial t} \right] = \frac{1}{\alpha} \left[ \tau \frac{\partial^2 \theta}{\partial t^2} + \frac{\partial \theta}{\partial t} \right] \tag{1.32}$$

Tavernier [Tavernier,1962] derives the same equation from the Boltzmann transport equation of electrons and phonons in solids:

$$\frac{\partial g}{\partial t} + v^i \nabla_i g + f_a \frac{\partial g}{\partial T} = \left[\frac{\partial g}{\partial t}\right]_{diff} \tag{1.33}$$

Where: $g$ is a statistical distribution of heat carriers (electrons, photons or phonons ...), $T$ is the momentum acting on this group of heat carriers, $f_a$ the force applied and $\left[\frac{\partial g}{\partial t}\right]_{diff}$ is the diffusion term also called collision term.
The Boltzmann equation therefore describes the variation in time of the distribution of the heat carriers because of the diffusion. Its reduced form in one dimension is expressed by:

$$\frac{\partial g}{\partial t} + v^i \frac{\partial g}{\partial x^i} = \left[\frac{\partial g}{\partial t}\right]_{diff} \tag{1.34}$$

In order to linearize it, Tavernier suggests the following approximation:

$$\left[\frac{\partial g}{\partial t}\right]_{diff} = -\frac{g - g_0}{\tau} \tag{1.35}$$

$g_0$ is a statistical distribution of heat carriers (i.e. electrons in the case of heat diffusion in metals) at equilibrium.
$\tau$ is the relaxation term corresponding to the heat carriers having a speed $v$.

The same hyperbolic model of heat conduction in [Osborne,1950, Vernotte,1961, Tavernier,1962] is consequently obtained:

$$\tau \frac{\partial \phi^i}{\partial t} = -\phi^i - \lambda I^{ij} \frac{\partial \theta}{\partial x^j} \tag{1.36}$$

Another textbook [Tzou,2014] presents also scales aspect, showing that Cattaneo's model was obtained by Maxwell from his kinetic theory [Maxwell,1867, Nayfeh and Nemat-Nasser,1971, Joseph and Preziosi,1989]. It can also be given by the linearized form of the Chapman-Enskog kinetic theory [Chapman and Cowling,1970]. Throughout this manuscript, Cattaneo's model is referring to Vernotte-Maxwell-Cattaneo's type model.

### 1.5.7 Effect of spatial scales on the treatment of the heat equation

The non-separation of scales can be a possible explanation of the reason of violation of causality principle in the heat conduction models [Auriault,2017]. According to Auriault, the problem derives from inconsistencies resulting from the application of the heat conduction model on different scales and that by distinction of scales the dilemma may vanish.

He claims that Fourier and Maxwell-Cattaneo-Vernotte models seek to explain the macroscopic behavior of the quantity $\theta$ valid at a scale $L$ larger than the atomic scale. He therefore distinguishes three characteristic lengths $l$, $L$ and $L_1$ which are respectively the atomic scale, the macroscopic scale where the Fourier's model and Maxwell-Cattaneo-Vernotte model are defined (i.e the scale large enough to be visible with the naked eye, without magnifying optical instruments [Reif,1965, Jaeger,2014]) and finally the upper macroscopic scale. These scales are defined such that:

$$\frac{l}{L} = \epsilon_1 \ll 1, \ , \ \frac{L}{L_1} = \epsilon_2 \ll 1 \tag{1.37}$$

Hence, according to Auriault, one cannot apply the classical models of behavior in the case where the scales are not clearly separated since the coefficients of the models will not be convenient. According to the argument of homogenisation used in [Auriault,2017], the macroscopic model equivalent to a heat conduction phenomenon and on which the application of equations of Fourier and Maxwell-Cattaneo-Vernotte is allowed,

derives from the separation of scales. Two equations derive from the approximations, they can be expressed in a $1D$ space by:

$$\lambda \frac{\partial^2 \theta}{\partial x^2} = \mathcal{C}_{m\omega} \widetilde{\rho_c} \frac{\partial \theta}{\partial t} + \mathrm{O}(\epsilon) \tag{1.38}$$

$$\lambda \frac{\partial^2 \theta}{\partial x^2} = \mathcal{C}_{m\omega} \widetilde{\rho_c} (\frac{\partial \theta}{\partial t} + \epsilon\tau \frac{\partial^2 \theta}{\partial t^2}) + \mathrm{O}(\epsilon^2) \tag{1.39}$$

The term $\mathrm{O}(\epsilon)$ includes the infinite speed of an infinitesimal heat signal.

Auriault deduces that the Maxwell-Cattaneo-Vernotte model describes the phenomenon of heat conduction well and is reduced to the Fourier model by a first-order Taylor expansion, only at a particular scale provided that the separation of scales should respect: $\epsilon_1 \ll 1$ and $\epsilon_2 \ll 1$ . In addition to that, all Newtonian models are defined at scales that are large compared to the atomic scale. This approximation shortens their domains of validity.

These spatial scales can be combined to temporal scales marked by three characteristic orders of time: the small time scale $t_{small} \leq 1\,\mu s$, the macroscopic time scale $t_{macro} \geq 1\,\mu s$ which is the temporal domain where Fourier's model and Maxwell-Cattaneo-Vernotte model are defined [Guillemet and Bardon,2000] and the large time scale $t_{large} \gg t_{macro} \Leftrightarrow \dfrac{t_{macro}}{t_{large}} = \epsilon_3 \ll 1$ i.e. thermal phenomenon taking a time considered large with respect to classical phenomena.

Others have also given similar arguments to explain this problem:

- According to Fichera [Fichera,1992], Fourier's model is a result of experimental observations, therefore it is related to the conditions and the nature of the matter considered. Fichera states:"*Fourier theory has a limited range which will become more and more restricted with the technical progress of the experimental instruments for measurements and of the computing facilities which, respectively, will permit more refined measures and sharper numerical approximations*". However, he admits that as a result the small heat flows that propagate at an infinitely high speed cannot be modeled using Fourier's hypothesis since they cannot be noticed experimentally. In [Fichera,1992], Fichera investigates also the value of the heat flow propagating at infinite speed based on Fourier's statements in [Fourier,1988] by taking the example of thermal propagation in a wire. He states:" *But while this influence can be expressed mathematically from the first instant, its numerical value is excessively small... The sensible propagation of heat, so far from being instantaneous, is excessively slow process and the time required to produce... change of temperature... is proportional to the square of the linear dimension (i.e. length of the wire)*".
  Hence according to Fichera, when it is not required to have extremely high precision on neither measurements nor evaluations/simulations, Fourier's heat conduction model results are quite satisfactory.

- According to Day [Day,1997], if a small fraction of the heat flow propagates at an infinitely high speed, therefore the physically most significant part of the signal (bulk of the signal), is at a finite speed.

### 1.5.8 Validity of the parabolic and hyperbolic models of heat conduction with respect to spatial and temporal domains

Guillemet and Bardon [Guillemet and Bardon,2000] raise the debate in their article on the spatial and temporal domains of the heat equation. According to [Guillemet and Bardon,2000], the time domain used by the heating engineer should be greater than the maximum duration for which the Fourier's model is questioned (it is of the order of $10^{-6}$ s). Thus, the utility of introducing relaxation time into the heat equation as a solution to the problem caused by the parabolic model is questioned. This term added for reasons of consistency is in fact negligible depending on the fields of use of the heat equation.

Moreover, the hyperbolic model supposed to be the answer to the problem of instantaneous heat propagation is needed just at the start of the transient regime. In this domain which corresponds generally to a distance smaller than 7 mean free path lengths ($7\,l_{pm}$) and a duration of ten relaxation times ($10\,\tau$), several disadvantages of the hyperbolic equation arise [Guillemet and Bardon,2000].

First, singular persistence appears numerically in the form of a temperature discontinuity front at a certain abscissa (corresponding to space) and propagates with time: its amplitude (corresponding to the amplitude of the variation of temperature) decreases over time but the front remains vertical giving 2 values of temperature at a given time: this can be physically interpreted by the lack of diffusion at the front. The front vanishes starting an abscissa of 7 mean paths. Second, the inertial term $\tau\dfrac{\partial^2\theta}{\partial t^2}$ gives a temperature behavior with apparent contradiction to the second law of thermodynamics. A heat flux from the cold zone towards a hot zone can be numerically observed and the points reach temperatures higher than the temperature imposed on the limit. This is due to the few interactions between heat carriers in this domain of space and time in which the local thermodynamics balance is not ensured. Beyond this domain the diffusive phenomenon covers the effect of this term.

Consequently, boundary conditions of the diffusion problem using the hyperbolic model are developed in [Guillemet and Bardon,2000] to solve the previous problems occurring at small spaces and small times. In [Guillemet and Bardon,2000], the possibility of extending the validity of the hyperbolic model up to a space scale of about one mean free path is investigated. In the resulting modified model, boundary conditions are added to compensate the discontinuity of macroscopic quantities at the observed space frontiers (ranging in $\leq 7\,l_{pm}$).

## 1.6 Compatibility of thermal models with constraints imposed by large transformation thermomechanics

A correct description of the thermal behavior of materials is often required in models dedicated to the large transformations of the matter. For example, a realistic heat conduction model is often essential for simulating forming processes [Battaglia,2007]. Researches nowadays are focusing on heat conduction models for applications including new materials especially at microscopic scales, such as nanomaterials [Pourasghar and Chen,2019], as well as for application to new forming processes, such as additive manufacturing [Stump and Plotkowski,2019]. Experimental works are also frequently performed in order to verify the proposed models by comparison [Both et al.,2016]. Numerous approaches have led to the existing heat conduction models whose descriptions can be found in the literature and are reviewed in [Liu et al.,2017]. Moreover, heat conduction is of primary importance for modeling dissipation. Its modeling requires to verify some general properties. These properties are not systematically fulfilled by the existing models. This aspect is discussed in the manuscript in order to improve the quality of the modeling and improve the identification of the dissipation.

### 1.6.1 Review on the frame indifference of Newtonian heat conduction models

Frame-indifference of thermomechanical fields and constitutive models is sought. This is also called objectivity in the solid thermomechanics community [Christov and Jordan,2005] (detailed in section 1.4).

However, frame-indifference is not verified by Newtonian quantities as the time derivative of temperature which may appear in the formulation of heat conduction models and does not take into account corrective terms describing the evolution of time. The following is a summary on the frame indifference of two Newtonian heat conduction models found in literature.

In a Newtonian framework, Fourier's model is frame-indifferent because temperature and spatial gradient of temperature are objective quantities but Cattaneo's model is not, due to the time derivative appearing in its equation. This is deeply discussed in [Christov and Jordan,2005, Christov,2009] who have proposed to

use one of the many existing objective transports to overcome this difficulty. [Christov and Jordan,2005] have further demonstrated that an objective transport has to be introduced in Cattaneo's model to prevent paradoxical evolution of thermal waves in a moving frame. No satisfying physical justification was proposed in [Christov and Jordan,2005] to validate the choice of an objective transport versus another. As in visco-elasticity, such formulations in terms of different objective time derivatives give different models (e.g. lower-convected or upper-convective Maxwell models, etc.), which are all objective but which exhibit different non-linear effects without generally satisfying physical justifications.

Other approaches adopting a microscopic scale as a starting point do not lead to frame-indifferent models either [Murdoch,1983]. The reason is that the Newtonian principle of dynamics leading to the kinetic theory of gases is not frame-indifferent. This characteristic propagates upscale, leading to heat conduction models that are not frame-indifferent at the macroscopic scale.

### 1.6.2 Causality and finite propagation of heat

Fourier's model of heat conduction (see section 1.5.3) is probably the most often cited heat model in the literature and the most often used for numerical applications. Fourier's heat equation is parabolic, i.e. corresponds to a diffusion of heat. In other words, the use of Fourier's model leads to consider that heat propagates at an infinite velocity [Straugham,2011] (this is detailed in section 1.5.4). Consequently, a material point submitted to a heat source may reach a given temperature at a velocity that might exceed the velocity of light. This is in contradiction with the theories of relativity, hence violating the causality principle [Auriault,2017, Landau and Lifshitz,1975]. This defect is shared by other models.

To solve this difficulty, several authors have proposed to add a relaxation term to Fourier's equation (see sections 1.5.5 and 1.5.6). The equation becomes hyperbolic, then corresponding to a model of heat propagation as opposed to heat diffusion for the classical Fourier's model [Vitokhin and Ivanova,2017, Mariano,2017]. Despite the fact that they agree with the necessity to improve Fourier's equation with a relaxation term, these authors have different points of view concerning the physical interpretation of this term [Cattaneo,1958, Christov,2009, Osborne,1950, Vernotte,1961, Tavernier,1962, Chapman and Cowling,1970].

Other models treat the previous problem in the framework of generalized continuous media. For example in [Liu et al.,2017], a micromorphic approach is proposed and a heat equation is derived from Helmholtz free energy potentials depending on an additional micromorphic temperature and its first gradient. Such a model takes non-local thermal effects into account and changes the heat equation in ways involving an internal length scale, which may represent a characteristic length of the system. This approach leads to various models of heat conduction avoiding the aforementioned problem of instantaneous propagation of heat.

It is worth noting that experimental results have clearly identified the heat propagation effect, as presented in [Ván et al.,2013, Kovács and Ván,2015, Ván,2016]. For the second sound characterizing this propagation, there are also investigations with experimental results at room temperature [Both et al.,2016, Ván et al.,2017]. It is remarkable that in those experiments, not the Cattaneo equation but one of its possible extension the Guyer-Krumhansl type heat conduction was frequently observed [Ván et al.,2017]. The later model is not investigated in this manuscript.

More details concerning causality can be found in [Fichera,1992]. Also the Cattaneo type finite speed has a material origin, and nothing prevents it to be larger than the speed of light in the material in a non-relativistic spacetime model. Finally, the best mathematical formulation of causality is the requirement of symmetric hyperbolicity of the governing partial differential equations, as proposed in the monograph of Müller and Ruggeri [Müller and Ruggeri,1998].

To conclude, on one hand, in a Newtonian Framework, Fourier's model is frame-indifferent but does not respect the causality principle [Fichera,1992]. On the other hand, Cattaneo's model alleviates the causality problem but its form depends on the choice of the observer or on the choice of an objective transport for its improved versions [Christov,2009]. None of these two models systematically satisfies both frame-indifference

and causality principles and open issues remain to be solved to construct a heat conduction model merging directly all physical requirements.

### 1.6.3 Irreversibility of transformations

The modeling of thermomechanical behavior of materials used in forming processes requires taking into account large deformations, the influence of temperature on the thermomechanical behavior, as well as the dissipative behavior of materials.

This last notion is essential in most of the applications e.g. in modeling the elastomers behavior, the dissipative mechanisms are in form of internal friction and reinforcement by loads [Boukamel,2006] and in modeling a fabrication process of a metal (which is intrinsically irreversible since it induces a change of shape), it is in form of modeling the evolution of temperature, viscosity and plasticity [Vitokhin and Ivanova,2017].

A dissipative behavior leads to thermodynamically irreversible changes. Hence, the state of the system at any given time depends on the history of its evolution.

In order to model this irreversible behavior, it is necessary to formulate the Clausius Duhem inequality deriving from the first and second laws of thermodynamics. The aim is to build models representing processes showing dissipation behaviors such as heat conduction, viscosity and plasticity via a thermodynamic approach with internal variables. We briefly recall the assumptions delimiting the corresponding thermodynamic framework:

- The formulation of models for large transformations (large strain, large displacement and finite variation of temperature).
- The decoupling of thermal and mechanical phenomena which allows us to consider the thermal behavior and the mechanical behavior separately.

Consequently, every model (including the spacetime models later discussed) should be thermodynamically compatible with these conditions.

## 1.7 Possible solutions to improve the heat conduction modeling

### 1.7.1 Covariance

The notion of frame-indifference is advantageously replaced with the covariance principle introduced by Einstein in the theories of relativity [Havas,1964, Muschik and Restuccia,2008, Panicaud et al.,2014, Rouhaud et al.,2013] (discussed in 1.4.3). Since the transformations corresponding to changes of observer involve space and time, it is relevant to explore the possibilities offered by a spacetime description of thermomechanical problems. This further ensures the fact that all equations and models are necessarily indifferent to changes of observer. The space and time components of spacetime tensors are obtained using projectors [Eckart,1940]. Also, the well-known difficulties associated with the choice of objective transports [Truesdell and Noll,2003, Rouhaud et al.,2013] are solved with the use of spacetime derivatives (covariant derivative in the direction of the velocity or the Lie derivative along the motion), which are by construction indifferent to changes of observers [Rouhaud et al.,2013]. This will be further detailed in sections 2.2.4 and 2.2.7.

### 1.7.2 Spacetime thermodynamics

The elements of the spacetime formalism in which a thermodynamical approach can be built are detailed in [Hayward,1999]. Furthermore, obtaining spacetime heat equations has already motivated many thermodynamical studies. These studies have developed relativistic theories of dissipation of first or second order. The

nomenclature corresponds to the degree of expansion of the variables used in the equations of these theories. Those theories extend the space of variables (heat, entropy, temperature...) of the classical theories to include some dissipation effects. The first order theories lead to the historically first relativistic and thermodynamics model proposed by Eckart [Eckart,1940]. He proposed the first generalization of Fourier's model in a spacetime formalism. Landau and Lifshitz come next to propose another model [Landau and Lifshitz,1975]. It has the same basis as Eckart's model with the only difference that it is written with respect to the proper observer, i.e. comoving with a material particle. It is worth to mention that [Bressan,1978] proposed an approach ending to spacetime heat conduction based on Stefan and Boltzmann's laws. As previously mentioned, the second order theories differ in the order of expansion of the variables. For example, Israel and Stewart's model [Israel and Stewart,1979a, Israel and Stewart,1979b, Stewart,1977] added second order corrections to the flux of entropy, while Carter's model [Carter,1988] is based on a multi-fluid approach. Section 1.8 expands the explanation on these relativistic models.

## 1.8 Relativistic models of heat conduction in literature

As discussed before, models deriving from linear thermodynamics lead to the instantaneous propagation of heat problem (the problem of causality is then identified) [Hayward,1999, Narasimhan,1999]. Other models introduce relaxation terms that change the structure of the heat equation, while having limited effects on the results [Eringen,1962, Auriault,2017, Ekoue et al.,2013, Tavernier,1962, Vernotte,1961, Liu et al.,2017]. In this section, several relativistic thermal behaviors are reviewed.

The heat conduction equation in the spacetime domain has been obtained in several studies based on a thermodynamic approach [López-Monsalvo,2011].

All relativistic theories of dissipation in these studies are similar in construction: they consist in proposing a form of the energy-momentum tensor and a definition of the entropy flow in order to apply the first and second laws of thermodynamics.

Below is a brief description of the models [Eckart,1940, Landau and Lifshitz,1975, Carter,1988, Israel and Stewart,1979b, Israel and Stewart,1979a, Stewart,1977] already cited in section 1.7.2. This does not restrict all possible models from theories of dissipation [Hayward,1999, López-Monsalvo,2011], but these listed relativistic models are among the most used models.

### 1.8.1 First order models

In this section, Eckart's model [Eckart,1940] and Landau and Lifshitz's model [Landau and Lifshitz,1975] are reviewed. Eckart's model [Eckart,1940](1940) is the result of the first development of thermodynamics in the relativistic framework. The relativistic theory of dissipation and the existence of a material whose number of particles is conserved with a local energy balance are assumed.

According to this model, the symmetric energy-momentum tensor can written using the following decomposition:

$$T^{\mu\nu} = \rho_c c^2 u^\mu u^\nu + u^\mu q^\nu + u^\nu q^\mu + T_\sigma^{\mu\nu} \tag{1.40}$$

Where: $\rho_c = \widetilde{\rho}_c \left(1 + \frac{e_{int}}{c^2}\right)$ is the mass density in case $e_{int} \neq 0$ in the convective frame, $u^\mu$ is the spacetime velocity, $q^\mu$ is the volume heat flux four-vector and $T_\sigma^{\mu\nu}$ is the stress four-tensor as measured by an observer moving with the particle flux, which is equivalent to the stress four-tensor expressed in the convective frame.
The simple definition of relativistic entropy leads to Eckart's model which is equivalent to a Fourier's model written in spacetime.

$$\phi^{\mu} = cq^{\mu} = -\lambda \Pi^{\mu\nu}(\nabla_{\nu}\theta + \theta \frac{du_{\nu}}{dt}) \tag{1.41}$$

Where: $\Pi^{\mu\nu} = g^{\mu\nu} + u^{\mu}u^{\nu}$ is the orthogonal projector to the observer's four-velocity. $g^{\mu\nu}$ is the metric four-tensor. Note that in the following chapters $\Pi^{\mu\nu}$ is defined differently due to the opposite signature of the metric taken into account. We presently respect the choice of Eckart.

The term $-\lambda \Pi^{\mu\nu}\theta \frac{\partial u_{\nu}}{\partial t}$ is an acceleration term that does not exist in the expression of the equivalent model built in a reference frame in the Newtonian approach. It represents a thermal heat flux which direction is opposite to the acceleration [López-Monsalvo,2011, Eckart,1940]. Hence, in this generalization of Fourier's model in spacetime, this term is associated to thermal inertia: it formally results from the local energy balance and reflects the effect of the world line curvature on the infinitesimal 3D spaces [Eckart,1940, López-Monsalvo,2011]. The resulting model of heat equation is parabolic. It keeps the defect of instantaneous propagation of heat flow and then leads to inconsistencies due to violating the causality principle.

The Landau and Lifshitz model [Landau and Lifshitz,1975] is another first order model. It does not differ fundamentally from Eckart's model. The only difference is the choice of the frame. In fact, the Eckart and Landau and Lifshitz models are particular applications of the same more general covariant model.

### 1.8.2 Second order models

The inconsistencies (due to the violation of the causality principle) caused by the previous theories lead to the necessity of "second-order" theories of dissipation. In this section, Israel and Stewart's model [Israel and Stewart,1979b, Israel and Stewart,1979a, Stewart,1977] and Carter's model [Carter,1988] are reviewed. In Israel and Stewart's model [Israel and Stewart,1979b, Israel and Stewart,1979a, Stewart,1977], the entropy flow is corrected such that it includes second order terms interpreted as truncated expansions due to the deviation from equilibrium. It leads naturally to a generalized heat conduction equation for Cattaneo's model [Christov,2009] in spacetime combined with a mechanical term. This is equivalent to an equation expressing the propagation of thermal signals for a model with relaxation terms. In this model the validity of the hypothesis of local equilibrium is assumed and a thermal propagation at finite speed is obtained. This assumption remains valid for small deviations to the equilibrium so that the energy density remains a function of the number of particles and of entropy densities.

This approach, which is based on the kinetic theory, is known as transient relativistic thermodynamics or as the relativistic second order theory of dissipation. The difference between this theory and Eckart's theory is in the energy-momentum tensor: the term related to viscosity and its resulting momentum are taken into account. Consequently this tensor is written:

$$T^{\mu\nu} = \rho_c c^2 u^{\mu}u^{\nu} + (\mathfrak{p} + \pi)\Pi^{\mu\nu} + u^{\mu}q^{\nu} + u^{\nu}q^{\mu} + \pi^{\mu\nu} \tag{1.42}$$

Where: $\mathfrak{p}$ is the hydrostatic pressure of the fluid defined through the trace of the stress tensor: $\mathfrak{p} = \frac{1}{3}tr(T_{\sigma})$. $\pi$ is a term related to viscous pressure. $\pi^{\mu\nu}$ is the mechanical stress not taking into account stress resulting from viscous pressure. In comparison with Eckart's model, the following definition is obtained:

$$T_{\sigma}^{\mu\nu} = (\mathfrak{p} + \pi)\Pi^{\mu\nu} + \pi^{\mu\nu} \tag{1.43}$$

Israel and Stewart also generalized the definition of the density entropy. The second order terms added to this definition must be measured separately by direct or indirect means of the kinetic theory.

In a purely thermal case $\mathfrak{p} = \pi = \pi^{\mu\nu} = 0$, the generalization of the Cattaneo's model in spacetime is then obtained including the relaxation term:

$$\phi^{\mu} = cq^{\mu} = -\lambda\theta\Pi^{\mu\nu}\left(\frac{1}{\theta}\nabla_{\nu}\theta + \frac{\partial u_{\nu}}{\partial t} + \frac{1}{2}\nabla_{\kappa}\left(\frac{\beta_1 u^{\kappa}}{\theta}\right)q_{\nu}\theta + \nabla_{\kappa}(q_{\nu})u^{\kappa}\beta_1\right) \tag{1.44}$$

Where: $\beta_1$ is introduced as a coupling parameter for the second order terms. It can be interpreted as a relaxation time for the propagation of thermal disturbances.

However, the stability conditions in this theory are rather artificial. Such theories do not systematically fulfill all the requirements.

A model is also proposed by Carter [Carter,1988]. Carter's theory is based on the multi-fluid approach of the relativistic dissipation study. This approach introduces the flux of entropy density.

### 1.8.3 A categorization by César Simón López-Monsalvo

In order to study the historical problem of heat conduction, a thesis was conducted in 2011 by César Simón López-Monsalvo [López-Monsalvo,2011]. This study recalls the bases of theories of dissipation of thermodynamics and applies the multi-fluid approach to solve the problems of temperature propagation. In this study the notions of linear classical irreversible thermodynamics and extended irreversible thermodynamics are introduced as in the definitions below. This categorization is added to the one based on the order of the theory of dissipation. We are interested in the terms that these theories add to the spacetime heat equation.

#### 1.8.3.1 Linear classical irreversible thermodynamics (CIT)

It is an approach developed by Onsager and extended by Prigogine [Prigogine,1980]. Its most important result are the reciprocal relations of Onsager, from which the Fourier's model can be derived. The only assumption taken into account is that at each point a local equilibrium is ensured at the macroscopic scale and for which the entropy satisfies the Gibbs law (although the system is not at global equilibrium).

In this approach, it is considered that the production of entropy $\eta_c$ is a bilinear form of the generalized thermodynamical forces $F_i$ (temperature gradients, chemical potential gradients ...) and fluxes $q_j$ which represent the irreversible processes which take place (heat flux, heat resulting from chemical reactions ...).

$$\eta_c = \sum_i F_i q_j \geq 0 \tag{1.45}$$

Despite the precise results that this approach provides experimentally, it shows failures when the thermal relaxation time scale is long compared to the dynamical one. The failures are shown, for example, in the case of superfluid Helium, even if the deviations of the equilibrium are not large. The CIT, however, retains the instantaneous character of the heat equation, hence the need for a more advanced development to overcome this problem.

#### 1.8.3.2 The hyperbolic equation of heat conduction based on extended irreversible thermodynamics (EIT)

Similarly to Fourier's model, Cattaneo's model can be constructed by interpreting heat conduction as an exchange of energy during the collisions of the particles of the material. This model takes two approximations into account: the heat flow $q^{\mu}$ is no longer linked to a force gradient as in the Fourier's model and that the quantity $\tau\frac{\partial}{\partial t}(\frac{\partial\theta}{\partial x})$ is small, thus corresponding to a long dissipation time compared to the dynamic evolution of the system.

In general, the EIT [Muller,2008, Jou et al.,1988] is designed to examine the variables varying slowly in phenomena extended by dissipation terms and describing the systems outside of their equilibrium state. For example, in the case of a fluid, the EIT considers the energy as a function of conserved quantities and slow dissipation fluxes, which transforms the Gibbs equation naturally to the hyperbolic heat equation.

We are talking here about the second order theories in which it is premature to simplify the higher order terms immediately at the deviation of equilibrium: these terms may revert to linear terms after the differentiation required by the second law of thermodynamics. In these theories the flow of entropy includes all the possible combinations of the dissipation effect. They show encouraging results with regard to stability and causality, however by introducing second order couples (introduced by the expansion of entropy flux) that are measurable.

The particular interest to this subject is greater because of its contribution in the field of the hydrodynamic description of relativistic energies of high plasma. However, the motivation of [López-Monsalvo,2011] is to carry out the modeling of the dynamics of superfluid neutron stars and high energy gas where photons contribute to the dominant pressure.

#### 1.8.3.3 On the multi-fluid approach developed [López-Monsalvo,2011]

One method of EIT is developped in [López-Monsalvo,2011]. It is the multi-fluid approach previously discussed in [Carter,1988]. In this investigation the entropy is considered as being a kind of fluid: the entropy density current is decomposed into a component corresponding to the one measured in the Eckart convective frame and another component which is transverse to the particles flow. In this case, we are dealing with both a flow of particles and entropy. Moreover, the principles of equivalence and covariance are the basis of this approach. The laws of thermodynamics then lead to the relativistic theory of heat conduction formulated in [López-Monsalvo,2011]. In addition to that, one of the most important results in this work is the analysis of the stability of the relativistic generalization of the heat equation.

To sum up, we notice that existing relativistic heat models fulfill the conditions of respecting the causality principle only if they derive from second order theories or in other words are built using EIT in a relativistic framework.

## 1.9 The self-heating phenomenon

In this part of the manuscript, we aim to build spacetime heat models respecting laws of thermodynamics, causality and the covariance principle. These models should be able to represent the reality of thermal phenomena. One possible way to test the reliability of the spacetime models in materials analysis is by using them in modeling the self-heating phenomenon occurring during fatigue tests.

As its name implies, the self-heating phenomenon is a thermomechanical transformation that leads to a variation of temperature of a material body without external heat supply [Doudard et al.,2009, Katunin,2017]. During such a transformation, a variable amount of mechanical energy is converted irreversibly into heat because of inelastic behaviors [Favier et al.,2016, Chrysochoos et al.,2009]. This phenomenon can be particularly investigated during fatigue tests [Favier et al.,2016, Chrysochoos et al.,2009, Boulanger et al.,2004, Benaarbia et al.,2016] during which, besides self-heating another amount of mechanical energy is converted reversibly into heat and is compensated at every mechanical cycle. Nowadays, very high cycle fatigue regime (VHCF) is becoming increasingly a topic of interest. A main reason is that many components used in aircraft, railway and automobile industries require to have a high fatigue lifetime exceeding the conventional range of megacycles [Cowles,1996].

VHCF corresponds typically to a gigacycle regime of fatigue [Ruben,2010]. Researches are actually focused on the resulting dissipation, which comes from the volume heat sources associated with irreversible

processes such as inelastic deformation mechanisms (internal friction [Guo et al.,2015] or microplasticity [Pu et al.,2019]) or heat diffusion.

### 1.9.1 Gigacycle fatigue testing machines

Fatigue strength is studied by applying cyclic load to specimens until their failure. $S-N$ curves diagram results from such tests [Ruben,2010] (e.g. Figure 7).

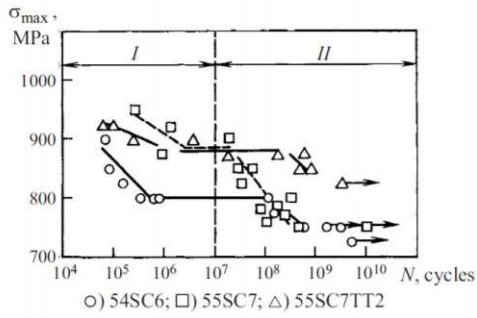


**Fig. 7:** Results of cyclic fatigue tests of various steels alloys in the range of high-cycle (I) and gigacycle regime (II) [Terentev,2004]. Tests are carried out at a load ratio R= –1 and a $20\,kHz$ frequency for high strength Cr-Si steel specimens.

Multiple classifications of fatigue testing machines can be found: classification by the type of load applied to the specimen (e.g. direct or axial stress, bending, torsion, applied strain, combined or complex stress) and classification related to the number of cycles that can be reached with the machine which depends on its testing frequency [Ruben,2010, Bathias and Paris,2005].

In order to reduce the total time of experiments of gigacycle fatigue tests, Bathias [Bathias and Paris,2005] develops an experimental method based on the application of the ultrasonic theory and technology. It is known as ultrasonic fatigue tests. The range of frequencies provided by ultrasonic fatigue machines is capable of producing $10^{10}$ cycles in less than one week while conventional fatigue machines took the average of three years to reproduce the same experiments [Blanche,2015].

Ultrasonic fatigue machines control the displacement. They mainly include a high frequency generator, a piezoelectric converter, and a displacement control system. Details on the function of each component are given in section 3.3 (see Figure 8). The nominal frequency is set to $20\,kHz$ (for the system shown in Figure 8). If a frequency of less than $19.5\,kHz$ is detected by the control system, the test system stops and reports a crack initiation.

### 1.9.2 Review on the measurement of self-heating in VHFC

The chronological development of self-heating investigation can be divided into 4 stages as detailed in [Munier,2012]. The first stage is between 1914 and 1937: The first investigations on the fatigue of materials were presented for the first time in [Wohler,1867] in 1867. The problem of identification of the time parameter $\tau_s$ characterizing the heat transfer perpendicular to the direction of heat conduction flux (also called characteristic time) arises. At the beginning of the $20^{th}$ century, the first identifications methods are discovered and empirical methods of determination of fatigue limit also appear [Stromeyer,1914, Moore and Kommers,1921, [Lehr,1926, Welter,1937]. Stromeyer's [Stromeyer,1914] work in 1914 is considered to be the first to study self-heating phenomenon.

His tests consisted of applying rotary bending on specimens. Temperature in his tests is measured using a differential temperature measurement device shown in Figure 9. A controlled flow of water at a certain

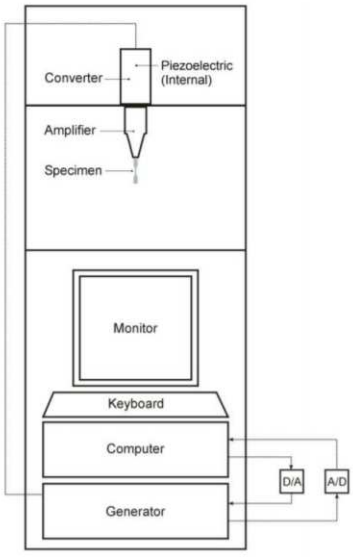


**Fig. 8:** Ultrasonic testing machine

temperature is introduced in his device through the input I. Once in contact with the specimen previously subjected to the fatigue test, the temperature of the water flow changes. It can be measured at the output O.

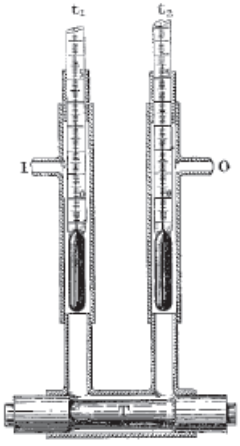


**Fig. 9:** Stromeyer's temperature measuring device for a conical specimen in rotary bending [Stromeyer,1914]

According to Stromeyer, the endurance limit (i.e. fatigue strength) is the minimum cyclic loading stress which leads to generate heat within the specimen. He showed the existence of a good correlation between his test results and the expression:

$$\pm \sigma_n = F_l + C(10^6/N)^{(1/4)} \tag{1.46}$$

where $\sigma_n$ (also known as $S_n$ in the literature) is the the amplitude of cyclic loading stress, $F_l$ the fatigue limit, $C$ a coefficient and $N$ is the number of cycles. These tests represent the birth of self-heating tests.

In the second stage between 1937 and 1980, research neglected the self-heating phenomenon. Only one study [Cazaud,1948] was published. Then in between 1980 and 2000 new methods based on experiments were published. Many materials were subject of study as well as the influence of the value of the stress

applied and the type of load [Galtier,1993, Luong,1998, Krapez et al.,1999]. The last stage is characterized by the research in modeling the mechanisms occurring during the change of temperature [Mareau,2007, Chrysochoos et al.,2009, Doudard et al.,2009, Maquin and Pierron,2009, Poncelet et al.,2011]. All the cited studies aimed to predict properties of material subjected to fatigue.

### 1.9.3 Recent methods of measurement of self-heating in VHFC

The resulting temperature from self-heating can be measured using different experimental arrangements: calorimeter [Shenogin et al.,2002], thermocouple [Zehnder et al.,1998], infrared (IR) sensors [Chrysochoos and Louche,2000, Wagner et al.,2009]. In general, according to the different studies, these measurements give similar results. A promising approach to study the dissipation is based on the use of quantitative IR thermography and optical extensometry [Boulanger et al.,2004, Berthel,2007, Maquin and Pierron,2009]. Indeed, these tools aim at assessing the dissipated energy associated with the cyclic loading. Specifically, IR and visible CCD cameras (charge-coupled device) can be used to record simultaneously fields corresponding to temperature variations and in-plane displacements over the sample gauge part [Chrysochoos et al.,2009]. Moreover, IR camera performances have been considerably improved with the discovery of infrared focal plane array sensors (IRFPA) [Poncelet et al.,2011]. These cameras nowadays provide IR films with a fine spatial resolution and low thermal noise. Consequently, several experimental approaches based on temperature measurements via quantitative IR techniques have recently been adopted to estimate the energy transformation [Chrysochoos et al.,2009, Boulanger et al.,2004, Blanche,2015]. Dissipation can be derived from thermal data fields by estimating the partial differential operators of the heat diffusion equation [Boulanger et al.,2004]. A number of simplified formulations, using different assumptions, can be then used for dissipation assessments. These assessments are based on averaging the variation of temperature through different directions which leads to emerging terms function of the time parameter $\tau_s$ detailed in section 3.3.3.

### 1.9.4 Self-heating models in literature

A realistic heat conduction model is an essential ingredient for modeling self-heating. The reason is that mechanical transformations occur in the body subject to ultrasonic fatigue tests which leads to an important change of its temperature: an evolution over time due to the dynamic character of the fatigue phenomenon which involves a spatial evolution due to heat conduction in all the specimen. However, the high cycle fatigue tests are considered as quasi-static processes from a thermodynamic point of view [Boulanger et al.,2004, Blanche,2015] (the statement of the local state axiom is found in [Germain,1983]). Thus considering high cycle fatigue, it is possible to study the heat conduction phenomenon occurring by starting from a quasi-static thermodynamical approach. A finite set of variables including: the absolute temperature $\theta$, the (small) strain tensor $\boldsymbol{\varepsilon}$ and a vector $\alpha_s$ of $n$ internal state variables that describe the material state, is considered. The first and second laws of thermodynamics, together with Fourier's heat conduction model, lead to the local heat conduction equation which can be expressed as in [Chrysochoos et al.,2009, Boulanger et al.,2004, Blanche,2015] by:

$$\widetilde{\rho}_c c_{m,v} \frac{\partial \theta}{\partial t} - \lambda \frac{\partial}{\partial x^i} \frac{\partial \theta}{\partial x^j} I^{ij} = d_1 + s_{the} + s_{thc} + f \tag{1.47}$$

Where: $I^{ij}$ is the $3D$ identity, $d_1 = \sigma^{ij} \dfrac{d\varepsilon^{ij}}{dt} - \widetilde{\rho}_c \dfrac{\partial \Psi}{\partial \varepsilon} \dfrac{d\varepsilon^{ij}}{dt} - \widetilde{\rho}_c \dfrac{\partial \Psi}{\partial \alpha_s} \dfrac{d\alpha_s}{dt}$ is the intrinsic dissipation, in which $\sigma^{ij}$ is the Cauchy stress tensor, $\varepsilon^{ij}$ is the elastic strain tensor and $\Psi$ is the specific free energy.
$s_{the} + s_{thc} = \widetilde{\rho}_c \theta \dfrac{\partial^2 \Psi}{\partial \theta \partial \varepsilon^e} \dfrac{d\varepsilon^{ij}}{dt} + \widetilde{\rho}_c \theta \dfrac{\partial^2 \Psi}{\partial \theta \partial \alpha_s} \dfrac{d\alpha_s}{dt}$ is the thermoelastic source and another possible thermomechanical coupling source due to internal state variable evolution (such as plasticity).
$f$ is the volume heat source. Some hypotheses were considered to simplify the local heat conduction equation:

the isotropic material conductivity $\lambda$ and the parameters $\widetilde{\rho_c}$ and $c_{m,v}$ are constant and independent of the state variables, thermoelastic effects were the only thermomechanical coupling factors considered hereafter, the convective terms of the total time derivative of the temperature are neglected, the external heat supply is time-independent then the equilibrium temperature field $\theta_f$ fulfilled $f = -\lambda\Delta\theta_f$ (where $\Delta$ represents the Laplace differential operator) and a change of variables $\theta_d = \theta - \theta_f$ can be applied.

Consequently, the left hand side of Eq. 1.47 is a differential operator that can be applied to $\theta_d$. The right hand side states different heat sources: the intrinsic dissipation $d_1$ and the thermoelastic source $s_{the}$. In this manuscript, the right hand side term is investigated, in the section 3.3.4 of chapter 3, in order to be used in the validation of the spacetime modeling of the phenomenon.

Analysis of temperature variations can be found in some references [Lemaitre and Chaboche,1990, Galtier,1993, La Rosa and Risitano,2000, Boulanger et al.,2004]. We analyse the temperature variation induced by thermoelastic coupling and dissipation during homogeneous uniaxial tests (Eq. 1.47). We define $\theta_{d(sthe)}$ and $\theta_{d(d1)}$ the temperatures induced respectively by $s_{the}$ and $d_1$.

#### 1.9.4.1 Thermoelastic coupling source

The thermoelastic behavior is assumed to be linear and isotropic [Boulanger et al.,2004]. The expression of the coupling source found in [Lemaitre and Chaboche,1990] shows that it is negative during loading and positive during unloading. Hence, the thermoelastic energy vanishes at the end of each complete loading cycle [Boulanger et al.,2004]. The span of $\theta_{d(sthe)}$ is noted $\Delta\theta_{d(sthe)}$. [Lemaitre and Chaboche,1990] also shows that $\Delta\theta_{d(sthe)}$ vanishes when the frequency of cyclic loading $f_L$ tends to 0 and for high frequencies ($\gg 1/(2\pi\tau_s)$) this quantity becomes independent of $f_L$(Figure 10).

#### 1.9.4.2 Dissipation source

The span of $\theta_{d(d1)}$, noted $\Delta\theta_{d(d1)}$ is always positive since it is the result of dissipation $d_1$ which must be positive. $d_1$ can derive from the strain rate $\dfrac{d\varepsilon^{ij}}{dt}$ and from the micro structural evolution represented by $\dfrac{d\alpha_s}{dt}$ (see Eq. 1.47). We can then conclude that the amplitude of $\theta_{d(d1)}$ is related to the amplitude of the strain rate. Moreover, in [La Rosa and Risitano,2000], it is shown that $\theta_{d(d1)}$ is proportional to $f_L$ and in [Galtier,1993] a linear expression is given.

Let us consider an example of fatigue test: a unixial test where $\Delta\sigma = 360\,MPa$ at $R = 0$ on a DP60 steel specimen [Boulanger et al.,2004] The evolution of $\Delta\theta_{d(sthe)}$ and $\Delta\theta_{d(d1)}$ through the time is observed for respectively $f_L = 50$, $f_L = 1$, $f_L = 30\,Hz$. Results show that for $f_L = 50\,Hz$, $\Delta\theta_{d(sthe)} \approx 0.3\ °C$ and $\Delta\theta_{d(d1)} = 1.8\ °C$ at the stabilized thermoelastic regime (Figure 10). This shows that the preponderant variation of temperature is related to dissipation (Figure 10). Moreover the same test at $f_L = 1\,Hz$, gives $\Delta\theta_{d(sthe)} \approx 0.3\ °C$ and $\Delta\theta_{d(d1)} \approx 0°C$. The same test at $f_L = 30\,Hz$, gives $\Delta\theta_{d(sthe)} \approx 0.3°C$ and $\Delta\theta_{d(d1)} \approx 1.1\ °C$. These results show the independence of $\theta_{d(sthe)}$ from $f_L$ and the proportionality between $\theta_{d(d1)}$ and $f_L$.

### 1.9.5 Summary of required assumptions for modeling self-heating

Fourier's model for heat conduction is often used to analyze self-heating occurring during fatigue tests in the Newtonian approach (see section 1.9.4). As reviewed in section 1.5, other models of heat conduction can be used in a Newtonian approach. We recall that the steady-state diffusion is described using these models in a continuous media where neither some of the thermomechanical couplings (the terms $s_{the}$ and $s_{thc}$ of Eq. 1.47) nor the heat transfer by radiation are taken into account. Only the resulting thermal dissipation $d_1$ is considered. Moreover, spacetime models of heat conduction can also be used in the study of self-heating: parabolic and hyperbolic heat conduction models derive respectively from first and second order theories of dissipation using a spacetime approach (see section 1.8).

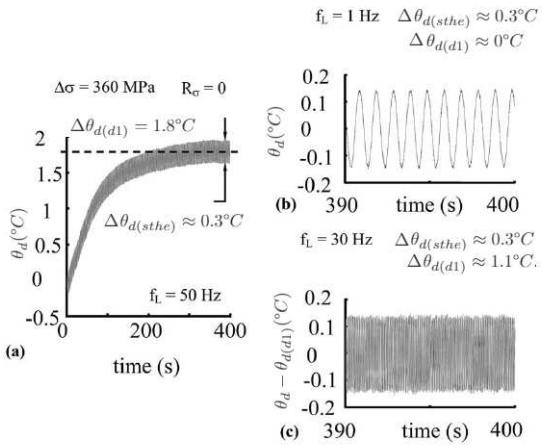


**Fig. 10:** Evolution of temperature of a specimen subjected to fatigue at (a) $f_L = 50\,Hz$, (b) $f_L = 1\,Hz$ at the stabilized regime, (c) $f_L = 30$Hz at the stabilized regime

The evolution of temperature in time during fatigue tests which also involves a spatial evolution of temperature due to heat conduction in the specimen, promotes the use of spacetime models of heat conduction. Besides, the necessity of coupling the mechanical behavior to the thermal behavior in the dissipation term, endorses the spacetime point of view to ensure the frame-indifference of such a coupling.

For all these reasons, we are considering the spacetime Fourier's model built with a spacetime thermodynamic approach. The convenience of solving thermal problems by the use of spacetime computation will be proved in this particular application. The study is based on experimental data resulting from fatigue test. Note that to avoid numerical inconsistencies, the models are defined in a macroscopic spatial domain of order $L$ and a temporal domain of order $t_{macro} = t$ (see section 1.5.7) where Fourier's heat conduction model is adapted.

## 1.10 Conclusions

In this chapter, definitions and notions of continuum thermodynamics are reviewed. First, definitions of classical 3D thermomechanics are given then the spacetime framework is introduced (section 1.2). Comparison of notions between these 2 frameworks is established in section 1.4.

Objectivity of the material is defined in Newtonian thermomechanics. It includes in its meaning the independence of models with respect to change of frames as well as with respect to superposition of rigid body motion. These two can not be distinguished in a 3D space. In spacetime thermomechanics, the notion of covariance used in Einstein's theory takes place. It postulates frame-indifference of laws and models. In such a formalism, spacetime tensors are covariant and covariant derivatives can be defined [Wang,2016].

The first part of this manuscript aims at modeling the thermal conduction behavior. Several Newtonian models in the literature exist [Fourier,1988, Cattaneo,1958, Tavernier,1962, Osborne,1950, Vernotte,1961, Battaglia,2007] (section 1.5). However, it has been identified that all the models do not fulfill all the requirements for an accurate modeling.

Here are the difficulties encountered in Newtonian thermomechanics (section 1.6): some of the models found in literature do not respect the causality principle [Fourier,1988], some are not covariant [Cattaneo,1958, Tavernier,1962, Osborne,1950, Vernotte,1961] (see table 3). Since both of these principles are necessary for a correct heat conduction model, together with taking into account correctly irreversibility for large transformations, a spacetime thermodynamical formalism guaranteeing covariance of models is needed (section 1.7). Its elements will be detailed in the following chapters.

| Properties/Models | Fourier | Cattaneo | Osborne | Vernotte |
|---|---|---|---|---|
| Verifies covariance principle in the 3D sense | Yes | No | No | No |
| Verifies causality principle | No | Yes | Yes | Yes |
| Thermod. compatibility | Yes | NA | NA | NA |

**Tab. 3:** List of the different Newtonian models reviewed in the literature with their properties (NA = not applicable)

Some relativistic models of heat conduction already exist in the literature [Eckart,1940, Carter,1988, Landau and Lifshitz,1975, Israel and Stewart,1979a, Israel and Stewart,1979b](section 1.8). Therefore, relativistic models deriving from CIT do not respect the causality principle [Eckart,1940, Landau and Lifshitz,1975]. Others deriving from EIT respect this principle [Israel and Stewart,1979a, Carter,1988] but the price to pay is to find coefficients of the second order corrections for the entropy sources (see table 4). Moreover the stability conditions in these models are rather artificial. Since existing relativistic models do not systematically meet all the requirements, complementary investigations on spacetime models are required.

| Properties/Models | Eckart | Landau and Lifshitz | Israel and Stewart | Carter |
|---|---|---|---|---|
| Verifies covariance principle | Yes | Yes | Yes | Yes |
| Verifies causality principle | No | No | Yes | Yes |
| Thermod. compatibility | Yes | Yes | Yes | Yes |

**Tab. 4:** List of the different spacetime models reviewed in the literature with their properties

Our aim is to develop a framework that guarantees covariance of heat conduction models, respects the causality principle and at the same time could be derived from classical irreversible thermodynamics. This framework will be built in a spacetime Euclidean domain without gravitation.

This framework will enable us to build spacetime heat conduction models that can be used for engineering applications (see chapter 2). The self-heating is one of the phenomena that can be modeled (section 1.9). It occurs during various processes especially fatigue tests. Newtonian studies of this self-heating are found in [Chrysochoos et al.,2009, Boulanger et al.,2004, Lemaitre and Chaboche,1990, La Rosa and Risitano,2000, Galtier,1993, Poncelet et al.,2011, Munier,2012]. The resulting dissipation enables the study of the fatigue limit. We will model this phenomenon in chapter 3 to prove the possibility of use of the spacetime heat models obtained in chapter 2 to represent materials analysis and characterization techniques and to improve the numerical resolution of such a phenomenon.

# 2 Spacetime modeling of thermal problems

## 2.1 Introduction and description of the problem

As discussed in chapter 1, frame-indifference of thermomechanical models has to be questioned to deal correctly with the behavior of matter undergoing large transformations. As reviewed, existing models show difficulties to verify frame-indifference [Cattaneo,1958] or/and causality principle [Fourier,1988]. Relativistic models verifying these two conditions may be derived from EIT, thus thermodynamically compatible, but this adds challenges to identify the coefficients of variables and laws [Israel and Stewart,1979a, Carter,1988].

In this chapter, we thus aim at obtaining heat conduction models verifying the covariance principle [Eringen,1962, Grot and Eringen,1966a, Rouhaud et al.,2013, Panicaud et al.,2014] and we will then systematically check the causality and the thermodynamics compatibility of the proposed models built from a CIT framework.

To do so, we will develop heat conduction models in a spacetime framework. The spacetime formalism developed in previous articles [Rouhaud et al.,2013, Panicaud et al.,2014, Panicaud et al.,2015, Wang,2016] is first briefly introduced. Then, we apply this framework to thermodynamics and derive a covariant form of the Clausius-Duhem inequality from the first and second principles of thermodynamics.

Two heat conduction models are proposed in this spacetime formalism. Models can be directly deduced from the thermodynamical approach or from inducing methods. A new method is especially proposed for the generalization of Cattaneo's model in the spacetime domain by use of a complexification method. Different expressions of the heat equation under their variational forms in the spacetime formalism are then presented, without mechanical couplings, in view of numerical investigations. Numerical simulations are then performed in order to emphasize the advantages and the drawbacks of Newtonian and spacetime formalisms. In the first formalism, time is discretized, while in the second it is a variable in the spacetime domain. These comparisons will be performed through an example. At the end of the chapter, the spacetime model obtained will be used in an engineering application: the study of heat diffusion through a cooling fin.

## 2.2 Spacetime formalism

The description of physical systems in this manuscript is built in a spacetime formalism, for which gravitation is not taken into account. The considered spacetime is (pseudo-) Euclidean and we define a metric tensor $\boldsymbol{g}$.

Throughout the manuscript, quantities that vary like the base vectors are called covariant e.g. $\mathbf{X}_\mu$ and those that vary like the dual base vectors are called contravariant e.g. $\mathbf{X}^\mu$ [Schouten,1954]. The upper indices denote contravariant quantities, while lower indices denote covariant quantities. We note that in Euclidean space (section 1.2), covariant and contravariant quantities are equivalent [Stover and Eric,2020].

### 2.2.1 Motion and frames

Consider a material body in space and time described by the spacetime continuum of hypervolume $\mathcal{D}$ with frontier $\partial\mathcal{D}$. The motion of the body is described by the specification of events $x^\mu$ corresponding to the coordinates of the material particles of the body within a four-dimensional spacetime manifold [Bressan,1963]. The motion of these particles corresponds to a set of worldlines that spans a linked open domain of the spacetime manifold. The quantities introduced in this work are defined for all $x^\mu$ in $\mathcal{D}$. The transformation from one coordinate system $x^\mu$ to another $\widetilde{x^\mu}$ is given by:

$$d\widetilde{x^\mu} = \frac{\partial \widetilde{x^\mu}}{\partial x^\nu} dx^\nu \tag{2.1}$$

As previously introduced in section 1.3, a frame is defined as a set of four base vectors of this spacetime. Therefore, a choice of a spacetime coordinate system defines a frame and spacetime coordinate

transformations describe changes of frames [Landau and Lifshitz,1975]. A specific coordinate system is associated to inertial frames, for which the covariant components of the metric tensor are:

$$g_{\mu\nu} = \eta_{\mu\nu} = \begin{pmatrix} -1 & 0 & 0 & 0 \\ 0 & -1 & 0 & 0 \\ 0 & 0 & -1 & 0 \\ 0 & 0 & 0 & +1 \end{pmatrix} \tag{2.2}$$

A proper frame is also defined, as a frame comoving with a material particle of the body (see section 1.3.3). It generalizes the notion of standard (imbedded) material coordinates and can be defined for any particle of the body. In this case, the fourth coordinate $x^4$ corresponds to the proper time of the material particle multiplied by a reference velocity, hence having a dimension that is homogeneous with a spatial length. We choose here this reference as the velocity of light $c$. The Minkowski tensor of components $\eta_{\mu\nu}$ is written in a form that does not depend on $c$ value. In this work, a hat is written above all quantities expressed for the specific proper frame, the coordinate system associated to this frame is thus $\hat{x}^\mu$. A particular case of proper and inertial frame are also considered. It corresponds to material particles that have a constant linear speed and does not have any acceleration. In this case, the hat above the quantity is not necessary.

An infinitesimal interval $ds$ between 2 close events is further defined as a generalized element of length:

$$ds^2 = g_{\mu\nu}(x^\kappa) dx^\mu dx^\nu \tag{2.3}$$

where $g_{\mu\nu}$ are the covariant components of the metric tensor in the coordinate system $x^\kappa$. The interval is invariant with respect to coordinate transformations.

### 2.2.2 Four-vector velocity

Using the definition of the interval above (Eq. 2.3), the four-vector velocity is defined as:

$$u^\mu = \frac{dx^\mu}{ds} \tag{2.4}$$

Note that it is a dimensionless quantity for all its components and that its norm is equal to one due to the definition of the interval $ds$. Depending on the choice of the frame, the velocity takes specific values:

- For an inertial frame, we deduce from Eqs. 2.2 and 2.3:

$$ds^2 = (cdt)^2 \left(1 - \frac{v^2}{c^2}\right) = (cdt/\gamma)^2 \tag{2.5}$$

  where $\gamma$ is the Lorentz factor and $v = ||v|| = \sqrt{v^i v_i}$ is the velocity norm as calculated in the Newtonian approach. The four-vector velocity is then given by:

$$u^\mu = \frac{\gamma}{c} v^\mu = \left(\frac{\gamma}{c}\frac{dx^i}{dt}, \gamma\right). \tag{2.6}$$

- For a proper frame (comoving with a material particle)(section 1.3.3), the four-vector velocity takes the particular value:

$$\hat{u}^\mu = (0, 0, 0, 1). \tag{2.7}$$

  Eq. 2.7 corresponds to a normalized speed and is independent of the $c$ value.

### 2.2.3 Tensor densities

In section 1.4.3 four-tensors densities are introduced. In the coordinate transformation below, the weight of tensor density $W$ has been introduced [Schouten,1954]. Typically the weight of Cauchy's stress tensor, is

equal to one ($W = 1$), while the weight of a deformation or strain tensor or temperature is equal to zero ($W = 0$) [Oldroyd,1950, Schouten,1954].

Through coordinate transformations from $x^\mu$ to $\widetilde{x^\mu}$, the scalar density $\mathcal{S}$, the components of a first-rank tensor density $\boldsymbol{\mathcal{V}}$ and the components of a second-rank tensor density $\boldsymbol{\mathcal{T}}$ verify the relations:

$$\widetilde{\mathcal{S}} = \left|\frac{\partial x^\alpha}{\partial \widetilde{x}^\beta}\right|^W \mathcal{S} \tag{2.8a}$$

$$\widetilde{\mathcal{V}}^\mu = \left|\frac{\partial x^\alpha}{\partial \widetilde{x}^\beta}\right|^W \frac{\partial \widetilde{x}^\mu}{\partial x^\nu}\mathcal{V}^\nu \tag{2.8b}$$

$$\widetilde{\mathcal{V}}_\mu = \left|\frac{\partial x^\alpha}{\partial \widetilde{x}^\beta}\right|^W \frac{\partial x^\nu}{\partial \widetilde{x}^\mu}\mathcal{V}_\nu \tag{2.8c}$$

$$\widetilde{\mathcal{T}}^{\mu\nu} = \left|\frac{\partial x^\alpha}{\partial \widetilde{x}^\beta}\right|^W \frac{\partial \widetilde{x}^\mu}{\partial x^\lambda}\frac{\partial \widetilde{x}^\nu}{\partial x^\kappa}\mathcal{T}^{\lambda\kappa} \tag{2.8d}$$

$$\widetilde{\mathcal{T}}_{\mu\nu} = \left|\frac{\partial x^\alpha}{\partial \widetilde{x}^\beta}\right|^W \frac{\partial x^\lambda}{\partial \widetilde{x}^\mu}\frac{\partial x^\kappa}{\partial \widetilde{x}^\nu}\mathcal{T}_{\lambda\kappa} \tag{2.8e}$$

where $\left|\frac{\partial \widetilde{x}^\mu}{\partial x^\nu}\right|$ is the determinant of the Jacobian matrix $\frac{\partial \widetilde{x}^\mu}{\partial x^\nu}$.

**Example** The weight of a mass density is equal to one. A coordinate transformations from $x^\mu$ to $\widetilde{x^\mu}$ of the mass density can be expressed by:

$$\widetilde{\rho} = \left|\frac{\partial x^\alpha}{\partial \widetilde{x}^\beta}\right|^W \rho = J\rho \tag{2.9}$$

where $J = \left|\frac{\partial x^\alpha}{\partial \widetilde{x}^\beta}\right|$ is the mass density ratio.

### 2.2.4 Projection operators

In order to construct the models, we wish to be able to separate temporal and spatial contributions of the four-dimensional tensors. Note that the spatial contribution does not necessarily correspond to the components that are associated to the first three coordinates: it depends on the chosen frame. For example, for an inertial frame, the direct projection is comparable to the Newtonian case. However, for other frames, the comparison may be not so simple. Therefore, if we require to clearly separate the different components of a spacetime tensor on the different directions of spacetime, either space or time or both, then we have to introduce projectors.

The time projection operator (or time projector) is simply $\boldsymbol{u}$ because the four-velocity by construction points toward the direction of the proper time (see Eq. 2.7). The spatial projection operator (or spatial projector) projects on the space that is perpendicular to the four-velocity and is defined as:

$$\Pi^{\mu\nu} = g^{\mu\nu} - u^\mu u^\nu \tag{2.10}$$

Projected variables using $\Pi^{\mu\nu}$ are denoted using a bar under variables ($\underline{.}$) e.g. $\underline{e}^{\mu\nu} = e^{\alpha\beta}(\delta^\mu{}_\alpha - u^\mu u_\alpha)(\delta^\nu{}_\beta - u^\nu u_\beta)$ is the projected spacetime elastic strain tensor.

### 2.2.5 Shift of a tensor

The contravariant components of a tensor can be changed to its covariant components and vice versa by use of the shift operation with the metric tensor. For a second-rank tensor, it can be done using the relations:

$$\mathcal{T}_{\mu\nu} = g_{\mu\alpha}g_{\nu\beta}\mathcal{T}^{\alpha\beta} \tag{2.11}$$

$$\mathcal{T}^{\mu\nu} = g^{\mu\alpha} g^{\nu\beta} \mathcal{T}_{\alpha\beta} \tag{2.12}$$

Moreover, mixed tensor densities can be shifted. For a second-rank tensor it can be done using the relation:

$$\mathcal{T}^{\mu}_{\nu} = g^{\mu\alpha} g_{\nu\beta} \mathcal{T}^{\beta}_{\alpha} \tag{2.13}$$

The same operations can be carried out for tensors densities of different orders. The contravariant components of a first-rank tensor (e.g. velocity) can be changed to its covariant components and vice versa, using the relations:

$$\mathcal{V}_{\mu} = g_{\mu\nu} \mathcal{V}^{\nu} \tag{2.14}$$

$$\mathcal{V}^{\mu} = g^{\mu\nu} \mathcal{V}_{\nu} \tag{2.15}$$

The theory of relativity intrinsically ensures the covariance of models through the use of tensors and spacetime operations. And as the change of coordinate system is equivalent to the change of frame, then the tensors and the spacetime equations are by construction form invariant with respect to change of frame.

### 2.2.6 The Newtonian hypothesis

Among the hypotheses that may be taken into account in this manuscript we note: $\frac{v}{c} << 1 \leftrightarrow \gamma \approx 1$, which corresponds to the hypothesis of Newton. It will be used to express models at the limit of the spacetime framework, which corresponds to the Newtonian framework (see section 5.5.3). Under this approximation, proper time can then be approximated to the absolute time. Moreover, the spacetime velocity is noted $v^{\mu}$ and expressed by:

$$v^{\mu} = \frac{dx^{\mu}}{dt} = \left( \frac{dx^{i}}{dt}, c \right) = (v^{i}, c) \approx c u^{\mu} \tag{2.16}$$

### 2.2.7 Covariant derivative

The use of covariant derivative is essential in the spacetime domain in order to write covariant models [Semay and Silvestre-Brac,2007]. The covariant derivatives of respectively, a scalar density $\mathcal{S}$ denoted $\nabla_{\lambda}\mathcal{S}$, a first-rank tensor density $\boldsymbol{\mathcal{V}}$ denoted $\nabla_{\lambda}\mathcal{V}^{\mu}$ (or $\nabla_{\lambda}\mathcal{V}_{\mu}$) and a second-rank tensor density $\boldsymbol{\mathcal{T}}$ denoted $\nabla_{\lambda}\mathcal{T}^{\mu\nu}$ (or $\nabla_{\lambda}\mathcal{T}_{\mu\nu}$) are given by:

$$\nabla_{\lambda}\mathcal{S} = \frac{\partial \mathcal{S}}{\partial x^{\lambda}} - W \Gamma^{\kappa}_{\kappa\lambda} \mathcal{S} \tag{2.17a}$$

$$\nabla_{\lambda}\mathcal{V}^{\mu} = \frac{\partial \mathcal{V}^{\mu}}{\partial x^{\lambda}} + \Gamma^{\mu}_{\kappa\lambda} \mathcal{V}^{\kappa} - W \Gamma^{\kappa}_{\kappa\lambda} \mathcal{V}^{\mu} \tag{2.17b}$$

$$\nabla_{\lambda}\mathcal{V}_{\mu} = \frac{\partial \mathcal{V}_{\mu}}{\partial x^{\lambda}} - \Gamma^{\kappa}_{\mu\lambda} \mathcal{V}_{\kappa} - W \Gamma^{\kappa}_{\kappa\lambda} \mathcal{V}_{\mu} \tag{2.17c}$$

$$\nabla_{\lambda}\mathcal{T}^{\mu\nu} = \frac{\partial \mathcal{T}^{\mu\nu}}{\partial x^{\lambda}} + \Gamma^{\mu}_{\kappa\lambda} \mathcal{T}^{\kappa\nu} + \Gamma^{\nu}_{\kappa\lambda} \mathcal{T}^{\mu\kappa} - W \Gamma^{\kappa}_{\kappa\lambda} \mathcal{T}^{\mu\nu} \tag{2.17d}$$

$$\nabla_{\lambda}\mathcal{T}_{\mu\nu} = \frac{\partial \mathcal{T}_{\mu\nu}}{\partial x^{\lambda}} - \Gamma^{\kappa}_{\mu\lambda} \mathcal{T}_{\kappa\nu} - \Gamma^{\kappa}_{\nu\lambda} \mathcal{T}^{\kappa\mu} - W \Gamma^{\kappa}_{\kappa\lambda} \mathcal{T}_{\mu\nu} \tag{2.17e}$$

where $\Gamma^{\alpha}_{\beta\gamma}$ are the coefficients of the metric connection identified with Christoffel's symbols [Talpaert,2000, Weinberg,1972] given by:

$$\Gamma^{\mu}_{\kappa\lambda} = \frac{1}{2} g^{\mu\alpha} \left( \frac{\partial g_{\alpha\kappa}}{\partial x^{\lambda}} + \frac{\partial g_{\alpha\lambda}}{\partial x^{\kappa}} - \frac{\partial g_{\kappa\lambda}}{\partial x^{\alpha}} \right) = \Gamma^{\mu}_{\lambda\kappa} \tag{2.18}$$

Note that in this case $\nabla_{\lambda} g^{\mu\nu} = 0$. Also not that for every point of the spacetime domain, for an inertial frame, all Christoffel's symbols vanish.

It is important to stress that, as a consequence of the absence of gravitation, the Riemann curvature tensor of this spacetime domain is equal to zero, although the Christoffel's symbols may not [Landau and Lifshitz,1975, Kobayashi and Nomizu,1996, Schellstede et al.,2014, Charnock,2017]. In other words, the considered spacetime is (pseudo-) Euclidean, thus flat, whether the frame is inertial ($\Rightarrow \Gamma^{\mu}_{\kappa\lambda} = 0$), or not ($\Rightarrow \Gamma^{\mu}_{\kappa\lambda} \neq 0$) [Landau and Lifshitz,1975].

A covariant transport corresponding to the projection of the covariant derivative on the proper time $u^{\lambda}\nabla_{\lambda}(.)$ is also defined. In an inertial coordinate system $z^{\mu}$, in which the Christoffel's symbols vanish, the covariant transport may be rewritten as:

$$u^{\lambda}\nabla_{\lambda}(.) = u^{\lambda}\frac{\partial}{\partial z^{\lambda}}(.) = u^{4}\frac{\partial}{\partial z^{4}}(.) + u^{i}\frac{\partial}{\partial z^{i}}(.) = \frac{d(.)}{ds} \tag{2.19}$$

### 2.2.8 Spacetime thermodynamics

In this section we introduce the elements needed to build models in a spacetime thermodynamical approach.

- Energy-momentum tensor

The energy-momentum tensor field $\boldsymbol{T}$ describes the density flux of energy and momentum in spacetime. It is defined $\forall x^{\mu}$ in the hypervolume $\mathcal{D}$ of the spacetime continuum of the material with frontier $\partial\mathcal{D}$. Remember that, in the present work, electromagnetism and gravitation phenomena are not considered. The energy-momentum tensor is advantageously decomposed into 3 parts [Eckart,1940, Carter,1988, Landau and Lifshitz,1975, Israel and Stewart,1979a], with the use of projectors in the direction of time and the space perpendicular to time (see section 2.2.4):

$$T^{\mu\nu} = T^{\mu\nu}_{\mathcal{U}} + T^{\mu\nu}_{q} + T^{\mu\nu}_{\sigma} \tag{2.20}$$

where

$$T^{\mu\nu}_{\mathcal{U}} = \mathcal{U}u^{\mu}u^{\nu} \text{ with } \mathcal{U} = u_{\alpha}T^{\alpha\beta}u_{\beta} \tag{2.21}$$

$$T^{\mu\nu}_{q} = q^{\mu}u^{\nu} + u^{\mu}q^{\nu} \text{ with } q^{\mu} = \Pi^{\mu}{}_{\alpha}T^{\alpha\beta}u_{\beta} \tag{2.22}$$

$$T^{\mu\nu}_{\sigma} = \Pi^{\mu}{}_{\alpha}T^{\alpha\beta}\Pi^{\nu}{}_{\beta} \tag{2.23}$$

In the particular proper frame where $\hat{u}^{\mu} = (0, 0, 0, 1)$, the components of this tensor are:

$$\hat{T}^{\mu\nu} = \begin{pmatrix} \hat{T}_{\sigma}^{\ 11} & \hat{T}_{\sigma}^{\ 12} & \hat{T}_{\sigma}^{\ 13} & \hat{q}^{1} \\ \hat{T}_{\sigma}^{\ 12} & \hat{T}_{\sigma}^{\ 22} & \hat{T}_{\sigma}^{\ 23} & \hat{q}^{2} \\ \hat{T}_{\sigma}^{\ 13} & \hat{T}_{\sigma}^{\ 23} & \hat{T}_{\sigma}^{\ 33} & \hat{q}^{3} \\ \hat{q}^{1} & \hat{q}^{2} & \hat{q}^{3} & \hat{\mathcal{U}} \end{pmatrix} \tag{2.24}$$

This particular form of the energy-momentum tensor in the proper frame enables an interpretation of its components, which are in this case: the energy density $\hat{\mathcal{U}} = \hat{u}_{\alpha}\hat{T}^{\alpha\beta}\hat{u}_{\beta}$, which equals to $\hat{\tilde{\rho}}_{c}(c^{2} + e_{int})$ because of the Einstein equivalence [Landau and Lifshitz,1975], the heat flux $\hat{q}^{\mu} = \hat{\Pi}^{\mu}{}_{\alpha}\hat{T}^{\alpha\beta}\hat{u}_{\beta}$, and the mechanical stress applied on the studied body $\hat{T}^{\mu\nu}_{\sigma} = \hat{\Pi}^{\mu}{}_{\alpha}\hat{T}^{\alpha\beta}\hat{\Pi}^{\nu}{}_{\beta}$. As a consequence, it is worth noting that $\hat{q}^{4} = 0$. The four projection is necessary but may not be sufficient to obtain covariant heat conduction. The main problem is that $q^{\mu}$ is not a simple spacelike vector, but a tensor component. That is reflected in the related entropy production expression as mentioned in [Ván and Biró,2012], and in the complicated non-relativistic transformation properties, see e.g. [Müller and Ruggeri,1998] in a kinetic theory context or [Ván et al.,2016] in a direct approach.

The definitions of the entities related to the energy-momentum tensor are summed up in Table 11:

| Variable | Physical interpretation in the proper frame | Unit in the international system |
|---|---|---|
| $\mathcal{U}$ | energy density | $kg.m^{-1}.s^{-2}$ |
| $\widetilde{\rho_c}$ | mass density at rest | $kg.m^{-3}$ |
| $e_{int}$ | specific internal energy | $J.kg^{-1}$ |
| $u^\mu$ | velocity four-vector | dimensionless |
| $q^\mu$ | volume heat flux four-vector | $J.m^{-3}$ |
| $T^{\mu\nu}_{\mathcal{U}}$ | energy four-tensor | $kg.m^{-1}.s^{-2}$ |
| $T^{\mu\nu}_{q}$ | heat four-tensor | $kg.m^{-1}.s^{-2}$ |
| $T^{\mu\nu}_{\sigma}$ | stress four-tensor | $Pa = kg.m^{-1}.s^{-2}$ |

**Tab. 5:** The spacetime variables used in the energy-momentum tensor

At this stage of the manuscript, we look to find models of the thermal behavior of materials only. Consequently, no mechanical stress is applied to the model and then the mechanical stress is supposed be null, which is equivalent to: $T^{\mu\nu}_{\sigma} = 0$. This assumption reduces the equation of energy-momentum to:

$$T^{\mu\nu} = \mathcal{U} u^\mu u^\nu + q^\mu u^\nu + u^\mu q^\nu \tag{2.25}$$

- Spacetime equations for thermodynamics of continuous media

The energy-momentum tensor enables to write the spacetime equations of thermodynamics for continuous media. To begin with, the first principle of thermodynamics leads to the conservation of internal energy in spacetime. It comes from the projection of the conservation of energy-momentum tensor ($\forall x^\mu \in \mathcal{D}, \nabla_\nu T^{\mu\nu} = 0$) on the proper time [Grot and Eringen,1966a]:

$$\forall x^\mu \in \mathcal{D}, u_\mu \nabla_\nu T^{\mu\nu} = 0 \tag{2.26}$$

Second, the flux of entropy in the spacetime domain $\mathcal{D}$ can be defined as a four-vector:

$$S^\mu = \widetilde{\rho_c} \eta_c u^\mu + \frac{q^\mu}{\theta} \tag{2.27}$$

where $\eta_c$ can be interpreted as the specific entropy for the proper frame and $\theta$ is the thermodynamics temperature [Landau and Lifshitz,1975]. Then, through the covariant variation of Eq. 2.27, it is possible to express the second principle of thermodynamics as [Eckart,1940, Muschik and Borzeszkowski,2015]:

$$\begin{aligned} &\forall x^\mu \in \mathcal{D}, \nabla_\mu S^\mu \geq 0 \\ &\Rightarrow \nabla_\mu (\widetilde{\rho_c} \eta_c u^\mu) + \nabla_\mu \left( \frac{q^\mu}{\theta} \right) \geq 0 \end{aligned} \tag{2.28}$$

- The four-dimensional form of the Clausius-Duhem inequality

The Clausius-Duhem inequality can be obtained at least by two ways. First, it can be derived by use of Eckart type Gibbs relation, as it can be found in [Eckart,1940, Landau and Lifshitz,1966]. For all points of the spacetime domain, we assume a local thermodynamic identity:

$$\forall x^\mu \in \mathcal{D}, \widetilde{\rho_c} (\theta d\eta_c - de_{int}) = -\widetilde{\rho_c} \frac{\partial e_{int}}{\partial \alpha_i} d\alpha_i \tag{2.29}$$

where $\alpha_i$ represents the state variables of the system other than temperature. A closed system is considered and $\alpha_i$ reduces to a mechanical variable (volume or strain). The second member of Eq. 2.29 has to be calculated along a reversible path. By use of Eq. 2.28, with the rest mass balance $\forall x^\mu \in \mathcal{D}, \nabla_\mu (\widetilde{\rho_c} u^\mu) = 0$, we can easily prove that $\widetilde{\rho_c} \theta d\eta_c \geq -\theta \nabla_\mu \left( \frac{q^\mu}{\theta} \right) ds$. From Eq. 2.26 and

expression of $T^{\mu\nu}$, we can also express the derivative of the specific internal energy $e$. Finally, after calculation, we can obtain the Clausius-Duhem inequality as proposed in Eq. 2.31.
Second, the first and second principles of thermodynamics can be combined to directly obtain the Clausius-Duhem inequality in the spacetime domain:

$$\forall x^\mu \in \mathcal{D}, \theta \nabla_\mu S^\mu - u_\mu \nabla_\nu T^{\mu\nu} \geq 0 \tag{2.30}$$

The terms of this inequality have been defined in the previous sections. It is worth noting that balance law has also to be simultaneously verified, i.e.: $\nabla_\nu T^{\mu\nu} = 0$. In Eq. 2.30, the use of the definitions of energy-momentum tensor (Eq. 2.25) and of entropy vector (Eq. 2.27), with the rest mass balance $\forall x^\mu \in \mathcal{D}, \nabla_\mu(\widetilde{\rho_c} u^\mu) = 0$ leads to the Clausius-Duhem inequality as proposed in Eq. 2.31. However, the inequality of Eq. 2.30 may be problematic in this form. It should be interpreted as a conditional inequality, where the energy-momentum balance is a constraint. Here the presentation is slightly different, as the Lagrange-Farkas multiplier is fixed in advance as an equivalent four-temperature, proportional to the four-velocity. The fact that equivalent temperature is moving with the rest mass is a questionable point, too. It is not obvious that one can choose such a velocity field. There are reasonable arguments that the origin of the instabilities of dissipative relativistic fluids are connected to that term, see in [Ván and Biró,2012]. This second way thus introduces different problems, which means that it may not be the best way for interpretation. Both methods however lead to the same Clausius-Duhem inequality given by Eq. 2.31:

$$\widetilde{\rho_c} \theta u^\mu \nabla_\mu \eta_c - \widetilde{\rho_c} u^\mu \nabla_\mu e_{int} - \frac{1}{\theta} q^\mu \nabla_\mu \theta + q_\nu u^\mu \nabla_\mu u^\nu \geq 0 \tag{2.31}$$

In this inequality, terms are related, respectively, to the evolution of entropy, the evolution of internal energy and the thermal dissipations (one is coupled to mechanics with the term $u^\mu \nabla_\mu u^\nu$).
The proposed equation shows an additional term compared to the classical form of the Clausius-Duhem inequality [Jou et al.,1988, Liu et al.,2017]. It is the acceleration, $a^\nu = u^\mu \nabla_\mu u^\nu$ (that takes the value $u^\mu \partial_\mu u^\nu = \dfrac{du^\nu}{ds}$ for an inertial frame), coupled to the heat flux and temperature. A similar term has already been proposed by Eckart [Eckart,1940], but with a non-covariant form. It is worth noting that this acceleration term is a relativistic one, depending on $c^{-2}$, which vanishes at the non-relativistic limit.

## 2.3 Spacetime Fourier's model of heat conduction

The goal of this section is to propose generalized Fourier's models written to suit the spacetime formalism, with 2 different methods.

### 2.3.1 General hypotheses

We remind that we place ourselves in a spacetime description in the context of general relativity in the sense of kinematics : gravitation is not taken into account, the metric is Euclidean and has null curvature (see table 2). The model which is built in a continuous media, is purely thermal. Indeed, thermomechanical couplings are not taken into account. Heat transfer by radiation are not taken into account.

All the material coefficients (especially the thermal conductivity) are assumed to be independent of time and temperature ($\forall x^\mu$). Moreover, the description is performed at the macroscopic scale and the thermal problem is supposed to be isotropic at this scale.

### 2.3.2 Method 1: Direct relativization of Fourier's model of heat conduction

One method to obtain a spacetime Fourier's model of heat conduction is to induce its generalization from the Newtonian Fourier's model of heat conduction.

- We start from Newtonian Fourier's model expressed for any frame by:

$$q^j = -\frac{\lambda}{c} I^{ji} \nabla_i \theta \tag{2.32}$$

  where $\lambda$ is the thermal conductivity of the considered material and $\boldsymbol{I}$ is the 3D metric of signature $(+1,+1,+1)$.
- We extend to spacetime by increasing the dimension of the heat vector. For the proper frame, we remind that $\hat{q}^4 = 0$ according to Eq. 2.24. Consequently, we have to use the spatial projector to link the heat vector to the temperature gradient. We induce the covariant expression for any frame of the heat flux:

$$q^\mu \quad = \quad \frac{\lambda}{c} \Pi^{\mu\nu} \nabla_\nu \theta = \frac{\lambda}{c} (g^{\mu\nu} - u^\mu u^\nu) \nabla_\nu \theta \tag{2.33}$$

  The positive sign before the second member of Eq. 2.33 is due to the signature of the 4D metric $(-1,-1,-1,+1)$.

Eq. 2.33 reduces to Eq. 2.32 (with hat on quantities) as expected, when expressed in the proper frame. The compatibility of Eq. 2.33 with the Clausius-Duhem inequality limited to the thermal dissipation (Eq. 2.35) is ensured at the non-relativistic limit or if the motion speed is strictly constant (to neglect the acceleration term), provided that $-\lambda\Pi^{\mu\nu}$ is a positive-definite matrix [Bressan,1978].

Moreover, for the proper frame, the spacetime model, for which the spatial components correspond to the Newtonian ones, violates similarly the causality principle when used in the internal energy balance (Eq. 2.34)(see sections 1.5.4 and 1.6.2).

### 2.3.3 Method 2: Spacetime thermodynamical approach

In this second method, we use the thermodynamic approach to obtain spacetime heat conduction models. This ensures thermodynamic compatibility for any motion. We start directly from the four-dimensional form of the Clausius-Duhem inequality limited to the thermal dissipation (Eq. 2.35).

By introducing the specific free energy defined by: $\Psi = e_{int} - \theta\eta_c$, the previous inequality is equivalent to:

$$-\widetilde{\rho_c}(u^\mu \nabla_\mu \Psi + \eta_c u^\mu \nabla_\mu \theta) \quad - \quad q^\mu \left( \frac{1}{\theta} \nabla_\mu \theta - u^\nu \nabla_\nu u_\mu \right) \geq 0 \tag{2.34}$$

Because of Eq. 2.29 for a closed system and without thermomechanical couplings, the first and second terms of Eq. 2.34 correspond to mechanical dissipations [Landau and Lifshitz,1966]. In the rest of this manuscript, we will only deal with the third term of Eq. 2.34, corresponding to "thermal" dissipations, theoretically coupled with acceleration:

$$\forall \theta, \Phi = -\frac{q^\mu}{\theta} \left( \nabla_\mu \theta - \theta u^\nu \nabla_\nu u_\mu \right) \geq 0 \tag{2.35}$$

As in method 1, we have to use the spatial projector to link the heat vector to the temperature gradient. Assuming $\theta$ positive, we propose the following expression of $q^\mu$, which verifies Eq. 2.35 for any motion, provided that $-\lambda\Pi^{\mu\nu}$ is a positive-definite matrix [Bressan,1978]:

$$q^\mu = \frac{\lambda}{c} (g^{\mu\nu} - u^\mu u^\nu)(\nabla_\nu \theta - \theta u^\kappa \nabla_\kappa u_\nu) \tag{2.36}$$

A similar additional term, linked to an acceleration effect, has already been proposed by Eckart [Eckart,1940], but with a non-covariant form (see section 1.8.1, Eq. 1.41).

For the proper frame, the spacetime model, for which the spatial components correspond to the Newtonian ones, violates similarly the causality principle when used in the internal energy balance (Eq. 2.26).

## 2.4 Spacetime Cattaneo's model of heat conduction

The goal of this section is to propose Cattaneo's model written to suit the spacetime formalism, with 2 different methods.

### 2.4.1 Method 3: Direct relativization of Cattaneo's model of heat conduction

A method to obtain a spacetime Cattaneo model of heat conduction is to induce its generalization from the Newtonian Cattaneo model of heat conduction.

- We assume a priori a Newtonian Cattaneo's type model expressed for any frame as in Eq. 2.37:

$$q^j - \tau \frac{\partial q^j}{\partial t} = -\frac{\lambda}{c} I^{ji} \left( \nabla_i \theta - \tau_1 \frac{\partial \nabla_i \theta}{\partial t} \right) \tag{2.37}$$

  where $\lambda$ is the thermal conductivity of the considered material and $\tau$ and $\tau_1$ are relaxation time constants of the material. The sign of the coefficients must be positive. That would be a natural consequence in a thermodynamic theory.
- To deal with covariant derivative valid for any frame, we use spacetime derivative; this treatment is different from the one proposed by Christov [Christov,2009]:

$$q^j - \tau c u^\nu \nabla_\nu q^j = -\frac{\lambda}{c} I^{ji} \left( \nabla_i \theta - \tau_1 c u^\kappa \nabla_\kappa (\nabla_i \theta) \right) \tag{2.38}$$

  This equation is still a Newtonian one in the sense defined in section 1.2.2.
- We then extend to spacetime by increasing the dimension of the heat vector. For the proper frame, we require that $\hat{q}^4 = 0$. Consequently, we have to use the spatial projector to relate the heat vector to the temperature gradient. We induce the covariant expression for any frame of the heat flux, which reduces to the expected expression for the proper frame (Eq. 2.38 with hat on the quantities):

$$q^\mu - \tau c u^\nu \nabla_\nu q^\mu = \frac{\lambda}{c} (g^{\mu\nu} - u^\mu u^\nu) \left( \nabla_\nu \theta - \tau_1 c u^\kappa \nabla_\kappa (\nabla_\nu \theta) \right) \tag{2.39}$$

  The positive sign before the second member of Eq. 2.39 is due to the signature of the 4D metric $(-1, -1, -1, +1)$.

By use of the Clausius-Duhem inequality limited to thermal dissipation (Eq. 2.35), we cannot directly verify whether this equation is thermodynamically compatible and thus physically plausible. The reason is further detailed (see section 2.4.2). However, this model verifies the causality principle.

All these equations reduce to their corresponding Fourier's versions when the relaxation time constants are equal to zero, i.e. $\tau_1 = \tau = 0$.

### 2.4.2 Method 4: Complexification of the spacetime Fourier's model of heat conduction from CIT

As illustrated in the previous section (see method 2), we can derive a model of heat conduction from the four-dimensional form of the Clausius-Duhem inequality limited to the thermal dissipation (Eq. 2.35). However, it is not possible to induce a solution that corresponds to a spacetime Cattaneo model. Indeed, we choose to limit the proposed methods to linear classical irreversible thermodynamics (CIT). As mentioned in the introduction, it corresponds to the first order of expansion of thermodynamic theories. To obtain

a model of Cattaneo's type could require to derive an extended irreversible thermodynamical approach (EIT) [Jou et al.,1988, López-Monsalvo,2011, Muller,2008]. The linear classical irreversible thermodynamics [Prigogine,1980] in the relativistic framework succeeds in describing motion for any frame (Eckart, Landau and Lifshitz), but cannot ensure the validity of the principle of causality of dissipative models. Many authors such as Israel and Stewart [Israel and Stewart,1979a], Carter [Carter,1988] have thus used the EIT approach. The theories of EIT consider that it is necessary to keep the second order terms of the thermodynamic equations. Then in these theories, the flux of entropy includes all the possible combinations of dissipative effects, as proposed in [Israel and Stewart,1979a]. It has been developed for thermomechanical aspects, and can then be applied for pure thermal effects. As mentioned in chapter 1, such approaches present also difficulties especially concerning stability.

Therefore, we are proposing an alternative way to obtain a spacetime model of Cattaneo's type. To achieve such a goal, we propose here to introduce relaxation time constants from complexification of dissipative relations (step 3 of the procedure below). The procedure is such that:

- We require at least to ensure the covariance for consistency. Galilean frames are highly special cases of the time-dependent Euclidean frames allowed by objectivity. Therefore, we start from the spacetime dissipative relation written for an inertial frame (Eq. 2.36). This can be obtained from the Clausius-Duhem inequality in a CIT framework.
  *Hyp1:* we assume that the projectors do not vary with time (in other word that the velocity is constant with time). Without loss of generality, we also further consider that $\frac{s}{c} \geq 0$, where $s$ is a spacetime variable.

$$q^\mu(s) \quad = \quad \frac{\lambda}{c}(\eta^{\mu\nu} - u^\mu u^\nu)(\partial_\nu \theta)(s) \tag{2.40}$$

- We apply the Laplace transform to this relation. The Laplace transform ($LT$) relates each function $f^\mu(s) \in \mathbb{R}^4$ to its associate in the complex numbers space $\mathcal{F}^\mu(p_L) \in \mathbb{C}^4$:

$$LT\left(f^\mu(s)\right) = \mathcal{F}^\mu(p_L) = \frac{1}{c}\int_{0^-}^{\infty} f^\mu(s) e^{-\frac{p_L s}{c}} ds \tag{2.41}$$

  This definition can easily be extended if the function depends on other variables. Now all the terms, in addition to the heat flux and temperature gradient, depend on the Laplace variable $p_L$.

$$\mathcal{Q}^\mu(p_L) = \frac{\lambda}{c}(\eta^{\mu\nu} - u^\mu u^\nu)(\mathcal{D}_\nu \Theta)(p_L) \tag{2.42}$$

  where $\mathcal{Q}^\mu(p_L) = LT(q^\mu(s))$ and $(\mathcal{D}_\nu\Theta)(p_L) = LT((\partial_\nu\theta)(s))$.
- To reach spacetime Cattaneo's model, it is now required to add an assumption.
  *Hyp2:* we assume that the conductivity can depend on the Laplace variable $p_L$, so we replace $\lambda$ by $\Lambda(p_L)$:

$$\mathcal{Q}^\mu(p_L) = \frac{\Lambda(p_L)}{c}(\eta^{\mu\nu} - u^\mu u^\nu)(\mathcal{D}_\nu \Theta)(p_L) \tag{2.43}$$

  It is worth noting that the dissipative relation is still linear in the Laplace space, even for $\Lambda(p_L) \in \mathbb{C}$.
- We now have to explicit the transfer function for conductivity as function of the Laplace variable $p_L$. We require that Cattaneo's model converges toward Fourier's model, for infinite times i.e. when $p_L \to 0$. It means that we must impose that:

$$\lim_{p_L \to 0} \Lambda(p_L) = \lambda \tag{2.44}$$

  The transfer function has thus to represent a low-pass filter, introducing two relaxation time constants $\tau$ et $\tau_1$;
  *Hyp3:* and we assume the simplest rational function:

$$\Lambda(p_L) = \lambda \frac{1 - \tau_1 p_L}{1 - \tau p_L} \tag{2.45}$$

- We apply the inverse Laplace transform ($LT^{-1}$) to the dissipative relation, with null initial boundaries:

$$\begin{aligned}
& LT^{-1}\left(\mathcal{Q}^{\mu}(p_L) = \frac{\Lambda(p_L)}{c}(\eta^{\mu\nu} - u^{\mu}u^{\nu})(\mathcal{D}_{\nu}\Theta)(p_L)\right) \\
\Leftrightarrow \quad & LT^{-1}\left(\mathcal{Q}^{\mu}(p_L) = \frac{\lambda}{c}\frac{1-\tau_1 p_L}{1-\tau p_L}(\eta^{\mu\nu} - u^{\mu}u^{\nu})(\mathcal{D}_{\nu}\Theta)(p_L)\right) \\
\Leftrightarrow \quad & LT^{-1}\left((1-\tau p_L)\mathcal{Q}^{\mu}(p_L)\right) = \frac{\lambda}{c}(\eta^{\mu\nu} - u^{\mu}u^{\nu})LT^{-1}\left((1-\tau_1 p_L)(\mathcal{D}_{\nu}\Theta)(p_L)\right) \\
\Leftrightarrow \quad & \left(1-\tau c\frac{d}{ds}\right)q^{\mu} = \frac{\lambda}{c}(\eta^{\mu\nu} - u^{\mu}u^{\nu})\left(1-\tau_1 c\frac{d}{ds}\right)\partial_{\nu}\theta
\end{aligned} \tag{2.46}$$

- We generalize the expression to any frame by replacing the "time" derivative and the gradients with a covariant spacetime form. It leads to:

$$q^{\mu} - \tau c u^{\nu}\nabla_{\nu}q^{\mu} = \frac{\lambda}{c}(g^{\mu\nu} - u^{\mu}u^{\nu})\left(\nabla_{\nu}\theta - \tau_1 c u^{\kappa}\nabla_{\kappa}(\nabla_{\nu}\theta)\right) \tag{2.47}$$

This equation is exactly the one obtained with method 3 (section 2.4.1) and it verifies the covariance principle. In addition to that, it has been obtained from a model built without using the EIT framework. More general models could be obtained from this method, by considering more complicated expressions instead of Eq. 2.45 in step 4 and introducing new time relaxation constants.

Laplace transform is used as a way to build a relativized version of a Cattaneo type equation (and not as a proof for generalisation relevance). Concerning the second relaxation time, method 3 aims at introducing it a priori, whereas method 4 aims at introducing it by use of the rational function (Eq. 2.45) that describes the conductivity behavior function of angular frequency that can be justified from experimental results.

We cannot verify whether this equation (Eq. 2.47) is thermodynamically compatible, with the Clausius-Duhem inequality limited to thermal dissipation (Eq. 2.35), as for method 3. The reason is that we should develop an EIT method. Similarly to method 3, it is possible to verify a posteriori that our propositions are eventually thermodynamically compatible with EIT by comparison with bibliography [Israel and Stewart,1979a, Carter,1988]. Moreover, it verifies the causality principle.

## 2.5 Resume on methods 1,2,3 and 4

It is worth noting that methods 3 (section 2.4.1) and 4 (section 2.4.2) lead to the same expression for spacetime Cattaneo's model (Eq. 2.39 compared to Eq. 2.47) for the choice of $\Lambda(p)$ given by Eq. 2.45, as well as methods 1 (section 2.3.2) and 2 (section 2.3.3) lead to the same expressions for spacetime Fourier's model (Eq. 2.33 compared to Eq. 2.36) if and only if acceleration term is neglected. In table 6, we have summarized the properties of the different heat conduction methods proposed in this work.

| **Methods**<br>**Properties/Models** | **1**<br>**Fourier** | **2**<br>**Fourier** | **3**<br>**Cattaneo** | **4**<br>**Cattaneo** |
|---|---|---|---|---|
| Eq. | 2.33 | 2.36 | 2.39 | 2.47 |
| Verifies covariance principle | Yes | Yes | Yes | Yes |
| Verifies causality principle | No | No | Yes | Yes |
| Order of expansion of the thermodynamics starting point | NA | Linear | NA | Linear |
| Coupling to acceleration | No | Yes | No | No |
| Thermod. compatibility with Eq. 2.35 | $\approx$ Yes (a post.) | Yes (a priori) | No (a post.) | No (a post.) |
| Thermod. compatibility with EIT | NA | NA | Yes | Yes |

**Tab. 6:** List of the different methods with their properties (NA = not applicable; a post. = a posteriori)

## 2.6 Spacetime weak integral forms for thermal problems

### 2.6.1 Introduction

We now solve heat conduction problems using the proposed spacetime models with a finite element method [Debard,2011]. In many domains of the physics, it is possible with the energy expression of the system to formulate the problem as a variational principle, from which we can derive an integral form [Oudin,2008]. The advantage is that we do not have to formulate the partial differential equations (local form of the problem) and express the related boundary conditions to obtain the integral forms (strong or weak integral forms). Moreover, it is useful to build weak integral forms, under a set of assumptions that lead to an existing unique solution due to the Lax-Milgram theorem [Clément and Martin,2016]. The assumptions can be resumed by:

- The weak integral forms are built in a Hilbert space $\mathcal{H}$ characterized by its scalar product and the norm denoted $||\,.\,||$ [Colmez,2009]
- The left hand-side denoted $a(.,.)$ is a bilinear functional verified to be continuous on $\mathcal{H}\times\mathcal{H}$ ($\exists c > 0, \forall (u,v)\in\mathcal{H}^2, |a(u,v)| \leq c||u||\,||v||$ and coercive on $\mathcal{H}$ ($\exists\alpha>0, \forall u\in\mathcal{H}, a(u,v)\geq\alpha||u||^2$).
- The right hand-side denoted $L(.)$ is a continuous linear form on $\mathcal{H}$

In the following, we are describing the different steps leading to the expressions of the heat conduction problem under its weak integral form with boundary conditions, in order to implement it in a programming environment (FEniCS project presented in section 2.7.1). We consider a spacetime numerical scheme of finite elements based directly on the previous spacetime physical models.

### 2.6.2 Specific assumptions for numerical resolution

### 2.6.3 Spacetime weak integral form with spacetime Fourier's model of heat conduction

Building the spacetime weak integral form derives first from injecting the spacetime Fourier's model of heat conduction in the local equation of balance for internal energy (Eq. 2.26), which can be written in the case of an inertial and proper frame as:

$$\widetilde{\rho_c}\frac{\partial e_{int}}{\partial t} + c\frac{\partial q^\mu}{\partial x^\mu} - f = 0 \tag{2.48}$$

where $f$ is an additional term representing the possible volume heat source. We assume here a linear relation between the specific energy $e_{int}$ and temperature $\theta$, with the proportional coefficient $\mathcal{C}_{m\omega}$ ($J.kg^{-1}.K^{-1}$) defined as the specific heat capacity at constant 3D volume. We also introduce the thermal diffusivity of the material as expressed by: $a = \dfrac{\lambda}{\widetilde{\rho_c}\mathcal{C}_{m\omega}}$; and the normalized volume heat source: $f_r = \dfrac{f}{\widetilde{\rho_c}\mathcal{C}_{m\omega}}$. It leads to:

$$\frac{\partial\theta}{\partial t} + \frac{ac}{\lambda}\frac{\partial q^\mu}{\partial x^\mu} - f_r = 0 \tag{2.49}$$

Eq. 2.49 represents the local equation of heat. Then, the weak integral form is obtained by multiplying this expression by an arbitrary temperature $\theta^*$, considered as a test function or virtual temperature field, and then integrating it on the spacetime hypervolume $\mathrm{d}H_\Omega$. For spacetime Fourier's model, Eq. 2.33 is used. By replacing the equation for heat flux in Eq. 2.49 by its expression in Eq. 2.33, the strong integral form of the problem is then obtained:

$$W(\theta,\theta^*) = \int_\Omega \theta^*\left(\frac{\partial\theta}{\partial t} + a\eta^{\mu\nu}\frac{\partial}{\partial x^\nu}\left(\frac{\partial}{\partial x^\mu}\theta\right) - a\frac{\partial}{\partial x^\mu}\left(u^\mu u^\nu\frac{\partial}{\partial x^\nu}\theta\right) - f_r\right)\mathrm{d}H_\Omega = 0, \forall\theta^* \tag{2.50}$$

It can also be written as:

$$W(\theta,\theta^*) = \int_\Omega \theta^* \frac{\partial\theta}{\partial t}\,\mathrm{d}H_\Omega - \int_\Omega a\eta^{\mu\nu}\frac{\partial\theta^*}{\partial x^\nu}\frac{\partial\theta}{\partial x^\mu}\,\mathrm{d}H_\Omega + \int_\Omega a\eta^{\mu\nu}\frac{\partial}{\partial x^\nu}\left(\theta^*\frac{\partial\theta}{\partial x^\mu}\right)\mathrm{d}H_\Omega + \int_\Omega a\frac{\partial\theta^*}{\partial x^\mu}u^\mu u^\nu\frac{\partial\theta}{\partial x^\nu}\,\mathrm{d}H_\Omega - \int_\Omega a\frac{\partial}{\partial x^\mu}\left(\theta^* u^\mu u^\nu\frac{\partial\theta}{\partial x^\nu}\right)\mathrm{d}H_\Omega - \int_\Omega \theta^* f_r\,\mathrm{d}H_\Omega = 0, \forall\theta^* \quad (2.51)$$

where $\Omega$ is the spacetime domain of integration, $\mathrm{d}H_\Omega = \mathrm{d}V_\omega \mathrm{d}t$ is the corresponding spacetime hypervolume of integration, $\mathrm{d}V_\omega$ is the 3D volume of integration.

#### 2.6.3.1 Dirichlet boundary conditions

In the particular case of Dirichlet boundary conditions, the third and the fifth integrals in Eq. 2.51 can be written as integrals over hypersurfaces using Green-Ostrogradski theorem. The test temperature $\theta^*$ is supposed to be null at the boundaries $\partial\Omega$. The problem is then formulated by:

$$W(\theta,\theta^*) = \int_\Omega \theta^*\frac{\partial\theta}{\partial t}\,\mathrm{d}H_\Omega + \int_\Omega aI^{ij}\frac{\partial\theta^*}{\partial x^i}\frac{\partial\theta}{\partial x^j}\,\mathrm{d}H_\Omega - \int_\Omega \theta^* f_r\,\mathrm{d}H_\Omega = 0, \forall\theta^* \quad (2.52)$$

Except for the integration domain, the terms in Eq. 2.52 are similar to their 3D equivalent [Debard,2011]. This is because we have expressed the model in the proper and inertial frame. It would exhibit differences if it was expressed for another frame and/or with thermomechanical couplings.

In order to place boundary conditions, we define: $\partial\Omega^j = \partial\omega \cup t$ as the space boundaries of the domain (where $\partial\omega = \partial x^j$) and $\partial\Omega^4 = \omega \cup \partial t$ as the time boundaries of the domain, where $\omega$ is the 3D spatial domain of integration.

Then, the boundary conditions of this weak integral form can be divided into boundary conditions on the space and on the time. The first type can be written: $\theta(x^\mu \in \partial\Omega^j) = f_{SC}(x^\mu \in \partial\Omega^j)$, where $f_{SC}$ is the function representing the space boundary conditions. The second type can be written: $\theta(x^\mu \in \partial\Omega^4) = f_{TC}(x^\mu \in \partial\Omega^4)$, where $f_{TC}$ is the function representing the initial time boundary conditions. The only condition required (on the temperature) on the time boundaries is at the initial time since the temperature at the final time has to be calculated as per the definition of a heat conduction problem. This aspect is detailed in section 2.6.5.

#### 2.6.3.2 Neumann-Dirichlet boundary conditions

In the particular case of Neumann-Dirichlet boundary conditions, the problem is formulated by:

$$\begin{aligned} W(\theta,\theta^*) &= \int_\Omega \theta^*\frac{\partial\theta}{\partial t}\,\mathrm{d}H_\Omega + \int_\Omega aI^{ij}\frac{\partial\theta^*}{\partial x^i}\frac{\partial\theta}{\partial x^j}\,\mathrm{d}H_\Omega - \int_\Omega \theta^* f_r\,\mathrm{d}H_\Omega \\ &- \int_{\partial\Omega_q} \theta^*\frac{c}{\widetilde{\rho_c}\mathcal{C}_{m\omega}}\frac{q^j_{ext}}{}n_j\,\mathrm{d}S_\Omega = 0, \forall\theta^* \end{aligned} \quad (2.53)$$

Where $q^j_{ext}$ is the surface heat flux in the proper frame imposed on the hypersurface $\partial\Omega_q$ and $n_j$ is the normal vector to the 3D surface. We have to remind that $q^4 = 0$, because the inertial frame is proper. The boundaries where the heat flux and temperature are applied should respect $\partial\Omega_q \cup \partial\Omega_\theta = \partial\Omega$ and $\partial\Omega_q \cap \partial\Omega_\theta = \varnothing$. The boundary conditions in this case are the flux boundary conditions (on $\partial\Omega_q$) represented by the imposed heat flux $q^j_{ext}$ and the temperature boundary conditions (on $\partial\Omega_\theta$).

### 2.6.4 Spacetime weak integral form with spacetime Cattaneo's model of heat conduction

The same scheme is used to write the spacetime weak integral form with Cattaneo's model of heat conduction. For this model, we use Eq. 2.47 with $\tau_1 = 0$ to simplify. Then the injection in the global balance of internal

energy (Eq. 2.49) leads to the the partial differential equation, which enables us to write the spacetime weak integral form for an inertial and proper frame:

$$\begin{aligned} W(\theta,\theta^*) &= \int_\Omega \theta^* \left( \frac{\partial \theta}{\partial t} + a\eta^{\mu\nu} \frac{\partial}{\partial x^\nu} \left( \frac{\partial}{\partial x^\mu}\theta \right) - a \frac{\partial}{\partial x^\mu} \left( u^\mu u^\nu \frac{\partial}{\partial x^\nu}\theta \right) - \tau \frac{\partial^2 \theta}{\partial t^2} - f_r \right) \mathrm{d}H_\Omega \\ &= 0, \forall \theta^* \end{aligned} \tag{2.54}$$

#### 2.6.4.1 Dirichlet boundary conditions

In the particular case of Dirichlet boundary conditions, the third and the fifth integrals in Eq.2.54 can be reduced as integrals over surfaces using Green-Ostrogradski theorem. The test temperature $\theta^*$ is supposed to be null at the boundaries $\partial\Omega$. The problem is then formulated by:

$$W(\theta,\theta^*) = \int_\Omega \theta^* \frac{\partial \theta}{\partial t} \mathrm{d}H_\Omega + \int_\Omega a I^{ij} \frac{\partial \theta^*}{\partial x^i} \frac{\partial \theta}{\partial x^j} \mathrm{d}H_\Omega + \int_\Omega \tau \frac{\partial \theta^*}{\partial t} \frac{\partial \theta}{\partial t} \mathrm{d}H_\Omega - \int_\Omega \theta^* f_r \mathrm{d}H_\Omega = 0, \forall \theta^* \tag{2.55}$$

Except for the integration domain, the terms in Eq. 2.55 are similar to their 3D equivalent [Debard,2011]. This is because we have expressed the model in the proper and inertial frame. It would exhibit differences if it was expressed in another frame and/or with thermomechanical couplings.

Similarly to the strategy leading to the weak integral form representing spacetime Fourier's model, boundary conditions have to be placed. We define: $\partial\Omega^j = \partial\omega \cup t$ as the space boundaries of the domain and $\partial\Omega^4 = \omega \cup \partial t$ as the time boundaries of the domain. Then, the boundary conditions of this weak integral form can be decomposed into boundary conditions on the space and on the time. The first type can be written: $\theta(x^\mu \in \partial\Omega^j) = f_{SC}(x^\mu \in \partial\Omega^j)$. The second type can be written: $\theta(x^\mu \in \partial\Omega^4) = f_{TC}(x^\mu \in \partial\Omega^4)$.

#### 2.6.4.2 Neumann-Dirichlet boundary conditions

In the particular case of Neumann-Dirichlet boundary conditions, the problem is formulated by:

$$\begin{aligned} W(\theta,\theta^*) = \int_\Omega \theta^* \frac{\partial \theta}{\partial t} \mathrm{d}H_\Omega + \int_\Omega a I^{ij} \frac{\partial \theta^*}{\partial x^i} \frac{\partial \theta}{\partial x^j} \mathrm{d}H_\Omega + \int_\Omega \tau \frac{\partial \theta^*}{\partial t} \frac{\partial \theta}{\partial t} \mathrm{d}H_\Omega - \int_\Omega \theta^* f_r \mathrm{d}H_\Omega \\ - \int_{\partial\Omega_q} \theta^* \frac{c\, q^j_{ext}}{\widetilde{\rho_c} c_{m,\omega}} n_j \mathrm{d}S_\Omega - \int_{\partial\Omega_q} \tau \theta^* \frac{\partial \theta}{\partial t} n_4 \mathrm{d}V = 0, \forall \theta^* \end{aligned} \tag{2.56}$$

where $q^j_{ext}$ is the surface heat flux in the proper frame imposed on the hypersurface $\partial\Omega_q$ and $n_j$ is the normal vector to the 3D surface. We have to remind that $q^4 = 0$, because the inertial frame is proper. $n_4$ is the time normal to the 3D volume ($= 1$ for final time; $= -1$ for initial time). The boundaries where the heat flux and temperature are applied should respect $\partial\Omega_q \cup \partial\Omega_\theta = \partial\Omega$ and $\partial\Omega_q \cap \partial\Omega_\theta = \varnothing$.

### 2.6.5 Discussion on the boundary conditions

In the spacetime formalism, the spacetime domain is meshed for use with a finite element method. Consequently, the boundary conditions should be given for all the spacetime domain. As in 3D, the space boundary conditions are either Dirichlet conditions (temperature) or Neumann-Dirichlet conditions (temperature and heat flux).

The time boundary conditions could also be a priori placed on the initial and the final times. The temperature of the initial time (in the case of Dirichlet conditions) is fixed as a constraint. The temperature of the final time is a priori unknown and left without conditions. This can be compared to space unconditioned boundaries when modeling in 3D.

Furthermore, from a numerical point of view, the present calculation is performed with the spacetime finite element method, which means that the integration of the forms is over an hypervolume including the

time in its domain. But when considering terms such as $\int_\Omega \theta^* \frac{\partial \theta}{\partial t} \, \mathrm{d}H_\Omega$, we notice that it is not necessary to have a final time condition on temperature since the weak integral form depends only on the first time derivative of the trial function. This argument presently holds for all the considered heat conduction models. Indeed, even if the corresponding partial differential equation is hyperbolic [Vitokhin and Ivanova,2017], the use of spacetime formalism enables to obtain weak integral form with only first time derivatives of the trial function requiring only one time condition.

## 2.7 Numerical simulations of heat conduction

### 2.7.1 Features of using FEniCS project

The following simulations are performed with FEniCS. FEniCS project is an automated programming environment for solving variational equations [Langtangen and Logg,2017]. Unlike other modeling environments where the user should follow predefined modules reproducing the physics of the phenomena, the user of FEniCS has only to specify the variational problem to be solved. This allows us to solve Newtonian thermal problems, as well as spacetime ones. Consequently, FEniCS is particularly useful for the implementation of the variational forms that we have introduced in section 2.6.

### 2.7.2 Numerical simulation of a spacetime Cattaneo's heat model

#### 2.7.2.1 An archetypal example

Let us consider Cattaneo's heat conduction model (Eq. 2.47) for an application in 1D+1D: one dimension is dedicated to the space in the direction $x$ and one to the time $t$. The spacetime boundary conditions are illustrated in Fig. 11.

We chose a geometry with small domains of space and time of the material in order to illustrate the physical and numerical problems that can occur at these scales to distinguish the considered heat conduction models. Indeed, at these scales, the different models for heat conduction may exhibit significant differences [Guillemet and Bardon,2000]. Furthermore, because of the chosen value of the thermal diffusivity, the corresponding relaxation time constant is around few $ns$.

The result is a map showing the evolution of temperature through space and time. The function $(1 - exp(-\beta t))$ introduced as a space boundary condition at $x = 0$ gives precision to the solution and help to obtain smoothed curves of temperature without noise near the boundaries, especially at the very short times. We notice in Fig. 12 that, for values of $\beta$ largely deviating from $1.3 \times 10^{10}$, accuracy on the temperature decreases. Moreover, the function on the border $(x = 0, t)$ does not contradict the condition on the border $(x, t = 0)$ at the intersection $(x = 0, t = 0)$.

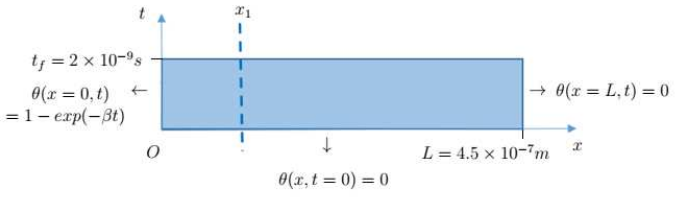


**Fig. 11:** Illustration showing the geometry, the boundary conditions and the section at a position $x = x_1$ through the time.

| Parameter | Value |
|---|---|
| Thermal diffusivity | $a = 10^{-5}\, m^2.s^{-1}$ |
| Relaxation time constant | $\tau = 0.8 \times 10^{-10}\, s$ |
| Volume heat source | $f_r = 0$ |

**Tab. 7:** Values of the variables used in the implemented heat model.

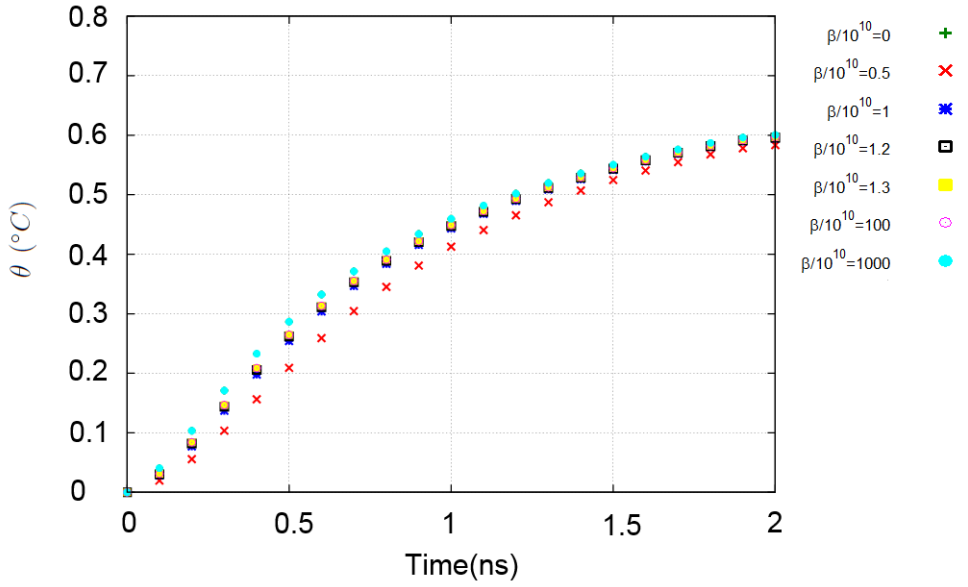


**Fig. 12:** Evolution of the temperature $\theta$ of an event at a given position $x$ as a function of the time $t$ for different values of the coefficient $\beta$. The study is applied with spacetime Cattaneo's model. The coefficients $\beta/(10^{10}) = 0, 0.5, 1, 1.2, 1.3, 100, 1000$ are respectively tested.

In the latter, we discuss, for Fourier's and/or Cattaneo's models respectively, the influence of spacetime meshing and of the material parameters. The variation of the parameters allows to examine their physical and numerical influences.

#### 2.7.2.2 Influence of the spacetime meshing

The mesh along the position and the time of the heat model, described in this section (for $\tau = 0$, i.e. considering spacetime Fourier's heat conduction model), is analyzed relatively to the admitted absolute error. This latter is computed with respect to the Newtonian analytical solution of the problem [Battaglia,2007] $\theta(x,t) = 1 - erf(\frac{x}{2\sqrt{at}})$, where $erf$ is the error function. Let us define $N_x$, to be the step along $x$ and $N_t$, the step along $t$. For a fixed $N_t = 150$, $N_x$ is changed, for an arbitrary position $x_1$ and time $t_1$, the temperature is investigated. The temperature converges toward values within the admissible margin for values of $N_x$ around 5550.

The tests are repeated at different instants of time and the relative error on the temperature is computed. The error decreases and tends to the admitted error at the same value of $N_x$. The same investigation can be led by varying $N_t$ for the same parameters of the model. Then, for this archetypal example, the meshing is required to be finer in the space than in the time dimension.

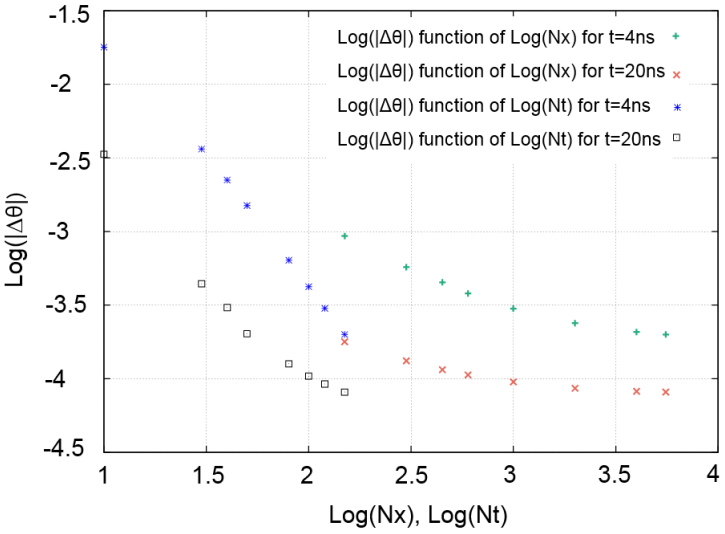


**Fig. 13:** The evolution of the logarithm of the error on the temperature value $\log(|\Delta\theta|)$ function of $\log(N_x)$ and $\log(N_t)$ at different times $t$. The evolution of the error is investigated at $x_1 = 10^{-7}m$ for a 1D+1D spacetime Fourier's model.

The graphs in Fig. 13 show that the logarithm of the error on the temperature has a faster rate decrease as a function of the time meshing than as a function of the space meshing. Indeed, for the time meshing, the linear regression gives $|\Delta\theta| = 0.1(N_t^{-1.68})$ at $t = 4ns$ with a coefficient of determination $R^2 = 0.89$ and $|\Delta\theta| = 0.06(N_t^{-1.36})$ at $t = 20ns$ with $R^2 = 0.96$. For the space meshing, the linear regression gives $|\Delta\theta| = 0.006(N_x^{-0.41})$ at $t = 4\,ns$ with a $R^2 = 0.94$ and $|\Delta\theta| = (N_x^{-0.202})$ at $t = 20\,ns$ with $R^2 = 0.99$. Although this meshing leads to plate elements, tests have been performed with balanced meshing on the spacetime domain and the results show that the variations of the temperature superimpose with the values obtained with plate elements. Consequently, the influence of the shape of the elements does not significantly affect the convergence.

#### 2.7.2.3 Influence of the material parameters

Concerning the material parameters, the thermal diffusivity and the relaxation time constant are examined for the heat model described in this section. As expected, tests show that the more the value of the thermal diffusivity is, the faster the temperature of a point subject to a source of heat raises (Fig. 14(a)) for all the models of heat conduction.

We have also tested the influence of the relaxation time constant $\tau$ used in Cattaneo's model. The longer the relaxation time is, the slower the temperature of a point subjected to a heat source raises (Fig. 14(b)). This can be explained by the decelerating effect on the conduction of heat.

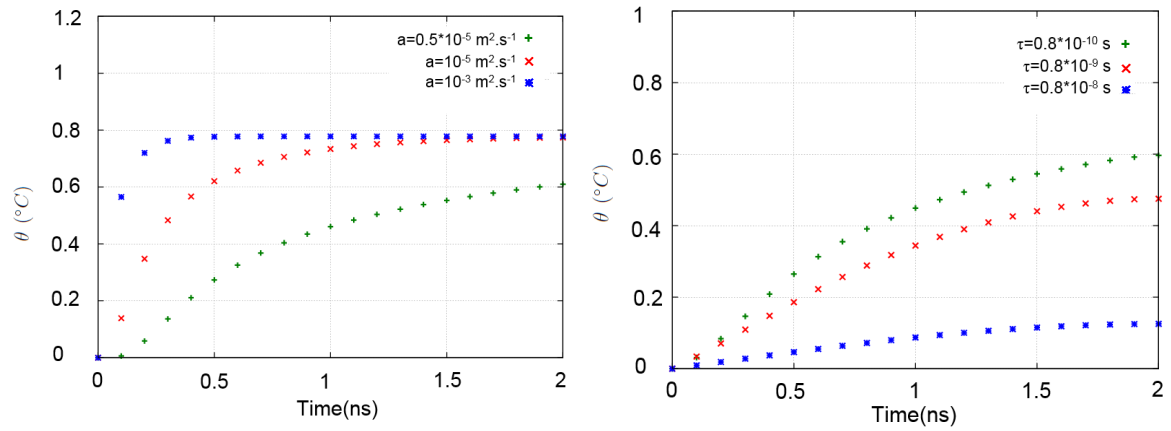


**Fig. 14:** On the left: Evolution of temperature for a 1D+1D spacetime Cattaneo's model function of the time at the position $x_1 = 10^{-7}m$ for different diffusivities $a = 0.5 \times 10^{-5}, 10^{-5}, 10^{-3}m^2 \cdot s^{-1}$ represented by the curves in green, red and blue respectively. On the right: Evolution of temperature for a 1D+1D spacetime Cattaneo's model function of the time at the position $x_1 = 10^{-7}m$ for different relaxation time constants of $\tau = 0.8 \times 10^{-10}, 0.8 \times 10^{-9}, 0.8 \times 10^{-8}s$ represented by the curves in green, red and blue curves respectively.

### 2.7.3 Comparison between spacetime Fourier's model and spacetime Cattaneo's model

A comparison between the two models of heat conduction has been also performed. Similarly to the Newtonian cases, the comparison between Fourier's model and Cattaneo's model shows a delay of the temperature conduction for this latter. This is illustrated in Fig. 15(a).

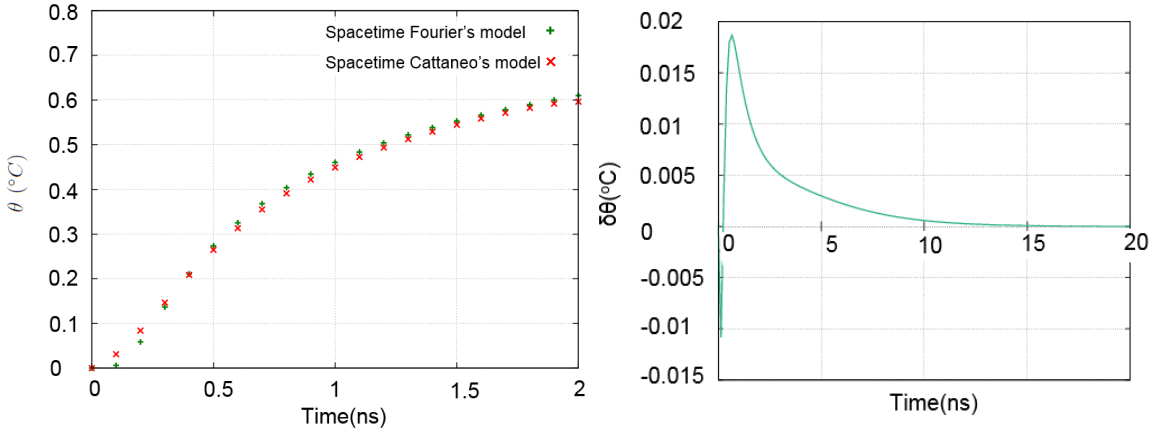


**Fig. 15:** On the left: Evolution of temperature through the time at a position $x$ for spacetime Fourier's model (green curve) and spacetime Cattaneo's model (red curve). On the right: Evolution of the difference of temperature through the time between spacetime Fourier's and Cattaneo's models.

It is noticed that the graph representing the spacetime Cattaneo's model has a delay in comparison with the graph representing the spacetime Fourier's model starting at a time $t_1 = 2.5 \times 10^{-10}\,s$. At the same time, the temperature obtained by the spacetime Cattaneo's model is lower, which is justified by the relaxation term that has been added to the model. Below this value of $t_1$ an inverse phenomenon is observed, it can be related to the boundaries effect (recovery of the boundary condition).

The evolution of the difference of temperature between both models through the time is shown in Fig. 15(b). It shows that at a certain inflection time $t_1$, the difference of temperature obtained by a Fourier's model and a Cattaneo's model for a same point is positive. It means that Cattaneo's model is delayed in respect to Fourier's model. Moreover the difference reaches a maximum near this inflection point $t_1$ and decreases through the time. As known and expected, the two models have the same results asymptotically for long times, since the difference between them vanishes. It emphasizes the importance for the choice of the domain of integration to be able to observe the phenomenon of delay modeled by Cattaneo's model for short times.

### 2.7.4 Comparison with Newtonian simulations using the discretization of time

In order to validate the simulations performed with spacetime finite elements, for each model, a comparison with the simulations in Newtonian approach with discretization of the time is done. In the latter, for the simulations, the space is solved with finite elements, while the time is discretized separately to be solved (finite differences).

We write the discretized weak integral form for Cattaneo's model or Fourier's model ($\tau = 0$) using the explicit method with a forward difference at the first time derivative and a second-order central difference at the second time derivative, which guarantees the stability of the numerical scheme [Debard,2011]. In the case of Dirichlet boundary conditions, the weak integral form is written as:

$$\begin{aligned} W^{3D}(\theta, \theta^*) \quad = \quad & \int_\omega \theta^* \left( \frac{\theta^{n+1} - \theta^n}{\Delta t} + \tau \frac{\theta^{n+1} - 2\theta^n + \theta^{n-1}}{\Delta t^2} \right) \mathrm{d}V_\omega \\ & + \int_\omega a I^{ij} \frac{\partial \theta^*}{\partial x^i} \frac{\partial \theta^{n+1}}{\partial x^j} \, \mathrm{d}V_\omega - \int_\omega \theta^* f_r \, \mathrm{d}V_\omega = 0, \forall \theta^* \end{aligned} \tag{2.57}$$

where $\omega$ is the 3D domain of integration. The weak integral form has the following boundary conditions: $\theta(x^j \in \partial\omega) = f_{SC}(x^j \in \partial\omega)$. An initial condition is also required such that: $\theta(t = t_0) = f_{TC}(t = t_0)(= 0\,°C$ for the example illustrated in Figures 16(a) and (b)).

The comparison between spacetime Fourier's model solved in spacetime finite elements and Newtonian Fourier's model with discretized time is shown in Fig. 16(a). Both models have been tested with the same conditions.

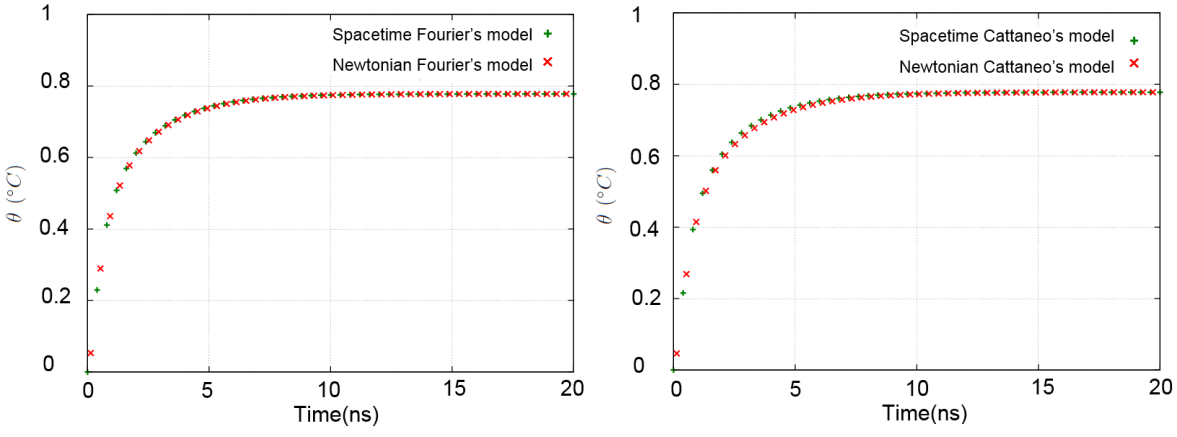


**Fig. 16:** On the left: evolution of temperature through the time at a position $x$ for spacetime Fourier's model (green curve) and Newtonian Fourier's model with discretized time (red curve), assuming $f_r = 0$. On the right: the same for Cattaneo's model.

The same study has been performed with Cattaneo's model. Similar results have been obtained as shown in Fig. 16(b). For all the heat conduction models, graphs closely superimpose, which verifies the spacetime simulation for these particular models.

### 2.7.5 Comparison of the computation time

The impact of using the spacetime finite element method on the computation time is studied. Fig. 17 shows that the variation of the computation time is function of the time mesh of a spacetime model. It changes exponentially to this latter, while the variation is linear in the case of the Newtonian model with discretization of time. The finer the mesh is, the bigger the difference is between the two approaches. In the example given, the ratio of the two computation times varies between 2 and 5 with the mesh refinement. Note that thermomechanical couplings are not taken into consideration in this example. Besides, the source of heat is constant in time.

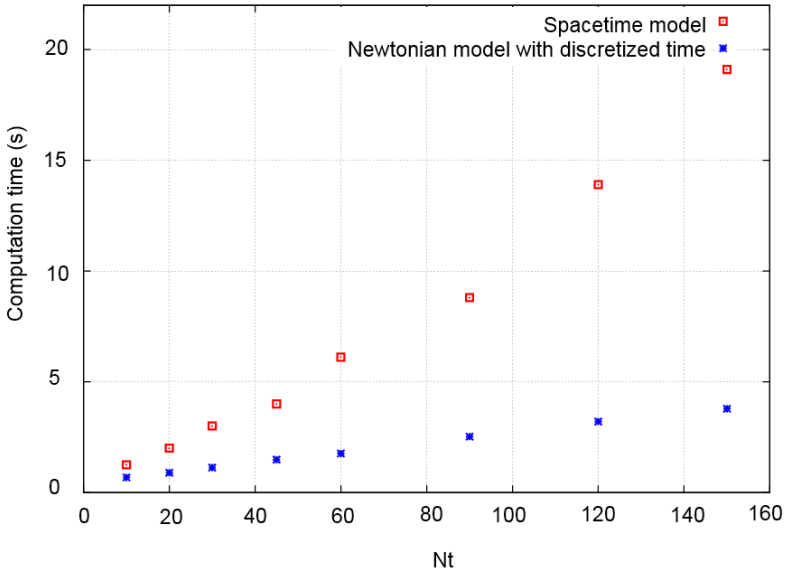


**Fig. 17:** Evolution of the computation time with the time mesh for spacetime Fourier's model (red squares) and the corresponding Newtonian model with the discretized time (blue stars).

### 2.7.6 Application: Spacetime modeling of the heat conduction for a cooling fin

This section presents an application of the spacetime modeling of the heat equation, previously proposed and formulated in the weak forms in Eqs. 2.51 and 2.54, for a 2D spatial geometry (2D cooling fin used in the industrial applications) using Neumann-Dirichlet boundary conditions. The flux representing the Neumann boundary condition is also a function of the temperature field [Lagrée,2010, Cengel,2008]. The field of temperature obtained with the spacetime method will be compared to the one obtained from the analytical formulation of the problem.

#### 2.7.6.1 Description of the problem

Fins are elements that extend the surface of an object in order to increase the rate of heat transfer with the environment by increasing the convection [Lagrée,2010]. Figure 18 shows a plate surface and a finned one. The convection flux exchanged differs between the two configurations since the surface of exchange of the

finned body is clearly larger than in the flat one, consequently the heat transfer is more important in the finned body.

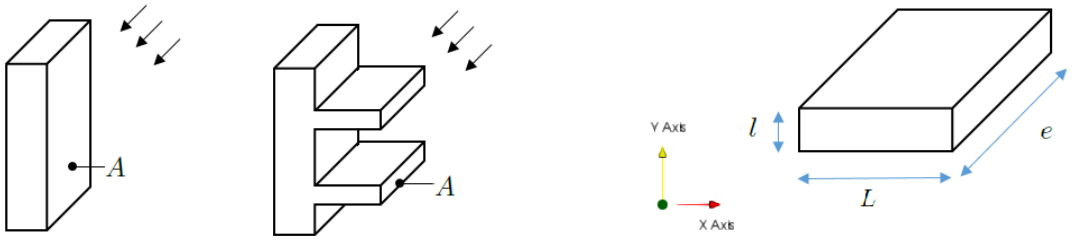


**Fig. 18:** On the left: The geometrical difference between a flat surface and a finned surface. On the right: The geometrical features of a fin.

We choose to do the simulation of a 2D spatial model, corresponding to the case for which $\theta(t, x, y)$ is homogeneous with respect to the $z$ axis. The corresponding geometry of the fin is represented in Figure 19.

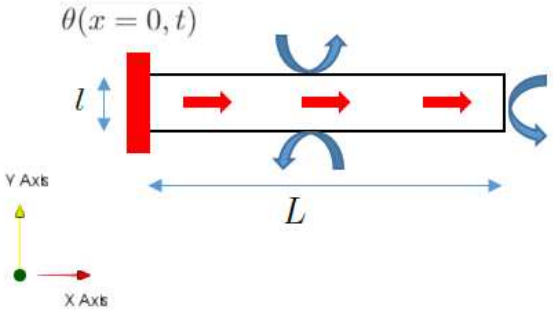


**Fig. 19:** The configuration of a 2D fin with the boundary conditions.

According to the application of the Vaschy-Buckingham theorem to the simulated fin, it is possible to prove that the solution of this problem can be written as $f(\frac{\theta-\theta_0}{\theta-\theta(x=0,t)}, \frac{at}{L^2}, \frac{x}{L}, \frac{y}{l}, \frac{l}{L}, Bi) = 0$ [Vaschy,1892, Buckingham,1914]. The Biot number $Bi$ is a dimensionless number used in heat transfer calculations. By definition, $Bi = \dfrac{hL_C}{\lambda}$, where $L_c$ is a characteristic length of the body. In the present case of the 2D fin: $Bi = \dfrac{hl}{\lambda}$ [Lagrée,2010].

The temperature is transported by conduction in the fin (Figure 19). The thermal diffusivity of the material is $a = \dfrac{\lambda}{\widetilde{\rho_c} c_{m,\omega}}$. The fin exchanges heat flux by convection with its surrounding environment through its external surfaces. The (surface) convective heat flux exchanged through any surface $dS_\omega$ can be written in the Newtonian inertial proper frame: $\phi^j dS_\omega = hI^{ij}(\theta - \theta_0)n_i dS_\omega$, where $h$ is the coefficient of convection of the surrounding medium, $\theta$ is the temperature at a point of the surface of the fin and $\theta_0$ is the temperature of the surrounding medium far away. No volume heat source is taken into account, i.e. $f_r = 0$.

The Newtonian Fourier's model is usually chosen in the literature in order to model this heat transfer [Lagrée,2010, Cengel,2008]. We choose to model the heat conduction using a spacetime Fourier's model. This choice guarantees obtaining a covariant model of the heat transfer. The weak form corresponding to

this problem is expressed with Eq. 2.53 where $cq^j_{ext}$ represents the convective heat flux imposed on the hyper-surface $\partial\Omega^j_q$.

The surface source of heat changing the thermal equilibrium, through the temperature of the hot base of the fin, is represented by a Dirichtet boundary condition at $x = 0$.

The boundary conditions can be resumed by: $\theta(x^\mu \in \partial\Omega^1) = f_{SC1}(x^\mu \in \partial\Omega^1) = 1000\,°C$, where $\partial\Omega^1$ is the space boundary where $x = 0$ and $\theta(x^\mu \in \partial\partial\Omega^j_q) = f_{SC2}(x^\mu \in \partial\Omega^1) = cq^j_{ext}$, where $\partial\Omega^j_q$ is the space boundary where $y = 0$, $y = l$ and $x = L$.

The time boundary condition can be written: $\theta(x^\mu \in \partial\Omega^2) = f_{TC}(x^\mu \in \partial\Omega^2) = 0°C$, where $\partial\Omega^2$ is the initial time boundary ($t = 0$).

To avoid contradictory boundary conditions of the temperature at $x = 0$, which is conditioned by spatial and initial boundary conditions at $t = 0$, it is considered to be function of the time such as: $\theta(x = 0, t) = 1000 - 1000\,exp(-130t)$ ($\beta = 130$ is obtained from an optimization method similar to the one done in section 2.7.2.1). This function enables to reach progressively but quickly $\theta(x = 0, t) = 1000°C$ without contradicting $\theta(x = 0, t = 0) = 0\,°C$.

By introducing the Biot number in the weak form, an equivalent equation of the problem can also be written as:

$$W(\theta, \theta^*) = \int_\Omega \frac{1}{a}\theta^* \frac{\partial\theta}{\partial t}\,\mathrm{d}H_\Omega + \int_\Omega \frac{\partial\theta^*}{\partial x^j}\frac{\partial\theta}{\partial x_j}\,\mathrm{d}H_\Omega + \int_{\partial\Omega^j_q} \theta^* \frac{Bi(\theta - \theta_0)}{l} n_j\,\mathrm{d}S_\Omega = 0, \forall\theta^* \tag{2.58}$$

#### 2.7.6.2 Simulation using FEniCS project

We consider the case of a 2D+1D fin (2 dimensions assigned to space and 1 to time) simulated using Eq. 2.58.

The Neumann condition that represents the convection heat flux imposed at the external surfaces is implemented carefully. This heat flux is function of the temperature of the position and is, at the same time, part of the two members of the bilinear form.

In fact, the term: $\int_{\partial\Omega^j_q} \theta^* \frac{Bi(\theta - \theta_0)}{l} n_j\,\mathrm{d}S_\Omega$ has to be divided into two parts corresponding to the right hand side and to the left hand side of the bilinear form such as: $\int_{\partial\Omega^j_q} (A\theta^*\theta + B\theta^*)\,\mathrm{d}S_\Omega = 0$, where $A$ and $B$ are constants. This could be avoided by normalizing the temperature and computing a normalized temperature field: $\theta_d = \theta - \theta_0$. Consequently, this term would not be an interesting issue and a post-treatment of results would be necessary to visualize the temperature field.

The selected material of the fin for the simulation is the aluminum. The parameters of the simulation are summarized in table 22 :

| Variable | Value |
|---|---|
| Thermal diffusivity of Al | $a = 9.7 \times 10^{-5}\, m^2/s$ |
| Conductivity of Al | $\lambda = 205\ W.m^{-1}.K^{-1}$ |
| Coefficient of heat convection of the air surrounding the fin | $h = 0.04\, kW.m^{-2}.K^{-1}$ |
| Temperature of the air surrounding the fin | $\theta_0 = 0\, K$ |
| Corresponding Biot number | $Bi = 0.01$ |
| Characteristic time of the conduction phenomenon | $\tau_c = \frac{L^2}{a}$ |
| Interval of time of simulation | $t_f = 10310\, s \geq \tau_c$ |
| Geometry | $L = 1\, m,\ l = 0.05\, m$ |
| Mesh | $N_x = 60,\ N_y = N_t = 30$ |

**Tab. 8:** The parameters of the simulation

As a result of the simulation, we obtain a cartography of the temperature propagating through the fin and dissipating through its surfaces, function of the time. The graphs of the evolution of the temperature through the fin can be obtained at any instant of time $t$, as presented in Fig. 20a.

#### 2.7.6.3 Comparison with analytical results

We compare the asymptotic temperature distribution that we previously get with respect to the analytic steady-state thermal distribution of the cooling fin. We chose the steady-state regime to compare since the previous simulation is reaching this state and since at this state the comparison of the temperature evolution through the position is time-independent. A comparison of evolution of temperature at a non-steady-state is also possible but the corresponding analytical solution takes a more complicated form.

Let us consider a uniform differential cross-section of the fin along the $x$-direction. In the analytical study, we include more hypothesis: The variation of the temperature transversely is considered to be negligible, then we consider the one-dimensional conduction through the $x$-direction. In addition to that, the convection across the surface area is considered to be uniform. Taking these assumptions into consideration, the energy balance on this cross section can be expressed by:

$$\frac{d^2\theta(x)}{dx^2} = \frac{h\mathcal{P}}{\lambda S}(\theta(x) - \theta_0) \tag{2.59}$$

where $\mathcal{P}$ is the perimeter of the fin and $S$ is the section of the fin in the orthogonal direction to $x$. It leads to write the fundamental equation of heat conduction of a fin, using the definition of $Bi$ number:

$$\frac{d^2\theta(x)}{dx^2} - \frac{2Bi}{a^2}(\theta(x) - \theta_0) = 0 \tag{2.60}$$

This differential equation has to be solved between $x = 0$ and $x = L$. The solution that can be obtained is:

$$\theta = \theta_0 + A' \cosh(\sqrt{2Bi}(x/l)) + B' \sinh(\sqrt{2Bi}(x/l)) \tag{2.61}$$

where $A'$ and $B'$ are constants. The boundary condition representing the temperature of the hot base of the fin can be written: $\theta(x = 0, t)$. The boundary at $x = L$ is free, the flux at this boundary is then:

$$\frac{d\theta(x = L)}{dx} - \frac{Bi}{l}(\theta(x = L) - \theta_0) = 0 \tag{2.62}$$

The analytical solution of Eq. 2.60 can be expressed as [Lagrée,2010]:

$$\frac{\theta(x) - \theta_0}{\theta(x = 0, t) - \theta_0} = \frac{\cosh(\sqrt{2Bi}(L/l - x/l)) + \sqrt{Bi/2}\sinh(\sqrt{2Bi}(L/l - x/l))}{\cosh(\sqrt{2Bi}(L/l)) + \sqrt{Bi/2}\sinh(\sqrt{2Bi}(L/l))} \tag{2.63}$$

The comparison between the results obtained from the analytical method and from the 2D+1D simulation shows that, for the same inputs of material parameters and boundary conditions, at a same position $y$ and for time $t$ in the steady-state regime for the numerical simulation (meaning a calculation time $t >> \tau_c$), the graphs of evolution of the temperature through the length of the fin superimpose (Fig. 20b).

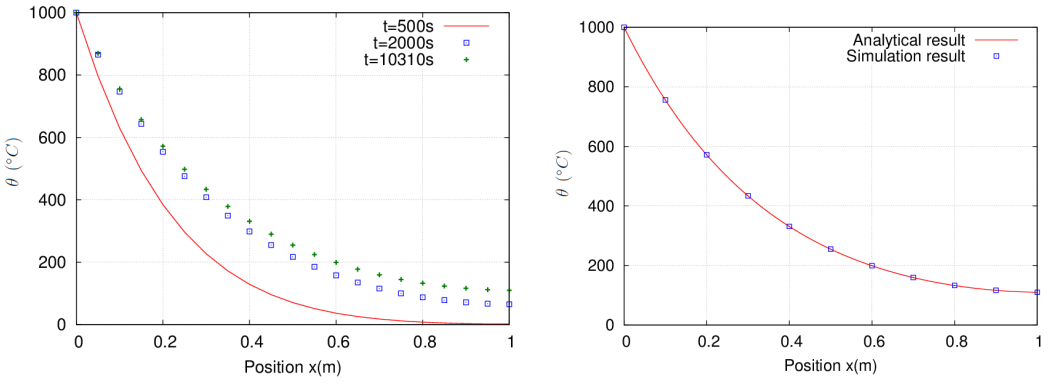


**Fig. 20:** a) On the left: Evolution of the temperature through the fin at $y = 0.025m$, at different instants of time: $t = 500s, 2000s$ and $10310s$ corresponding respectively to the red, blue and green graphs. and b) On the right: Comparison between the evolution of temperature through the length of the fin at $y = 0.025m$ and $t = 10310s$ for the theoretical model represented by the analytical formula and the numerical 2D+1D heat model simulated in section 2.7.6.2, respectively represented by the red and the blue graphs. The results superimpose.

The results show a compatibility of the 2D+1D numerical model of the heat conduction with analytical results for the cooling fin in the steady-state regime. It is a simple application of the use of one of the proposed heat models of the manuscript (spacetime Fourier's heat model with Neumann-Dirichlet boundary conditions) for industrial applications demanding precision on the temperature on different time intervals. Different geometries can be applied and the boundary conditions can be easily adapted.

## 2.8 Conclusions

In this chapter of the manuscript, we first investigated the modeling of a thermal behavior using a thermodynamical approach. The originality comes from the systematic use of a spacetime formalism to ensure the indifference to change of frames, for both the physical models as well as for the numerical resolution schemes. Using the conservation of internal energy written in the spacetime domain and the variation of the four-vector entropy flux, a covariant statement of the Clausius-Duhem is proposed with covariant terms.

The pure thermal evolution in case of heat conduction is specifically focused. Spacetime counterparts of Fourier's and Cattaneo's equations have been obtained through the spacetime generalization of the Newtonian equations, or deduced from the aforementioned covariant statement of Clausius-Duhem inequality, or obtained from a complexification method. Without thermomechanical dissipative couplings, two kinds of models have been obtained from these different methods. It is worth noting that a particular methodology involving only the CIT framework has been also proposed to obtain Cattaneo's model in the spacetime domain, by use of Laplace transform and complexification. It can be easily generalized to obtain other models leading to third order (or more) space/time derivatives of temperature in the heat equation. Different covariant models which generalize Cattaneo's Newtonian model can thus be obtained from a CIT framework without the need to use an EIT framework. Such terms remain to be deeply studied from a numerical point of view.

As in its original form, Cattaneo's model contains relaxation terms that delay the conduction of heat in the body. The existence of these terms consequently lead to overcome the problems of causality faced in some other thermal models, which assume a heat propagation at an infinite velocity. Therefore, this spacetime formalism reaches its goal in building covariant spacetime heat conduction models and respecting simultaneously the causality principle.

Numerical simulations with FEniCS have been also performed to illustrate this approach without thermomechanical couplings. For pure thermal problems, the proposed spacetime weak integral forms (Eqs.2.52, 2.53, 2.55 and 2.56) for heat conduction models differ from the Newtonian ones (Eq. 2.57) only through the integration domain. In the first ones, the time is a dimension of the domain of integration. However in the second, it is generally discretized using the explicit method with a forward difference for the first time derivative and a second-order central difference for the second time derivative (if required for Cattaneo's model). This clears up the difference in the integration forms obtained. Corollary, the initial required condition on the discretized time becomes a boundary condition on the spacetime integration domain.

The numerical models have been successfully benched with respect to the classical version of Fourier's and Cattaneo's models. However, the spacetime finite element method has a CPU time complexity of higher order (second order) than the one of the classical approach. Moreover, the influence of the domain of integration, the mesh and the material parameters have been studied with 1D+1D models that show no difficulty to perform such a new method for thermal problems. It has been successfully applied to the cooling fin problem and the spacetime model is able to predict the heat diffusion in this particular application.

Eventually, the use of a spacetime formalism seems to have less numerical interest in the case of motionless body experiencing only heat transfer by conduction. However, in the next chapter, we will prove some numerical advantage of the spacetime method. Moreover, this chapter is considered as a prequel to the cases of bodies experiencing simultaneously heat transfers and mechanical finite transformations at large scales, as in forming processes, in a way that accommodates simultaneously the covariance and causality principles. It will be further investigated in the second part of the manuscript (chapters 4 and 5).

# 3 Application of spacetime modeling to self-heating

## 3.1 Introduction

Self-heating phenomenon represents thermal evolution in materials resulting from mechanical loading. It can be especially investigated during fatigue tests (see section 1.9). The aim of this chapter is to compute the variation of temperature of a material body due to self-heating from an innovative point of view: requiring a covariant formulation of the thermomechanical behavior (detailed in section 1.7), we use a spacetime heat conduction model as developed in the previous chapter (section 2.3). Then computational methods performed with FEniCS platform lead to a new approach for investigating self-heating.

However, other steps have also to be investigated, especially the identification process of numerical values of the different parameters to see its influence on the accuracy and reliability of this new kind of numerical simulations. This optimization by inverse analysis is performed by use of a classical Newtonian approach.

Some numerical values for these parameters are provided, as well as the integral form of the spacetime problem with the adapted boundary conditions that can directly be used.

The layout of the chapter is as follows: section 3.3 describes the fatigue tests, in which the self-heating phenomenon is occurring. In this section, we also discuss the different methods used in the Newtonian approach to identify the dissipation term and the time parameter and we explain the data treatment required for their calculation and/or optimization. In section 3.4, based on section 2.3, the spacetime Fourier heat model for self-heating is built. The identified parameters in section 3.3 are input parameters of the spacetime heat model. The variational problem is thus proposed in the spacetime approach in order to be solved. In Section 3.5, numerical simulations of the spacetime variational problem are done using FEniCS project. Moreover, some comparative results with experimental data are illustrated in order to prove the reliability of the present approach in the case of self-heating.

## 3.2 Methodology for modeling of the self-heating phenomenon in spacetime

In order to fulfill the task of modeling the self-heating phenomenon in a spacetime domain, many steps are necessary:

- Study of parameters of the fatigue test which includes analyzing experimental data and identification of the parameters of the Newtonian model (section 3.3). The thermal dissipation, expressed in Eq. 2.35, is one important parameter to be computed. Based on previous studies [Favier et al.,2016, Chrysochoos et al.,2009, Boulanger et al.,2004], several identification methods are developed in order to reduce the probable errors of this step.
- Injection of the resulting thermal dissipation in a spacetime heat model representing the self-heating phenomenon. The boundary conditions are investigated in order to reproduce the conditions of the fatigue test provided by the experimental data (section 3.5.1.1).
- Numerical simulation of the spacetime variational problem of the model. The evolution of the temperature in a spacetime domain is then obtained (section 3.5).
- Comparison between the evolution of the temperature occuring during self-heating obtained from experimental results and that obtained by a spacetime approach (results of the simulation of the spacetime heat model, see section 3.5.2).

This last step aims to validate the spacetime model by showing its ability to reproduce the self-heating phenomenon and consequently validate the spacetime heat conduction equation used as well as the method/framework proposed to build it.

## 3.3 Self-heating study based on experimental data measurements

### 3.3.1 Description of the gigacycle fatigue tests

Gigacycle fatigue testing using piezoelectric devices is used to test smooth samples under axial loading. Frequency of the cycle usually stands around $20kHz$ in order to rapidly achieve fatigue life up to $10^{10}$ cycles. The ultrasonic machines used offer a significant reduction in test time compared to conventional testing machines. In addition to that, high frequency loading raises the intrinsic dissipation and consequently induces large temperature variations easily detectable even by standard temperature measurement devices [Favier et al.,2016].

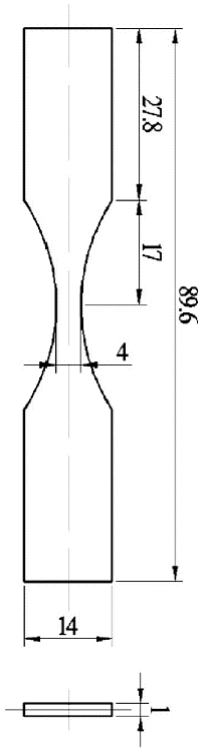


**Fig. 21:** Specimen geometry and dimensions in mm.

| Variable | Value |
|---|---|
| Mass density $\widetilde{\rho_c}$ | $7800\,kg.m^{-3}$ |
| Specific heat capacity (constant volume) $\mathcal{C}_{m\omega}$ | $473\,J.kg^{-1}.K^{-1}$ |
| Thermal conductivity $\lambda$ | $50.2\ W.m^{-1}.K^{-1}$ |
| Thermal diffusivity $a = \dfrac{\lambda}{\widetilde{\rho_c}\mathcal{C}_{m\omega}}$ | $13.6 \times 10^{-6}\ m^2.s^{-1}$ |

**Tab. 9:** Thermophysical properties of the considered C65 steel [ASM,1998]

The fatigue specimen is thin and flat hourglass shaped (Fig. 21). The fatigue tests were carried out at 20 $kHz$ using an ultrasonic fatigue device at the Laboratory of Energetics Mechanics and Electromagnetism (LEME) of the University Paris-Nanterre. The cyclic loading is stress imposed at 221 $MPa$ and at a load ratio of $R = -1$. No cooling device (air or gas flow) is used during the tests. The studied specimen is made of C65 steel frequently used in parts fabrication. Table 9 shows the thermophysical properties of the considered steel.

The specimen is subjected to natural convection with its surrounding environment (having convective heat transfer coefficient $h$ and being at room temperature $\theta_0$). It is also subjected to heat conduction with the titanium horn, on which the specimen is clamped during the tests using a small piece of steel. The temperature of the horn remains fairly close to the room temperature during the test.

The piezoelectric fatigue machine used to perform the fatigue tests is designed according to [Bathias and Paris,2005]. The vibratory fatigue system illustrated in Fig. 22 is made of several elements. The first one is the generator that can reach a power of 2 $kW$ and whose frequency is tuned between 19.5 $kHz$ and 20.5 $kHz$. It gives a sinusoidal signal to the converter, which produces vibrations. The function of this latter is to turn electric vibrations into mechanical ones. Moreover, an amplifier called

"booster" increases or decreases (1.5 times) the displacement of the converter. At last, a horn made of a cylindrical part followed by a cone-shaped profile section completes the equipment. As the displacement amplitude of the system (converter and booster) is limited, the cone allows to increase the vibratory amplitude of the specimen in order to reach the required stress. The specimen is screwed to the horn and its bottom extremity is stress-free. A calibration of the setup is needed to set the required stress. It consists of finding a linear relation existing between control voltage and displacement amplitude of the horn/specimen's boundary. This latter is measured by a laser sensor.

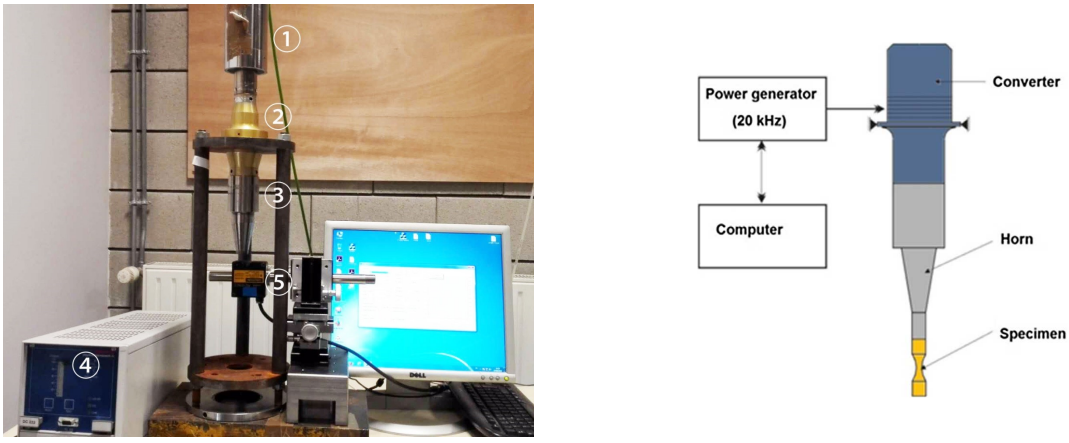


**Fig. 22:** (a) On the left: Components of the fatigue testing machine: 1) converter, 2) amplifier, 3) horn, 4) generator, 5) laser sensor, (b) On the right: Illustration corresponding to the testing machine

Thermography detection was performed using an infrared FLIR A325sc camera. This is a microbolometer-based camera with a $320 \times 240$ detector and a thermal resolution (noise equivalent temperature difference, NETD) of 0.1 $^oC$. It is the mean used to measure the surface temperature of the specimen at different intervals of time $t$. During the tests, the lens axis of the camera was kept fixed and perpendicular to the surface of the specimen. The adopted spatial resolution enables us to observe the central gauge part of the specimen. The frame-rate of the IR camera is 3.75 pictures per second (i.e. sampling frequency $f_{IR} = 3.75\ Hz$).

### 3.3.2 Experimental results

Pictures provided by the camera between $t_i = 0\ s$ and $t_f = 3\ min\ 46.366\ s$ are presently processed in order to compute dissipation and temperature evolution during this interval of time corresponding to $\approx 45 \times 10^5$ cycles to illustrate the methodology. We must note that $t_i$ and $t_f$ are chosen in such a way that a large temporal variation of temperature can been observed.

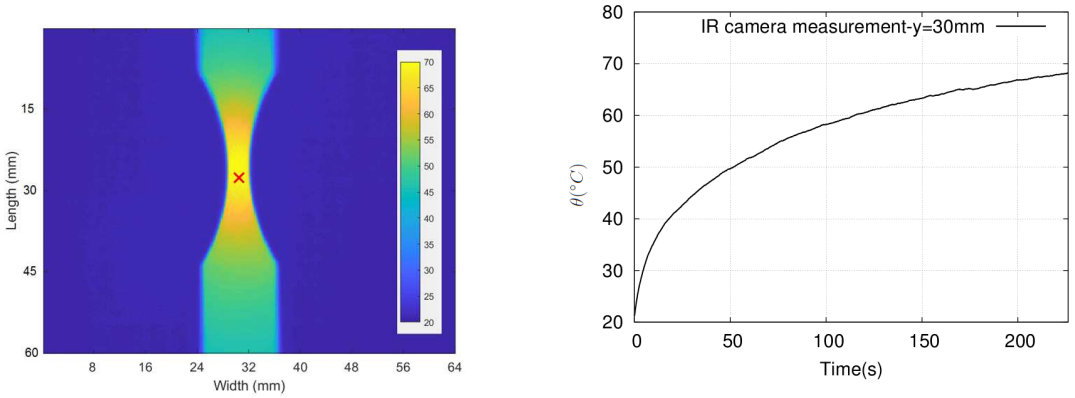


**Fig. 23:** (a) On the left: Example of an infrared picture taken by the IR camera at a time $t$, (b) On the right: Evolution of the measured specimen temperature $\theta(t)$ at a surface point located around its center as function of the time (red cross in left figure)

At each time step, we obtain a 2D cartography showing the distribution of temperature as illustrated in Fig. 23(a). On each picture obtained at a time step, the high and low parts of the specimen are cut for further data treatment. Furthermore, the specimen is connected to the horn at the top, consequently the temperature profile at the center of the specimen is slightly asymmetrical, due to the heat conduction with the horn. The obtained map of temperature of the sample surface will further be used as a reference for comparison with the spacetime simulations. The sequence of the maps through the time enables to deduce the evolution of the temperature at each point of the specimen through the time. Fig. 23(b) shows the evolution of the measured specimen temperature $\theta(t)$ at a surface point located around its center as function of the time.

### 3.3.3 Newtonian self-heating modeling for parameters identification

The spacetime simulations require to have input parameters. The latter should be related as close as possible to the experimented systems. Specific experiments could be used for such identifications of parameters, but we choose to deduce them from the one presented in section 3.3.2. For the identification process, we propose to test the following hypothesis: identification can be done by use of classical thermomechanical modeling with less accuracy than the spacetime simulations; in other words, identification can be performed with very simple modeling with rough approximation because of the material features (thermal diffusivity is small) and geometric dimensions (thickness $\ll$ width $\ll$ length).

It enables to propose the use of a spacetime approach only for numerical simulations. Therefore, we will only consider Newtonian approaches for identification process, with simplified equations. The aim is eventually to test the robustness of the process: how simple identifications influence the spacetime simulations in terms of accuracy and reliability?
Whatever the modeling is, its error due to a lack of causality is negligible providing that the sampling of the experimental results is less than $10^5\,kHz$ calculated by a Cattaneo time of $10ns$ [Ván et al.,2013] for the studied material, as previously explained in section 1.6. However, other errors due to modelling or calculating can occur that may require to use spacetime simulations as further demonstrated.

All material parameters are also supposed to be temperature-independent in the temperature range of the tests $[0; 100\ °C]$, whatever the temperature variations induced by fatigue test are. As a consequence, thermal diffusivity, mass density and specific heat capacity are not affected and remain constant.

In addition to that, in order to simplify the heat conduction models, many assumptions are usually made about the type of the heat flux diffusing through the specimen dimensions. The result of these assumptions leads to different methods of computation (designated as 2D, 1D or 0D method) [Favier et al.,2016,

Chrysochoos et al.,2009, Boulanger et al.,2004] as illustrated in Fig. 24. In particular, given the small thickness, the temperature can be considered constant through the thickness; it can be checked by calculating the Biot number ($Bi \approx 5.10^{-4} << 1$). Moreover, the 2D method will not be further used, considering that the variations of temperature along the width of the specimen are negligible compared to the variations along its length. We only propose to test the 1D and 0D methods.

The implementation of these methods requires a spatial averaging process: for a field $X(x_N)$, one can calculate its averaged value on coordinate $x_N$ as $\bar{X} = \frac{1}{L_N}\int X(x_N)dx_N$ where $L_N$ is the length of the spatial domain for the considered coordinate/direction.

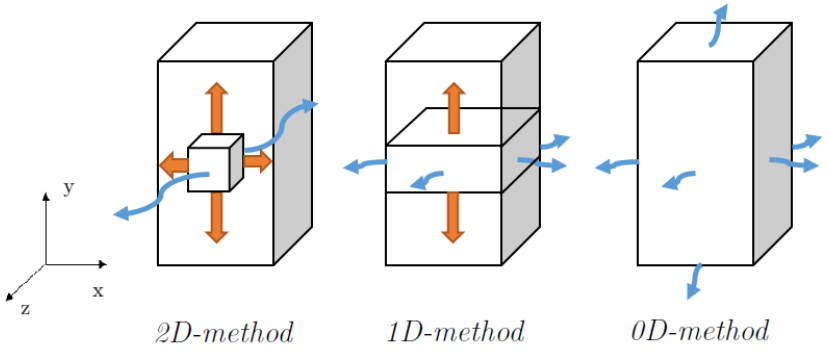


**Fig. 24:** Illustration of the 2D, 1D or 0D methods of computation for the heat transfers models

Two parameters are used in the different models. A characteristic time $\tau_{ND}$ with $N$ depending on the dimension of the modeling is first introduced. This parameter characterizes the thermal inertia related to heat conduction along the averaged directions and balanced at boundaries by heat convection flux. This parameter is theoretically and possibly related to thermophysical quantities $\widetilde{\rho_c}\mathcal{C}_{m\omega}$, heat convection flux $h$ and radiation out the surface. A heat source term $\frac{d_1}{\widetilde{\rho_c}\mathcal{C}_{m\omega}}$ is also considered. This parameter characterizes the intrinsic dissipation related to the mechanical power dissipated by irreversible processes within the material through thermomechanical couplings. With a Newtonian approach for elastoplastic behavior, it can be calculated with $d_1 = \sigma : \dot{\varepsilon} - \widetilde{\rho_c}\sum_i \frac{\partial \psi}{\partial \alpha_i}\dot{\alpha_i}$ with $\sigma$ the stress tensor, $\dot{\varepsilon}$ the strain rate tensor, $\alpha_i$ the internal states variables other than temperature or total strain, and $\psi$ the specific free energy [Chrysochoos and Louche,2000].

#### 3.3.3.1 The 2D method

In this method, we assume that the variations of temperature are negligible through the thickness of the specimen. This hypothesis allows reducing the 3D problem to a 2D problem. Consequently, this method is called the 2D method. It allows working with the surface temperature fields as those provided by an IR thermographic device, assuming that these surface temperature fields are representative of the average temperature through the thickness [Blanche,2015]. A Newtonian approach can be proposed [Chrysochoos and Louche,2000] to obtain the corresponding heat equation as following:

$$\frac{\partial \bar{\theta_d}(x,y,t)}{\partial t} + \frac{\bar{\theta_d}(x,y,t)}{\tau_{2D}(y)} - a\left(\frac{\partial^2 \bar{\theta_d}(x,y,t)}{\partial x^2} + \frac{\partial^2 \bar{\theta_d}(x,y,t)}{\partial y^2}\right) = \frac{\bar{d_1}(x,y,t)}{\widetilde{\rho_c}\mathcal{C}_{m\omega}} \tag{3.1}$$

where: $\bar{\theta_d} = \bar{\theta} - \theta_0$ is the average difference between the specimen temperature and the room temperature (assumed to be independent of time and space, and equal to the initial temperature of the specimen). The average, denoted here by the "bar", is made in this case over the thickness ($z$ direction). $\tau_{2D}$ is the time parameter characterizing the heat transfer perpendicular to the direction of heat conduction flux. It is

worth noting that it may be function of the length $y$; it would be linked to the variation of the thickness of the specimen through the length. In this case, it characterizes the heat transfer through the $z$ direction. $\frac{\bar{d}_1(x,y,t)}{\widetilde{\rho_c}\mathcal{C}_{m\omega}}$ is the average intrinsic dissipation term over the thickness.

A computation of heat sources using the 2D-method can be found in [Benaarbia et al.,2016]. Moreover, [Benaarbia et al.,2014, Berthel,2007] develop extensively imaging techniques (i.e. infrared thermography (IR) and digital image correlation (DIC)) related to the use of this method.

#### 3.3.3.2 The 1D method

In this method, we assume that the variations of temperature are negligible/not considered through the thickness and the width of the specimen. This hypothesis allows reducing the 3D problem to a 1D problem. Consequently, this method is called the 1D method. It allows working with the surface temperature fields as those provided by an IR thermographic device. A Newtonian approach can be proposed [Chrysochoos and Louche,2000] to obtain the corresponding heat equation as following:

$$\frac{\partial \bar{\bar{\theta}}_d(y,t)}{\partial t} + \frac{\bar{\bar{\theta}}_d(y,t)}{\tau_{1D}(y)} - a\left(\frac{\partial^2 \bar{\bar{\theta}}_d(y,t)}{\partial y^2}\right) = \frac{\bar{\bar{d}}_1(y,t)}{\widetilde{\rho_c}\mathcal{C}_{m\omega}} \tag{3.2}$$

where: $\bar{\bar{\theta}}_d = \bar{\bar{\theta}} - \theta_0$ is the average difference between the specimen temperature and the room temperature (assumed to be independent of time and space, and equal to the initial temperature of the specimen). The average, denoted here by the "double bar", is made in this case over the thickness ($z$ direction) and the width ($x$ direction). $\tau_{1D}$ is the time parameter characterizing the heat transfer perpendicular to the direction of heat conduction flux. In this case, it characterizes the heat transfer through the $x$ and $z$ directions. $\frac{\bar{\bar{d}}_1(y,t)}{\widetilde{\rho_c}\mathcal{C}_{m\omega}}$ is the average intrinsic dissipation term over the thickness and the width corresponding to self-heating. The described 1D method takes less time of treatment of the fatigue tests than the 2D method, while generally ensuring accurate results.

#### 3.3.3.3 The 0D method

In this method, we assume that the variations of temperature are negligible/not considered through the thickness, length and width of the specimen. This hypothesis allows reducing the 3D problem to a 0D problem. Consequently, this method is called the 0D method. It allows working with the surface temperature fields as those provided by an IR thermographic device. A Newtonian approach can be proposed [Chrysochoos and Louche,2000] to obtain the corresponding heat equation as following:

$$\frac{\partial \bar{\bar{\theta}}_d(t)}{\partial t} + \frac{\bar{\bar{\theta}}_d(t)}{\tau_{0D}} = \frac{\bar{\bar{d}}_1(t)}{\widetilde{\rho_c}\mathcal{C}_{m\omega}} \tag{3.3}$$

where: $\bar{\bar{\theta}}_d = \bar{\bar{\theta}} - \theta_0$ is the difference between the average specimen temperature and the room temperature (assumed to be independent of time and space, and equal to the initial temperature of the specimen). The average is made in this case over the thickness ($z$ direction), the width ($x$ direction) and the length ($y$ direction). We note the averaged quantities in this case by the "triple bar". $\frac{\bar{\bar{d}}_1(t)}{\widetilde{\rho_c}\mathcal{C}_{m\omega}}$ is the average dissipation term over the thickness, the length and the width corresponding to self-heating. $\tau_{0D}$ is the time parameter characterizing the heat transfer perpendicular to the direction of heat conduction flux. In this case, it characterizes the heat transfer through all the spatial directions.

For Eq. 3.3, in the case of constant value for $\frac{\bar{\bar{d}}_1}{\widetilde{\rho_c}\mathcal{C}_{m\omega}}$ and for initial conditions $\bar{\bar{\theta}}_d(t_i) = 0$, the analytical solution is (for initial time $t_i = 0$):

$$\bar{\bar{\theta}}_d(t) = \frac{\bar{\bar{d}}_1}{\widetilde{\rho_c}\mathcal{C}_{m\omega}}\tau_{0D}\left(1 - \exp\left(-\frac{t}{\tau_{0D}}\right)\right) \tag{3.4}$$

### 3.3.4 Data treatment methods for parameters identification

In addition to the thermophysical parameters (table 9), several parameters are required for further calculations and comparison, such as the time parameter $\tau_{ND}$, with $N = 0, 1$ and the dissipation term $\frac{d_1}{\widetilde{\rho_c}\mathcal{C}_{m\omega}}$, that is now noted $f_r$ for simplification/convenience. In order to identify these parameters, several methods are presently investigated by use of the 0D or 1D method (presented in section 3.3.3).

Average is performed on experimental data by considering spatial averaging as previously defined in section 3.3.3, either on two or three directions. It is applied to temperature $\theta_d$ or to intrinsic dissipation $d_1$ for Newtonian computation:

- To apply the 0D method, the maps of surface temperature obtained at each time step by the IR camera are thus subjected to temperature averaging through the width and length. The result is a temperature field only function of time $\overline{\overline{\theta}}(t)$. The averaged difference between the specimen temperature $\overline{\overline{\theta}}(t)$ and its surrounding temperature leads to $\overline{\overline{\theta}}_d(t)$.
- When 1D method is considered, then only an average of surface temperature through the width is performed. The result is a temperature field function of space and time $\overline{\theta}(y,t)$. The averaged difference between the specimen temperature $\overline{\theta}(y,t)$ and its surrounding temperature leads to $\overline{\theta}_d(y,t)$.

For both models, 1D and 0D, it is reminded that the surface temperature measured by the camera can be considered as the mean temperature through the specimen thickness ($Bi \ll 1$).

| $f_r$ **identification** | **global optimization** | **global optimization** | **local calculation** |
|---|---|---|---|
| $\tau_{ND}$ identification | calculation from $h$ | global optimization | global optimization * |
| 0D method | Meth. A | Meth. B | Meth. C |
| 1D method | × | × | Meth. D |

**Tab. 10:** Features of the different methods to identify $\tau_{ND}$ and $f_r$ (* for method C, it is used from method B; whereas for method D, it is simultaneous)

The different methods and their features are summarized in Table 10, then detailed in the different next paragraphs.

#### 3.3.4.1 Method A: use of the 0D method and parameters identification by calculation of $\tau_{0D}$ and global optimization of $f_r$

- First, identification of the time parameter $\tau_{0D}$
  The time parameter is directly computed using its definition: it is the constant characterizing the perpendicular heat exchanges through the specimen. It is demonstrated that it corresponds to the approximation [Chrysochoos and Louche,2000]: $\tau_{0D} \approx \frac{\widetilde{\rho_c}\mathcal{C}_{m\omega}e_s}{2h} \approx 123\ s$ if losses by radiation are neglected. $e_s = 1\ mm$ is the specimen thickness and $h = 15\ W.m^{-2}.K^{-1}$ is the heat transfer coefficient for natural convection. The latter value is evaluated from bibliography for similar experimental conditions. However, the hypothesis of natural convection and the uncertainty on the heat transfer coefficient lead to a significant uncertainty on the $\tau_{0D}$ value (as discussed in section 3.3.5). For this reason, further methods are also studied in order to obtain this time parameter with more accuracy.
- Second, identification of the dissipation term $f_r$ assumed as constant
  Assuming that the time parameter is known from the previous step, the solution of Eq. 3.3 , given by

Eq. 3.4, is:

$$\overline{\overline{\theta}}_{d(sol)}(t, c_1) = c_1\ \tau_{0D}\left(1 - \exp\left(-\frac{t}{\tau_{0D}}\right)\right) \tag{3.5}$$

In Eq. 3.5, parameter $c_1$ is a priori unknown. So we optimize a functional to this parameter to obtain the less distance between the experimental data and the solution given by Eq. 3.5:

$$c_1 = Inf_k\left(\sum_j \left\{\overline{\overline{\theta}}_{d(sol)}(t_j, c_{1k}) - \overline{\overline{\theta}}_{d(exp)}(t_j)\right\}^2\right) \tag{3.6}$$

The optimization process has been programmed with Matlab by using the "fminsearch" function of Matlab toolbox to get a local minimum of the function. This is a nonlinear programming solver that searches for the minimum of a problem. This function strongly depends on the initial value of the iteration process, that is why we have systematically tested different initial values to be sure to obtain the same minimum, which thus becomes global (in the tested range). By plotting the error function (see Fig. 25(a)), we can also check that this minimum is global (in the tested range). The error function for this method shows a narrow minimum for the dissipation term. The value obtained for $c_1 = f_r$ is 0.34825 $°C.s^{-1}$.

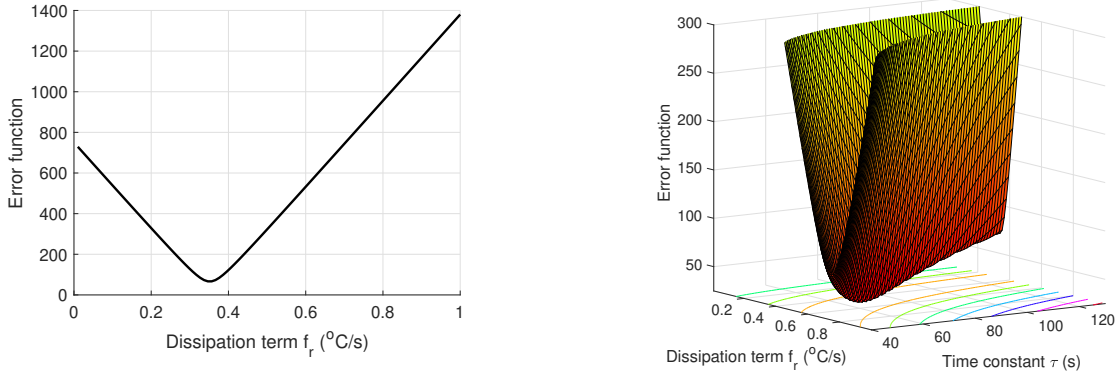


**Fig. 25:** On the left: a) Error function $\sum_j \left\{\overline{\overline{\theta}}_{d(sol)}(t_j, c_1) - \overline{\overline{\theta}}_{d(exp)}(t_j)\right\}^2$ obtained from method A as function of $c_1 = f_r$ in the range $[0; 1]C.s^{-1}$. On the right: b) Error function $\sum_j \left\{\overline{\overline{\theta}}_{d(sol)}(t_j, c_1, c_2) - \overline{\overline{\theta}}_{d(exp)}(t_j)\right\}^2$ obtained from method B as function of $c_1 = f_r$ in the range $[0; 1]\ C.s^{-1}$ and of $c_2 = \tau_{0D}$ in the range $[40; 130]\ s$

#### 3.3.4.2 Method B: use of the 0D method and parameters identification by simultaneous and global optimization of $\tau_{0D}$ and $f_r$

We consider here that both parameters are unknown and should be simultaneously optimized. The solution of Eq. 3.3 , given by Eq. 3.4, is:

$$\overline{\overline{\theta}}_{d(sol)}(t, c_1, c_2) = c_1\ c_2\left(1 - \exp\left(-\frac{t}{c_2}\right)\right) \tag{3.7}$$

In Eq. 3.7, parameters $c_1$ and $c_2$ are a priori unknown. So we optimize a functional to these parameters to obtain the less distance between the experimental data and the solution given by Eq. 3.7:

$$(c_1, c_2) = Inf_{k,m}\left(\sum_j \left\{\overline{\overline{\theta}}_{d(sol)}(t_j, c_{1k}, c_{2m}) - \overline{\overline{\theta}}_{d(exp)}(t_j)\right\}^2\right) \tag{3.8}$$

The optimization process has been also programmed with Matlab by using the "fminsearch" function of Matlab toolbox to get a local minimum of the function, as explained in the previous section. The value obtained for the two parameters are $c_1 = f_r = 0.47519\ °C.s^{-1}$ and $c_2 = \tau_{0D} = 72.73\ s$. The error function for this method is mapped in Fig. 25(b) and shows a narrow minimum for the dissipation term, whereas the minimum for the time parameter is broader, but convergence is ensured.

#### 3.3.4.3 Method C: use of the 0D method and parameters identification by global optimization of $\tau_{0D}$ and local calculation of $f_r$

- First, identification of the time parameter $\tau_{0D}$ assumed as constant
  We choose to use the value optimized from method B, corresponding to $\tau_{0D} = 72.73\ s$.

- Second, identification of the dissipation term $f_r(t)$
  By use of Eq. 3.3, we can directly write:

$$f_r(t) = \frac{d\bar{\bar{\theta}}_{d(exp)}}{dt} + \frac{\bar{\bar{\theta}}_{d(exp)}}{\tau_{0D}} \tag{3.9}$$

  with $\tau_{0D}$ the time parameter chosen in the previous step. The time gradient of temperature is directly computed using mathematical tool of Matlab (numerical derivative by centred finite differences). The injection of this calculation in Eq. 3.9 leads to the evolution of the dissipation term as function of time. The result is shown in Fig. 26. Between $t = t_i = 0$ and $t = t_f$, where $\bar{\bar{\theta}}_d(t)$ varies between 0 and 34.02 $°C$, the value of $f_r$ tends to 0.51 $°C.s^{-1}$. Except at short times, the dissipation term could be roughly considered as constant with time. For further calculations, the full time-dependence of this parameter is considered.

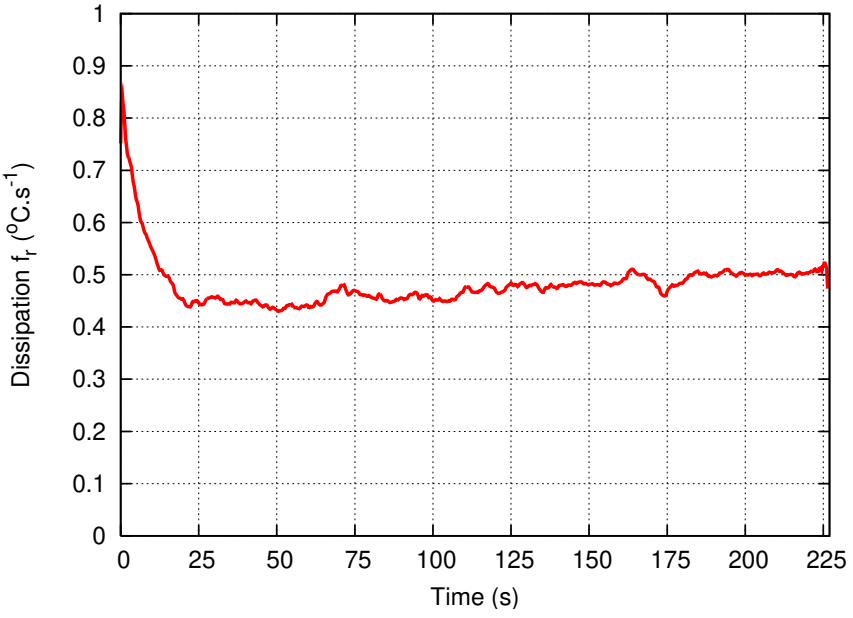


**Fig. 26:** Dissipation $f_r(t) = \frac{\bar{\bar{d}}_1(t)}{\widetilde{\rho_c}\mathcal{C}_{m\omega}}$ varying with time, obtained from method C

#### 3.3.4.4 Method D: use of the 1D method and parameters identification by simultaneous global optimization of $\tau_{1D}$ and local calculation of $f_r$

Since the experimental temperature maps show variations through the length ($y$ direction), it is interesting to compute an identification process using the 1D method for comparison with the previous methods (A, B, C). We then expect more accuracy on the dissipation values and thus on the temperature prediction.

We note that a variation of $\tau_{1D}$ with the length $y$ could also be considered: it would be linked to the variation of the width of the specimen through the length. We neglect this effect in what follows. We assume thus that the value of $\tau_{1D}$ does not depend on the $y$ direction at first approximation. Calculations (not presented here) have been performed to check this assumption, which show that no significant difference occurs.

Moreover, the identification of the time parameter by optimization is relevant but numerical value has to be adapted because of the use of the 1D method. We look thus for simultaneous identification of both the dissipation term $f_r(y,t)$ by local calculation and the time parameter $\tau_{1D}$ as a result of global optimization. By the use of Eq. 3.2, we can write:

$$f_r(y,t,\tau_{1D}) = \frac{\partial \bar{\bar{\theta}}_{d(exp)}}{\partial t} + \frac{\bar{\bar{\theta}}_{d(exp)}}{\tau_{1D}} - a\left(\frac{\partial^2 \bar{\bar{\theta}}_{d(exp)}}{\partial y^2}\right) \tag{3.10}$$

An optimisation process similar to that of methods A and B is implemented to obtain simultaneously the characteristic time $\tau_{1D}$ and the heat source term $f_r(y,t)$:

$$c_2 = Inf_k\left(\sum_i \sum_j \left\{\bar{\bar{\theta}}_{d(sol)}(y_i,t_j,c_{2k},f_r(y_i,t_j,c_{2k})) - \bar{\bar{\theta}}_{d(exp)}(y_i,t_j)\right\}^2\right) \tag{3.11}$$

Unlike previous methods, $f_r$ is a function of $\tau_{1D}$. This function is introduced in the optimisation process by numerically calculating Eq. 3.2 whose numerical solution is denoted $\bar{\bar{\theta}}_{d(sol)}$. The computation process has been programmed with Matlab. The time gradient and the space Laplacian operators in Eq. 3.10 can directly be computed using mathematical tools in Matlab based on finite differences scheme. Because of the derivative in Eq. 3.10, the results for heat dissipation source presents important noise. Consequently, a smooth step is added using moving average filter on dissipation. The result of the calculation is eventually the (smoothed) heat source term $f_r(y,t)$ depending on space and time and the time parameter $c_2 = \tau_{1D} = 43\ s$. The results are presented in Fig. 27. The negative values of $f_r(y,t)$ seen on Fig. 27 b) are due to the noise in experimental data, therefore these values are insignificant.

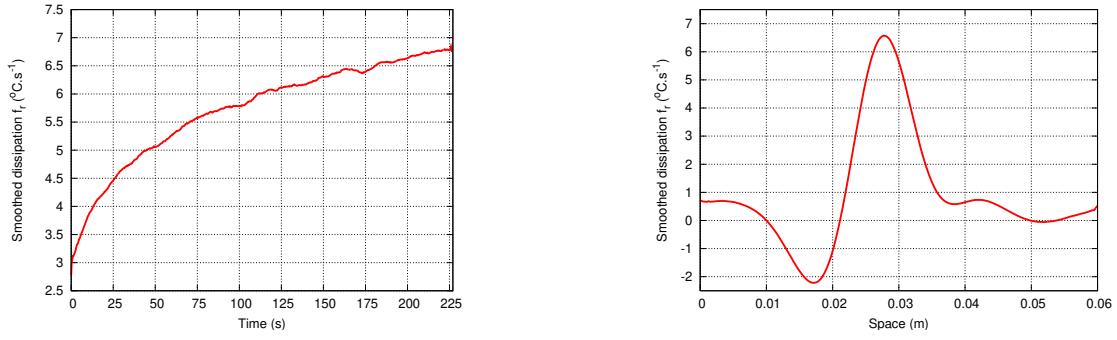


**Fig. 27:** Evolution of $f_r(y,t) = \dfrac{\bar{\bar{d}}_1(y,t)}{\widetilde{\rho_c}\mathcal{C}_{m\omega}}$ obtained from the Newtonian computation (method D): a) On the left, as function of the time at $y = 30\ mm$, b) On the right, as function of the space at $t_f = 226.366\ s$

### 3.3.5 Uncertainties estimation

Uncertainty of the Newtonian thermal model can derive from a lack of knowledge on the thermomechanical parameters, from the error on measurement/sampling (e.g. error on the camera measurements) or from the choice of models [Makowski,2009]. We are looking for the uncertainties of the characteristic time $\Delta\tau_{ND}, N = 0, 1$ and of the intrinsic dissipation $\Delta f_r = \Delta\left(\frac{d_1}{\widetilde{\rho_c}\mathcal{C}_{m\omega}}\right)$. We can divide the types of uncertainty as follows:

- Relative uncertainty on the physical properties of the model as: relative uncertainty on the thermal diffusivity $\frac{\Delta a}{a} = 7\%$, relative uncertainty on the heat convection coefficient $\frac{\Delta h}{h} = 25\%$ and relative uncertainty on the specific heat capacity $\frac{\Delta\mathcal{C}_{m\omega}}{\mathcal{C}_{m\omega}} = 5\%$ [Ogawa et al.,2001, Conner,2013]
- Measurement errors related to the camera features. The uncertainty of the measured temperature is $\Delta\bar{\bar{\theta}}_{d(exp)}(t) = \Delta\bar{\theta}_{d(exp)}(t) = 0.1\ °C$, it is a marked-up value of that given by the manufacturer. The uncertainty on the Laplacian operator of temperature is thus $\Delta\left(\frac{\partial^2\bar{\bar{\theta}}_{d(exp)}}{\partial y^2}\right) = 0.02\left(\frac{\partial^2\bar{\bar{\theta}}_{d(exp)}}{\partial y^2}\right)$; it is deduced from the spatial resolution of the camera and the uncertainty on the measured temperature, but this latter is numerically negligible. Finally, the uncertainty of the camera frequency is assumed to be negligible, thus uncertainty of the time gradient of temperature is supposed to be null: $\Delta\left(\frac{d\bar{\bar{\theta}}_{d(exp)}}{dt}\right) = \Delta\left(\frac{\partial\bar{\bar{\theta}}_{d(exp)}}{\partial t}\right) = 0$

Looking for uncertainties is applicable for the methods A (for $\tau_{0D}$, having a direct consequence on the identification of $f_r$), C (for $f_r$), and D (for $\tau_{1D}$ and $f_r$). For method B with full optimization for both parameters, it is useless to consider.

For method A, because $\tau_{0D} \approx \frac{\widetilde{\rho_c}\mathcal{C}_{m\omega}e_s}{2h}$, we can calculate its relative uncertainty by propagating uncertainties of heat convection coefficient and specific heat capacity according to the GUM recommendation [JCGM,1995], leading to $\frac{\Delta\tau_{0D}}{\tau_{0D}} = 25.5\%$. Even if it is not calculated with the same approach, we can assume the same value for $\frac{\Delta\tau_{1D}}{\tau_{1D}} = 25.5\%$. We notice that the uncertainty is quite important for this parameter. It can be related to the difficulty of its identification as seen for the different methods.

Concerning intrinsic dissipation, it depends on the dimension of the method. For method C (0D), we can calculate the uncertainties by use of Eq. 3.9:

$$\begin{aligned}
\Delta^2 f_r(t) &= \left|\frac{\partial f_r}{\partial\left(\frac{d\bar{\bar{\theta}}_{d(exp)}(t)}{dt}\right)}\right|^2 \Delta^2\left(\frac{d\bar{\bar{\theta}}_{d(exp)}}{dt}\right) + \left|\frac{\partial f_r}{\partial\bar{\bar{\theta}}_{d(exp)}(t)}\right|^2 \Delta^2\bar{\bar{\theta}}_{d(exp)}(t) \\
&\quad + \left|\frac{\partial f_r}{\partial\tau_{0D}}\right|^2 \Delta^2\tau_{0D} \\
\Rightarrow \Delta f_r(t) &= \frac{1}{\tau_{0D}}\sqrt{0.1^2 + 0.255^2\,\bar{\bar{\theta}}^2_{d(exp)}(t)}
\end{aligned} \tag{3.12}$$

Thus $\Delta f_r(t)$ is a function of time. We notice that the uncertainty $\Delta f_r(t)$ varies between 0 and 0.119 $°C.s^{-1}$ for method C, which corresponds to a relative uncertainty $\frac{\Delta f_r(t)}{f_r(t)} \times 100$ varying between 0 and 23.5%. Similarly, the expression for uncertainty of intrinsic dissipation obtained using method D and corresponding

to Eq. 3.10 can be calculated as:

$$\Delta f_r(y,t) = \sqrt{\frac{1}{\tau_{1D}^2}\left(0.1^2 + 0.255^2\,\bar{\bar{\theta}}^2_{d(exp)}(y,t)\right) + (0.02^2 + 0.07^2)\left(a\frac{\partial^2 \bar{\bar{\theta}}_{d(exp)}(y,t)}{\partial y^2}\right)^2} \tag{3.13}$$

Thus $\Delta f_r(y,t)$ is a function of space and time. The uncertainty $\Delta f_r(y,t)$ varies between 0 and 0.497 $°C.s^{-1}$ for method D, which corresponds to a relative uncertainty varying between 0 and 4.43%. We notice that the relative uncertainty of $f_r$ obtained using method D corresponding to the $1D$ model is almost five times smaller than that obtained by using method C corresponding to the $0D$ model. This is due to the additional information on the parameters dependence to spatial length provided by the $1D$ model.

### 3.3.6 Discussion on the results of the parameters identification

We can see that the four previous Newtonian methods lead to different values for $\tau_{ND}, N = 0, 1$ and $f_r$. For the time parameter, the optimization process, used in methods B and C, gives a value (72.73 $s$) approximately two times smaller than the direct calculation by use of its definition (123 $s$), as used in method A. The latter is strongly dependent on the choice for the numerical value of the natural convection coefficient $h$ with a significant uncertainty as proved in section 3.3.5.

In the literature, values of the time parameter are given for similar experiments: In [Boulanger et al.,2004], computations give $\tau_{ND} = 80s$ for a dual phase steel (DP 60) specimen, knowing that its width is 2.5 $mm$. Also experiments for different loadings in [Munier,2012] show that $\tau_{ND}$ is around 36.9 $s$, knowing that the dual phase steel (DP 600) specimen had a width of 3.6 $mm$.

For the heat source term, values for methods A to C are in the range of 0.34825 $°C.s^{-1}$ to 0.8424 $°C.s^{-1}$ (for long times). This is quite consistent with values found in bibliography [Munier,2012] (the heat source value is 0.022 $°C.s^{-1}$ for a variation of temperature of 1.8 $°C$). We see that its evolution with time tends to a constant value, which strongly depends on the type of 0D method used.

Considering thermal diffusivity with a Laplacian term in method D increased the accuracy on the values of the parameters. For self-heating, the heat source term is related to thermomechanical couplings [Boulanger et al.,2004, Lemaitre and Chaboche,1990, Saanouni,2012]. The space variations of $f_r(y,t)$ are directly related to the stress amplitude variations in the sample with the length ($y$ direction). Through the method D, we are then able to take it into account. For a time parameter $\tau_{1D} = 43$ $s$, the heat source term is a function of space and time, reaching a maximum at $f_r(y = 30\ mm, t_f = 226.366\ s) = 11.2\ °C.s^{-1}$ (non-smoothed data).

We remind that even if the identification process does not provide unique and accurate values of $\tau_{ND}, N = 0, 1$ and $f_r$, the introduced discrepancies will enable to test the spacetime simulations and its influence on the numerical results in comparison to experimental results.

## 3.4 Spacetime heat model

### 3.4.1 Spacetime heat equation of the model

The spacetime heat model of self-heating is constructed based on a spacetime Fourier's heat model (Eq. 2.51) with the Neumann-Dirichlet boundary conditions reproducing the fatigue tests conditions. To complete the heat model, we have to take into consideration that it is also subject to external conditions of temperature and heat flux. Therefore comes the necessity of writing the spacetime weak integral form with spacetime Fourier's model of heat conduction in the Neumann-Dirichlet boundary conditions that will be useful for modeling self-heating experiments.

In the particular case of Neumann-Dirichlet boundary conditions, the third and the fifth integrals in Eq. 2.51 can be written as integrals over hypersurfaces using Green-Ostrogradski theorem. The test temperature

$\theta^*$ is supposed to be null at the boundaries $\partial\Omega$. After simplification, the problem is then formulated by:

$$W(\theta,\theta^*) = \int_\Omega \theta^* \frac{\partial\theta}{\partial t}\,\mathrm{d}H_\Omega + \int_\Omega aI^{ij}\frac{\partial\theta^*}{\partial x^i}\frac{\partial\theta}{\partial x^j}\,\mathrm{d}H_\Omega - \int_\Omega \theta^* f_r\,\mathrm{d}H_\Omega + \int_\Omega \theta^*\frac{\theta}{\tau_{ND}}\,\mathrm{d}H_\Omega - \int_{\partial\Omega_q} \theta^*\frac{c\,q^j_{ext}}{\widetilde{\rho_c}\mathcal{C}_{m\omega}}n_j\,\mathrm{d}S_\Omega = 0, \forall\theta^* \tag{3.14}$$

where $I^{ij}$ is the 3D identity matrix. $q^j_{ext}$ is the surface heat flux imposed on the hypersurface $\partial\Omega_q$ in the proper observer and $n_j$ is the normal vector to the 3D surface. We remind that $q^4 = 0$, because the inertial observer is also proper. In the considered approximations (especially without thermomechanical couplings), the variational problem is very similar to the Newtonian one, except for the integral over space volume that is replaced by a spacetime hypervolume.

The last two terms of Eq. 3.14 are related to the boundary condition effect. Indeed, by analogy with the equations in Newtonian approach, an additional term is added to the spacetime formulation. This additional term $\int_\Omega \theta^*\frac{\theta}{\tau_{ND}}\,\mathrm{d}H_\Omega$, which value varies between the 0D, 1D and 2D methods, has to be introduced if some averages are performed to simplify the simulation: it corresponds to the perpendicular heat exchanges. This term is then the result of the averaging of the temperature necessary to the transition to a 2D, 1D or 0D model and which has direct impact on the boundary conditions. In order to place boundary conditions, we define: $\partial\Omega^j = \partial\omega \cup t$ as the space boundaries of the domain and $\partial\Omega^4 = \omega \cup \partial t$ as the time boundaries of the domain, where $\omega$ is the 3D spatial domain of integration.

Then, the boundary conditions of this weak integral form can be divided into boundary conditions on the space and on the time. The first type can be written: $\theta(x^\mu \in \partial\Omega^j) = f_{SC}(x^\mu \in \partial\Omega^j)$, where $f_{SC}$ is the function representing the space boundary conditions. The second type can be written: $\theta(x^\mu \in \partial\Omega^4) = f_{TC}(x^\mu \in \partial\Omega^4)$, where $f_{TC}$ is the function representing the initial time boundary conditions. The only condition required (on the temperature) on the time boundaries is at the initial time since the temperature at the final time has to be calculated by the resolution of the heat diffusion problem (incrementally).

The boundaries where the heat flux and temperature are applied should respect $\partial\Omega_q \cup \partial\Omega_\theta = \partial\Omega$ and $\partial\Omega_q \cap \partial\Omega_\theta = \varnothing$. The boundary conditions in this case are the flux boundary conditions (on $\partial\Omega_q$) represented by the imposed heat flux $q^j_{ext}$ and the temperature boundary conditions (on $\partial\Omega_\theta$).

## 3.5 Self-heating computation using FEniCS project

### 3.5.1 Input data requirement

In this paragraph, we discuss the input data required for the simulations of the self-heating problem by use of weak forms. Data about the material and geometrical dimensions of the specimen must be precised, as well as time parameter, heat source term and boundary conditions. The simulation is based on the resolution of Eq. 3.14.

First, the parameters $a$, $\widetilde{\rho_c}$ and $\mathcal{C}_{m\omega}$ are related to the material corresponding to the studied fatigue tested specimen and are supposed to be known (as given in table 9).

Second, the numerical model is eventually a 1D+1D geometry of dimension $L = 60\ mm$ dedicated for the space (corresponding to the $y$ direction) and $t_f = 226.366\ s$ dedicated for the time. The associated meshing is defined by the number of divisions in the dimensions of space and time respectively: $N_y = N_t = 850$.

Third, for the time parameter $\tau_{ND}$, we will use the different values obtained by the identification methods A to D (see section 3.3.4) to investigate their influence on the calculation.

Fourth, the dissipation term $f_r(x^\mu)$ resulting from the mechanical loading represents the source of heat in the spacetime model. This intrinsic dissipation is computed with values obtained by the different methods A to D illustrated in section 3.3.4 and are also used to investigate their influence on the calculation. In the methods A and B, it is assumed as constant value, which is directly implemented in the 1D+1D simulation.

However, in the methods C and D the result is respectively function of time $f_r(t)$ and function of space and time $f_r(y,t)$. Remind that $\hat{x}_4 = x_4 = ct$ such that expressing a function with $t$ or $x^4$ is equivalent.

#### 3.5.1.1 Boundary conditions

Since the specimen is clamped to the horn from one side and free from the other side, a Neumann condition on the upper spatial boundary of the specimen represents the conductive flux through the horn and a Neumann condition on the other spatial boundary represents the convective heat flux, on the external surfaces. The boundaries of the specimen where the conductive heat flux and the convective heat flux are applied, are represented in Figure 28.

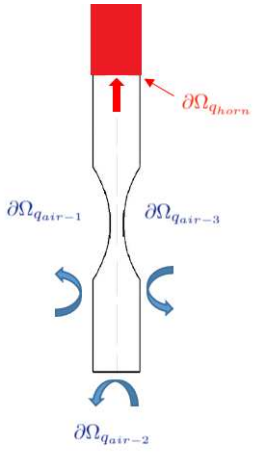


**Fig. 28:** Boundaries of the specimen where the conductive heat flux and the convective heat flux are applied. The red part represents the horn..

In the present experiment, the flux of heat due to the existence of the horn holding the specimen depends on time. It can be obtained by the computation of $c\ q^y_{horn}(t) = -\lambda \dfrac{\partial \bar{\bar{\theta}}_d}{\partial y}$ at $y = 0$, applied on $\partial\Omega_{q_{horn}}$. The conductive heat flux direction is from the specimen (the hot body) to the horn. According to the experimental results, identification of this function leads to $\dfrac{c\ q^y_{horn}(t)}{\widetilde{\rho}_c \mathcal{C}_{m\omega}} = -0.0035 + 0.004\ \exp(-0.01752t)$ $(°C.m.s^{-1})$.

Calculations to study the influence of this flux on the influence of temperature distribution have been performed. Results show a negligible effect. Therefore, it can be neglected in the further simulations.

The other spatial boundary is subjected to a Neumann condition representing the thermal exchange (convection flux) with the surrounding environment at the lower spatial boundary. Since the convection coefficient of the surrounding air is not directly measured in the experiment, it can be approximated using: $h \approx \dfrac{\widetilde{\rho}_c \mathcal{C}_{m\omega} e_s}{2\tau_{ND}}$. The boundary condition in this case is a convection flux at $y = L$, applied on $\partial\Omega_{q_{air}}$ with $c\ q^y_{air}(t) = h\ \bar{\bar{\theta}}_d$. A Dirichlet boundary condition defines the temperature at the initial time. It represents the initial state of temperature at $t = t_i = 0$. It can be expressed by $\forall y, \bar{\bar{\theta}}_d(y, t = 0) = 0$.

The mathematical problem to be solved is thus as follows with the unknown function $\bar{\bar{\theta}}_d(x^\mu) = \bar{\bar{\theta}}_d(y,t)$:

$$\begin{aligned} W(\bar{\bar{\theta}}_d, \theta^*) \quad = \quad & \int_\Omega \theta^* \frac{\partial \bar{\bar{\theta}}_d}{\partial t} \, \mathrm{d}H_\Omega + \int_\Omega a \frac{\partial \theta^*}{\partial y} \frac{\partial \bar{\bar{\theta}}_d}{\partial y} \, \mathrm{d}H_\Omega - \int_\Omega \theta^* f_r(x^\mu) \, \mathrm{d}H_\Omega \\ & + \int_\Omega \theta^* \frac{\bar{\bar{\theta}}_d}{\tau_{ND}} \, \mathrm{d}H_\Omega - \int_{\partial\Omega_{q_{horn}}} \theta^* \frac{c \, q^y_{horn}(t)}{\widetilde{\rho_c \mathcal{C}}_{m\omega}} \, \mathrm{d}S_\Omega \\ & - \int_{\partial\Omega_{q_{air}}} \theta^* \frac{c \, q^y_{air}(t)}{\widetilde{\rho_c \mathcal{C}}_{m\omega}} \, \mathrm{d}S_\Omega = 0, \forall \theta^* \end{aligned} \tag{3.15}$$

$$\text{and} \qquad \forall y \in [0; L], \ \bar{\bar{\theta}}_d(x^\mu \in \partial\Omega^4) = f_{TC}(y, t=0) = 0 \tag{3.16}$$

$$\text{and} \qquad \forall t \in [0; t_f], \ c \, q^y_{horn}(t) = 0 \tag{3.17}$$

$$\text{and} \qquad \forall t \in [0; t_f], \ c \, q^y_{air}(t) = h \, \bar{\bar{\theta}}_d(y = L, t) \tag{3.18}$$

#### 3.5.1.2 Review of the numerical approach

To sum up, as follows the spacetime numerical approach is based on:

- the parameter identifications methods ($f_r$ and $\tau_{ND}$) obtained from different identification methods using the experimental results fatigue tests
- the choice of the spacetime method (in this case the 1D+1D method) corresponding to the weak integral form given by Eq. 3.15
- the different system parameters: material and geometry of the specimen, the boundary conditions expressed by Dirichlet conditions and Neumann conditions with flux terms in the weak integral form of the problem, the IR camera frequency and the loading frequency. These last two parameters allow the computation of the total time, and the time step which are input parameters of the numerical simulation.

Figure 29 describes briefly the procedure used in 1D+1D modeling of self-heating in this chapter. The parameters in red are computed using the experimental data.

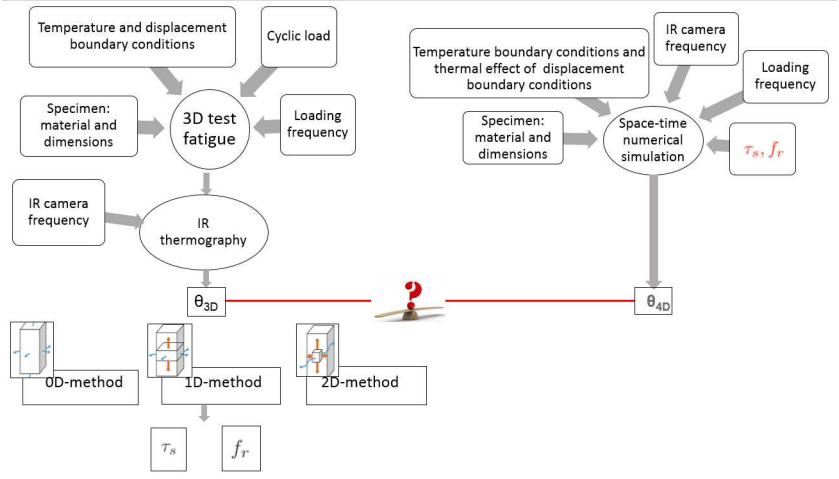


**Fig. 29:** Scheme resuming the spacetime modeling of self-heating

### 3.5.2 Simulation results

#### 3.5.2.1 Influence of the identification process with 0D methods (A,B,C)

In section 3.3.4, 3 different identification methods are discussed using the Newtonian 0D method. The results of these methods are 3 different sets of the time parameter and dissipation term. The latter is either constant $f_r$ or slightly varying with time $f_r(t)$ (see in Fig. 26). In the latter, the prediction of temperature using a spacetime model is consequently more accurate. The implementation of these sets on the 1D+1D FEniCS script gives maps of temperature function of space and time. From this spacetime simulation, we can then compute the average of temperature through the dimension of space used in the model ($y$ direction); for this computation, we use a sampling step of 2 time divisions and then compute the average over these steps. Consequently we can compare this average to the average of temperature through the space obtained from experimental data. Results of this comparison are shown in Fig. 30.

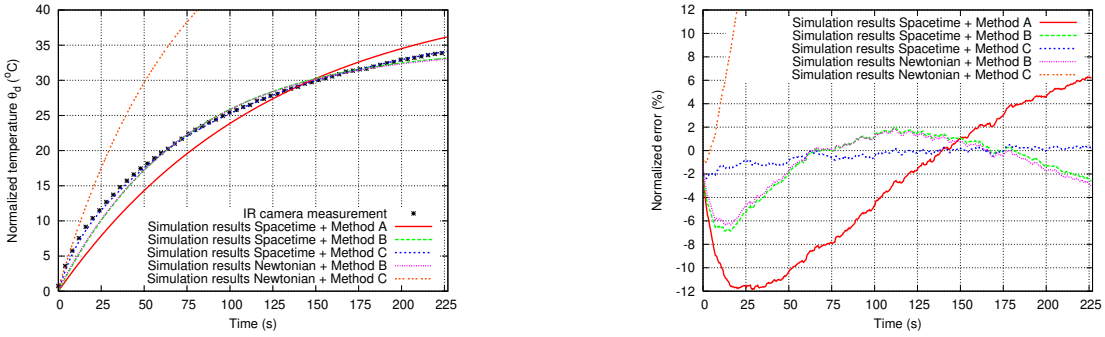


**Fig. 30:** On the left: a) Evolution of $\overline{\overline{\theta}}_d(t)$ obtained from experimental measurements and from the different spacetime simulations as function of the time. On the right: b) Evolution of the relative error, between $\overline{\overline{\theta}}_d(t)$ obtained from experimental measurements and from the different spacetime simulations compared to the maximum value of temperature over the time, as function of the time

A quantitative study between the spacetime simulation results and the experimental data shows their compatibility, as presented in Fig. 30. Graphs of variation of $\overline{\overline{\theta}}_d(t)$ through the time obtained by different methods show a similar behavior trend in the studied time interval, for the different sets of input parameters values. For method C, where considering time evolution of the dissipation term, graph of the simulation results and the experimental results nearly superimpose in the studied time interval. This superposition shows that temperatures resulting from self-heating computed with the spacetime approach are close to those experimentally measured. This consequently validates the spacetime approach in the modeling of self-heating for space-averaged temperatures varying with time, providing that the temporal dynamic of the dissipation term is accurate enough.

The slight differences seen in Fig. 30(a) are surveyed by computation of the model error. The relative error is computed by finding the difference between $\overline{\overline{\theta}}_d(t)_{(exp)}$ obtained from experimental measurements and $\overline{\overline{\theta}}_d(t)_{(simu)}$ obtained from the different spacetime simulations compared to the maximum value of temperature over the time, as:

$$\%\text{relative error}(t) = 100 \times \left( \frac{\overline{\overline{\theta}}_d(t)_{(exp)} - \overline{\overline{\theta}}_d(t)_{(simu)}}{max(\overline{\overline{\theta}}_{d(exp)})} \right) \tag{3.19}$$

The relative error is always less than 12% (in absolute value). This relative error (in absolute value) of modeling is roughly maximum at the beginning and is decreasing with time and for method C tends toward zero for the steady-state temperature. For method C, the error is less than 2% (in absolute value). Whatever the method, the error is mainly due to the step of identification. Its evolution with time at long times for

method A and B should be related to the final value of temperature calculated for those methods. The final value of temperature (for $t \to \infty$) is different for the different methods. The error increases outside of the studied time interval, especially for method A and B. It means that a better identification for methods A and B (global optimization with time) could be obtained with more experimental points beyond the final time $t_f$ that would lead to a better fitting at long times, and thus would reduce the relative error at long times. At the contrary, method C does not depend on additional points at long times (local calculation with time of $f_r$), providing that the time parameter is correctly fitted. According to these results, averaging the temperature in the 3 directions of space is relevant when studying only the time dynamics of the temperature of self-heating through numerical simulations. Eventually, the identification method C seems to be more adapted to provide the most accurate input parameters in the studied time interval.

We can also compare the results of the 1D+1D simulation performed with a spacetime model with the 1D simulation performed with a Newtonian model, which has the same input parameters as obtained in sections 3.3.4.2 or 3.3.4.3. The evolution of temperature through time obtained from these two models for a given method can then be compared. The relative error of the Newtonian model can also be obtained using Eq. 3.19. When comparing simulation obtained with method B, the temperature values are almost similar (magenta to green lines). The calculation with Newtonian or spacetime approach are thus similar in the case of constant input parameters. However, when considering method C that is more accurate in terms of the dissipation term, because time-dependent, the Newtonian numerical scheme (finite difference in time) is not relevant for calculation of the distribution of temperature compared to the spacetime numerical scheme (blue to orange lines). It proves the interest of the spacetime approach for the temperature evolution in a self-heating system, from a numerical point of view.

#### 3.5.2.2 Influence of the identification process with 1D method (D)

Moreover, simulations based on data from method D corresponding to the Newtonian 1D method have been also performed. Figs.31 present respectively the comparison of the evolution of $\bar{\bar{\theta}}_d(y,t)$ as function of the time at different positions $y = \frac{L}{2} = 30\ mm$ and $y = 9\ mm$, and the evolution of $\bar{\bar{\theta}}_d(y,t)$ as function of the space at different times $t = 147.36\ s$ and $t = t_f = 226.366\ s$. Graphs present similar trends showing that the simulation results are close to the experimental ones. Furthermore, the relative model error is studied and plotted in Figs.32. The relative error in this case is computed by finding the difference between $\bar{\bar{\theta}}_d(y,t)_{(exp)}$ obtained from experimental measurements and $\bar{\bar{\theta}}_d(y,t)_{(simu)}$ obtained from the different spacetime simulations compared to the maximum value of temperature over the time and space, as:

$$\%\text{relative error}(y,t) = 100 \times \left( \frac{\bar{\bar{\theta}}_d(y,t)_{(exp)} - \bar{\bar{\theta}}_d(y,t)_{(simu)}}{max(\bar{\bar{\theta}}_{d(exp)})} \right) \tag{3.20}$$

The evolution of the relative error as function of the time shows a peak (around 8.5% in absolute value) at the beginning of the experiment then decreases and tends to a roughly constant value (less than 3%). However, its evolution as function of the space shows a different behavior with oscillations. The error value is less than 5% whatever the time is (in absolute value). It means that the spacetime simulation is relevant for modeling the space and time variations of temperature. However, its accuracy strongly depends on the input parameters accuracy and on the choices performed during the identification step.

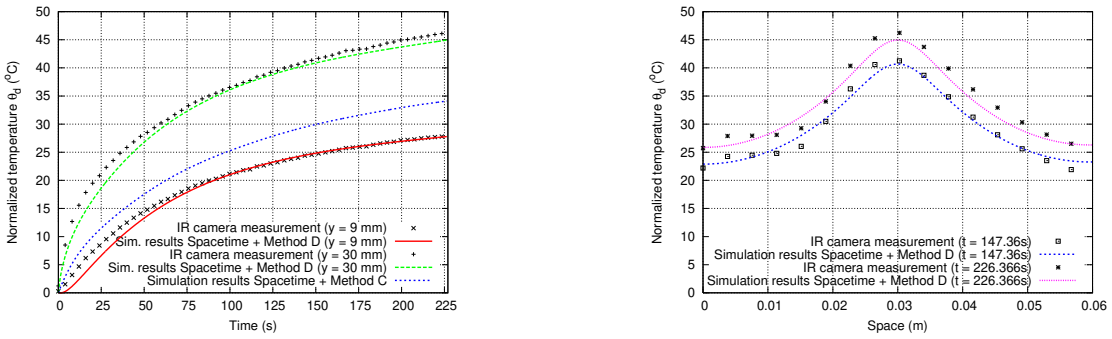


**Fig. 31:** On the left: a) Evolution of $\bar{\bar{\theta}}_d(t)$ obtained from experimental measurements and from the spacetime simulation based on method D as function of the time at different positions. On the right: b) Evolution of $\bar{\bar{\theta}}_d(y)$ obtained from experimental measurements and from the spacetime simulation based on method D as function of space at different times

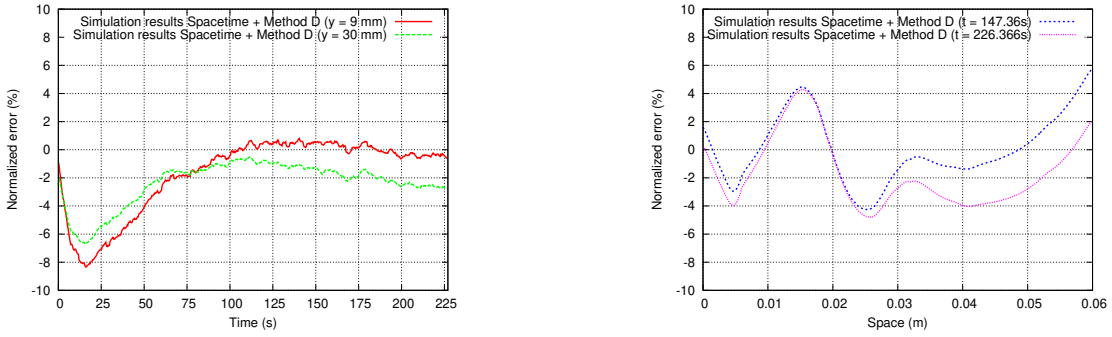


**Fig. 32:** On the left: a) Evolution of the relative error between $\bar{\bar{\theta}}_d(t)$ obtained from experimental measurements and from spacetime simulation using method D compared to the maximum value of temperature as function of the time at different positions. On the right: b) Evolution of the relative error between $\bar{\bar{\theta}}_d(y)$ obtained from experimental measurements and from the spacetime simulation using method D compared to the maximum value of temperature as function of space at different times

We also highlight from the results of Fig. 31 the influence of the variability of the input parameters especially the dissipation $f_r$ on the results of the simulations. In other words, we are studying the influence on the simulation results of the choice of the Newtonian identification method leading either to $f_r(t)$ (method C) or to $f_r(y,t)$ (method D). By comparing the time evolution of $\bar{\bar{\theta}}_d(y,t)$ and $\bar{\bar{\theta}}_d(t)$ at $y = 30\ mm$ (geometric center of the specimen) obtained from FEniCS spacetime simulations with the evolution obtained from experimental measurements, it can be noticed that a significantly better agreement is found when using parameters values from method D in spacetime simulation than from method C.

#### 3.5.2.3 Sensibility to the thermal diffusivity

Another questioning aspect is the importance of the thermal diffusivity in the heat conduction equation. Thus, we aim here at studying the effect of the thermal diffusivity on the time evolution and space distribution of the temperature. We consider respectively values of $a = 13.6 \times 10^{-5}\ m^2.s^{-1}$, $a = 13.6 \times 10^{-6}\ m^2.s^{-1}$ (corresponding to the material used in the experiment) and $a = 13.6 \times 10^{-7}\ m^2.s^{-1}$. Input parameters $\tau_{1D}$ and $f_r$ obtained from method D are used. Evolutions of $\bar{\bar{\theta}}_d(y,t)$ through the time and space obtained from FEniCS spacetime simulations related to different values of thermal diffusivity are reported in Fig. 33. The temperature profiles obtained from experimental measurements are also added into the graphs for comparison.

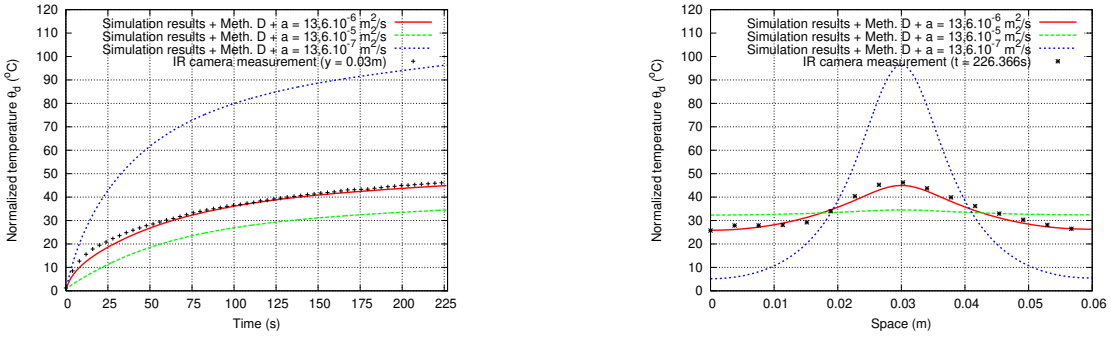


**Fig. 33:** On the left: a) Evolution of $\bar{\bar{\theta}}_d(y = 30mm, t)$ as function of the time obtained respectively from experimental measurements, spacetime simulations using method D for different diffusivities. On the right: b) Evolution of $\bar{\bar{\theta}}_d(y, t = 226.366s)$ as function of the space obtained respectively from experimental measurements, spacetime simulations using method D for different diffusivities

Large discrepancies on the temperature profiles are observed, emphasizing the important role played by the thermal diffusivity in the heat conduction equation. The thermal diffusivity term occurs in the Laplacian term. This term strongly influences the distribution of intrinsic dissipation in the hourglass specimen, which reflects the distribution of stress resulting from the fatigue tests. This conclusion is also supported by the identification step, for which the thermal diffusivity has strong influence on the accuracy when spatial distribution of temperature (method D) is considered. The resulting behaviors are consistent with the heat conduction model's logic: for $a = 13.6 \times 10^{-5}\, m^2/s$, the heat diffuses faster than for $a = 13.6 \times 10^{-6}\, m^2/s$, which leads to lower temperatures at a certain position of the specimen. Similarly, for $a = 13.6 \times 10^{-7}\, m^2/s$ the heat diffuses slower than for $a = 13.6 \times 10^{-6}\, m^2/s$, which leads to higher temperatures at a certain position of the specimen.

Even if the thermal diffusivity of the material is small (compared to other materials), it has a crucial effect on the prediction of the temperature evolution of the specimen. Especially when looking for spatial distribution of the temperature, it has to be taken into account both in the identification step (for an accurate space and time distribution of the heat source term) and in the simulation step.

## 3.6 Conclusions

This chapter investigates the use of the spacetime approach in the modeling of self-heating phenomenon. The self-heating phenomenon occurs particularly during fatigue tests. The mechanical transformation during these tests causes thermal changes and especially dissipation. We investigate the transformation by measurement of the variations of temperature and its analyze for VHCF tests. Indeed, gigacyclic fatigue tests are studied in order to obtain significant values of finite variations of temperature. Consequently we focus on the study of intrinsic dissipation related to self-heating. Data of the resulting variation of temperature have been obtained using an IR camera and then processed with different data treatments.

To compute these variations in a spacetime domain, we require the identification of intrinsic dissipation term and characteristic time parameter. Many methods are possible in order to compute these parameters. We have studied different methods of identification especially for the intrinsic dissipation, either by direct calculation with the Newtonian heat equation or by optimization of an analytic solution in specific cases. The obtained values depending on time and/or space are consistent with bibliography for the studied material (C65 steel). The different methods present slight discrepancies. The heat source term is roughly time independent, but not strictly, when averaged over the space. Its variation with space has also been obtained when considering the 1D method. Such a method provides more information. However, its variation is difficult to deeply analyze in terms of material mechanisms. The trend is directly related to the mechanical loading leading to self-heating for the geometry of the specimen, because of the stress variation along its

length. In fact, the hourglass specimen geometry leads to the stress variation hence to the variation of temperature through the length, since a constant fatigue load is applied on surfaces varying along the length of the specimen.

We have also proposed spacetime variational forms directly adapted for modeling the self-heating. The resulting spacetime simulations from the obtained model give the variations of temperature through space and time, by use of a suitable programming environments (e.g. FEniCS project). In this chapter, we choose to use the 1D+1D method for application to the self-heating. Simulations of the spacetime model have been compared with the experimental data measurements. Results show a good agreement with slight differences deriving from thermal inertia and/or approximation of smoothing of the experimental data (especially $f_r$). Agreement is correct when comparing fully space averaged values of temperature, whatever the identification method is. It means that averaged values of the parameters identified with less accurate model than the one used for simulation are relevant to obtain a further reliable, accurate and quick simulations.

Considering spatial dependence of the dissipation, through the use of thermal diffusivity in the identification step, is also required for a correct description of the temperature variations along the sample length, provided that the spatial boundary condition are realistic enough. More accurate results could be obtained by complexifying the identification step. The effect of thermal diffusivity on the 1D+1D simulations has also directly been studied and shows a strong influence on the results when considering space variation of the temperature and of the heat source term.

The agreement between simulation and experimental results leads to admit the spacetime modeling introduced in the manuscript as a convenient approach to describe the self-heating phenomenon especially when parameters are time dependent. The detailed study of self-heating induced by gigacylic fatigue, in this chapter, is a concrete example. More accuracy could be obtained by modeling the mechanical behavior and adding explicitly the thermomechanical couplings that will be investigated in the following chapters (Chapters 4 and 5). More research could be done in order to provide a complete spacetime approach in modeling self-heating by finding a spacetime method for the parameters identification step.

# Part 2: Modeling of thermo-mechanical behavior in materials

# 4 Bibliographic review on mechanical modeling and illustrations for large deformations

## 4.1 Introduction

In part 1 of the manuscript, spacetime models of heat conduction are developed and applied to a thermal engineering application and a study of self-heating. In this second part, spacetime thermomechanical models will be developed based on the spacetime thermal models already obtained and taking into account the mechanical stress.
In this first chapter of part 2, mechanical models taking into account the large deformation of materials are introduced. A deformation is generally defined as the variation of form (linear/angular length) thus the variation of a scalar product [Sidoroff]. Large deformations are characterized by a difference between the Lagrangian and Eulerian measure of the variables (see section 1.4.4). Geometrical/kinematics non-linearities with respect to the reference configuration are not neglected in this case. Practically, deformations not negligible with respect to 1 are considered as large deformations.

First, the existing mechanical models built in a Newtonian framework are reviewed. Numerical simulations using these models are performed using FEniCS project. The results of the corresponding models will be used for comparison between Newtonian and spacetime models further developed (see chapter 5). The difficulties faced while modeling the mechanical or thermomechanical behaviors of material considering large deformations in a Newtonian framework are then listed: difficulties in modeling non-linear classical behaviors written in rate forms (plasticity, viscosity, large deformations or a combination of non-linearity) and respecting material objectivity (see section 4.3). These problems can be alleviated by means of spacetime thermodynamical modeling. Spacetime models introduced by previous studies are reviewed. In order to overcome the aforementioned problems of the Newtonian models and the existing spacetime models, a spacetime thermodynamical approach will be proposed in the next chapter of this part. It extends the one used in part 1 by taking into account the mechanical stress.

## 4.2 Newtonian thermomechanical models

We first review existing Newtonian mechanical/thermomechanical models built in the classical Newtonian continuum. Among the models, we will focus on the elastic, hyperelastic, thermoelastic and elastoplastic models. In this section, the weak integral forms of these models are written.

### 4.2.1 Strain tensors for small and large deformations

One important parameter in modeling Newtonian behavior is the definition of Newtonian strain. The concept of strain is used to evaluate variation of displacement with respect to a reference length [Belytschko et al.,2006]. The models are developed in cases of small and large deformations which require the introduction of different definitions of strain.

In a specific frame, it is possible to specify the positions of each of the particles of the material body. The coordinates of the particles in the reference configuration are noted $Z^i$, which defines the material or Lagrangian coordinates (see section 1.4.4). After deformation, the current configuration is defined at the current time $t$, with the spatial or Eulerian coordinates $z^i$ (see section 1.4.4). Both the material and spatial configurations are usually expressed using the same frame $(\mathbf{e}_i, \xi^i, t)$. The deformation of the continuum can thus be described using $Z^i$ or $z^i$.

The deformation gradient $F^i_j$ and its inverse $F'^i_j$ can then be defined as:

$$F^i_j = \frac{\partial z^i}{\partial Z^j} \tag{4.1}$$

$$F'^{i}_{j} = \frac{\partial Z^{i}}{\partial z^{j}} \tag{4.2}$$

From this deformation gradient, several strain tensors may then be defined on the reference or spatial configurations.

In the small deformation theory, the Eulerian strain tensor is linearized such as [Bertram,2012]:

$$\varepsilon^{ij} = \frac{1}{2}(F^{ij} + F^{ij}) - I^{ij} \tag{4.1}$$

where $\varepsilon^{ij}$ is the symmetric strain tensor (symmetric gradient of displacement), and $F^{ij}$ corresponds to the transpose of $F^{ij}$. Another definition for the small strain can be expressed using the displacement vector $dep^{i}$ [Brunet,2009]:

$$\varepsilon^{ij} = \frac{1}{2}(\nabla_{j} dep^{i} + \nabla_{i} dep^{j}) \tag{4.2}$$

The relationship between $dep^{i}$ and $F^{i}_{j}$ can be expressed by:

$$F^{i}_{j} = I^{i}_{j} + \nabla_{j} dep^{i} \tag{4.3}$$

For large deformations, a Lagrangian description can be used. The Newtonian right Cauchy-Green deformation [Bertram,2012, Lai et al.,2010] is given by:

$$C_{ij} = F^{a}_{i} F^{b}_{j} I_{ab} \tag{4.4}$$

The Green-Lagrange strain tensor is then defined as:

$$E_{ij} = \frac{1}{2}(C_{ij} - I_{ij}) \tag{4.5}$$

For large deformations, a Eulerian description can also be used. The Newtonian left Cauchy-Green deformation [Bertram,2012] is given by:

$$\beta^{ij} = F^{i}_{a} F^{j}_{b} I^{ab} \tag{4.6}$$

Its inverse is given by:

$$b_{ij} = F'^{a}_{i} F'^{b}_{j} I_{ab} \tag{4.7}$$

The Euler-Almansi strain tensor is then defined as:

$$e_{ij} = \frac{1}{2}(I_{ij} - b_{ij}) \tag{4.8}$$

In this section we will designate by the tensor "$strain^{ij}$" indifferently one of these 3 types of strain. To represent variations with respect to time, several quantities are defined. First, we introduce the Newtonian velocity as this parameter will later interfere generally in the projection on the space domain of: the balance of molecules number and the components of energy four-tensor in the spacetime approach. In an inertial frame, it is defined as:

$$v^{i} = \frac{dz^{i}}{dt} \tag{4.9}$$

We also introduce the definition of the variation with time of the strain which is used for example in modeling the rate-form constitutive models. Generally, we can define the velocity gradient as the derivative of the velocity, denoted $L^{i}_{j}$ and such that:

$$L^{i}_{j} = \frac{dF^{i}_{a}}{dt} F'^{a}_{j} \tag{4.10}$$

The rate of deformation and spin then correspond to the symmetric and antisymmetric parts of the velocity gradient [Bertram,2012] and are respectively:

$$d_{ij} = \frac{1}{2}(L_{ij} + L_{ji}) \tag{4.11}$$

$$\omega_{ij} = \frac{1}{2}(L_{ij} - L_{ji}) \tag{4.12}$$

Note that the operator $\frac{d(.)}{dt}$ (in Eq. 4.9 and Eq. 4.10) corresponds to a total derivative in the Newtonian space and is also called the material derivative defined as:

$$\frac{d(.)}{dt} = \frac{\partial(.)}{\partial t} + v^i \frac{\partial(.)}{\partial \xi^i} \tag{4.13}$$

Note that this operator is an expression of a variation with respect to time and it has to be applied in an inertial frame to be properly used. Otherwise, Christoffel symbols have to be taken into account. In other words, this operator is not frame-indifferent. In classical Newtonian mechanics and in spacetime mechanics, many objective transports are proposed to fix the non-objectivity of total derivatives [Venturi,2009, Eshraghi et al.,2013, Rouhaud et al.,2013]. The covariant derivative is one of them, thus the material derivative will be replaced by the covariant derivative while developing covariant models (see section 2.2.7).

Generally, the variation of stress for a mechanical body at equilibrium i.e. that experiences neither linear acceleration nor angular acceleration, under Cauchy's general theory of stress, can be expressed by [Ugural and Fenster,2003]:

$$-\nabla_j \sigma^{ij} = \widetilde{\rho_c} f_M^i \tag{4.14}$$

where $\sigma^{ij}$ is the Cauchy Newtonian stress tensor, $f_M^j$ is the mechanical body force per unit volume. Note that the subscript "$M$" corresponds to mechanical. Eq. 4.14 corresponds to the equation of mechanical balance.

Further, we will investigate Newtonian thermomechanical/mechanical models taking into account the following assumptions:

- Thermomechanical/mechanical models are built for continuous media
- Thermomechanical couplings (thermoelastic coupling corresponding to the thermal expansion) are taken into account in the modeling.
- The hypothesis of local thermodynamic equilibrium is assumed.
- Material coefficients are constant ($\forall t$, $\forall x^i$) and thus are temperature independent except if mentioned otherwise.
- Materials are assumed to be homogeneous and isotropic.
- Gravitation could be considered under the Newtonian hypothesis, but in this manuscript it is not.

### 4.2.2 Elastic constitutive models

The stress and strain inside a continuous elastic material are connected by a linear relationship that is analogous to Hooke's spring model, and is often referred to by that name [Ugural and Fenster,2003].

The equation governing small elastic deformations of a body $\Omega$ can be written as:

$$\sigma^{ij} = \Lambda \varepsilon^{ab} I_{ab} I^{ij} + 2\mu \varepsilon^{ij} \tag{4.15}$$

where $\Lambda = \frac{E\,\nu}{(1+\nu)(1-2\nu)}$ and $\mu = \frac{E}{2(1+\nu)}$ are Lamé's elasticity parameters for the material in $\Omega$, $E$ is Young's modulus, $\nu$ is Poisson coefficient and $I^{ij}$ is the identity tensor.

The modern theory of elasticity generalizes Hooke's model to say that the strain (as well as the deformation i.e. stretch) of an elastic object or material is proportional in a tensorial/matricial point of view to the stress applied to it.

This linear model can be generalized to the case of large deformations.

**Characteristics of the elastic model in light of large deformation using Green-Lagrange strain or Euler-Almansi strain**

Eq. 4.15 can be transformed to express the elastic behavior for large deformations using Green-Lagrange strain (Eq. 4.5) or Euler-Almansi strain (Eq. 4.8). This can be done by the replacement of the small strain by the Green-Lagrange strain or Euler-Almansi strain. In this case:

- we consider large deformation instead of small deformation. Therefore, the undeformed and deformed configurations of the continuum are significantly different requiring a clear distinction between them
- using Green-Lagrange strain, we consider a Lagrangian description of the motion of the continuum
- using Euler-Almansi strain, we consider an Eulerian description of the motion. Thus parameters of the elastic model, e.g. density, are dependent on the current configuration.
- for small deformations or large deformations defined using Euler-Almansi strain, the stress (see Eq. 4.16) corresponds to Cauchy stress tensor. However, in the case of elastic constitutive models for large deformations defined using Green-Lagrange strain, the stress (see Eq. 4.16) is a second Piola-Kirchhoff stress which can be expressed as: $\sigma_{PK2}^{ij} = J\, F_{\alpha}'^{\,i}\, \sigma_c^{\alpha\beta}\, (F_{\beta}'^{\,j})^T$, where $J$ is the determinant of $F_j^i$ and $\sigma_c^{\alpha\beta}$ is the Cauchy stress tensor.

The generalized form of Eq. 4.15 can be written:

$$\sigma^{ij} = \Lambda strain^{ab} I_{ab} I^{ij} + 2\mu strain^{ij} \tag{4.16}$$

The $strain^{ij}$ tensor will then be replaced with the corresponding type of strain (Eqs. 4.2,4.5 or 4.8) to obtain the elastic constitutive models corresponding respectively to small deformation and large deformations defined using Green-Lagrange (Kirchhoff Saint-Venant model) or Euler-Almansi strain tensors [Bertram,2012, Sidoroff, Lejeunes,2014]. In case of small deformations and large deformations using Euler-Almansi strain, we have $\sigma^{ij} = \sigma_c^{ij}$. In case of large deformations using Green-Lagrange strain, we have $\sigma^{ij} = \sigma_{PK2}^{ij}$.

**Newtonian weak integral form of the elastic models**

In order to solve a mechanical problem using the proposed Newtonian elastic model with a finite element method, we write the weak integral of the problem [Oudin,2008]. The weak integral form is obtained by multiplying Eq. 4.14 by an arbitrary displacement $dep_i^* \in V_{dep_i}$, considered as a test function or virtual displacement field ($V_{dep_i}$ is the displacement function space), and then integrating it on the 3D volume $\omega$:

$$-\int_{\omega} (\nabla_j \sigma^{ij}) dep_i^* dV_\omega = \int_{\omega} \widetilde{\rho_c} f_M^i dep_i^* dV_\omega, \forall dep_i^* \tag{4.17}$$

Since $\nabla_j \sigma^{ij}$ contains second-order derivatives of the primary unknown $dep_i$, we integrate this term by parts:

$$-\int_{\omega} (\nabla_j \sigma^{ij}) dep_i^* dV_\omega = \int_{\omega} \sigma^{ij} \nabla_j dep_i^* dV_\omega - \int_{\partial\omega} (\sigma^{ij} n_j) dep_i^* dS_\omega, \forall dep_j^* \tag{4.18}$$

where $n_j$ is the outward unit normal to the 3D surface. The quantity $\sigma^{ij} n_j$ is known as the stress vector at the boundary, and is often prescribed as a boundary condition [Langtangen and Logg,2017]. We here assume that it is prescribed on a part $\partial\omega_{T_M}$ of the boundary as a Neumann boundary condition: $\sigma^{ij} n_j = T_M^i$. Note that the subscript "$M$" corresponds to mechanical. On the remaining part of the boundary, we assume that the value of the displacement is given as a Dirichlet condition therefore the associated terms in the integral are null. Thus, for Neumann-Dirichlet boundary conditions we obtain:

$$\int_{\omega} \sigma^{ij} \nabla_j dep_i^* dV_\omega = \int_{\omega} \widetilde{\rho_c} f_M^i dep_i^* dV_\omega + \int_{\partial\omega_{T_M}} T_M^i dep_i^* dS_\omega, \forall dep_i^* \tag{4.19}$$

We then obtain a variational form function of $dep_i$ and $dep_i*$, such that:

$$W(dep_i, dep_i^*) = \int_{\omega} \sigma^{ij}(dep_i) \nabla_j dep_i^* dV_\omega - \int_{\omega} \widetilde{\rho_c} f_M^i dep_i^* dV_\omega - \int_{\partial\omega_{T_M}} T_M^i dep_i^* dS_\omega, \forall dep_i^* \tag{4.20}$$

One can show that the inner product of a symmetric tensor $A$ and an antisymmetric tensor $B$ vanishes. If we express $\nabla_j dep_i^*$ as a sum of its symmetric and antisymmetric parts, only the symmetric part will remain in the product $\sigma^{ij}(dep_i)\nabla_j dep_i^*$ since $\sigma^{ij}(dep_i)$ is a symmetric tensor (as a consequence of to the conservation of angular momentum [Brunet,2009]). Thus the replacement of the terms by their values rise to the slightly different variational form:

$$W(dep_i, dep_i^*) = \int_\omega \sigma^{ij}(dep_i) strain_{ij}(dep_i^*) dV_\omega - \int_\omega \widetilde{\rho_c} f_M^i dep_i^* dV_\omega - \int_{\partial\omega_{T_M}} T_M^i dep_i^* dS_\omega, \forall dep_j^* \quad (4.21)$$

By replacing $strain_{ij}$ by the definitions of strain previously introduced in section 4.2.1, we obtain:

- In the small deformation theory [Bertram,2012, Lejeunes,2014]:

$$W(dep_i, dep_i^*) = \int_\omega \sigma_c^{ij}(dep_i) \varepsilon_{ij}(dep_i^*) dV_\omega - \int_\omega \widetilde{\rho_c} f_M^i dep_i^* dV_\omega - \int_{\partial\omega_{T_M}} T_M^i dep_i^* dS_\omega, \forall dep_i^* \quad (4.22)$$

- In a Lagrangian description of large deformations [Bertram,2012, Lejeunes,2014]:

$$W(dep_i, dep_i^*) = \int_\omega \sigma_{PK2}^{ij}(dep_i) E_{ij}(dep_i^*) dV_\omega - \int_\omega \widetilde{\rho_c} f_M^i dep_i^* dV_\omega - \int_{\partial\omega_{T_M}} T_M^i dep_i^* dS_\omega, \forall dep_i^* \quad (4.23)$$

- In an Eulerian description of large deformations [Bertram,2012, Lejeunes,2014]:

$$W(dep_i, dep_i^*) = \int_{\omega(t)} \sigma_c^{ij}(dep_i) e_{ij}(dep_i^*) dV_\omega - \int_{\omega(t)} \widetilde{\rho_c}(dep_i) f_M^i dep_i^* dV_\omega - \int_{\partial\omega_{T_M}(t)} T_M^i dep_i^* dS_\omega, \forall dep_i^* \quad (4.24)$$

  where $\omega(t)$ and $\partial\omega_{T_M}(t)$ are respectively the domain of integration and the boundary where Neumann boundary conditions are applied, that both depend on time.

We remind that in case the Eulerian description is used, $\widetilde{\rho_c}$ is a function of $dep_i$. We also note that the non-linearity of Eq. 4.23 and Eq. 4.24 caused by the introduction of large deformations, lead to the necessity of use of a non-linear resolution type of resolution methods when implemented for numerical simulation (in this manuscript this is done using FEniCS project).

$\partial\omega$ is the space boundary of the domain. It is divided into $\partial\omega_{dep_i}$ where the Dirichlet conditions on displacement are applied and $\partial\omega_{T_M}$ where the surface force is applied. They should respect: $\partial\omega_{dep_i} \cup \partial\omega_{T_M} = \partial\omega$ and $\partial\omega_{dep_i} \cap \partial\omega_{T_M} = \varnothing$.

A function representing the space boundary conditions is denoted $f_{SC}$. Dirichlet boundary conditions of this problem can then be written: $f_{SC}(x^i \in \partial\omega_{dep_i}) = dep_i(x^i \in \partial\omega_{dep_i}, t)$ and Neumann boundary conditions of this problem can be written: $f_{SC}(x^i \in \partial\omega_{T_M}) = T_M^i(x^i \in \partial\omega_{T_M}, t)$.

### 4.2.3 Thermoelastic constitutive models

Thermoelastic models are used in modeling reversible thermomechanical behaviors, for example when modeling the behavior of near-incompressible elastomers [Nicholson and Lin,1996]. The linearized thermoelastic constitutive equations (for small deformations) are given by:

$$\sigma^{ij} = \Lambda \varepsilon^{ab} I_{ab} I^{ij} + 2\mu\varepsilon^{ij} - 3\kappa\alpha(\theta - \theta_0) I^{ij} \quad (4.25)$$

$$\widetilde{\rho_c}\eta_c = \widetilde{\rho_c}\eta_{c0} + \frac{\widetilde{\rho_c} c_{mv}}{\theta_0}(\theta - \theta_0) + 3\kappa\alpha\varepsilon^{ij} I_{ij} \quad (4.26)$$

where $\kappa = \Lambda + 2\mu/3$, $\alpha$ is the thermal expansion coefficient and $\theta_0$ is the reference temperature. In addition to that, we can derive from Eq. 1.20 the heat equation by replacing the total derivative by a

covariant derivative and using the definition of entropy (Eq. 4.26) when the deformation is null:

$$\theta_0 \widetilde{\rho_c} \frac{d\eta_c}{dt} - \nabla_i \phi^i = 0 \tag{4.27}$$

where isotropic Fourier's model of heat conduction is considered to calculate $\phi^i = -\lambda I^{ij} \nabla_j \theta$. As seen in Eq. 4.27, we suppose that no volume heat source is applied to $\omega$.

**Newtonian weak integral form of the thermoelastic models**

Eqs. 4.26 and 4.27, together with the expression of heat flux in Fourier's model and with replacing the time derivatives by an implicit Euler scheme lead to the thermal weak integral form of the problem in the inertial proper frame at the time increment $n+1$:

$$\begin{aligned} W(\theta, \theta^*) &= \int_\omega \left( \widetilde{\rho_c} c_{mv} \frac{\theta^{n+1} - \theta^n}{\Delta t} + 3\kappa\alpha\theta_0 \frac{(\varepsilon^{ij})^{n+1} - (\varepsilon^{ij})^n}{\Delta t} I_{ij} \right) \theta^* dV_\omega + \int_\omega \lambda I^{ij} \frac{\partial \theta^{n+1}}{\partial x^i} \frac{\partial \theta^*}{\partial x^j} dV_\omega \\ &- \int_{\partial\omega_q} \lambda I^{ij} \frac{\partial \theta^{n+1}}{\partial x^i} \theta^* n_j dS_\omega, \forall \theta^* \end{aligned} \tag{4.28}$$

where $\theta$ and $\varepsilon^{ij}$ are the unkown fields of temperature and strain at the time increment $n+1$. Note that in section 2.7.4 a similar Newtonian model is used under the assumption that no mechanical stress nor surface heat flux are applied. Contrarily, in section 2.7.4 a volume heat source is taken into consideration as well as relaxation term corresponding to the use of a Cattaneo-like heat conduction model. Moreover, in [Lejeunes,2014, Farhat et al.,1991], a similar thermoelastic model was found. The generalisation of Eq. 4.28 in order to include other definitions of strain for application to large deformation, is then:

$$\begin{aligned} W(\theta, \theta^*) &= \int_\omega \left( \widetilde{\rho_c} c_{mv} \frac{\theta^{n+1} - \theta^n}{\Delta t} + 3\kappa\alpha\theta_0 \frac{(strain^{ij})^{n+1} - (strain^{ij})^n}{\Delta t} I_{ij} \right) \theta^* dV_\omega \\ &+ \int_\omega \lambda I^{ij} \frac{\partial \theta^{n+1}}{\partial x^i} \frac{\partial \theta^*}{\partial x^j} dV_\omega - \int_{\partial\omega_q} \lambda I^{ij} \frac{\partial \theta^{n+1}}{\partial x^i} \theta^* n_j dS_\omega, \forall \theta^* \end{aligned} \tag{4.29}$$

The $(strain^{ij})^{n+1}$ tensor will then be replaced with the corresponding type of strain (Eqs. 4.2,4.5 or 4.8). In case the Eulerian description is used, $\widetilde{\rho_c}$ is a function of $dep_i$. In addition to the previous thermal weak form, the mechanical weak form is as expressed in Eq. 4.21 that has to be simultaneously resolved. For simplification, the unknown temperature $\theta^{n+1}$, respectively $\theta^n$ are replaced by the temperature variation $\Delta\theta^{n+1} = \theta^{n+1} - \theta_0$, respectively $\Delta\theta^n = \theta^n - \theta_0$ which appear naturally in the stress constitutive relation (Eq. 4.25). Then, the solution of the coupled problem at $t = t^{n+1}$ is now $(dep_i^{n+1}, \Delta\theta^{n+1}) = (dep_i, \Delta\theta)$.

The spatial domain is divided into $\partial\omega_{dep_i}$ where the Dirichlet conditions on displacement are applied and $\partial\omega_{T_M}$ where the surface force is applied. They should respect: $\partial\omega_{dep_i} \cup \partial\omega_{T_M} = \partial\omega$ and $\partial\omega_{dep_i} \cap \partial\omega_{T_M} = \varnothing$.

In addition to that, Dirichlet conditions on temperature are applied on $\partial\omega_{\Delta\theta}$.

Dirichlet boundary conditions of this problem can be written: $f_{SC}(x^i \in \partial\omega_{dep_i}) = dep_i(x^i \in \partial\omega_{dep_i}, t)$, $f_{SC}(x^i \in \partial\omega_{\Delta\theta}) = \Delta\theta(x^i \in \partial\omega_{\Delta\theta}, t)$ on the space and $f_{TC}(t = t_0) = \Delta\theta(t = t_0)$ on the time. Neumann boundary conditions of this problem can be written: $f_{SC}(x^i \in \partial\omega_{T_M}) = T_M^i(x^i \in \partial\omega_{T_M}, t)$.

### 4.2.4 Hyperelastic constitutive models

The behavior of some materials can not be accurately described using the linear elastic models reviewed in section 4.2.2. Many examples can be found in the literature such as rubber materials [Muhr,2005], elastomers, biological tissues [Gao et al.,2014]... Moreover elastic models may not derive from a potential

energy, consequently the deformation may depend on the path of transformation. Such a behavior is dissipative hence irreversible. This shows the need to develop hyperelastic models [Lejeunes,2014].

A material is called hyperelastic, if a differentiable function of the deformation gradient $F$ called specific strain energy exists and the specific stress power is equal to the rate of this function [Bertram,2012]. Consequently, the mechanical behavior is totally defined by the specific strain energy which is a form of potential energy. Moreover, the hyperelastic behavior is reversible and, as a definition, no mechanical dissipation occurs with such a behavior [Lejeunes,2014].

This notion is also called perfect elasticity or "Green" elasticity. According to [Bertram,2012], any hyperelastic material is elastic, however the inverse is not true.

By definition, boundary value problems for hyperelastic media can be expressed as minimization problems [Bechir et al.,2006, Khajehsaeid,2013]. The total potential energy to minimize is given by:

$$P = \int_{\omega} \widetilde{\rho_c} \Psi(dep_i)\,\mathrm{d}\omega - \int_{\omega} \widetilde{\rho_c} f_M^i dep_i\,\mathrm{d}\omega - \int_{\partial\omega_{T_M}} T_M^i dep_i\,\mathrm{d}S_\omega \tag{4.30}$$

where $\Psi$ is the specific free energy, $f_M^i$ is a body force (per unit reference volume) and $T_M^i$ is a surface force (per unit reference area).

At minimum points of $P$, the directional derivative of $P$ with respect to change in $dep_i$:

$$L(dep_i, dep_i^*) = \frac{dP(dep_i + \epsilon\, dep_i^*)}{d\epsilon}|_{\epsilon=0} \tag{4.31}$$

is equal to zero for all $dep_i \in V_{dep_i}$:

$$L(dep_i, dep_i^*) = 0, \forall dep_i \in V_{dep_i} \tag{4.32}$$

To minimize the potential energy, a solution of the variational equation above is sought. Depending on the specific free energy $\Psi$, $L(dep_i, dep_i^*)$ can be nonlinear in $dep_i$. In such a case, the Jacobian of $L$ is required in order to solve this problem using Newton-Raphson method [Galántai,2000]. The Jacobian of $L$ is defined as [Langtangen and Logg,2017]:

$$A(dep_i; \Delta dep_i, dep_i^*) = \frac{dL(dep_i + \epsilon\Delta dep_i, dep_i^*)}{d\epsilon}|_{\epsilon=0} \tag{4.33}$$

where $\Delta dep_i$ is the variation of $dep_i$ defining the direction of derivative.

**Newtonian weak integral form of the hyperelastic models**

The weak integral form is expressed by:

$$W(dep_i, dep_i^*) = A(dep_i, dep_i^*) - L(dep_i, dep_i^*) \tag{4.34}$$

The specific strain energy for a Hooke-like model is:

$$\widetilde{\rho_c}\Psi(dep_i) = \frac{\Lambda}{2}\left(strain^{ij}\, I_{ij}\right)^2 + \mu\, strain^{ij}\, strain_{ij} \tag{4.35}$$

In case the Eulerian description is used, $\widetilde{\rho_c}$ is a function of $dep_i$. The $strain^{ij}$ tensor will then be replaced with the corresponding type of strain (Eqs. 4.2,4.5 and 4.8). $\partial\omega$ is the space boundary of the domain. It is divided into $\partial\omega_{dep_i}$ where the Dirichlet conditions on displacement are applied and $\partial\omega_{T_M}$ where the surface force is applied. They should respect: $\partial\omega_{dep_i} \cup \partial\omega_{T_M} = \partial\omega$ and $\partial\omega_{dep_i} \cap \partial\omega_{T_M} = \varnothing$.

Dirichlet boundary conditions of this problem can be written: $f_{SC}(x^i \in \partial\omega_{dep_i}) = dep_i(x^i \in \partial\omega_{dep_i}, t)$ and Neumann boundary conditions of this problem can be written: $f_{SC}(x^i \in \partial\omega_{T_M}) = T_M^i(x^i \in \partial\omega_{T_M}, t)$.

### 4.2.5 Illustration of the elastic and hyperelastic behaviors using a Hooke-like model

#### 4.2.5.1 Description of the problem

Let us consider a beam geometry fixed at its left boundary and subjected to a traction load applied in the form of stretch at its right boundary (see Fig. 34). Let us define the stretch as a process parameter evolving linearly with time and that is imposed as an input for the calculation: $\chi(t) = dep_n/L\, t$ in the $x$-direction, where $dep_n$ is the increment of displacement at each increment of time, chosen as a constant, $dep_n = 0.1\, m$ for this example, $L$ is the length of the beam and $t$ is the time varying between 0 and $t_{max}$. $t_{max}$ is the time at which the maximum loading of stretch is applied.

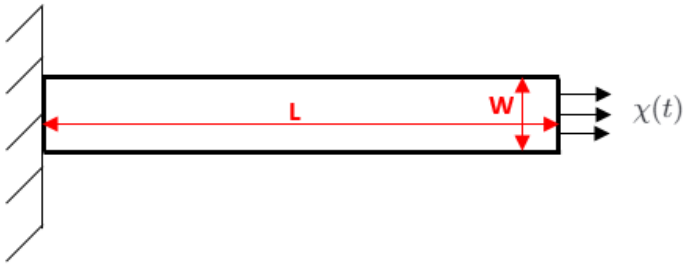


**Fig. 34:** Beam subjected to traction load.

Let us consider that the beam has the behavior of a Hooke-like model. We will investigate this model in case of elasticity (Eq. 4.21) and hyperelastacity (Eq. 4.34), consequently we assume that the yield stress of the material is not reached such that no plasticity occurs. Then for each case, we will simulate traction using small strain (Eq. 4.2), Green-Lagrange strain (Eq. 4.5) and Euler-Almansi strain (4.8).

In the following example, we are applying a significant value of $\chi(t)$ to the beam, as it enables us to clearly show the different behaviors of evolution of the stress through time for the different models. Time is here introduced as proportional to loading.

#### 4.2.5.2 Weak integral forms and boundary conditions corresponding to the elastic and hyperelastic modeling of the beam subjected to traction

In order to simulate the model described in section 4.2.5.1 using FEniCS project, we need to explicit the weak integral forms related to the behaviors simulated and the boundary conditions corresponding to the studied case. Eqs. 4.22, 4.23 and 4.24 represent the weak integrals forms of elastic models using respectively small strain, Green-Lagrange strain and Euler-Almansi strain.

For the hyperelastic models, Eq. 4.34 represents the weak integral form together with Eq. 4.35, where the $strain^{ij}$ tensor is respectively replaced with the corresponding type of strain (Eqs. 4.2, 4.5 and 4.8) to obtain models using respectively small strain, Green-Lagrange strain and Euler-Almansi strain.

For the boundary conditions, all the models are constrained by:

- $\forall y \in \partial\omega_1, \forall t,\ f_{SC1} = dep(x = 0, y) = (0, 0)$ on the clamped boundary of the beam.
- $\forall y \in \partial\omega_2, \forall t,\ f_{SC2} = dep(x = L, y) = (\chi(t) \times L, 0) = (0.1\, t, 0)$ on the right boundary of the beam.

#### 4.2.5.3 Parameters of the numerical simulation

As follows are the input parameters of the numerical simulation of the Hooke-like model subjected to traction:

| | Parameter | Value |
|---|---|---|
| Geometry | Length | $L = 1\,(m)$ |
| | Width | $W = 0.1\,(m)$ |
| | Thickness | $H = 0.1\,(m)$ |
| Material | Young's modulus | $E = 250000\,(MPa)$ |
| | Poisson coefficient | $\nu = 0\,(adim)$ |
| | Density | $\widetilde{\rho_c} = 7850\,(kg/m^3)$ |
| | Thermal expansion | $\alpha = 0\ (K^{-1})$ |
| | Thermal conductivity | $\lambda = 500000\ (w.m^{-1}.K^{-1})$ |
| | Specific heat capacity at constant 3D volume | $\mathcal{C}_{m\omega} = 520\ (J.kg^{-1}.K^{-1})$ |
| Mesh and time stepping | Number of nodes through the $x-$direction of space | $N_x = 100\,(adim)$ |
| | Number of nodes through the $y-$direction of space | $N_y = 10\,(adim)$ |
| | Number of loading steps | $N_{step} = 40\,(adim)$ |
| Loading | Time at which the maximum loading is applied | $t_{max} = 10\,(s)$ |
| | Stretch applied on the right boundary of the beam | $\chi(t) = 0.1\,t$ |
| | Volume force vector | $f_M = (0, 0)\,(N)$ |
| | Surface force vector | $T_M = (0, 0)\,(N)$ |

**Tab. 11:** Parameters of the numerical simulation of the beam subjected to traction (except for the stretch on the right boundary, all other paratemers are applied in all the integration domain $\omega$)

The space mesh of the model (2D triangular) is given in Fig. 35. In the next section the evolution of $\sigma^{11}$ is given at the center of the beam marked by the red dot.

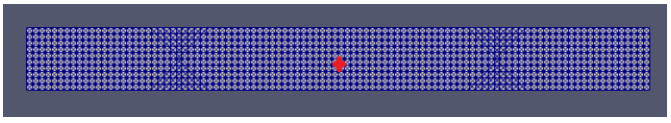

**Fig. 35:** Meshing used in the numerical simulation of the beam subjected to traction load.

Below (Fig. 36) is the result of evolution of $\sigma_c^{11}$ at the center of the beam, as a function of time (thus loading increment) for Newtonian elastic models (using small deformation, Green-Lagrange large deformation and Euler-Almansi large deformation) and the hyperelastic model function of Euler-Almansi large deformation. Note that the evolution of stress corresponding to the hyperelastic models using small deformation and Green-Lagrange large deformation is identical to that obtained using the elastic model respectively function of small deformation and Green-Lagrange large deformation. Fig. 37 a) and Fig. 37 b) show respectively the evolution of $\sigma_c^{11}$ in function of $x$ at $y = W/2$ and in function of $y$ at $x = L/2$.

The error as well as the percentage of error on the field $\sigma_c^{11}(x, y, t)$ are computed by finding the difference between $\sigma_c^{11}(x, y, t)_{(sol)}$ obtained from analytical computation of the solution $(\sigma_c^{11}{}_{(sol)} = E\,\chi(t))$ and $\sigma_c^{11}(x, y, t)_{(simu)}$ obtained from the spacetime simulation compared to the norm value of stress over the time and space $||\sigma_c^{11}(x, y, t)_{(sol)}||$, as:

$$\text{error}(x, y, t) = \int_{\omega} \left(\sigma_c^{11}(x, y, t)_{(sol)} - \sigma_c^{11}(x, y, t)_{(simu)}\right)^2 d\omega \tag{4.36}$$

and

$$\%\text{relative error}(x, y, t) = 100 \times \left(\frac{\text{error}(x, y, t)}{||(\sigma_c^{11}(x, y, t)_{(sol)}||}\right) \tag{4.37}$$

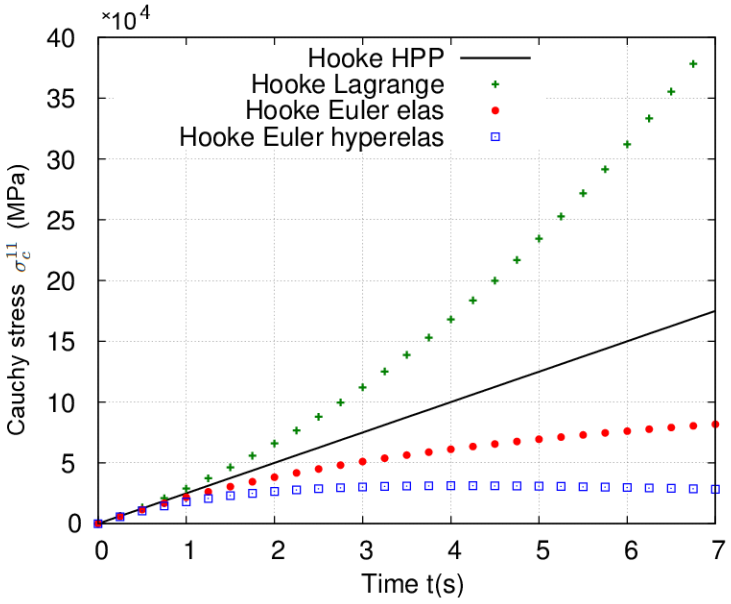


**Fig. 36:** The variation of $\sigma_c^{11}$ as a function of time for a beam under traction load for different Newtonian elastic and hyperelastic models between $0$ and $7s$.

The error and percentage of error on $\sigma_c^{11}$ are respectively around $1.59 \times 10^{-8}\, MPa$ and $2.01 \times 10^{-13}\,\%$.

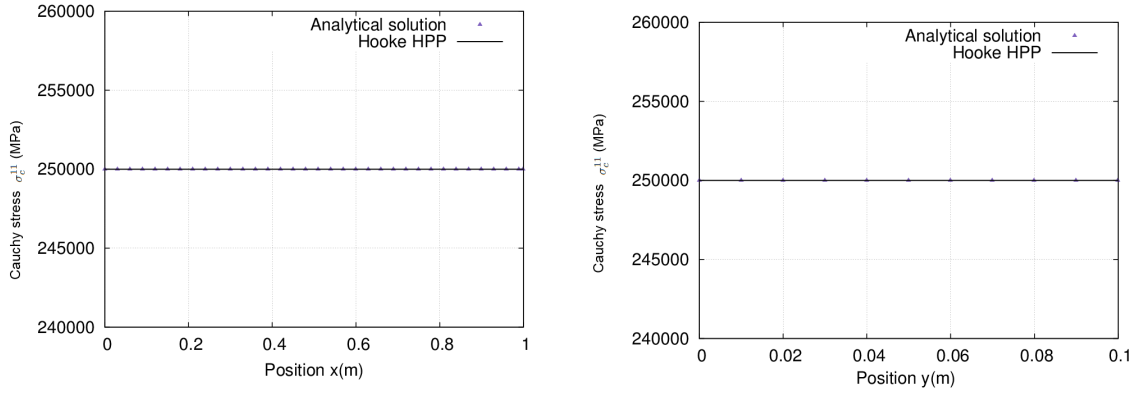


**Fig. 37:** On the left: a) Evolution of $\sigma_c^{11}(x, y, t)$ obtained from analytical solution ($\sigma_c^{11}{}_{(sol)} = E\,\chi(t_{max})$) and simulation for a Newtonian elastic model as function of the space in the $x$-direction at $y = W/2$ and $t = t_{max}$. On the right: b) Evolution of $\sigma_c^{11}(x, y, t)$ obtained from analytical solution ($\sigma_c^{11}{}_{(sol)} = E\,\chi(t_{max})$) and simulation for a Newtonian elastic model as function of the space in the $y$-direction at $x = L/2$ and $t = t_{max}$.

A similar case study of a beam subjected to a bending load can be found in appendix A. Moreover, the Cauchy stress values obtained in this illustration for different models are significant. In reality, non-linear behaviors interfere preventing these high values of stress e.g. the plasticity which is reviewed in section 4.2.6.

### 4.2.6 Elasto-plastic constitutive model

The material is now represented by an isotropic elasto-plastic von Mises yield condition of uniaxial strength $\sigma_0$ and with isotropic hardening of modulus $H$. The yield condition in case of normal stress with linear

isotropic hardening is thus given by [Bonnet,2014, Brunet,2009]:

$$f(\sigma^{ij}) = \sqrt{\frac{3}{2} s^{ij} s_{ij}} - \sigma_0 - H\, p \tag{4.38}$$

where $s^{ij}$ is the deviatoric part of $\sigma^{ij}$, $\sigma_0$ is the yield strength, $H$ is the hardening modulus which can be obtained from tangent modulus: $E_t = \dfrac{EH}{E+H}$ and $p$ is the cumulated equivalent plastic strain. We define ${\sigma^{ij}}^{eq}_{elas} = \sqrt{\frac{3}{2} s^{ij} s_{ij}}$

Before writing the variational form, we consider $\sigma^{ij}$ obtained from a Hooke-like model as in Eq. 4.15 [Bonnet,2014].

The return mapping procedure consists in finding a new stress $(\sigma^{ij})^{n+1}$ and internal variable $p^{n+1}$ state verifying the current plasticity condition from a previous stress $(\sigma^{ij})^n$ and internal variable $p^n$ state for an increment of total deformation $\Delta\epsilon$ applied.

- An elastic predictor stress $\sigma^{ij}_{elas} = (\sigma^{ij})^n + \sigma^{ij}(\Delta strain^{ij})$ is first computed [Bonnet,2014].
- The plasticity criterion is then evaluated with the previous plastic strain using Eq. 4.38. If $f_{elas} < 0$, no plasticity occurs during this time increment and $\Delta p, \Delta strain^{ij}_P = 0$, where $strain^{ij}_P$ is the strain due to plasticity behavior. Otherwise, plasticity occurs and in the case of linear isotropic hardening, the increment of plastic strain is given by :

$$\Delta p = \frac{f_{elas}}{3\mu + H} \tag{4.39}$$

where $f_{elas} = {\sigma^{ij}}^{eq}_{elas} - \sigma_0 - H\, p$. The final stress state is corrected by the plastic strain as follows $(\sigma^{ij})^{n+1} = \sigma^{ij}_{elas} - \dfrac{3\mu}{{\sigma^{ij}}^{eq}_{elas}} s^{ij} \Delta p$, this is the plastic corrector [Bonnet,2014]. It can be observed that the last term vanishes in case of elastic evolution so that the final stress is the one calculated from the elastic predictor.

In order to use a Newton-Raphson procedure to resolve global equilibrium, we also need to derive the algorithmic consistent tangent matrix. In this problem, it corresponds to minimizing the specific free energy given by $\Psi$ in Eq. 4.35.

**Newtonian weak integral form of the elasto-plastic models**

The global problem with its associated Newton-Raphson procedure can then be derived. Each iteration will require establishing equilibrium by driving to zero the residual between the internal forces associated with the current stress state $(\sigma^{ij})^n$ and the external force vectors $f^i_M$ and $T^i_M$. The weak integral form resolved at each iteration for the elastic prediction is:

$$\begin{aligned} W(\Delta dep_i, \Delta dep_i^*) &= \int_\omega \widetilde{\rho_c} \Psi(\Delta dep_i)\, \mathrm{d}\omega + \int_\omega (\sigma^{ij})^n \frac{\partial strain^{ij}(\Delta dep_i + \epsilon \Delta dep^{j*})}{\partial \epsilon}|_{\epsilon=0}\, \mathrm{d}\omega \\ &- \int_\omega \widetilde{\rho_c} f^i_M \Delta dep_i\, \mathrm{d}\omega - \int_{\partial\omega_{T_M}} T^i_M \Delta dep_i\, \mathrm{d}S_\omega \end{aligned} \tag{4.40}$$

Where $\Delta dep_i$ is the increment of elastic displacement and $\Delta dep_i^*$ is the corresponding test function. The $strain^{ij}$ tensor is then replaced with the corresponding type of strain (Eqs. 4.2,4.5 and 4.8). In case the Eulerian description is used, $\widetilde{\rho_c}$ is a function of $\Delta dep_i$. $\partial\omega$ is the space boundary of the domain. It is divided into $\partial\omega_{\Delta dep_i}$ where the Dirichlet conditions on displacement are applied and $\partial\omega_{T_M}$ where the surface force is applied. They should respect: $\partial\omega_{\Delta dep_i} \cup \partial\omega_{T_M} = \partial\omega$ and $\partial\omega_{\Delta dep_i} \cap \partial\omega_{T_M} = \varnothing$.

Dirichlet boundary conditions of this problem can be written: $f_{SC}(x^i \in \partial\omega_{\Delta dep_i}) = \Delta dep_i(x^i \in \partial\omega_{\Delta dep_i}, t)$ on the space. Neumann boundary conditions of this problem can be written: $f_{SC}(x^i \in \partial\omega_{T_M}) = T^i_M(x^i \in \partial\omega_{T_M}, t)$.

### 4.2.7 Numerical simulation of the elasto-plastic behavior

#### 4.2.7.1 Description and parameters of the problem

Let us consider the same beam geometry as in section 4.2.5.1 fixed at its left boundary and subjected to a traction load applied in the form of stretch at its right boundary (see Fig. 34). However, this time the yield stress is set to be $\sigma_0 = 60000\,MPa$ and the hardening modulus is $H = 25000\,MPa$.

This stretch causes a mechanical stress exceeding the yield stress in the beam, hence causing a plastic behavior of the material. The other parameters of the simulation concerning the geometry, the material, the mesh and time step as well as volume and surface force vectors remain the same (see table 11).

#### 4.2.7.2 Weak integral forms and boundary conditions corresponding to the elasto-plastic modeling of the beam subjected to traction

In order to simulate the model described in section 4.2.7.1 using FEniCS project, we need to explicit the weak integral forms related to the behaviors simulated and the boundary conditions corresponding to the studied case.

Eq. 4.40 represents the weak integral form, where the $strain^{ij}$ tensor is respectively replaced with the corresponding type of strain (Eqs. 4.2,4.5 and 4.8) to obtain elasto-plastic models using respectively small strain, Green-Lagrange strain and Euler-Almansi strain.

As for the boundary conditions, all the models are constrained by:

- $\forall y \in \partial\omega_1, \forall t,\ f_{SC1} = \Delta dep(x = 0, y) = (0, 0)$ on the clamped boundary of the beam.
- $\forall y \in \partial\omega_2, \forall t,\ f_{SC2} = \Delta dep(x = L, y) = (dep_n, 0) = (0.1, 0)$ on the right boundary of the beam.

Below (Fig. 38) is the result of evolution of $\sigma_c^{11}$ at the center of the beam, as a function of time for Newtonian elasto-plastic models (using small deformation, Green-Lagrange large deformation and Euler-Almansi large deformation).

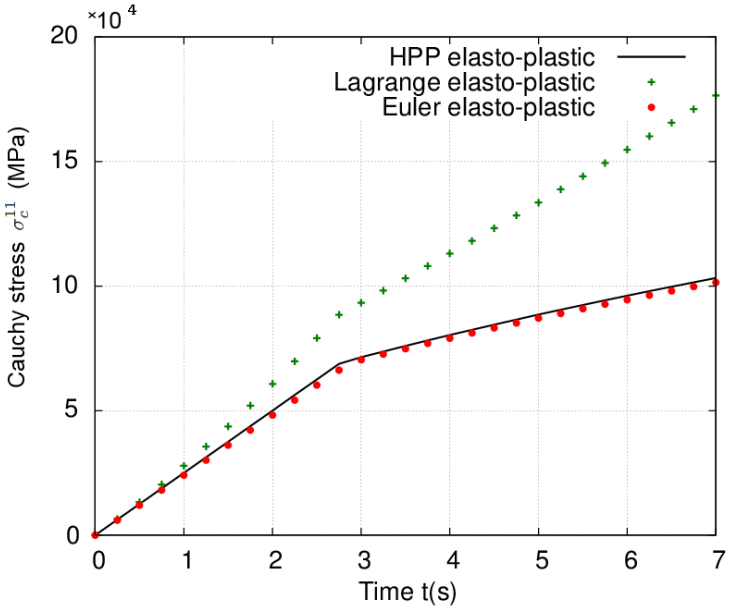


**Fig. 38:** The variation of $\sigma_c^{11}$ as a function of time for a beam under traction load for different Newtonian elasto-plastic models examined.

## 4.3 Difficulties encountered during Newtonian modeling of the thermomechanical behavior of materials

### 4.3.1 Classical continuum behavior models

In the second part of the manuscript, we are interested in modeling the mechanical behavior of models in order to couple it with the thermal behavior as detailed in part 1. Besides Hooke's model for linear elasticity which is convenient in modeling the behavior of materials in small transformations, most constitutive models in solid mechanics lead to non-linear problems. These are conveniently formulated under a rate form. Examples of such a difficulty are: plasticity [Valanis,1970, Lubliner,1984, Prasolov,1997] (illustrated in section 4.2.7), viscosity depending on time [Wiechert,1893, Zener,1948, Oldroyd,1950, Wineman,2009], elasticity for large deformation used to model elastomers [Mooney,1940, Rivlin,1948, Rivlin and Saunders,1951, Ogden,1984, Boyce and Arruda,2000, Steinmann et al.,2012, Hossain and Steinmann,2013] (illustrated in section 4.2.5), or even a combination of these difficulties in the cases of biomaterials [Prost-Domasky et al.,1997] or metal manufacturing [Saanouni,2012]. Such constitutive models take the form of relations between stress and strain tensors, and their respective rates. Consequently, rate-form modeling is often convenient, and these types of time-dependent phenomena require an incremental formulation of the chosen elastic model. Note that such so called hypoelastic models need to be strictly equivalent to the initial elastic one; if not, it can lead to the well-known deficiencies of hypoelastic formulations, such as hysteresis with dissipation for elastic loading [Altemeyer et al.,2016].

### 4.3.2 The problem of material objectivity

There are many possible definitions of stress rate for use in large deformation, due to the choice of the stress tensor as well as the choice of the time transport [Dogui and Sidoroff,1985]. Moreover, constitutive models shall not generate stress when the material undergoes a rigid body motion. This is classically referred to as (material) objectivity (see 1.4.2). Objectivity may then be enforced by using objective transports (see details in [Frewer,2009]), but a particular attention has to be paid when using such operators in large deformation [Truesdell,1966, Prost-Domasky et al.,1997]. A large number of these transports verifying material objectivity can be found in the literature [Jaumann,1911, Green and Naghdi,1965, Bruhns and Meyers,1998], but none seems to be strictly better than the others [Truesdell,1966] and their use does not guarantee a priori a reversible behavior for large elastic deformations, which would contradict thermodynamics. Differences and similarities between objectivity and frame-indifference are also discussed in [Panicaud et al.,2014, Romano et al.,2018].

In addition to the invariance of stress with respect to rigid body motion, including translation and rotation, the covariance of equations with respect to any observer is required, and that for any diffeomorphism of a spacetime continuum. The notion of the action of diffeomorphism on a spacetime continuum introduces differential geometry. Using a geometric point of view on continuum mechanics has lead so far to important contributions [Eringen,1962, Truesdell and Noll,2003, Marsden and Hughes,1994, Venturi,2009] (see section 1.4.3). For example, Marsden and Hughes use geometry to clarify the exposition of the kinematics of continuum and of mechanical principles [Marsden and Hughes,1994]. Recent works on the geometry for non-linear elasticity can also be found in [Romano et al.,2014].

## 4.4 Possible solutions for modeling the thermomechanical behavior of materials

### 4.4.1 A solution using a spacetime formalism

As in the case of thermal modeling (introduced in section 1.7), the difficulties faced in mechanical modeling can also be solved using a spacetime formalism. These can be summarized by the violation of material objectivity

and the difficulty to choose and guarantee objective transports. The interest of using differential geometry in this formalism is to impose covariance to the equations of continuum mechanics. Especially, differential geometry introduces a very powerful tool, the Lie derivative along the motion, which answers the need expressed by [Eringen,1962, Nemat-Nasser,2004, Besson et al.,2009, Xiao et al.,1999, Eshraghi et al.,2013] of a cautious construction of a rate-form elastic model. By use of a spacetime framework, the Lie derivative along the motion guarantees simultaneously the covariance of the transport and the invariance to the superposition of rigid body motion [Rouhaud et al.,2013]. Since frame changes proceed on space and time, it leads to the use of four-dimensional vectors and four-dimensional tensors. In this manuscript and in the articles [Rouhaud et al.,2013, Panicaud et al.,2014], this refers to spacetime formalism.

The use of a spacetime diffeomorphisms group makes a clear distinction between this work and others [Romano et al.,2018, Romano et al.,2014, De Saxce and Vallée,2016] that intended to be a geometric representation of Newtonian mechanics using a Galilean group. On the one hand, the mathematical structure is more simple comparing to when using a Poincaré group (group of motion in the Minkowski spacetime of special relativity [Hehl,2012]), compared to the use of a Galilean group, since it is possible to use a spacetime (pseudo-)metric. On the other hand, we will just have to lug some negligible terms in the equations that can be killed when the velocity of the material is small compared to a reference velocity [Weinberg,1972]. Moreover, as mentioned in part 1, in the present manuscript, we do not deal with gravitation, thus we only consider a flat spacetime (i.e. not Riemannian) [Weinberg,1972].

### 4.4.2 Thermodynamics in a spacetime formalism for mechanical modeling

As detailed in section 1.7.2, to obtain suitable constitutive models, it is useful to deal with thermodynamics. Thermodynamics and spacetime formalism have led to numerous publications concerning theoretical aspects, such as balance equations or constitutive models [Eckart,1940, Havas,1964, Grot and Eringen,1966a, Grot and Eringen,1966b, Muller,1969, Maugin,1971a, Maugin,1971b, Maugin,1973, Israel,1987, Muller,2008, Ottinger,1998, Kijowski and Magli,1997, Beig and Schmidt,2005, Vallée,1981, Yavari and Ozakin,2008, Romano and Barretta,2011, Yavari and Marsden,2012, Schellstede et al.,2014, Bressan,1978]. For example, significant works on relativistic thermodynamics have been performed by Tolman [Tolman,1930], Moller [Moller,1972], Lichnerowicz [Lichnerowicz,1994] and Tsallis [Tsallis et al.,1995]. These works aim at a covariant formulation of thermodynamics, especially including the coupling between the mechanical and the thermal behavior independently of the frame, or at some generalizations of the Clausius-Duhem inequality [Muschik and Borzeszkowski,2015, Bressan,1978, Muschik and Borzeszkowski,2014]. Relations between relativistic and non-relativistic thermodynamics have been specifically detailed in [Schellstede et al.,2014].

In this manuscript, we aim to propose an innovative method to obtain mechanical behavior. We will use the modeling of reversible processes as an illustration. One important goal is to derive new covariant constitutive models for large deformation. We will see the advantages of the spacetime method compared to the Newtonian case, especially by the use of the spacetime Lie derivative. An approach considering a spacetime thermodynamical framework is thus proposed in chapter 5. The aim is to obtain a general method fully covariant, i.e. that can be adapted for any frame, and thus any motion, to be applied to the construction of thermomechanical constitutive models.

## 4.5 Complements for the spacetime formalism for thermomechanical modeling

### 4.5.1 Spacetime deformation in different frames

In Newtonian continuum mechanics, a mapping from one configuration to another is used to describe the deformation of a material continuum. When this concept is extended to a spacetime formalism, the configuration can be characterized directly by the spacetime coordinates of the events, because it contains simultaneously the information on both space and time. Here we introduce the deformation of the domain

$\mathcal{D}$ that can be described by the mapping $\mathcal{F}$:

$$\forall x^\mu \in \mathcal{D}, x^\mu = \mathcal{F}^\mu(X^\kappa) \Leftrightarrow \left\{ \begin{array}{l} x^i = \mathcal{F}^i(X^k, X^4) \\ x^4 = \mathcal{F}^4(X^k, X^4) \end{array} \right. \tag{4.41}$$

Here two particular coordinate systems can be specified:

1. The inertial spacetime frame, whose base vectors $\mathbf{e}_\mu$ are homogeneous in the spacetime, with the metric tensor components $\eta_{\mu\nu}$ (see section 1.3.2). For simplicity, the 3D space part of the frame (i.e. coordinate system) is chosen to be Cartesian, whatever the configuration is. Coordinates in the inertial spacetime frame correspond to the observed coordinates $x^\mu$ in the current configuration and $X^\mu$ in the reference configuration, as defined previously and used in Eq. 4.41.
2. The proper spacetime frame, in which the current configuration is always considered as a reference configuration:

$$\hat{x}^\mu = X^\mu \tag{4.42}$$

The proper frame is the one previously introduced in section 1.3.3. This frame is spacetime curvilinear, including possible acceleration and rotation because of the deformation of materials. Moreover, for all the configurations, this coordinate system is chosen to be identical to the spacetime inertial coordinate system at the time of reference (i.e. only initially).

The different configurations and spacetime frames are summarized in Table 12.

| | | **inertial frame** $z^\mu$ | **proper frame** $\hat{x}^\mu$ |
|---|---|---|---|
| current configuration | coordinate | $x^\mu$ | $\hat{x}^\mu = X^\mu$ |
| | base vectors | $\mathbf{g}_\mu = \mathbf{e}_\mu$ | $\hat{\mathbf{g}}_\mu$ |
| | metric | $g_{\mu\nu} = \eta_{\mu\nu}$ | $\hat{g}_{\mu\nu}$ |
| reference configuration | coordinates | $X^\mu$ | $\hat{X}^\mu$ |
| | base vectors | $\mathbf{G}_\mu = \mathbf{e}_\mu$ | $\hat{\mathbf{G}}_\mu = \mathbf{e}_\mu$ |
| | metric | $G_{\mu\nu} = \eta_{\mu\nu}$ | $\hat{G}_{\mu\nu} = \eta_{\mu\nu}$ |

**Tab. 12:** Configurations and frames; for simplicity and for the reference configuration, all the coordinate systems used are considered with 3D Cartesian coordinates.

### 4.5.2 Spacetime deformation gradient and strain tensor

In a spacetime formalism, the deformation gradient and strain tensors can be defined, following the general definitions proposed by Lamoureux-Brousse [Havas,1964]. To define spacetime strain tensors, it is proposed to compare two different configurations of the same material continuum: its current configuration and its reference configuration (see section 1.4.4). The choice of a reference configuration should not enter directly in a constitutive relation, as being completely arbitrary.

These two configurations are described indifferently with two different frames either $x^\mu$ or $\hat{x}^\mu$, associated with the two respective covariant components of the metric tensor $\eta_{\mu\nu}$ or $\hat{g}_{\mu\nu}$. The material continuum is defined at a given instant of reference, with a unique reference configuration that is described either by $X^\mu$ or $\hat{X}^\mu$, within each respective frame.

To define a spacetime deformation gradient, the two coordinate sytems are compared by defining the gradient $F^\mu{}_\nu$ and its inverse $F'^\mu{}_\nu$ such that:

$$F^\mu{}_\nu = \frac{\partial x^\mu}{\partial \hat{x}^\nu} \text{ and } F'^\mu{}_\nu = \frac{\partial \hat{x}^\mu}{\partial x^\nu} \tag{4.43}$$

In other words, these equations define the deformation gradient as the matrix of the coordinate transformation between the proper and inertial frames, independently of the reference configuration. Moreover, because of Eq. 4.42, Eqs. 4.43 turns to be quantities similar to the definitions of deformation gradient in the classical Newtonian continuum mechanics:

$$F^{\mu}_{\ \nu} = \frac{\partial x^{\mu}}{\partial X^{\nu}} \text{ and } F'^{\mu}_{\ \ \nu} = \frac{\partial X^{\mu}}{\partial x^{\nu}} \tag{4.44}$$

Hence, as usually done in Newtonian continuum mechanics, the comparison between two configurations is done through the definition of the strain tensors. According to Lamoureux-Brousse [Havas,1964], a spacetime Euler-Almansi's strain tensor $\boldsymbol{e}$ can be defined as:

$$e_{\mu\nu} = \frac{1}{2}(g_{\mu\nu} - b_{\mu\nu}) \tag{4.45}$$

It has the same form as the 3D Euler-Almansi's strain tensor, where the tensor $\boldsymbol{b}$ is the spacetime generalization of the inverse of the left Cauchy-Green deformation tensor defined by:

$$b_{\mu\nu} = F'^{\alpha}_{\ \ \mu} F'^{\beta}_{\ \ \nu} G_{\alpha\beta} \tag{4.46}$$

Note that there is also a "material" counterpart of the above strain tensor [Panicaud et al.,2014]. A spacetime Green-Lagrange's strain tensor $\boldsymbol{E}$ can also be defined as:

$$E_{\mu\nu} = \frac{1}{2}(C_{\mu\nu} - g_{\mu\nu}) \tag{4.47}$$

It has the same form as the 3D Green-Lagrange's strain tensor, where the tensor $\boldsymbol{C}$ is the spacetime generalization of the inverse of the right Cauchy-Green deformation tensor defined by:

$$C_{\mu\nu} = F^{\alpha}_{\ \ \mu} F^{\beta}_{\ \ \nu} G_{\alpha\beta} \tag{4.48}$$

We have preserved, with the capital letters, the usual notations proposed by Eringen [Grot and Eringen,1966a] for the definitions of the spacetime deformation and strain tensors. After the choice of the inertial or proper frames, using Eqs. 2.8d, 2.8e and 4.42, the relations for the different metrics components can be obtained:

$$\hat{g}^{\mu\nu} = F'^{\mu}_{\ \ \alpha} F'^{\nu}_{\ \ \beta} \eta^{\alpha\beta} \tag{4.49a}$$

$$\hat{g}_{\mu\nu} = F^{\alpha}_{\ \ \mu} F^{\beta}_{\ \ \nu} \eta_{\alpha\beta} \tag{4.49b}$$

From the definitions of spacetime strain tensors, it is easy to find the transformation between the different counterparts:

$$E_{\mu\nu} = F^{\alpha}_{\ \ \mu} F^{\beta}_{\ \ \nu} e_{\alpha\beta} = \hat{e}_{\mu\nu} \tag{4.50}$$

Because of Eq. 4.42 and definition of the 4D transformation gradient, it can be proved that Eq. 4.50 can be interpreted as a change of frames between two equivalent measures/components of the same strain tensor (corresponding to different observers). The detailed proof can be found in [Panicaud et al.,2014]. Briefly, we have thus $E_{\mu\nu} = \hat{e}_{\mu\nu}$, because $\hat{g}_{\mu\nu} = \hat{C}_{\mu\nu} = C_{\mu\nu}$ and $\hat{b}_{\mu\nu} = \hat{G}_{\mu\nu} = G_{\mu\nu}$ in Eqs. 4.45 and 4.47. This shows that $E_{\mu\nu}$ (Eq. 4.47) actually corresponds to some components of $e_{\mu\nu}$ written in the proper frame. These respectively correspond to the Lagrangian and Eulerian expressions of the strain.

### 4.5.3 Spacetime Lie derivative

In addition to the frame-indifferent covariant transport (introduced in section 2.2.7), it is possible to define a spacetime rate operator whose result is both frame-indifferent and invariant to the superposition of rigid body motions. Among the spacetime rate operators, the spacetime Lie derivative is the only derivative that fulfills the two aspects of the principle of objectivity [Rouhaud et al.,2013].

The explicit expressions of the Lie derivative with along the velocity four-vector $\boldsymbol{u}$ (defined in section 2.2.2) of a 4-scalar density $\mathcal{S}$, of the covariant components and of the contravariant components of a second-rank four-tensor density $\boldsymbol{\mathcal{T}}$ with a weight of tensor density $W$ [Schouten,1954], are:

$$\mathcal{L}_u(\mathcal{S}) = u^\lambda \frac{\partial \mathcal{S}}{\partial x^\lambda} + W\mathcal{S}\frac{\partial u^\lambda}{\partial x^\lambda} \tag{4.51a}$$

$$\mathcal{L}_u(\mathcal{T}_{\mu\nu}) = u^\lambda \frac{\partial \mathcal{T}_{\mu\nu}}{\partial x^\lambda} + \mathcal{T}_{\lambda\nu}\frac{\partial u^\lambda}{\partial x^\mu} + \mathcal{T}_{\mu\lambda}\frac{\partial u^\lambda}{\partial x^\nu} + W\mathcal{T}_{\mu\nu}\frac{\partial u^\lambda}{\partial x^\lambda} \tag{4.51b}$$

$$\mathcal{L}_u(\mathcal{T}^{\mu\nu}) = u^\lambda \frac{\partial \mathcal{T}^{\mu\nu}}{\partial x^\lambda} - \mathcal{T}^{\lambda\nu}\frac{\partial u^\mu}{\partial x^\lambda} - \mathcal{T}^{\mu\lambda}\frac{\partial u^\nu}{\partial x^\lambda} + W\mathcal{T}^{\mu\nu}\frac{\partial u^\lambda}{\partial x^\lambda}. \tag{4.51c}$$

The Lie derivative is intrinsic because the derivative of tensor field is taken along a physical vector field: the velocity. This operator could be interpreted as a Lagrangian entity (as it is defined for a particle of matter), and it is computed within an Eulerian formalism (as it is defined at a given event of spacetime). Moreover, the Lie derivative obeys to Leibnitz's rule [Protter,1985] and chain's rule [Rodriguez and Lopez Fernandez,2010].

Note that in particular the Lie derivative of the metric tensor $\mathbf{g}$ does not vanish, except if the motion is isometric. This is the reason why the formulas are different for contravariant or covariant components.

### 4.5.4 Rate of deformation and spin tensors

The definition of the variation of the strain with time is important. For example, it is used in modeling the rate-form constitutive models. Generally, in spacetime, we can define the velocity gradient as the covariant derivative of the velocity, denoted $\boldsymbol{L}$ and such that:

$$L^\mu{}_\nu(u^\alpha) = \nabla_\nu u^\mu = \frac{\partial u^\mu}{\partial x^\nu} + \Gamma^\mu_{\kappa\nu}u^\kappa \tag{4.52}$$

The symmetric and antisymmetric parts of the velocity gradient correspond respectively to the rate of deformation $\boldsymbol{d}$ and spin $\boldsymbol{\omega}$ tensors, defined by:

$$d^\mu{}_\nu(u^\alpha) = \frac{1}{2}(\nabla_\nu u^\mu + \nabla_\mu u^\nu) \tag{4.53a}$$

$$\omega^\mu{}_\nu(u^\alpha) = \frac{1}{2}(\nabla_\nu u^\mu - \nabla_\mu u^\nu) \tag{4.53b}$$

Here the velocity gradient $\boldsymbol{L}(u^\mu)$, rate of deformation $\boldsymbol{d}(u^\mu)$ and spin $\boldsymbol{\omega}(u^\mu)$ are functions depending on the chosen velocity fields, so they can also be defined with the four-vector velocity $v^\mu$ instead of the four-vector velocity $u^\mu$ (see Eq. 2.6). As follows, when using $\boldsymbol{L}$ or $\boldsymbol{d}$ or $\boldsymbol{\omega}$ without precision, it will refer to the definition using the dimensionless four-velocity $u^\mu$.

Moreover, by giving the definition of the Lie derivative and of the rate of deformation, it can be derived such that [Rouhaud et al.,2013]:

$$\mathcal{L}_u(g_{\mu\nu}) = 2d_{\mu\nu} \text{ and } \mathcal{L}_u(g^{\mu\nu}) = -2d^{\mu\nu} \tag{4.54}$$

Then, with the definition of the Euler-Almansi strain tensor $\boldsymbol{e}$ (Eq. 4.45), it is possible to verify that the rate of deformation represents the variation of the Euler-Almansi strain in the sense of the Lie derivative, such that [Rouhaud et al.,2013]:

$$\mathcal{L}_u(e_{\mu\nu}) = d_{\mu\nu} \quad \text{and} \quad \mathcal{L}_u(e^{\mu\nu}) = d^{\mu\nu} - 2e_{\alpha\beta}d^{\alpha\nu}g^{\beta\mu} - 2e_{\alpha\beta}g^{\alpha\nu}d^{\beta\mu} \tag{4.55}$$

## 4.6 Example on the principle of covariance applied to Euclidean mechanical transformations

Now that we have introduced the elements of a spacetime modeling which enable us to obtain covariant mechanical models, let us illustrate the importance of such a modeling. The notion of objectivity defined

in section 1.4.2 is now discussed under the light of the principle of covariance in order to illustrate this principle.

Let us consider 2 Euclidean spacetime frames noted $(\mathbf{e}_\mu, \xi^\mu)$ and $(\widetilde{\mathbf{e}}_\mu, \widetilde{\xi^\mu})$ such that:

$$\xi^i = Q^i_j \widetilde{\xi^j} + \lambda^i \tag{4.56}$$

$$\xi^4 = \widetilde{\xi^4} = ct \tag{4.57}$$

where the orthogonal matrix $Q^i_j$ describes a rigid body rotation and the vector $\lambda^i$ represents a translation. This represents an Euclidean transformation in spacetime. Note that Euclidean transformations (i.e rigid body transformations in classical Newtonian continuum) preserve the 3D Euclidean distance between any two points [Thurston,1997, Gurtin,1982, Garrigues,2007, De Souza Neto et al.,2011]. The Jacobian matrix of this transformation is expressed by:

$$\frac{\partial \xi^\mu}{\partial \widetilde{\xi^\nu}} = \begin{pmatrix} Q^i_j & & & \frac{1}{c}\left[\frac{dQ^i_j}{dt}\widetilde{\xi^j} + \frac{d\lambda^i}{dt}\right] \\ 0 & 0 & 0 & 1 \end{pmatrix} \tag{4.58}$$

The determinant of this Jacobian matrix is then:

$$\left|\frac{\partial \xi^\mu}{\partial \widetilde{\xi^\nu}}\right| = \left|Q^i_j\right| = 1 \tag{4.59}$$

The velocity of one frame with respect to the other is expressed by:

$$\frac{d\xi^i}{dt} = c\frac{\partial \xi^i}{\partial \widetilde{\xi^4}} = \frac{dQ^i_j}{dt}\widetilde{\xi^j} + \frac{d\lambda^i}{dt} \tag{4.60}$$

As an illustration on the application of the objectivity and the covariance principles, let us consider the second-rank tensor $\boldsymbol{\tau}$. The principle of covariance applied in spacetime leads to write (see Eq. 2.8e):

$$\tau^{\mu\nu} = \frac{\partial \xi^\mu}{\partial \widetilde{\xi^\alpha}}\frac{\partial \xi^\nu}{\partial \widetilde{\xi^\beta}}\widetilde{\tau}^{\alpha\beta} \tag{4.61}$$

We consider the spatial components of this tensor; they can be expressed by:

$$\tau^{ij} = \frac{\partial \xi^i}{\partial \widetilde{\xi^m}}\frac{\partial \xi^j}{\partial \widetilde{\xi^n}}\widetilde{\tau}^{mn} + \frac{\partial \xi^i}{\partial \widetilde{\xi^m}}\frac{\partial \xi^j}{\partial \widetilde{\xi^4}}\widetilde{\tau}^{m4} + \frac{\partial \xi^i}{\partial \widetilde{\xi^4}}\frac{\partial \xi^j}{\partial \widetilde{\xi^n}}\widetilde{\tau}^{4n} + \frac{\partial \xi^i}{\partial \widetilde{\xi^4}}\frac{\partial \xi^j}{\partial \widetilde{\xi^4}}\widetilde{\tau}^{44} \tag{4.62}$$

We assume that the tensor $\boldsymbol{\tau}$ is symmetric and the Euclidean transformation expressed in Eq. 4.56 and 4.57 is applied to this tensor, then:

$$\tau^{ij} = Q^i_m Q^j_n \widetilde{\tau}^{mn} + \frac{2}{c}\left(\frac{d\lambda^j}{dt} + \frac{dQ^j_k}{dt}\widetilde{\xi^k}\right)Q^i_m \widetilde{\tau}^{m4} + \frac{1}{c^2}\left(\frac{d\lambda^i}{dt} + \frac{dQ^i_l}{dt}\widetilde{\xi^l}\right)\left(\frac{d\lambda^j}{dt} + \frac{dQ^j_k}{dt}\widetilde{\xi^k}\right)\widetilde{\tau}^{44} \tag{4.63}$$

The second and third terms of Eq. 4.63 are the result of application of the covariance principle (on the spatial components of a second-rank tensor). If these terms are omitted, the equation corresponds exactly to the definition of objectivity for a second-rank tensor in the classical Newtonian continuum (see Eq. 1.9). These terms are respectively proportional to $\frac{\widetilde{\tau}^{m4}\, v}{c}$ and $\frac{\widetilde{\tau}^{44}\, v^2}{c^2}$. In other words, the objectivity of the tensor $\boldsymbol{\tau}$ is respected in a motion for which $\frac{\widetilde{\tau}^{m4}\, v}{c} << \widetilde{\tau}^{mn}$ and $\frac{\widetilde{\tau}^{44}\, v^2}{c^2} << \widetilde{\tau}^{mn}$.

Otherwise the covariance of the tensor $\boldsymbol{\tau}$ is ensured thanks to all the additional terms which can be obtained from the development of the last 2 terms of Eq. 4.63.

## 4.7 Spacetime thermomechanical models in previous studies

One main objective of this study is to build models which can describe the thermomechanical phenomena taking place during forming processes by the use of a spacetime formalism. The spacetime thermal modeling has been discussed in part 1 of the manuscript. As for the spacetime mechanical modeling, many authors have evoked this subject [Vitokhin and Ivanova,2017, Badreddine,2006, Bertram,2012, Besson et al.,2009, Zhang et al.,2011, Borja,2013]. As follows, thermomechanical/mechanical models found in the literature are reviewed.

The spacetime modeling is possible using different methods [Panicaud et al.,2014, Panicaud et al.,2015, Wang,2016]:

1. Copying the existing Newtonian relationships and replace their variables with their spacetime equivalent. This is known as the direct relativization of Newtonian models or the 3D analogy method.
2. Starting from a thermodynamic approach by deriving a free energy function under non-dissipative conditions (which leads to spacetime hyperelastic models).
3. Using the representation theory in spacetime, between strain/strain-rate and stress/stress-rate tensors.
4. Building a specific spacetime stiffness for linear behaviors.
5. Deriving the spacetime hyperelastic/elastic models to obtain hypoelastic models.

Other methods to obtain various spacetime models can also be found in the literature. As follows, the spacetime thermoelastic, thermo-hyperelastic and hypoelastic models, as well as the methods used in the literature to obtain them, are reviewed.

### 4.7.1 Spacetime thermoelastic model

This model can be constructed by a direct relativization of the classical thermoelastic constitutive model [Panicaud et al.,2014]. This generalization is summarized by:

$$\sigma^{\mu}_{\nu} = f(\Delta\theta, b^{\lambda}_{\kappa}) \tag{4.64}$$

where $f$ is a function of the variables $\Delta\theta$ and $b^{\lambda}_{\kappa}$ previously defined in Eq. 4.46.

Eq. 4.64 is constrained by the 2 assumptions that: the material is homogeneous and 11 degrees of freedom have been chosen corresponding to $\Delta\theta$ and the 10 components of the symmetrical spacetime tensor $b^{\lambda}_{\kappa}$. As discussed in section 4.2.4, the thermoelastic model is not suitable to describe the behavior of all materials. Furthermore, this model is not ensured to be reversible since it does not derive from a 4D potential energy. Hence, spacetime thermo-hyperelastic models are generally required.

### 4.7.2 Spacetime thermo-hyperelastic model

To build a constitutive relation in the classical three-dimensional space, one possible approach consists of expressing the problem in a variational form [Bertram,2012]. In the spacetime formalism, the same methodology can be used. The advantage of such a method is that the use of four-tensors and four-operators ensures the covariance of models [Panicaud et al.,2014]. In order to obtain the constitutive relation, [Panicaud et al.,2014] assumes the existence of a function $F_{4D} = \Psi(\Delta\theta, \mathbf{b})$ such that:

$$\sigma^{\mu}_{\nu} = -2\frac{\widetilde{\rho_c}}{\widetilde{\rho_c}'} b^{\mu}_{\kappa} \frac{\partial \Psi(\Delta\theta, \mathbf{b})}{\partial b^{\nu}_{\kappa}} \tag{4.65}$$

Where $\widetilde{\rho_c}$ and $\widetilde{\rho_c}'$ are respectively associated to $\partial\Omega$ and $\partial\Omega'$ representing the respective hypervolumes of the undeformed and deformed matters.

Eq. 4.65 represents a constitutive relation for thermo-hyperelastic materials where no assumption has been done on $\Psi(\Delta\theta, \mathbf{b})$. It is frame-indifferent because it is constructed following the covariant principle.

However, its generality (i.e. ability to represent any 3D constitutive model) is not guaranteed as demonstrated in [Panicaud et al.,2015]; it depends on the 3D constitutive model chosen.

Note that, a similar spacetime formulation can also be obtained starting from a spacetime thermodynamical approach [Muller,1969, Vallée,1981, Landau and Lifshitz,1966]. However, there is still a debate regarding these works, especially on coupling different phenomena or concerning irreversible processes [Israel and Stewart,1979a, Israel and Stewart,1979b, Jou et al.,1988]. For simple elastic behavior and isothermal conditions, this approach can be considered as valid [Muller,1969, Panicaud et al.,2014].

In the following, the material is assumed to be isotropic. To ensure material isotropy together with the indifference with respect to the change of frames of $\Psi$, the representation theory is used. $\Psi(\Delta\theta, \mathbf{b})$ is formulated using the invariants of $b$: $b_I, b_{II}, b_{III}, b_{IV}$ [Broer,2019] such that:

$$\Psi(\Delta\theta, b) = \Psi(\Delta\theta, b_I, b_{II}, b_{III}, b_{IV}) \tag{4.66}$$

The invariants of $\mathbf{b}$ being:

$$b_I = g^\nu_\kappa b^\kappa_\nu; \quad b_{II} = b^\nu_\kappa b^\kappa_\nu; \quad b_{III} = b^\nu_\kappa b^\kappa_\lambda b^\lambda_\nu \tag{4.67}$$

The expression of $\sigma^\mu_\nu$ is then deduced by developing Eqs.4.65 and 4.66:

$$\sigma^\mu_\nu = a_I b^\mu_\nu + a_{II} b^\mu_\kappa (b^\kappa_\nu - b^\kappa_\lambda b^\lambda_\nu) \tag{4.68}$$

where: $a_K$ ($K$ running from $I$ to $III$, and $a_{III} = -a_{II}$) are three scalar valued functions depending on $\Delta\theta$, invariants of $\mathbf{b}$ and properties of the material studied and expressed by:

$$a_K(\Delta\theta, \mathbf{b}) = -2K \frac{\rho}{\rho'} \frac{\partial \Psi}{\partial b_K} \tag{4.69}$$

Note that if $a_{III} = 0$, Eq. 4.69 can be interpreted as a direct relativization in spacetime of Newtonian Eulerian elastic model. Another assumption is done on the form of $a_K$: the coefficients $a_i$ ($i$ running from 0 to 2) are introduced such that they only depend on the temperature variation. It leads to the spacetime thermo-hyperelastic model:

$$\sigma^\mu_\nu = \sqrt{|b^\alpha_\beta|}(a_1 b^{\mu\lambda}(g_{\mu\lambda} - b_{\mu\lambda}) + a_0 \Delta\theta) b^\mu_\nu + \sqrt{|b^\alpha_\beta|} a_2 b^\mu_\kappa (b^\kappa_\nu - b^\kappa_\lambda b^\lambda_\nu) \tag{4.70}$$

This model is constrained by the choice of $\Psi(\Delta\theta, b)$ resulting from the assumption of isotropic material. Moreover, the generalization to anisotropic behaviors is possible but quite complex.

Furthermore, a definition of spacetime stiffness of linear behaviors can be obtained by considering a general linear relationship between second-order stress tensor and second-order elastic strain tensor [Truesdell and Noll,2003, Panicaud et al.,2015]. Using this method, a spacetime hyperelastic model is proposed in [Panicaud et al.,2015] for isotropic behavior, with isothermal conditions at a macroscopic scale such that:

$$\sigma^{\mu\nu} = 2a_1(g_{\alpha\beta} e^{\alpha\beta}) g^{\mu\nu} + 2a_2 e^{\mu\nu} \tag{4.71}$$

$$\iff \sigma_{\mu\nu} = 2a_1(g^{\alpha\beta} e_{\alpha\beta}) g_{\mu\nu} + 2a_2 e_{\mu\nu} \tag{4.72}$$

This spacetime model is considered as a reference model for comparing other material behaviors (e.g. spacetime hypoelastic models). However, it is limited by the assumptions used to obtain it.

### 4.7.3 Spacetime hypoelastic model

The Newtonian hypoelastic model is first reviewed since it is used in developing the spacetime hypoelastic model [Panicaud et al.,2015, Wang,2016]. The hypoelastic model in classical Newtonian continuum mechanics is associated with the system of ordinary differential equation [Eringen,1962, Grot and Eringen,1966a] such that:

$$D_{3D}^{X}\sigma_{ij} = F_{3D}(\sigma_{ij}, D_{ij}) \tag{4.73}$$

where: $D_{ij}$ represents the Lagrangian rate of deformation tensor in the classical 3D space, $D_{3D}^{X}$ an objective rate operator of $D_{ij}$ ($X$ represents the randomness of type of the objective rate operator) and $F_{3D}$ is a function of $\sigma_{ij}$ and $D_{ij}$ in the classical 3D space. The dependence on $D_{ij}$ must be linear and the relation is integrable on a closed domain and the result is not necessarily null which shows a dissipative effect throughout the domain.

A spacetime hypoelastic model can then be deduced using the direct relativization of Newtonian hypoelastic model such that:

$$D_{4D}^{X}\sigma^{\mu\nu} = F_{4D}(g^{\mu\nu}, \sigma^{\mu\nu}, D_{\mu\nu}) \tag{4.74}$$

where: $D_{4D}^{X}$ is a spacetime rate operator which can be the covariant derivative or Lie derivative. It can be also obtained from spacetime thermodynamics and using the representation theory. The assumptions, hence the limitations of these models are similar to the ones discussed for thermo-hyperelastic models in section 4.7.2.

The derivation of hyperelastic models such as the models mentioned in section 4.7.2 can also be used to obtain hypoelastic models. Hence, models will carry the same defects of the models derived.

Hooke-like hypoelastic models obtained using different methods can be classified according to the integrability criterion [Panicaud et al.,2015, Wang,2016]. The models obtained are:

- Non-integrable hypo-elastic models obtained by replacing the deformation and the stress by their spacetime rate. The model obtained is expressed by:

$$D_{4D}^{X}\sigma^{\mu\nu} = 2a_1(g^{\alpha\beta}D_{\alpha\beta})g^{\mu\nu} + 2a_2 g^{\mu\alpha}g^{\nu\beta}D_{\alpha\beta} \tag{4.75}$$

  These correspond to the models obtained by the first three methods previously reviewed and match the definition of a spacetime hypoelastic model as given by Eq. 4.74.
- Integrable non-hypo-elastic models obtained by deriving the reference model (Eq. 4.71) which correspond to the models obtained by the fourth method previously reviewed. The model obtained is expressed by:

$$D_{4D}^{X}\sigma^{\mu\nu} = D_{4D}^{X}(2a_1(g^{\alpha\beta}D_{\alpha\beta})g^{\mu\nu} + 2a_2 g^{\mu\alpha}g^{\nu\beta}D_{\alpha\beta}) \tag{4.76}$$

- Integrable hypo-elastic models obtained by replacing the strain $e_{\mu\nu}$ in Eq. 4.76 by its definition and the use of Lie derivative. The model obtained is expressed by:

$$\mathcal{L}_u(\sigma^{\mu\nu}) = \varphi_1 g^{\mu\nu} + \varphi_2 g^{\mu\alpha}g\nu\beta D_{\alpha\beta} + \varphi_3\sigma^{\mu\nu} - 4g^{\mu\alpha}D_{\alpha\beta}g^{\beta\nu} \tag{4.77}$$

  where:

$$\varphi_1 = \frac{2(a_1)^2}{a_2(Na_1 + a_2)}(g^{\alpha\beta}D_{\alpha\beta})(g^{\alpha\beta}\sigma_{\alpha\beta}) + 2a_1(g^{\alpha\beta}D_{\alpha\beta}) - \frac{2a_1}{a_2}(\sigma^{\alpha\beta}D_{\alpha\beta}) \tag{4.78}$$

$$\varphi_2 = \frac{2a_1}{Na_1 + a_2}(g^{\alpha\beta}\sigma_{\alpha\beta}) + 2a_2 \tag{4.79}$$

$$\varphi_3 = (g^{\alpha\beta}D_{\alpha\beta}) \tag{4.80}$$

  This model shows advantages because of the use of Lie derivative [Grot and Eringen,1966a, Bressan,1978] which corresponds to a true time derivative: it includes naturally the effect of time variation, it is independent to any rigid body superposition and it is frame-indifferent.
  In [Panicaud et al.,2014], these proposed models are numerically tested. The third model shows particular advantages since it is integrable and covariant because of the use of Lie derivative.

### 4.7.4 Spacetime mechanical models discussed in [Wang,2016]

A PhD thesis carried out by Wang [Wang,2016] at the LASMIS laboratory at the University of Technology of Troyes investigates the spacetime mechanical models. In [Wang,2016], the thermodynamical approach is used under some assumptions to obtain these models:

- A framework as described in [Eckart,1940, Grot and Eringen,1966a] is considered. In this framework three field variables: the momentum-energy tensor $T^{\mu\nu}$, the particle current and the entropy vector, have been chosen to construct balance equations.
- The particle current is as described in [Eckart,1940].
- The decomposition of momentum-energy tensor results from the assumptions made on the form of the spacetime Cauchy stress tensor (see section 2.2.8).
- Thermal phenomena and thermomechanical couplings are not taken into account in this study.
- Relativistic models are developed. However, numerical simulations are performed at the non-relativistic limit. Hence, approximations are applied directly within the spacetime balance equations even if they are initially formulated in a spacetime formalism.

In this spacetime formalism, in addition to the isotropic hyperelastic and hypoelastic models previously discussed (sections 4.7.2 and 4.7.3 ), Wang has developed anisotropic elastic then elastoplastic models [Rougée,1997, Mandel,1983, Lubarda,2002, Maugin,1971a, Nemat-Nasser,1974].

The anisotropic elastic model is obtained using the definition spacetime stiffness of linear behaviors: it is a generalization of the elastic isotropic model reviewed in section 4.7.2. The elastoplastic models are constructed using the flow theory for plasticity from thermodynamics. Under the assumption of a specific choice of the state variables, the specific strain energy used was written:

$$\Psi = \Psi_{elasticity}(\Lambda/\widetilde{\rho_c}, \mu/\widetilde{\rho_c}, strain_{\mu\nu}, g^{\mu\nu}) + \Psi_{plasticity}(p, H_m) \tag{4.81}$$

where $strain_{\mu\nu}$ is the elastic strain, $p$ is the cumulated plastic strain and $H_m$ are $m$ constants of material for isotropic hardening. Besides, an additive decomposition of rate of deformation is considered such that: $d_{\mu\nu} = d_{E\mu\nu} + d_{P\mu\nu}$, where $d_{\mu\nu}$, $d_{E\mu\nu}$ and $d_{P\mu\nu}$ are respectively the total, elastic and plastic rate of deformations. Under the assumption of isotropic hardening, 3 elastoplastic models are developed: an elastoplastic model with a reversible hypoelastic part constructed with a Lie derivative, an elastoplastic model with an irreversible hypoelastic part constructed with a Lie derivative, and an elastoplastic model with an irreversible hypoelastic part constructed with a Jaumann transport.

The first model is the only one to have a non-linear hypoelastic part that can be proved to be reversible. Hence, it is the only model that corresponds to the assumption that only the plastic deformation causes dissipations of energy.

In general, models developped in [Wang,2016] are covariant since they are built in a spacetime framework. For incremental models, the Lie derivative is used [Panicaud et al.,2015], allowing to express variation with respect to time, while being simultaneously covariant and invariant with respect to the superposition of rigid body motion. However, thermomechanical couplings are not taken into account in these models and models are limited by the assumptions made (the choice of variables and decomposition of momentum-energy tensor). Besides this thesis was limited to the development of these models, although this formalism could cover other models such as the viscoelastic and viscoplastic models.

Simulations are done to compare different spacetime models. However, Wang implemented numerically the spatial components of these spacetime models (i.e. their projection on the classical Newtonian continuum) and not directly the spacetime model. Simulations of these models using "Zset", which does not consider numerical spacetime scheme of resolution, are done for different geometries and loading (Fig. 39).

Simulations using projection of the spacetime hypoelastic models are performed for two geometries using different loads. First, the case of a cubic element subjected to gliding, traction load and then unloaded is studied. Then, the case of a bar meshed with 320 reduced quadrilateral elements subjected to torsion, traction and then unloaded, is studied. The hypoelastic reversible model constructed with the Lie derivative shows a total compatibility with the Hookean model of reference for these two cases (example in Fig. (39)). However, the use of this model takes a computation time superior by 15% to that required when using the spacetime hypoelastic irreversible models constructed respectively with the Lie derivative and with the Jaumann derivative.

Similarly, simulations using the projection of the 3 spacetime elastoplastic models previously described are performed for two geometries. The case of a cubic element subjected to gliding then unloaded is studied,

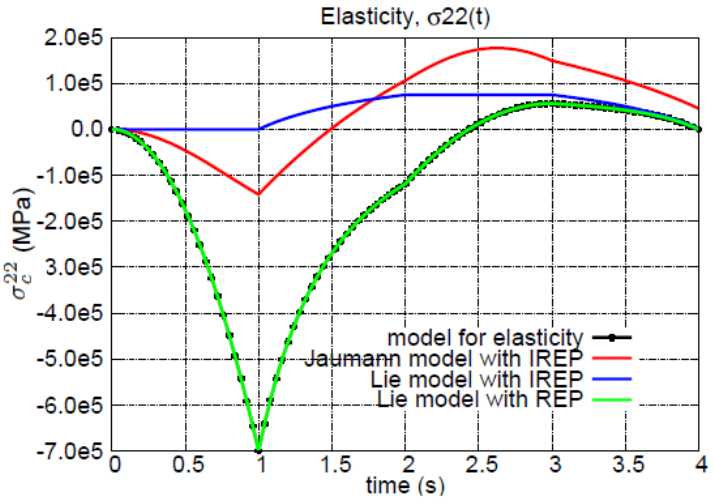


**Fig. 39:** The variation of $\sigma_c^{22}$ as a function of time for a cycle of deformation (gliding, traction, release), obtained using Zset, of a cubic element at large deformation and without plasticity for the different models examined: the elastic model, the hypoelastic irreversible model (IREP) constructed with the Lie derivative, the hypoelastic irreversible model constructed with the Jaumann derivative and the hypoelastic reversible model (REP) constructed with the Lie derivative.

as well as the case of a beam meshed into 320 quadrilateral elements subjected to the same cycle of stress. The spacetime elastoplastic model with a reversible elastic part and the Lie derivative is shown to be the most precise.

These simulations compare advantageously different methods used to obtain spacetime models by illustrating the results of these models (Fig. 40). However, the projection of the models obtained in spacetime and the numerical simulations in the Newtonian domain, show advantageous results compared to the Newtonian models numerical results (due to the projection of additional terms obtained in spacetime modeling, e.g. expressed by the difference between the blue and black curves of Fig. 40) but do not illustrate all the benefits of covariant models. This is why the space projection studied in [Wang,2016] is not enough to illustrate the benefits of the use of the spacetime formalism. Contrarily, the spacetime models are covariant and therefore carry additional terms derived from this fact and that the spatial projection may neglect. These differences will be studied in the next chapter of the manuscript and this will be possible by the use of spacetime projectors in the modeling and using a simulation tool enabling a full spacetime numerical resolution. We therefore expect more accurate models than Newtonian models that might be matched more correctly with reality in case of large deformations.

## 4.8 Conclusions

In this chapter, the mechanical modeling for large deformations found in the literature was reviewed. The non-linearity of mechanical models was introduced by the use of Green-Lagrange and Euler-Almansi strains (section 4.2.1). Using these definitions and the mechanical balance law (Eq. 4.14), the Newtonian elastic, thermoelastic, hyperlastic and elasto-plastic models and corresponding weak integral forms for small then large deformations (sections 4.2.2, 4.2.3, 4.2.4 and 4.2.6) were reminded for continuous media in the case of homogeneous isotropic materials. Thermomechanical couplings were taken into account only for the thermoelastic models. Lagrangian and Eulerian descriptions were used for large deformations models using respectively Green-Lagrange and Euler-Almansi strains. The weak forms of these models were then deduced by multiplying the models by arbitrary test functions and integrating them on the 3D domain. This step will be further useful in order to compare the Newtonian models to different spacetime models which will be later developed in chapter 5.

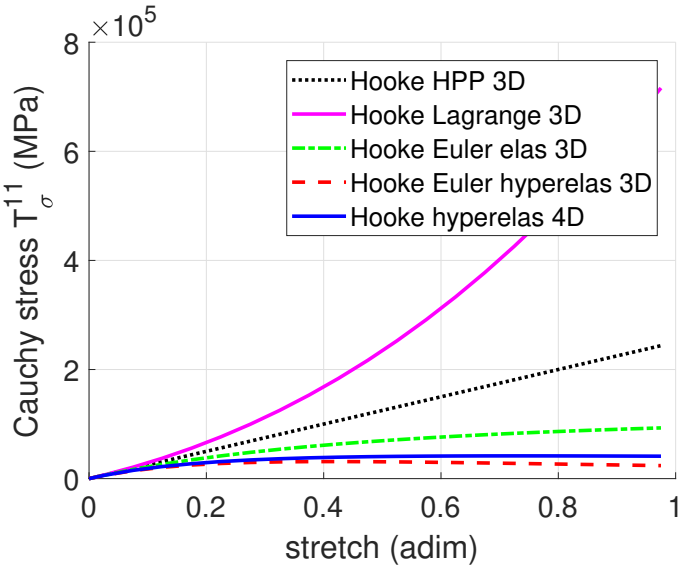


**Fig. 40:** The variation of $T_{\sigma}^{11}$ as a function of stretch for a beam under traction without plasticity for the different Newtonian elastic and hyperelastic models and the spacetime hyperelastic model projected [Wang,2016]. These models are implemented using "MATLAB" and using the same material parameters as in section 4.2.5.3 and for a the stretch of $\chi(t) = 0.1\,t$, where $0 < t < t_{max} = 10s$.

Two examples illustrated the Newtonian models reviewed. In the first example, elastic and hyperelastic models were illustrated (section 4.2.5). It consisted in applying a traction load using a Dirichlet boundary condition on a beam geometry. The evolution of the Cauchy stress tensor in the $x$-direction $\sigma_c^{11}$ in function of time shows that the model using Green-Lagrange strain has different elastic and hyperelastic behaviors while the other models have the same elastic and hyperelastic behaviors.

In the second example, the plastic behavior was observed: the same geometry, load and boundary conditions as in the previous example were applied (section 4.2.7). Results of the evolution of $\sigma^{11}$ in function of time show that the plastic model using Green-Lagrange has a different evolution of $\sigma^{11}(t)$ than the one using small strain and Euler-Almansi strain due to its different elastic behavior. These examples help to visualize the behavior of different models using different strain definitions and thus give some expected behaviors of such models when considering spacetime approach.

Moreover, the difficulties facing the mechanical modeling in a classical Newtonian continuum can be summarized by: the non linearity of the models (e.g. plastic models) and the need to fulfill the material objectivity of the models. The use of a thermodynamical approach built in a spacetime formalism (as the one introduced in part 1 of the manuscript) seems to be able to alleviate these problems. Since the spacetime method will be further used, the spacetime tools necessary for mechanical modeling in a spacetime formalism were introduced e.g. spacetime deformation gradient, spacetime strain tensors, the Lie derivative, the rate of deformation, spin tensors. In section 4.6, an example was used to illustrate the additional terms resulting from applying the covariance principle on transformations and especially in the case of a second-order tensor.

Eventually, in the literature, different spacetime mechanical models were proposed, such as spacetime expansions of the Hooke's model taking into account kinematic/geometric non-linearities. In [Rouhaud et al.,2013] and [Panicaud et al.,2015], spacetime thermoelastic, thermo-hyperelastic and hypoelastic models were obtained using different methods such as direct relativization of Newtonian models, thermodynamics approach, using the representation theory... However, in [Rouhaud et al.,2013] and [Panicaud et al.,2015] the covariant models were obtained under hypotheses that limit their use (isotropy, isothermal conditions, macroscopic scale...)and the numerical simulation were not conducted with spacetime resolution. Besides, in some models, Lie derivative and projection operators were not used in the methodology, which requires further development of the constitutive models obtained.

Furthermore, a study by Wang [Wang,2016] (section 4.7.4) investigated the spacetime anisotropic elastic and elastoplastic models. This study was limited to the mechanical modeling thus the modeling of thermal behavior of material and thermomechanical coupling was neglected in the resulting models. In addition to that, only the spatial projection of the spacetime models were implemented for simulation and were compared to Newtonian mechanical models. This limits the ability to study the impact of a spacetime approach on the mechanical models from a numerical point of view since the resolution of the problem is Newtonian. Thus, the advantages of a spacetime numerical resolution: use of covariant derivatives, spacetime metric, expression of the spacetime energy-momentum tensor... were not reached yet.
In the next chapter, we propose a spacetime thermodynamical methodology leading to a spacetime thermomechanical coupled model. This methodology respects the covariance principle and the use of covariant derivatives. It also respects the use of projection operators in the development of spacetime models. The weak form of the problem will be then implemented for simulation without any spatial projection using FEniCS project which actually enables a spacetime numerical resolution. The results obtained from spacetime models will then be compared to results obtained from the corresponding Newtonian models.

# 5 Spacetime modeling of the thermomechanical behavior of materials

## 5.1 Introduction

In the aim of building thermomechanical models respecting laws of thermodynamics as well as the causality and covariance principles, spacetime weak integral forms for thermomechanical behaviors are developed in this chapter. We also aim to obtain a spacetime numerical resolution of the thermomechanical problem, this is why the spacetime methodology will be further developed to take into account projectors, the definitions of covariant derivatives and thermomechanical couplings (beyond the assumption made in chapters 2 and 3).

In the following, we suggest a spacetime thermomechanical model obtained by the same procedure used in chapter 2 for obtaining spacetime thermal models. On one hand, the thermomechanical model will be formulated using the spacetime formalism. On the other hand, thermomechanical models showing dissipative behavior should be compatible with the second principle of thermodynamics. This latter combined with the first principle leads to the inequality of Clausius-Duhem for thermomechanics [Bertram,2012, Besson et al.,2009, Bonet and Wood,2008].

To obtain the first and second principles of thermodynamics, the energy-momentum balance law coupling thermal and mechanical phenomena will be introduced [Landau and Lifshitz,1975]. The spacetime formulation of thermomechanical models and weak forms can then be deduced for general applications to large deformations, as well as for small deformations..

Furthermore, in order to compare the Newtonian and the spacetime modeling, test cases similar to the examples of chapters 4, are done to compare the use of both approaches. The case of a bimetallic element is also simulated as an application of the spacetime thermo-hyperelastic modeling for small deformations.

## 5.2 Energy-momentum tensor

At this stage of the manuscript, we look to find models of the thermo-mechanical behavior of materials. Consequently, the mechanical stress applied to the material body is now taken into consideration, which is equivalent to: $T_{\sigma}^{\mu\nu} \neq 0$. We remind that the modeling is done under the following assumptions: gravitation, electromagnetic fields, volume heat source, diffusion of molecules, chemical reactions, change in physical states are not taken into account. The hypothesis of local thermodynamic equilibrium is assumed.

The equation of energy-momentum for this case of study (see section 2.2.8):

$$T^{\mu\nu} = T_{\mathcal{U}}^{\mu\nu} + T_{q}^{\mu\nu} + T_{\sigma}^{\mu\nu} = \mathcal{U}u^{\mu}u^{\nu} + q^{\mu}u^{\nu} + u^{\mu}q^{\nu} + T_{\sigma}^{\mu\nu} \tag{5.1}$$

where: $\mathcal{U}$ is the energy density and $q^{\mu}$ is the volume heat flux four-vector (see table 11).

### 5.2.1 Energy four-tensor

Using the definition of mass density $\rho$, the mass density in a convective frame for $e_{int} \neq 0$ denoted $\rho_c$ and the mass density at rest in the convective frame, considering no internal energy denoted $\widetilde{\rho}_c$, the energy four-tensor $T_{\mathcal{U}}^{\mu\nu}$ can be further developed to:

$$\mathcal{U} = \rho c^2/\gamma = \rho_c c^2 = \widetilde{\rho}_c c^2 \left(1 + \frac{e_{int}}{c^2}\right) \tag{5.2}$$

$$\Rightarrow T_{\mathcal{U}}^{\mu\nu} = \mathcal{U}u^{\mu}u^{\nu} = \widetilde{\rho}_c c^2 \left(1 + \frac{e_{int}}{c^2}\right) u^{\mu}u^{\nu} \tag{5.3}$$

where $\rho_c = \widetilde{\rho}_c \left(1 + \frac{e_{int}}{c^2}\right)$ is the mass density in case $e_{int} \neq 0$ and the specific internal energy $e_{int}$ depends on the following state variables: the temperature $\theta$ and the displacement $dep^{\mu}$. This term naturally includes the macroscopic kinetic energy.

### 5.2.2 Heat four-tensor

The heat four-tensor $T_q^{\mu\nu}$ is developed in part 1 of this manuscript. Four methods are illustrated in sections 2.3 and 2.4 in order to obtain respectively the spacetime Fourier's and Cattaneo's models of heat conduction. Cattaneo's model of heat conduction can be expressed as in Eq. 2.38. This model verifies the covariance principle, the causality principal and is built using a thermodynamical approach. When $\tau$ and $\tau_1$ (of the order of $ns$) are negligible with respect to the time ($t \in t_{macro}$, see section 1.5.7), the advantages of this model are limited. We thus propose to use in this chapter the spacetime Fourier model of heat conduction expressed in Eq. 2.32.

$$
\begin{aligned}
T_q^{\mu\nu} &= q^\mu u^\nu + u^\mu q^\nu && (5.4)\\
&= \frac{\lambda}{c}\Pi^{\mu\kappa}\left(\nabla_\kappa\theta\right)u^\nu + u^\mu\frac{\lambda}{c}\Pi^{\nu\kappa}\left(\nabla_\kappa\theta\right) && (5.5)\\
&= \frac{\lambda}{c}(\Pi^{\mu\kappa}u^\nu + \Pi^{\nu\kappa}u^\mu)\nabla_\kappa\theta && (5.6)
\end{aligned}
$$

### 5.2.3 Stress four-tensor

We assume that the stress four-tensor $T_\sigma^{\mu\nu}$ depends on the following state variables: the temperature $\theta$ and the displacement $dep^\mu$. In addition to this, it depends on the projection operator, thus on the metric tensor $g^{\mu\nu}$. The impact of use of the projection operator is one of the aims of this chapter. It will be further expressed for spacetime hyperelastic models as a function of the specific free energy $\Psi$ (see section 5.5).

## 5.3 Four-dimensional balance laws for continuous media

### 5.3.1 Balance of the molecules number

We assume that the molecules cannot be created or annihilated, which leads to the principle of balance of molecules number. We consider again the spacetime global domain of the material of hypervolume $\mathcal{D}$ with frontier $\partial\mathcal{D}$. We introduce the molecules current $n^\mu$ which thus verifies:

$$\forall x^\mu \in \mathcal{D}, \nabla_\mu n^\mu = 0 \quad (5.7)$$

Problems occur when defining this molecule current four-vector velocity. In the general context of relativistic physics, this molecule current may be defined as:

$$n^\mu = nu^\mu + \nu^\mu \quad (5.8)$$

where the scalar $n$ represents the molecules number density (per unit of volume) in the proper frame and the four-vector velocity $\nu^\mu$ represents the molecules diffusion current. When non-thermomechanical dissipation occurs, two different assumptions can be adopted: they are proposed by [Eckart,1940] and by [Landau and Lifshitz,1975]. Different authors have attempted to merge these two approaches [Schellstede et al.,2014, Israel,1989]. In this manuscript, since such dissipations are not considered, the diffusion term is chosen such that $\nu^\mu = 0$. Consequently, the balance equation of all the molecules in $\mathcal{D}$ eventually leads to:

$$\forall x^\mu \in \mathcal{D}, \nabla_\mu(\widetilde{\rho}_c u^\mu) = 0 \quad (5.9)$$

It corresponds to the balance of the rest mass per unit of volume. At the non-relativistic limit, it would lead to the classical continuity equation.

### 5.3.2 Balance of the momentum and energy

The spacetime energy-momentum balance can be obtained from the definition of the energy-momentum tensor. In a general frame of reference, it can be locally written as:

$$\forall x^\mu \in \mathcal{D}, \nabla_\nu T^{\mu\nu} = 0 \tag{5.10}$$

$$\Leftrightarrow \forall x^\mu \in \mathcal{D}, \nabla_\nu T^{\mu\nu}_{\mathcal{U}} + \nabla_\nu T^{\mu\nu}_{q} + \nabla_\nu T^{\mu\nu}_{\sigma} = 0 \tag{5.11}$$

Using Eq. 5.1 and Eq. 5.6, we obtain:

$$\forall x^\mu \in \mathcal{D}, \nabla_\nu (T^{\mu\nu}_{\mathcal{U}} + T^{\mu\nu}_{q} + T^{\mu\nu}_{\sigma}) = 0 \tag{5.12}$$

$$\Leftrightarrow \forall x^\mu \in \mathcal{D}, \nabla_\nu \left( \widetilde{\rho}_c c^2 \left( 1 + \frac{e_{int}}{c^2} \right) u^\mu u^\nu + \frac{\lambda}{c} (\Pi^{\mu\kappa} u^\nu + \Pi^{\nu\kappa} u^\mu) \partial_\kappa \theta + T^{\mu\nu}_{\sigma} \right) = 0 \tag{5.13}$$

The expressions of $e_{int}(\theta, dep^\mu)$ and $T^{\mu\nu}_{\sigma}(\theta, dep^\mu, g^{\mu\nu})$ can then be injected in Eq. 5.13 leading to:

$$\nabla_\nu \left( \widetilde{\rho}_c c^2 \left( 1 + \frac{e_{int}(\theta, dep^\mu)}{c^2} \right) u^\mu u^\nu + \frac{\lambda}{c} (\Pi^{\mu\kappa} u^\nu + \Pi^{\nu\kappa} u^\mu) \partial_\kappa \theta + T^{\mu\nu}_{\sigma}(\theta, dep^\mu, g^{\mu\nu}) \right) = 0 \tag{5.14}$$

We now have to determine the expression of $e_{int}$ and $T^{\mu\nu}_{\sigma}$ which can be connected.

### 5.3.3 Balance of the internal energy

It is interesting to calculate the balance of the energy-momentum tensor along the direction of the velocity four-vector to obtain the balance of internal energy of the system. With the time projector (see section 2.2.4), it leads locally to:

$$\forall x^\mu \in \mathcal{D}, u_\mu \nabla_\nu T^{\mu\nu} = 0 \tag{5.15}$$

In order to develop Eq. 5.15, we use :

$$u_\mu \nabla_\nu T^{\mu\nu} = \nabla_\nu (u_\mu T^{\mu\nu}) - T^{\mu\nu} \nabla_\nu u_\mu = 0 \tag{5.16}$$

First using the fact that $\nabla_\nu (u_\mu T^{\mu\nu}_{\sigma}) = 0$ because $u_\mu T^{\mu\nu}_{\sigma} = 0$ (because of its construction by the projection of $T^{\mu\nu}$, see section 2.2.8 [Wang,2016]) and $u_\mu T^{\mu\nu}_{q} = q^\nu$ which is obtained using Eq. 2.21:

$$\begin{aligned} u_\mu T^{\mu\nu}_{q} &= u_\mu q^\nu u^\mu + u_\mu q^\mu u^\nu \\ &= q^\nu + (\delta^\mu_\alpha - u^\mu u_\alpha) u_\mu T^{\alpha\beta} u_\beta u^\nu = q^\nu \end{aligned} \tag{5.17}$$

We obtain:

$$\nabla_\nu (u_\mu T^{\mu\nu}) = \nabla_\nu (\tilde{\rho_c} (c^2 + e_{int}) u^\nu) + \nabla_\nu q^\nu \tag{5.18}$$

Second, using $u_\mu u^\mu = 1$, we can deduce that: $u^\mu \nabla_\nu u_\mu = u_\mu \nabla_\nu u^\mu = 0$. Then:

$$T^{\mu\nu} \nabla_\nu u_\mu = q^\mu u^\nu \nabla_\nu u_\mu + T^{\mu\nu}_{\sigma} \nabla_\nu u_\mu \tag{5.19}$$

Eqs. 5.18 and 5.19 lead to:

$$u_\mu \nabla_\nu T^{\mu\nu} = \nabla_\nu (\tilde{\rho_c} (c^2 + e) u^\nu) + \nabla_\nu q^\nu - q^\mu u^\nu \nabla_\nu u_\mu - T^{\mu\nu}_{\sigma} \nabla_\nu u_\mu \tag{5.20}$$

If $T^{\mu\nu}$ is symmetric, then according to its definition (Eq. 2.23), $T^{\mu\nu}_{\sigma}$ is symmetric. Eq. 5.20 can then be rewritten using the rate of deformation $d^{\mu\nu}$ (symmetric part of the velocity gradient):

$$u_\mu \nabla_\nu T^{\mu\nu} = \nabla_\nu (\tilde{\rho_c} (c^2 + e_{int}) u^\nu) + \nabla_\nu q^\nu - q^\mu u^\nu \nabla_\nu u_\mu - T^{\mu\nu}_{\sigma} d_{\mu\nu} = 0 \tag{5.21}$$

We then conclude on the internal energy balance :

$$\nabla_\nu(\tilde{\rho_c}(c^2+e_{int})u^\nu)+\nabla_\nu q^\nu - q^\mu u^\nu \nabla_\nu u_\mu = T_\sigma^{\mu\nu} d_{\mu\nu} \tag{5.22}$$

In the special case of adiabatic behavior and because $u^\mu u^\nu d_{\mu\nu}=0$ (meaning that $\underline{d}_{\mu\nu}=d_{\mu\nu}$), it is also possible to write the internal energy balance directly as a function of the total energy-momentum tensor such that:

$$\forall x^\mu \in \mathcal{D}, \nabla_\nu(\tilde{\rho_c}(c^2+e_{int})u^\nu) \quad = \quad T^{\mu\nu} d_{\mu\nu} \tag{5.23}$$

We can now derive Eq. 5.22:

- In an inertial frame with the choice of a 3D Cartesian coordinate system, the covariant derivative reduces to the partial derivative and the four-vector velocity can be expressed as in Eq. 2.6.

$$\begin{aligned} \widetilde{\rho}_c u^\nu \partial_\nu((c^2+e_{int})) + \partial_\nu q^\nu - q^\mu u^\nu \partial_\nu u_\mu &= T_\sigma^{\mu\nu} d_{\mu\nu} \\ \Leftrightarrow \widetilde{\rho}_c \frac{d}{ds}(c^2+e_{int}) + \frac{\partial q^i}{\partial x^i} + \frac{\partial q^4}{cdt} - q^\mu \frac{du_\mu}{ds} &= T_\sigma^{\mu\nu} d_{\mu\nu} \\ \Leftrightarrow \widetilde{\rho}_c \frac{de_{int}}{ds} + \frac{\partial q^i}{\partial x^i} + \frac{\partial q^4}{cdt} - q^\mu \frac{du_\mu}{ds} &= T_\sigma^{\mu\nu} d_{\mu\nu} \end{aligned} \tag{5.24}$$

- In an inertial frame with the choice of a 3D Cartesian coordinate system, for which the motion would be non-relativistic ($v \ll c$), we obtain:

$$\widetilde{\rho}_c \frac{de_{int}}{dt} + \frac{\partial \phi^i}{\partial x^i} + \frac{\partial q^4}{\partial t} - q^\mu \frac{du_\mu}{dt} \quad = \quad c(T_\sigma^{ij} d_{ij} + 2T_\sigma^{i4} d_{i4} + T_\sigma^{44} d_{44}) \tag{5.25}$$

Since $\frac{\partial q^4}{\partial t}$ is negligible with respect to $\frac{\partial \phi^i}{\partial x^i}$, Eq. 5.25 can then be approximated to:

$$\widetilde{\rho}_c \frac{de_{int}}{dt} + \frac{\partial \phi^i}{\partial x^i} - q^\mu \frac{du_\mu}{dt} \quad \approx \quad c(T_\sigma^{ij} d_{ij} + 2T_\sigma^{i4} d_{i4} + T_\sigma^{44} d_{44}) \tag{5.26}$$

Eq. 5.26 is the non-relativistic balance of internal energy. If the acceleration term $\frac{du_\mu}{dt}$ is null, in addition to $T_\sigma^{4j} = T_\sigma^{44} = 0$ or $\approx 0$, and/or if $d^{4j} = d^{44} = 0$ or $\approx 0$, it reduces to the Newtonian balance of internal energy [Brunet,2009], noting that $c\boldsymbol{d(u)} \approx \boldsymbol{d(v)}$.

### 5.3.4 Balance of the entropy

Now we can locally express the balance of entropy through the inequality:

$$\forall x^\mu \in \mathcal{D}, \nabla_\nu S^\nu \quad = \quad \frac{\Phi}{\theta\ c} \tag{5.27}$$

where $\Phi$ is the dissipation, which is the irreversibility source with the constraint that $\Phi \geq 0$, and $\theta$ is the temperature also assumed to be strictly positive. Besides, we can define the entropy current as in Eq. 2.27 which leads to:

$$\forall x^\mu \in \mathcal{D}, \nabla_\nu(\widetilde{\rho}_c \eta_c u^\nu) + \nabla_\nu(\frac{q^\mu}{\theta}) \quad = \quad \frac{\Phi}{\theta\ c} \tag{5.28}$$

This is the equivalent to Eq. 2.28.

- For an inertial frame with the choice of a 3D Cartesian coordinate system, the covariant derivative reduces to the partial derivative and the four-vector velocity can be expressed as in Eq. 2.16. We can then write:

$$\widetilde{\rho}_c \frac{d\eta}{ds} + \frac{\partial}{\partial x^i}(\frac{q^i}{\theta}) + \frac{\partial}{c\partial t}(\frac{q^4}{\theta}) \quad = \quad \frac{\Phi}{\theta\ c} \tag{5.29}$$

- For an inertial frame with the choice of a 3D Cartesian coordinate system, for which the motion would be non-relativistic ($v \ll c$), we obtain:

$$\widetilde{\rho}_c \frac{d\eta}{dt} + \frac{\partial}{\partial x^i}(\frac{\phi^i}{\theta}) \quad \approx \quad \frac{\Phi}{\theta} \tag{5.30}$$

Eq. 5.30 is the balance of entropy in the absence of chemical phenomena or diffusion species. It corresponds to the second principle of thermodynamics written in the Newtonian case [Brunet,2009].

## 5.4 The four-dimensional form of the Clausius-Duhem inequality

As in Newtonian mechanics, it is possible to locally express the second principle by construction of a generalized spacetime expression of the Clausius-Duhem inequality. Consequently:

$$\forall x^\mu \in \mathcal{D}, \theta \nabla_\nu S^\nu - u_\mu \nabla_\nu T^{\mu\nu} = \frac{\Phi}{c} \quad \geq \quad 0 \tag{5.31}$$

$$\Rightarrow \forall x^\mu \in \mathcal{D}, \theta \nabla_\nu(\widetilde{\rho}_c \eta_c u^\nu) + \nabla_\nu(\frac{q^\mu}{\theta}) - \nabla_\nu(\rho_c c^2 u^\nu)$$

$$-\nabla_\nu(q^\nu) + q^\mu u^\nu \nabla_\nu(u_\mu) + T^{\mu\nu} d_{\mu\nu} = \frac{\Phi}{c} \quad \geq \quad 0$$

$$\widetilde{\rho}_c \theta u^\mu \nabla_\mu \eta_c - \widetilde{\rho}_c u^\mu \nabla_\mu e_{int} - \frac{1}{\theta} q^\mu \nabla_\mu \theta + q_\nu u^\mu \nabla_\mu u^\nu + T_\sigma^{\mu\nu} d_{\mu\nu} \quad \geq \quad 0 \tag{5.32}$$

In this inequality, terms are related, respectively, to the evolution of entropy, the evolution of internal energy, the thermal dissipations (one is coupled to mechanics with the term $u^\mu \nabla_\mu u^\nu$) and the internal mechanical power $T_\sigma^{\mu\nu} d_{\mu\nu}$.

By introducing the specific free energy defined by: $\psi = e_{int} - \theta \eta_c$, the previous inequality is equivalent to:

$$-\widetilde{\rho_c}(u^\mu \nabla_\mu \psi + \eta_c u^\mu \nabla_\mu \theta) \quad - \quad q^\mu \left( \frac{1}{\theta} \nabla_\mu \theta - u^\nu \nabla_\nu u_\mu \right) + T_\sigma^{\mu\nu} d_{\mu\nu} = \frac{\Phi}{c} \geq 0 \tag{5.33}$$

In the following, the spacetime form of Clausius-Duhem inequality is expressed in different frames:

- In an inertial frame with the choice of a 3D Cartesian coordinate system, the covariant derivative reduces to the partial derivative and the four-vector velocity can be expressed as in Eq. 2.6. We can then write using Eq. 2.35:

$$\widetilde{\rho}_c c \left( \theta \frac{d\eta}{ds} - \frac{de_{int}}{ds} \right) - c \frac{q^\mu}{\theta} (\partial_\mu \theta - \theta \frac{du_\mu}{ds}) + c T_\sigma^{\mu\nu} d_{\mu\nu} = \Phi \quad \geq \quad 0 \tag{5.34}$$

- For an inertial frame with the choice of a 3D Cartesian coordinate system, for which the motion would be non-relativistic ($v \ll c$), we obtain:

$$\widetilde{\rho}_c \left( \theta \frac{d\eta}{dt} - \frac{de_{int}}{dt} \right) - \frac{\phi^i}{\theta} \partial_i \theta - \frac{q^4}{\theta} \frac{\partial \theta}{\partial t} + q^i \frac{du_i}{dt} + q^4 \frac{du_4}{dt}$$

$$+ c(T_\sigma^{ij} d_{ij} + 2 T_\sigma^{i4} d_{i4} + T_\sigma^{44} d_{44}) = \Phi \quad \geq \quad 0 \tag{5.35}$$

Since $\frac{\partial q^4}{\partial t}$ is negligible with respect to $\frac{\partial \phi^i}{\partial x^i}$, Eq. 5.35 can then be approximated to:

$$\widetilde{\rho}_c \left( \theta \frac{d\eta}{dt} - \frac{de_{int}}{dt} \right) - \frac{\phi^i}{\theta} \partial_i \theta + q^i \frac{du_i}{dt} + q^4 \frac{du_4}{dt}$$

$$+ c(T_\sigma^{ij} d_{ij} + 2 T_\sigma^{i4} d_{i4} + T_\sigma^{44} d_{44}) \approx \Phi \quad \geq \quad 0 \tag{5.36}$$

Eq. 5.36 is the non-relativistic expression of the Clausius-Duhem inequality. It corresponds to another expression of the second principle of thermodynamics. If the acceleration term $\frac{du_\mu}{dt}$ is null, in addition to $T_\sigma^{4j} = T_\sigma^{44} = 0$ or $\approx 0$, and/or if $d^{4j} = d^{44} = 0$ or $\approx 0$, it reduces to the expected Newtonian Clausius-Duhem inequality (see Eq. 1.17), noting that $c\boldsymbol{d(u)} \approx \boldsymbol{d(v)}$.

## 5.5 Spacetime thermo-hyperelastic model formulation

From the spacetime generalization of the Clausius-Duhem, it is possible to obtain constitutive behaviors of materials. In this section, we aim to obtain a formulation of the spacetime thermo-hyperelastic behavior of materials. As in the Newtonian case, it is assumed that hyperelasticity also ensures that the material models are non-dissipative (i.e. $\Phi = 0$). Moreover, we build the constitutive behavior using Lie derivative since this rate is objective in spacetime (see section 4.5.3). In order to obtain directly the constitutive behavior, we replace equivalently the covariant derivative by the Lie derivative where possible in Eq. 5.33: especially for occurrence of $u^\mu \nabla_\mu(.)$ for scalars that have a weight $W = 0$ (this is the case of the specific free energy and temperature). It is an important innovative step of the proposed methodology. Eq. 5.33 can then be rewritten as:

$$-\widetilde{\rho}_c(\eta_c \mathcal{L}_u(\theta) + \mathcal{L}_u(\Psi)) \quad - \quad q^\mu \left( \frac{1}{\theta} \nabla_\mu \theta - u^\nu \nabla_\nu u_\mu \right) + T^{\mu\nu}_\sigma d_{\mu\nu} = 0 \tag{5.37}$$

It is worth noting that the use of the Lie derivative is a particular choice that is, at this step of the derivation, not better than an other choice. In order to develop Eq. 5.37, it is necessary to define all the arguments of the Lie derivative: the materials parameters, the kinematic tensors and the temperature. Choosing the constitutive model consists in choosing a specific free energy $\Psi$.

**Assumptions:**

Several assumptions are made at this stage:

- We suppose that the temperature is coupled to the mechanical behavior through a strong coupling.
- We assume an isotropic behavior of materials at macroscopic scale. Full isotropic behavior requires at least 2 independent material parameters (for example the Lamé coefficients) [Wang,2016]. Therefore, the chosen behavior is also invariant under spacetime rotation, consequently invariant to the Galilean translation at the non-relativistic limit. This full symmetry is assumed in the following.

Moreover, the resulting model should satisfy:

- The balance of molecules number (Eq. 5.7), the balance of momentum and energy (Eq. 5.11), the balance of internal energy (Eq. 5.15), the balance of entropy (Eq. 5.27) and the Clausius-Duhem inequality (Eq. 5.32).
- $T^{\mu\nu}_\sigma u_\mu = 0$ to respect the construction of $T^{\mu\nu}$.
- The symmetry of $T^{\mu\nu}$ and $T^{\mu\nu}_\sigma$.
- $T^{\mu\nu}_\sigma$ is as a function of the specific free energy $\Psi$. Thus, the designated $\Psi$ should a priori depend on spatial projected quantities at least for its mechanical part.

Therefore, we consider the following partition of $\Psi$ such that:

$$\Psi = \Psi_\theta(\mathcal{C}_{mP}, \theta) + \Psi_\sigma(\Lambda/\widetilde{\rho}_c, \mu/\widetilde{\rho}_c, \underline{I}_I, \underline{I}_{II}) + \Psi_{\theta,\sigma}(\kappa\alpha/\widetilde{\rho}_c, \Delta\theta, \underline{I}_I) + \Psi_0 \tag{5.38}$$

where $\mathcal{C}_{mP}$ is the specific heat coefficient at constant pressure, $\Lambda/\widetilde{\rho}_c$ and $\mu/\widetilde{\rho}_c$ are the Lamé specific coefficients for elasticity (per unit of mass). $\kappa\alpha/\widetilde{\rho}_c$ is a specific coefficient coupling the bulk modulus $\kappa = \Lambda + 2\mu/3$ and the thermal expansion coefficient $\alpha$. These 3 coefficients are supposed to be temperature independent. $\underline{I}_I$ and $\underline{I}_{II}$ are the invariants of the projected strain tensor. The thermomechanical coupling is expressed by $\Psi_{\theta,\sigma}$ in which $\Delta\theta = \theta - \theta_0$ is the variation of temperature caused by the thermoelastic behavior, measured with respect to a reference temperature $\theta_0$. This choice is a general form of the specific free energy $\Psi$ depending on invariants. Other equivalent choices of $\Psi_\sigma$ and $\Psi_{\theta,\sigma}$ are possible:

- We could consider the functions $\Psi_\sigma(\Lambda/\widetilde{\rho}_c, \mu/\widetilde{\rho}_c, \underline{e}_{\mu\nu}, \underline{g}^{\mu\nu})$ and $\Psi_{\theta,\sigma}(\kappa\alpha/\widetilde{\rho}_c, \Delta\theta, \underline{e}_{\mu\nu}, \underline{g}^{\mu\nu})$, where $\underline{e}_{\mu\nu}$ is the Eulerian covariant component of the projected elastic strain tensor, and $\underline{g}^{\mu\nu}$ is the contravariant component of the projected metric tensor.
- We could also consider the functions $\Psi_\sigma(\Lambda/\widetilde{\rho}_c, \mu/\widetilde{\rho}_c, \underline{b}_{\mu\nu}, \underline{g}^{\mu\nu})$ and and $\Psi_{\theta,\sigma}(\kappa\alpha/\widetilde{\rho}_c, \Delta\theta, \underline{b}_{\mu\nu}, \underline{g}^{\mu\nu})$, with $b_{\mu\nu}$ defined in Eq. 4.46. Note that $\mathcal{L}_u(b_{\mu\nu}) = 0$, which could help in simplifying the expression of the behavior model.

For simplification, we use the Euler-Almansi strain $\underline{e}^{\mu\nu}$ when referring to the elastic strain in this chapter. It is worth noting that the specific free energy $\Psi$ is supposed to be, at the macroscopic scale, a function of the only state variables temperature $\theta$ and projected elastic strain $\underline{e}^{\mu\nu}$. However, because of the use of the Lie derivative, all the arguments/parameters have to be listed for further derivation.

### 5.5.1 Application for a specific free energy based on the invariants of the projected strain tensor

Using Eq. 5.37, we can write for a reversible behavior:

$$-\widetilde{\rho}_c(\eta_c\mathcal{L}_u(\theta)+\mathcal{L}_u(\Psi_\theta))-\widetilde{\rho}_c\mathcal{L}_u(\Psi_\sigma)-\widetilde{\rho}_c\mathcal{L}_u(\Psi_{\theta,\sigma})-q^\mu\left(\frac{1}{\theta}\nabla_\mu\theta-u^\nu\nabla_\nu u_\mu\right)+T^{\mu\nu}_\sigma d_{\mu\nu}=0 \tag{5.39}$$

$$\begin{aligned}\Leftrightarrow\ \widetilde{\rho}_c\left(\eta_c\mathcal{L}_u(\theta)+\frac{\partial\Psi_\theta}{\partial\mathcal{C}_{mP}}\mathcal{L}_u(\mathcal{C}_{mP})+\frac{\partial\Psi_\theta}{\partial\theta}\mathcal{L}_u(\theta)\right)\ &+\\ \widetilde{\rho}_c\left(\frac{\partial\Psi_\sigma}{\partial(\Lambda/\widetilde{\rho}_c)}\mathcal{L}_u(\Lambda/\widetilde{\rho}_c)+\frac{\partial\Psi_\sigma}{\partial(\mu/\widetilde{\rho}_c)}\mathcal{L}_u(\mu/\widetilde{\rho}_c)+\frac{\partial\Psi_{\theta,\sigma}}{\partial(\kappa\alpha/\widetilde{\rho}_c)}\mathcal{L}_u(\kappa\alpha/\widetilde{\rho}_c)+\frac{\partial\Psi_{\theta,\sigma}}{\partial\Delta\theta}\mathcal{L}_u(\Delta\theta)\right)\ &+\\ \widetilde{\rho}_c\left(\frac{\partial\Psi_\sigma}{\partial\underline{I}_I}\mathcal{L}_u(\underline{I}_I)+\frac{\partial\Psi_{\theta,\sigma}}{\partial\underline{I}_I}\mathcal{L}_u(\underline{I}_I)+\frac{\partial\Psi_\sigma}{\partial\underline{I}_{II}}\mathcal{L}_u(\underline{I}_{II})\right)+q^\mu\left(\frac{1}{\theta}\nabla_\mu\theta-u^\nu\nabla_\nu u_\mu\right)\ &=\\ T^{\mu\nu}_\sigma d_{\mu\nu}\end{aligned} \tag{5.40}$$

The specific free energy is expressed in Eq. 5.38 as an additive decomposition of three effects. The two invariants $\underline{I}_I$ and $\underline{I}_{II}$ should physically correspond respectively to the deformation of volume and deformation of surface of the material continuum. We propose for the expressions of the specific free energy terms by analogy with Newtonian approaches [Farhat et al.,1991, Nayfeh and Nemat-Nasser,1971]:

$$\Psi_\sigma = \frac{\Lambda}{\widetilde{\rho}_c}\frac{\underline{I}_I^{\mathfrak{n}_1}}{\mathfrak{n}_1}+\frac{\mu}{\widetilde{\rho}_c}\frac{\underline{I}_{II}^{\mathfrak{n}_2}}{\mathfrak{n}_2} \tag{5.41}$$

$$\Psi_{\theta,\sigma} = -\frac{3\kappa\alpha}{\widetilde{\rho}_c}\Delta\theta\underline{I}_I \tag{5.42}$$

with $\mathfrak{n}_1$ and $\mathfrak{n}_2$ exponents of the power laws ($\in\mathbb{N}^{+*}$). The invariants $\underline{I}_I$ and $\underline{I}_{II}$ are supposed to be independent to get a decoupling of the mechanical effects, but they will be expressed as a function of the strain tensor $\boldsymbol{e}$ and/or the metric tensor $\boldsymbol{g}$. According to Eqs. 4.54 to 4.55, the Lie derivatives of these invariants are linear functions of the deformation rate tensor $\boldsymbol{d}$, as it will be illustrated further. We can then calculate the different terms of Eq. 5.40 with:

$$\frac{\partial \Psi_\sigma}{\partial(\Lambda/\widetilde{\rho}_c)} = \frac{\underline{I}_I^{\mathfrak{n}_1}}{\mathfrak{n}_1} \tag{5.43}$$

$$\mathcal{L}_u(\Lambda/\widetilde{\rho}_c) = \frac{\Lambda}{\widetilde{\rho}_c}\underline{g}^{\mu\nu}d_{\mu\nu} \tag{5.44}$$

$$\frac{\partial \Psi_\sigma}{\partial(\mu/\widetilde{\rho}_c)} = \frac{\underline{I}_{II}^{\mathfrak{n}_2}}{\mathfrak{n}_2} \tag{5.45}$$

$$\mathcal{L}_u(\mu/\widetilde{\rho}_c) = \frac{\mu}{\widetilde{\rho}_c}\underline{g}^{\mu\nu}d_{\mu\nu} \tag{5.46}$$

$$\frac{\partial \Psi_{\theta,\sigma}}{\partial(\kappa\alpha/\widetilde{\rho}_c)} = -3\Delta\theta\underline{I}_I \tag{5.47}$$

$$\mathcal{L}_u(\kappa\alpha/\widetilde{\rho}_c) = \frac{\kappa\alpha}{\widetilde{\rho}_c}\underline{g}^{\mu\nu}d_{\mu\nu} \tag{5.48}$$

$$\frac{\partial \Psi_\sigma}{\partial \underline{I}_I} + \frac{\partial \Psi_{\theta,\sigma}}{\partial \underline{I}_I} = \frac{\Lambda}{\widetilde{\rho}_c}\underline{I}_I^{\mathfrak{n}_1-1} - \frac{3\kappa\alpha}{\widetilde{\rho}_c}\Delta\theta \tag{5.49}$$

$$\mathcal{L}_u(\underline{I}_I) = A_I^{\mu\nu}d_{\mu\nu} \tag{5.50}$$

$$\frac{\partial \Psi_\sigma}{\partial \underline{I}_{II}} = \frac{\mu}{\widetilde{\rho}_c}\underline{I}_{II}^{\mathfrak{n}_2-1} \tag{5.51}$$

$$\mathcal{L}_u(\underline{I}_{II}) = A_{II}^{\mu\nu}d_{\mu\nu} \tag{5.52}$$

$$\mathcal{L}_u(\Delta\theta) = \mathcal{L}_u(\theta) - \mathcal{L}_u(\theta_0) = \mathcal{L}_u(\theta) \tag{5.53}$$

$$\mathcal{L}_u(\mathcal{C}_{mP}) = 0 \tag{5.54}$$

with $A_I^{\mu\nu}$ and $A_{II}^{\mu\nu}$ tensorial functions that remain to be explicited. Note that the Lie derivative of a constant scalar of density $W = 0$ is null. By using Eqs. 5.43 to 5.54 in Eq. 5.40, then it is possible to write:

$$\widetilde{\rho}_c\left(\eta\mathcal{L}_u(\theta) + \tfrac{\partial\Psi_\theta}{\partial\theta}\mathcal{L}_u(\theta)\right) + \widetilde{\rho}_c\left(\tfrac{\underline{I}_I^{\mathfrak{n}_1}}{\mathfrak{n}_1}\tfrac{\Lambda}{\widetilde{\rho}_c}\underline{g}^{\mu\nu}d_{\mu\nu} + \tfrac{\underline{I}_{II}^{\mathfrak{n}_2}}{\mathfrak{n}_2}\tfrac{\mu}{\rho_c}\underline{g}^{\mu\nu}d_{\mu\nu} - 3\Delta\theta\underline{I}_I\tfrac{\kappa\alpha}{\widetilde{\rho}_c}\underline{g}^{\mu\nu}d_{\mu\nu} - 3\tfrac{\kappa\alpha}{\widetilde{\rho}_c}\underline{I}_I\mathcal{L}_u(\theta)\right)$$

$$+ \quad \widetilde{\rho}_c\left((\tfrac{\Lambda}{\widetilde{\rho}_c}\underline{I}_I^{\mathfrak{n}_1-1} - \tfrac{3\kappa\alpha}{\widetilde{\rho}_c}\Delta\theta)A_I^{\mu\nu}d_{\mu\nu} + \tfrac{\mu}{\rho_c}\underline{I}_{II}^{\mathfrak{n}_2-1}A_{II}^{\mu\nu}d_{\mu\nu}\right) - q^\mu\left(\frac{1}{\theta}\nabla_\mu\theta - u^\nu\nabla_\nu u_\mu\right) = T_\sigma^{\mu\nu}d_{\mu\nu} \tag{5.55}$$

By considering independent and reversible transformations, we obtain simultaneously:

$$\forall\mathcal{L}_u(\theta), \eta_c = -\frac{\partial\Psi_\theta}{\partial\theta} + 3\frac{\kappa\alpha}{\widetilde{\rho}_c}\underline{I}_I \tag{5.56}$$

$$\forall\theta, q^\mu\left(\frac{1}{\theta}\nabla_\mu\theta - u^\nu\nabla_\nu u_\mu\right) \geq 0 \tag{5.57}$$

$$\forall d_{\mu\nu}, T_\sigma^{\mu\nu} = \frac{\underline{I}_I^{\mathfrak{n}_1}}{\mathfrak{n}_1}\Lambda\underline{g}^{\mu\nu} + \frac{\underline{I}_{II}^{\mathfrak{n}_2}}{\mathfrak{n}_2}\mu\underline{g}^{\mu\nu} - 3\Delta\theta\underline{I}_I\kappa\alpha\underline{g}^{\mu\nu}$$
$$+ \quad \left((\Lambda\underline{I}_I^{\mathfrak{n}_1-1} - 3\kappa\alpha\Delta\theta)A_I^{\mu\nu} + \mu\underline{I}_{II}^{\mathfrak{n}_2-1}A_{II}^{\mu\nu}\right)^{Sym} \tag{5.58}$$

As expected, this equation is symmetric and the choice of $\underline{I}_I^{\mathfrak{n}_1-1}$ has to respect $T_\sigma^{\mu\nu}u_\mu = 0$ (the other terms already respect this condition).

### 5.5.2 Spacetime thermo-hyperelastic behavior of a specific reversible model

In this model, spatial projectors to define the specific free energy. The invariants of the projected strain tensor are chosen by generalizing the invariants of Newtonian Hookean-like models [Ugural and Fenster,2003]. The first invariant, related to the spatial volume variation, is given by:

$$\underline{I}_I = \underline{e}_{\mu\nu}\underline{g}^{\mu\nu} = \underline{e}_{\mu\nu}g^{\mu\nu} = e_{\mu\nu}\underline{g}^{\mu\nu} \tag{5.59}$$

that leads then to:

$$\mathcal{L}_u(\underline{I}_I) = A_I^{\mu\nu}d_{\mu\nu} = (\underline{g}^{\mu\nu} - 2\underline{e}^{\mu\nu})d_{\mu\nu} \tag{5.60}$$

The second invariant, related to the spatial surface variation, is:

$$\underline{I}_{II} = \underline{e}_{\mu\nu}\underline{e}^{\mu\nu} = \underline{e}_{\mu\nu}e^{\mu\nu} = e_{\mu\nu}\underline{e}^{\mu\nu} \tag{5.61}$$

that leads then to:

$$\mathcal{L}_u(\underline{I}_{II}) = A^{\mu\nu}_{II}d_{\mu\nu} = (2\underline{e}^{\mu\nu} - 2\underline{e}^{\mu}{}_{\beta}e^{\beta\nu} - 2\underline{e}^{\mu\beta}\underline{e}_{\beta}{}^{\nu})d_{\mu\nu} \tag{5.62}$$

Assuming a quadratic form for the specific free energy, according to the choice of these invariants, it leads to $\mathfrak{n}_1 = 2$ and $\mathfrak{n}_2 = 1$. Using Eqs. 5.59 to 5.62 and 5.58, the stress-strain curve can be obtained:

$$\begin{aligned} T^{\mu\nu}_{\sigma} &= \frac{(e_{\alpha\beta}\underline{g}^{\alpha\beta})^2}{2}\Lambda\underline{g}^{\mu\nu} + (\underline{e}_{\alpha\beta}\underline{e}^{\alpha\beta})\mu\underline{g}^{\mu\nu} + \Lambda(e_{\alpha\beta}\underline{g}^{\alpha\beta})(\underline{g}^{\mu\nu} - 2\underline{e}^{\mu\nu}) \\ &+ 2\mu\underline{e}^{\mu\nu} - 4\mu\left(\underline{e}^{\mu}{}_{\beta}\underline{e}^{\beta\nu}\right)^{Sym} - 3\kappa\alpha\Delta\theta(e_{\alpha\beta}\underline{g}^{\alpha\beta})\underline{g}^{\mu\nu} - 3\kappa\alpha\Delta\theta(\underline{g}^{\mu\nu} - 2\underline{e}^{\mu\nu}) \qquad (5.63) \\ &= \Lambda(e_{\alpha\beta}\underline{g}^{\alpha\beta})\left(\underline{g}^{\mu\nu} + \frac{1}{2}(e_{\alpha\beta}\underline{g}^{\alpha\beta})\underline{g}^{\mu\nu} - 2\underline{e}^{\mu\nu}\right) \\ &+ 2\mu\left(\underline{e}^{\mu\nu} + \frac{1}{2}(e_{\alpha\beta}\underline{e}^{\alpha\beta})\underline{g}^{\mu\nu} - 2\left(\underline{e}^{\mu}{}_{\beta}\underline{e}^{\beta\nu}\right)^{Sym}\right) \\ &- 3\kappa\alpha\Delta\theta\left((e_{\alpha\beta}\underline{g}^{\alpha\beta})\underline{g}^{\mu\nu} + \underline{g}^{\mu\nu} - 2\underline{e}^{\mu\nu}\right) \qquad (5.64) \end{aligned}$$

As expected, this expression is symmetric because the spatial projector keeps the property of symmetry. Moreover, Eq. 5.64 verifies $T^{\mu\nu}_{\sigma}u_{\mu} = 0$ (since it can be proved that $\underline{e}^{\mu\nu}u_{\mu} = 0$ and $\underline{g}^{\mu\nu}u_{\mu} = 0$). The non-linear terms in Eq. 5.58 correspond to terms in the Lie derivative that can be related to the derivative to the material parameters and to the metric components. By use of $\Psi_{\sigma}(\Lambda/\widetilde{\rho}_c, \mu/\widetilde{\rho}_c, \underline{e}_{\mu\nu}, \underline{g}^{\mu\nu})$ and $\Psi_{\theta,\sigma}(\kappa\alpha/\widetilde{\rho}_c, \Delta\theta, \underline{e}_{\mu\nu}, \underline{g}^{\mu\nu})$ instead of $\Psi_{\sigma}(\Lambda/\widetilde{\rho}_c, \mu/\widetilde{\rho}_c, \underline{I}_I, \underline{I}_{II})$ and $\Psi_{\theta,\sigma}(\kappa\alpha/\widetilde{\rho}_c, \Delta\theta, \underline{I}_I)$, we would obtain exactly the same constitutive model. As expected, Eq. 5.64 leads to the absence of spacetime stress for $\underline{e}^{\alpha\beta} = 0$ and $\Delta\theta = 0$.

### 5.5.3 The thermo-hyperelastic behavior under different assumptions

#### 5.5.3.1 For small deformations and finite temperature variation

We assume that the deformations are small ($\forall\mu,\nu, e^{\mu\nu} \ll 1 \Leftrightarrow ||e|| \ll 1$) and the variation of temperature is finite, then Eq. 5.64 leads to:

$$\begin{aligned} T^{\mu\nu}_{\sigma} &= (\Lambda - 3\kappa\alpha\Delta\theta)(e_{\alpha}{}^{\beta}(\delta^{\alpha}{}_{\beta} - u^{\alpha}u_{\beta}))(g^{\mu\nu} - u^{\mu}u^{\nu}) \\ &+ 2(\mu + 3\kappa\alpha\Delta\theta)e^{\alpha\beta}(\delta^{\mu}{}_{\alpha} - u^{\mu}u_{\alpha})(\delta^{\nu}{}_{\beta} - u^{\nu}u_{\beta}) \\ &- 3\kappa\alpha\Delta\theta(g^{\mu\nu} - u^{\mu}u^{\nu}) \qquad (5.65) \end{aligned}$$

Eq. 5.65 shows that $e^{\alpha\beta} = 0$ or $e^{\alpha\beta} = \mathcal{N}u^{\alpha}u^{\beta}$, with $\mathcal{N} \in \mathbb{R}^*$ (and $\Delta theta = 0$) leads to the absence of spacetime stress. When expressed in an inertial frame, Eq. 5.65 leads to:

$$\begin{aligned} T^{\mu\nu}_{\sigma} &= (\Lambda - 3\kappa\alpha\Delta\theta)(e_{\alpha}{}^{\beta}(\delta^{\alpha}{}_{\beta} - \gamma^2 v^{\alpha}v_{\beta}/c^2))(\eta^{\mu\nu} - \gamma^2 v^{\mu}v^{\nu}/c^2) \\ &+ 2(\mu + 3\kappa\alpha\Delta\theta)e^{\alpha\beta}(\delta^{\mu}{}_{\alpha} - \gamma^2 v^{\mu}v_{\alpha}/c^2)(\delta^{\nu}{}_{\beta} - \gamma^2 v^{\nu}v_{\beta}/c^2) \\ &- 3\kappa\alpha\Delta\theta(\eta^{\mu\nu} - \gamma^2 v^{\mu}v^{\nu}/c^2) \qquad (5.66) \end{aligned}$$

where $e^{\mu\nu} = \frac{1}{2}(\eta^{\mu\nu} - b^{\mu\nu})$ from Eq. 4.45. At the non-relativistic limit, it leads to:

$$\begin{aligned} T^{\mu\nu}_{\sigma} &\approx (\Lambda - 3\kappa\alpha\Delta\theta)(e_{\alpha}{}^{\beta}\delta^{\alpha}{}_{\beta})\eta^{\mu\nu} + 2(\mu + 3\kappa\alpha\Delta\theta)e^{\mu\nu} - 3\kappa\alpha\Delta\theta\eta^{\mu\nu} \qquad (5.67) \\ &\approx (\Lambda - 3\kappa\alpha\Delta\theta)(e_{a}{}^{b}\delta^{a}{}_{b})\eta^{\mu\nu} + 2(\mu + 3\kappa\alpha\Delta\theta)e^{\mu\nu} - 3\kappa\alpha\Delta\theta\eta^{\mu\nu} \qquad (5.68) \end{aligned}$$

In absence of thermomechanical coupling, Eq. 5.68 leads to the Hookean-like model for small deformation for thermoelasticity, assuming that $e_4{}^4 \approx 0$ if the loading speed is non-relativistic, so that only the spatial components remain in the trace of $e^{\mu\nu}$.

When expressed in the proper frame, where $\hat{u}^\mu = (0,0,0,1)$, Eq. 5.65 leads for the spatial components to:

$$\begin{aligned}\hat{T}_\sigma^{ij} &= J(\Lambda - 3\kappa\alpha\Delta\theta)(\hat{e}_a{}^b\delta^a{}_b + \hat{e}_4{}^4 - \hat{e}_4{}^\beta\hat{u}_\beta)\hat{g}^{ij} + 2J(\mu + 3\kappa\alpha\Delta\theta)\hat{e}^{ij} \\ &- 3J\kappa\alpha\Delta\theta\hat{g}^{ij} \end{aligned} \tag{5.69}$$

where $\hat{e}^{\mu\nu} = \frac{1}{2}(\hat{g}^{\mu\nu} - \hat{b}^{\mu\nu}) = \frac{1}{2}(\hat{g}^{\mu\nu} - \hat{g}^{\mu\alpha}\hat{g}^{\nu\beta}\eta_{\alpha\beta})$ from Eq. 4.45. Because $\Lambda$ and $\mu$ are scalar densities, the determinant $J$ has to be introduced and for small deformations $J \approx 1$. It leads to the Hookean-like model for small deformation (Eq. 4.25), with new terms coupling the deformation to the finite temperature variation $-3\kappa\alpha\Delta\theta(\hat{e}_a{}^b\delta^a{}_b)\hat{g}^{ij} + 6\kappa\alpha\Delta\theta\hat{e}^{ij}$ and the term $\hat{e}_4{}^4 - \hat{e}_4{}^\beta\hat{u}_\beta$ that strictly vanishes when the proper frame is also locally inertial ($\hat{g}^{\mu\nu} = \eta^{\mu\nu}$ leading to $\hat{u}_\mu = (0,0,0,1)$). In the proper but non-inertial frame, this term may be neglected if and only if the loading speed is non-relativistic [Panicaud et al.,2014]. And for the time components, it leads to:

$$\begin{aligned}\hat{T}_\sigma^{i4} &= J(\Lambda - 3\kappa\alpha\Delta\theta)(\hat{e}_a{}^b\delta^a{}_b + \hat{e}_4{}^4 - \hat{e}_4{}^\beta\hat{u}_\beta)\hat{g}^{i4} + 2J(\mu + 3\kappa\alpha\Delta\theta)\hat{e}^{i\beta}(\delta^4{}_\beta - \hat{u}_\beta) \\ &- 3J\kappa\alpha\Delta\theta\hat{g}^{i4} \end{aligned} \tag{5.70}$$

and

$$\begin{aligned}\hat{T}_\sigma^{44} &= J(\Lambda - 3\kappa\alpha\Delta\theta)(\hat{e}_a{}^b\delta^a{}_b + \hat{e}_4{}^4 - \hat{e}_4{}^\beta\hat{u}_\beta)(\hat{g}^{44} - 1) \\ &+ 2J(\mu + 3\kappa\alpha\Delta\theta)\hat{e}^{\alpha\beta}(\delta^4{}_\alpha - \hat{u}_\alpha)(\delta^4{}_\beta - \hat{u}_\beta) \\ &- 3J\kappa\alpha\Delta\theta(\hat{g}^{44} - 1) \end{aligned} \tag{5.71}$$

Eq. 5.71 vanishes if and only if the proper frame is also inertial ($\hat{g}^{\mu\nu} = \eta^{\mu\nu}$ leading to $\hat{u}_\mu = (0,0,0,1)$). For other frames, some terms appear for the time components, which can be considered as very small, as for example for the proper frame, if the loading speed is non-relativistic. In this proper frame, because of the choice of the strain tensor, Eq. 5.69 vanishes for $\hat{e}^{\alpha\beta} = 0$, only if the additional hypothesis $\Delta\theta = 0$ is taken into account. The use of projector in the specific free energy ensures the modeling of spatial contributions for the stress and strain expressions for the proper frame if the loading speed is small enough.

#### 5.5.3.2 For small deformations and small temperature variation

We assume the deformations and the temperature variation are small ($\forall\mu,\nu, e^{\mu\nu} \ll 1 \Leftrightarrow ||e|| \ll 1$ and $\Delta\theta \ll \theta_0$, such that $\Delta\theta e^{\mu\nu} \to 0$, Eq. 5.65 leads to:

$$\begin{aligned}T_\sigma^{\mu\nu} &= \Lambda(e_\alpha{}^\beta(\delta^\alpha{}_\beta - u^\alpha u_\beta))(g^{\mu\nu} - u^\mu u^\nu) \\ &+ 2\mu e^{\alpha\beta}(\delta^\mu{}_\alpha - u^\mu u_\alpha)(\delta^\nu{}_\beta - u^\nu u_\beta) \\ &- 3\kappa\alpha\Delta\theta(g^{\mu\nu} - u^\mu u^\nu) \end{aligned} \tag{5.72}$$

Eq. 5.72 shows that $e^{\alpha\beta} = 0$, $\Delta\theta = 0$ or $e^{\alpha\beta} = \mathcal{N}u^\alpha u^\beta$, $\Delta\theta = 0$, with $\mathcal{N} \in \mathbb{R}^*$ leads to the absence of spacetime stress. When expressed in an inertial frame, Eq. 5.72 leads to:

$$\begin{aligned}T_\sigma^{\mu\nu} &= \Lambda(e_\alpha{}^\beta(\delta^\alpha{}_\beta - \gamma^2 v^\alpha v_\beta/c^2))(\eta^{\mu\nu} - \gamma^2 v^\mu v^\nu/c^2) \\ &+ 2\mu e^{\alpha\beta}(\delta^\mu{}_\alpha - \gamma^2 v^\mu v_\alpha/c^2)(\delta^\nu{}_\beta - \gamma^2 v^\nu v_\beta/c^2) \\ &- 3\kappa\alpha\Delta\theta(\eta^{\mu\nu} - \gamma^2 v^\mu v^\nu/c^2) \end{aligned} \tag{5.73}$$

where $e^{\mu\nu} = \frac{1}{2}(\eta^{\mu\nu} - b^{\mu\nu})$ from Eq. 4.45. At the non-relativistic limit, it leads to:

$$T_\sigma^{\mu\nu} \approx \Lambda(e_\alpha{}^\beta\delta^\alpha{}_\beta)\eta^{\mu\nu} + 2\mu e^{\mu\nu} - 3\kappa\alpha\Delta\theta\eta^{\mu\nu} \tag{5.74}$$

$$\approx \Lambda(e_a{}^b\delta^a{}_b)\eta^{\mu\nu} + 2\mu e^{\mu\nu} - 3\kappa\alpha\Delta\theta\eta^{\mu\nu} \tag{5.75}$$

Eq. 5.75 leads to the Hookean-like model for small deformation coupled with small temperature variation, assuming that $e_4{}^4 \approx 0$ if the loading speed is non-relativistic, so that only the spatial components remain.

When expressed in the proper frame, where $\hat{u}^\mu = (0,0,0,1)$, Eq. 5.72 leads for the spatial components to:

$$\begin{aligned}\hat{T}_\sigma^{ij} &= J\Lambda(\hat{e}_a{}^b\delta^a{}_b + \hat{e}_4{}^4 - \hat{e}_4{}^\beta\hat{u}_\beta)\hat{g}^{ij} + 2J\mu\hat{e}^{ij} \\ &- 3J\kappa\alpha\Delta\theta\hat{g}^{ij} \end{aligned} \tag{5.76}$$

where $\hat{e}^{\mu\nu} = \frac{1}{2}(\hat{g}^{\mu\nu} - \hat{b}^{\mu\nu}) = \frac{1}{2}(\hat{g}^{\mu\nu} - \hat{g}^{\mu\alpha}\hat{g}^{\nu\beta}\eta_{\alpha\beta})$ from Eq. 4.45. Because $\Lambda$ and $\mu$ are scalar densities, the determinant $J$ has to be introduced and for small deformations $J \approx 1$. It leads to the Hookean-like model for small deformation coupled with small temperature variation, with a new term $\hat{e}_4{}^4 - \hat{e}_4{}^\beta\hat{u}_\beta$ that strictly vanishes when the proper frame is also locally inertial ($\hat{g}^{\mu\nu} = \eta^{\mu\nu}$ leading to $\hat{u}_\mu = (0,0,0,1)$). In the proper but non-inertial frame, this term may be neglected if and only if the loading speed is non-relativistic [Panicaud et al.,2014]. And for the time components, it leads to:

$$\begin{aligned}\hat{T}_\sigma^{i4} &= J\Lambda(\hat{e}_a{}^b\delta^a{}_b + \hat{e}_4{}^4 - \hat{e}_4{}^\beta\hat{u}_\beta)\hat{g}^{i4} + 2J\mu\hat{e}^{i\beta}(\delta^4{}_\beta - \hat{u}_\beta) \\ &- 3J\kappa\alpha\Delta\theta\hat{g}^{i4} \end{aligned} \tag{5.77}$$

and

$$\begin{aligned}\hat{T}_\sigma^{44} &= J\Lambda(\hat{e}_a{}^b\delta^a{}_b + \hat{e}_4{}^4 - \hat{e}_4{}^\beta\hat{u}_\beta)(\hat{g}^{44} - 1) \\ &+ 2J\mu\hat{e}^{\alpha\beta}(\delta^4{}_\alpha - \hat{u}_\alpha)(\delta^4{}_\beta - \hat{u}_\beta) \\ &- 3J\kappa\alpha\Delta\theta(\hat{g}^{44} - 1) \end{aligned} \tag{5.78}$$

As previously said, these two expressions vanish if and only if the proper frame is also inertial ($\hat{g}^{\mu\nu} = \eta^{\mu\nu}$ leading to $\hat{u}_\mu = (0,0,0,1)$). For other frames, some terms appear for the time components, which can be considered as very small, as for example for the proper frame, if the loading speed is non-relativistic.

In this proper frame, because of the choice of the strain tensor, Eq. 5.76 vanishes for $\hat{e}^{\alpha\beta} = 0$, since $\Delta\theta$ is small. However, this condition is equivalent to consider that the proper frame is inertial. Indeed, because of the definition of the strain tensor, we have $\hat{e}_{\mu\nu} = \frac{1}{2}(\hat{g}_{\mu\nu} - \hat{b}_{\mu\nu})$ that is equivalent to $\hat{b}_{\mu\nu} = \hat{g}_{\mu\nu} - 2\hat{e}_{\mu\nu}$. The definition of $\boldsymbol{b}$ leads to $\hat{b}_{\mu\nu} = \eta_{\mu\nu}$. Moreover, if the proper frame is inertial, then $\hat{g}_{\mu\nu} = \eta_{\mu\nu}$, thus $\hat{b}_{\mu\nu} = \hat{g}_{\mu\nu}$. Consequently, $\hat{g}_{\mu\nu} = \eta_{\mu\nu}$ is equivalent to have $\hat{e}_{\mu\nu} = 0$. The last equations are three equivalent expressions leading to say that if the proper frame is inertial, the elastic strain components vanish which leads to the absence of spacetime stress for the considered hyperelastic material. Reciprocally, no spacetime strain corresponds to the undeformed configuration that is necessarily inertial.

#### 5.5.3.3 For large transformations (i.e. large deformations and finite temperature variation)

For small deformations, no difference is expected between the spacetime formalism at the non-relativistic approximation and the classical Newtonian approach from a modeling point of view as proved in section 5.5.3.2. It is now interesting to investigate the relations obtained for large deformations. We consider Eq.

5.64 expressed in the proper frame, for the spatial components:

$$\begin{aligned}
\hat{T}^{ij}_{\sigma}/J &= (\Lambda - 3\kappa\alpha\Delta\theta)(\hat{e}_{\alpha\beta}(\hat{g}^{\alpha\beta} - \hat{u}^{\alpha}\hat{u}^{\beta}))\hat{g}^{ij} + 2(\mu + 3\kappa\alpha\Delta\theta)\hat{e}^{ij} \\
&\quad + \frac{1}{2}\Lambda(\hat{e}_{\alpha\beta}(\hat{g}^{\alpha\beta} - \hat{u}^{\alpha}\hat{u}^{\beta}))^2\hat{g}^{ij} + \mu(\hat{e}_{\kappa\lambda}(\hat{g}^{\kappa\alpha} - \hat{u}^{\kappa}\hat{u}^{\alpha})(\hat{g}^{\lambda\beta} - \hat{u}^{\lambda}\hat{u}^{\beta})\hat{e}_{\alpha\beta})\hat{g}^{ij} \\
&\quad - 2\Lambda(\hat{e}_{\alpha\beta}(\hat{g}^{\alpha\beta} - \hat{u}^{\alpha}\hat{u}^{\beta}))\hat{e}^{ij} - 4\mu(\hat{e}^{i\alpha}\hat{e}_{\alpha}{}^{j} - \hat{e}^{i\alpha}\hat{e}_{4}{}^{j}\hat{u}_{\alpha})^{Sym} \\
&\quad - 3\kappa\alpha\Delta\theta\hat{g}^{ij} \qquad (5.79) \\
&= (\Lambda - 3\kappa\alpha\Delta\theta)(\hat{e}_{a}{}^{b}\delta^{a}{}_{b} + \hat{e}_{4}{}^{4} - \hat{e}_{4}{}^{\beta}\hat{u}_{\beta})\hat{g}^{ij} + 2(\mu + 3\kappa\alpha\Delta\theta)\hat{e}^{ij} \\
&\quad + \frac{1}{2}\Lambda(\hat{e}_{a}{}^{b}\delta^{a}{}_{b} + \hat{e}_{4}{}^{4} - \hat{e}_{4}{}^{\beta}\hat{u}_{\beta})^2\hat{g}^{ij} + \mu(\hat{e}^{\alpha\beta}\hat{e}_{\alpha\beta} - \hat{e}^{\alpha}{}_{4}\hat{e}_{\alpha 4} - \hat{e}_{\alpha}{}^{4}\hat{e}_{4\beta} + \\
&\quad + \hat{e}_{44}\hat{e}_{44})\hat{g}^{ij} - 2\Lambda(\hat{e}_{a}{}^{b}\delta^{a}{}_{b} + \hat{e}_{4}{}^{4} - \hat{e}_{4}{}^{\beta}\hat{u}_{\beta})\hat{e}^{ij} \\
&\quad - 4\mu(\hat{e}^{ia}\hat{e}_{a}{}^{j} + \hat{e}^{i4}\hat{e}_{4}{}^{j} - \hat{e}^{ia}\hat{e}_{4}{}^{j}\hat{u}_{a} - \hat{e}^{i4}\hat{e}_{4}{}^{j}\hat{u}_{4})^{Sym} \\
&\quad - 3\kappa\alpha\Delta\theta\hat{g}^{ij} \qquad (5.80) \\
&\approx (\Lambda - 3\kappa\alpha\Delta\theta)(\hat{e}_{a}{}^{b}\delta^{a}{}_{b})\hat{g}^{ij} + 2(\mu + 3\kappa\alpha\Delta\theta)\hat{e}^{ij} + \frac{1}{2}\Lambda(\hat{e}_{a}{}^{b}\delta^{a}{}_{b})^2\hat{g}^{ij} + \mu(\hat{e}^{\alpha\beta}\hat{e}_{\alpha\beta})\hat{g}^{ij} \\
&\quad - 2\Lambda(\hat{e}_{a}{}^{b}\delta^{a}{}_{b})\hat{e}^{ij} - 4\mu(\hat{e}^{ia}\hat{e}_{a}{}^{j})^{Sym} - 3\kappa\alpha\Delta\theta\hat{g}^{ij} \qquad (5.81)
\end{aligned}$$

Eq. 5.81 has been obtained by considering that the loading speed is non-relativistic. In this equation, four non-linear geometrical terms correspond to a natural expansion of the Hookean model for large deformations. Besides, the linear terms $-3\kappa\alpha\Delta\theta(\hat{e}_{a}{}^{b}\delta^{a}{}_{b})\hat{g}^{ij}$ and $6\kappa\alpha\Delta\theta\hat{e}^{ij}$ correspond to the expansion of the Hookean model resulting from finite temperature variation. These two terms strongly couple the deformation and the quadratic deformation respectively to the finite variation of temperature. The resulting effect of these terms depend on the value of the deformation. For large deformations, their value is important with respect to the last term of Eq. 5.81. Thus, by comparison with a Hookean Newtonian thermoelastic model (Eq. 4.25), six terms depending on three material parameters are added to the model for large transformations. In case the transformation is isothermal $\Delta\theta = 0$, Eq. 5.81 can be compared with a Hookean Newtonian elastic model (Eq. 4.15), four quadratic terms depending on two material parameters are added to the model for large transformations.

### 5.5.4 Summary on the equations and the variables for a reversible spacetime thermo-hyperelastic model

**Input data and summary of the model:**

The governing equations of the thermoelastic model are written under the following assumptions:

- The thermoelastic behavior is reversible.
- The strain in these equations is the total strain caused by the thermal and the mechanical behaviors.
- The residual stress is null.
- The material parameters: $\Lambda$, $\mu$, $\mathcal{C}_{mP}$, $\lambda$, $\kappa = (\Lambda + 2\mu)/3$ and $\alpha$ are constants.

The governing equations of the thermo-hyperelastic model are summarized by:

- The balance of molecules number given in Eq. 5.9.
- The specific free energy given in Eq. 5.38, Eq. 5.41 and Eq. 5.42 where the invariants are defined in Eq. 5.59 and Eq. 5.61.
- The stress-strain relation given in 5.64 which is expressed in the chosen frame for the type of transformation considered (small or large deformation, small or finite temperature variation).
- The heat equation of the phenomena which should be compatible with Eq. 5.57 for the heat conduction model.
- The definition of the spacetime strain tensor used given in: Eq. 4.2 for small deformations and Eq. 4.45 for a spacetime Euler-Almansi's strain tensor in case of large deformations.

For the output of the problem, the unknown variables of the problem are: $\theta(x^\alpha)$ and $dep^\lambda(x^\alpha)$.

## 5.6 Spacetime weak integral form of a thermomechanical problem

Eq. 5.10 represents the local balance of spacetime energy-momentum tensor. The weak integral form of a thermomechanical problem is obtained by multiplying this expression by a test function $r^*_\mu$ combining the virtual temperature field $\theta^*$ and the virtual displacement field $dep^*_\mu$ such that:

$$r^*_\mu = \begin{pmatrix} \theta^* \\ dep^*_\mu \end{pmatrix} \tag{5.82}$$

Then the resultant expression is integrated on the spacetime hypervolume $\mathrm{d}H_\Omega$.

$$\mathcal{W}(r_\mu, r^*_\mu) = \int_\Omega r^*_\mu \nabla_\nu T^{\mu\nu}\, dH_\Omega \quad = \quad 0, \forall r^*_\mu \tag{5.83}$$

where the trial function $r_\mu$ is given by:

$$r_\mu = \begin{pmatrix} \theta \\ dep_\mu \end{pmatrix} \tag{5.84}$$

Eq. 5.83 can be developed to:

$$\mathcal{W}(r_\mu, r^*_\mu) = \int_\Omega \left(\nabla_\nu (T^{\mu\nu}\, r^*_\mu) - T^{\mu\nu} \nabla_\nu r^*_\mu\right)\, dH_\Omega \quad = \quad 0, \forall r^*_\mu \tag{5.85}$$

Using Green-Ostrogradski theorem, Eq. 5.85 can be written:

$$\mathcal{W}(r_\mu, r^*_\mu) = \int_\Omega T^{\mu\nu}\, \nabla_\nu r^*_\mu\, dH_\Omega - \int_{\partial\Omega} T^{\mu\nu}\, r^*_\mu n_\nu\, \mathrm{d}S_\Omega = 0, \forall r^*_\mu \tag{5.86}$$

where $n_\nu$ is the normal vector to the hypersurface of integration $\mathrm{d}S_\Omega$.
The boundary conditions of the problem are summarized in table 13.

| Type of boundary conditions | Variable | Boundary | Condition | Functions representing the boundary conditions |
|---|---|---|---|---|
| Dirichlet boundary conditions | $dep_\mu$ | $\partial\Omega_{dep_\mu}$ | $\partial\Omega_{dep_\mu} \cup \partial\Omega_{T_M} = \partial\Omega$ | $f_{SC}(x^\mu \in \partial\Omega_{dep_\mu}) = dep_\mu(x^\mu \in \partial\Omega_{dep_\mu})$ on the space |
| | | | $\partial\Omega_{dep_\mu} \cap \partial\Omega_{T_M} = \varnothing$ | $f_{TC}(x^\mu \in \partial\Omega_{dep_\mu}) = dep_\mu(x^\mu \in \partial\Omega_{dep_\mu})$ on the time |
| | $\theta$ | $\partial\Omega_\theta$ | - | $f_{SC}(x^\mu \in \partial\Omega_\theta) = \theta(x^\mu \in \partial\Omega_\theta)$ on the space<br>$f_{TC}(x^\mu \in \partial\Omega_\theta) = \theta(x^\mu \in \partial\Omega_\theta)$ on the time |
| Neumann boundary conditions | $T_M$ | $\partial\Omega_{T_M}$ | $\partial\Omega_{dep_\mu} \cup \partial\Omega_{T_M} = \partial\Omega$ | $f_{SC}(x^\mu \in \partial\Omega_{T_M}) = T_M(x^\mu \in \partial\Omega_{T_M})$ on the space |
| | | | $\partial\Omega_{dep_\mu} \cap \partial\Omega_{T_M} = \varnothing$ | $f_{TC}(x^\mu \in \partial\Omega_{T_M}) = T_M(x^\mu \in \partial\Omega_{T_M})$ on the time |

**Tab. 13:** Boundary conditions for a spacetime thermomechanical model

**Specific developments for numerical resolution:**

In order to implement this example for simulation using FEniCS project, we need to determine the weak integral forms related to the behaviors simulated and the corresponding boundary conditions.

To implement the weak integral form obtained in section 5.6, Eq. 5.83 is further developed to:

$$\mathcal{W}(r_\mu, r_\mu^*) = \int_\Omega r_\mu^* \nabla_\nu (T_{\mathcal{U}}^{\mu\nu} + T_q^{\mu\nu} + T_\sigma^{\mu\nu})\, dH_\Omega \quad = \quad 0, \forall r_\mu^* \tag{5.87}$$

The first term of Eq. 5.87 can be developed to:

$$\begin{aligned} \int_\Omega r_\mu^* \nabla_\nu T_{\mathcal{U}}^{\mu\nu}\, dH_\Omega &= \int_\Omega r_\mu^* \nabla_\nu (\tilde{\rho_c}(c^2 + e_{int}) u^\mu u^\nu)\, dH_\Omega \\ &= \int_\Omega r_\mu^* \nabla_\nu (\tilde{\rho_c} e_{int} u^\mu u^\nu)\, dH_\Omega \\ &= \int_\Omega (\tilde{\rho_c} e_{int} u^\mu u^\nu)\, \nabla_\nu r_\mu^*\, dH_\Omega - \int_{\partial\Omega} (\tilde{\rho_c} e_{int} u^\mu u^\nu)\, r_\mu^* n_\nu \, \mathrm{d}S_\Omega \end{aligned} \tag{5.88}$$

Using Green-Ostrogradski theorem, Eq. 5.87 can be written:

$$\begin{aligned} \mathcal{W}(r_\mu, r_\mu^*) &= \int_\Omega (\tilde{\rho_c} e_{int} u^\mu u^\nu)\, \nabla_\nu r_\mu^*\, dH_\Omega - \int_{\partial\Omega} (\tilde{\rho_c} e_{int} u^\mu u^\nu)\, r_\mu^* n_\nu \, \mathrm{d}S_\Omega \\ &+ \int_\Omega (T_q^{\mu\nu} + T_\sigma^{\mu\nu})\, \nabla_\nu r_\mu^*\, dH_\Omega - \int_{\partial\Omega} (T_q^{\mu\nu} + T_\sigma^{\mu\nu})\, r_\mu^* n_\nu \, \mathrm{d}S_\Omega \\ &= 0, \forall r_\mu^* \end{aligned} \tag{5.89}$$

Then the thermomechanical problem is written for a proper frame convenient to study material behaviors (see section 1.3.3) and for which $\hat{u}^\mu = (0, 0, 0, 1)$. In a proper frame, Eq. 5.89 can be written:

$$\begin{aligned} \mathcal{W}(r_\mu, r_\mu^*) &= \int_\Omega (\tilde{\rho_c} e_{int})\, \nabla_4 r_4^*\, dH_\Omega - \int_{\partial\Omega} (\tilde{\rho_c} e_{int})\, r_4^* \hat{n}_4 \, \mathrm{d}S_\Omega \\ &+ \int_\Omega (\hat{T}_q^{\mu\nu} + \hat{T}_\sigma^{\mu\nu})\, \nabla_\nu r_\mu^*\, dH_\Omega - \int_{\partial\Omega} (\hat{T}_q^{\mu\nu} + \hat{T}_\sigma^{\mu\nu})\, r_\mu^* \hat{n}_\nu \, \mathrm{d}S_\Omega \\ &= 0, \forall r_\mu^* \end{aligned} \tag{5.90}$$

**Verification for purely thermal problem:**

In the case of an inertial proper frame, assuming a linear relation between the specific energy $e_{int}$ and temperature $\theta$ with the proportional coefficient $\mathcal{C}_{m\omega}$ $(J.kg^{-1}.K^{-1})$, and in absence of $\hat{T}_\sigma^{\mu\nu}$ and the thermomechanical coupling (the function $r_\mu$ is reduced to $r_4 = \theta$), Eq. 5.90 can be written:

$$\begin{aligned} \mathcal{W}(r_\mu, r_\mu^*) &= \int_\Omega \left( (\tilde{\rho_c} \mathcal{C}_{m\omega} \theta)\, \nabla_4 r_4^* + \hat{T}_q^{4\nu}\, \nabla_\nu r_4^* \right) dH_\Omega \\ &- \int_{\partial\Omega} \left( \hat{T}_q^{4\nu}\, r_4^* \hat{n}_\nu + \tilde{\rho_c} \mathcal{C}_{m\omega} \theta\, r_4^* \hat{n}_4 \right) \mathrm{d}S_\Omega = 0, \forall r_\mu^* \end{aligned}$$

Besides in this particular frame, $\hat{q}^4 = 0$. Then Eq. 5.91 can then be written:

$$\begin{aligned}\mathcal{W}(r_\mu, r_\mu^*) &= \int_\Omega \left( (\tilde{\rho_c}\mathcal{C}_{m\omega}\theta)\, \nabla_4 r_4^* + q^i u^4\, \nabla_i r_4^* \right)\, dH_\Omega \\ &- \int_{\partial\Omega} \left( q^i u^4\, r_4^* \hat{n}_i + \tilde{\rho_c}\mathcal{C}_{m\omega}\theta\, r_4^* \hat{n}_4 \right)\, \mathrm{d}S_\Omega = 0, \forall r_\mu^*\end{aligned}$$

Dividing Eq. 5.91 by $\frac{\tilde{\rho_c}\mathcal{C}_{m\omega}}{c}$ and replacing $q^i = \frac{\lambda}{c} I^{ij} \nabla_j \theta$ since it is written in an inertial proper frame, we obtain:

$$\mathcal{W}(\theta, \theta^*) = \int_\Omega \left( \theta\, \frac{\partial \theta^*}{\partial t} + a I^{ij}\, \frac{\partial \theta}{\partial x^j}\, \frac{\partial \theta^*}{\partial x^i} \right)\, dH_\Omega - \int_{\partial\Omega} \left( \theta^*\, \frac{c\, q^i}{\widetilde{\rho_c}\mathcal{C}_{m\omega}} n_i + c\theta\, \theta^* \hat{n}_4 \right)\, \mathrm{d}S_\Omega = 0, \forall r_\mu^*$$

Besides, $-\int_{\partial\Omega} c\theta\, \theta^* \hat{n}_4\, \mathrm{d}S_\Omega = -\int_\Omega c \frac{\partial(\theta\, \theta^*)}{c\partial t}\, dH_\Omega = -\int_{\partial\Omega} \theta^*\, \frac{\theta}{\partial t}\, dH_\Omega - \int_{\partial\Omega} \theta \frac{\theta^*}{\partial t}\, dH_\Omega$. Eq. 5.91 can then be written:

$$\mathcal{W}(\theta, \theta^*) = \int_\Omega \left( \theta^*\, \frac{\partial \theta}{\partial t} + a I^{ij}\, \frac{\partial \theta}{\partial x^j}\, \frac{\partial \theta^*}{\partial x^i} \right)\, dH_\Omega - \int_{\partial\Omega_q} \theta^*\, \frac{c\, q^i}{\widetilde{\rho_c}\mathcal{C}_{m\omega}} n_i\, \mathrm{d}S_\Omega = 0, \forall r_\mu^*$$

Thus, we obtain again the spacetime weak integral form with spacetime Fourier's model of heat conduction (section 2.6.3.2). Eq. 5.91 will reduce to Eq. 2.53 with $f_r = 0$ and $q^i_{ext} = q^i$.

## 5.7 Newtonian vs spacetime modeling

The spacetime modeling which we have proposed can be compared to the Newtonian classical modeling. The main difference between the two approaches is that the spacetime modeling enables us to obtain covariant models which can be then written in the proper frame and should properly deal with large deformations. A spacetime thermomechanical model systematically has 4 degrees of freedom (including the displacement and temperature) even if the external source of heat and temperature are null. This is not the case for a Newtonian thermomechanical model for which the existence of the fourth degree of freedom is necessary only if in the existence of external source of heat or temperature.

Table 14 summarizes the main differences and similarities between the Newtonian and spacetime modeling of the thermomechanical behavior, for respectively small and large deformations.

| | Newtonian modeling | Spacetime modeling |
|---|---|---|
| Small deformations theory | Use of small deformation $^{ij}$<br>Variational form function of $\epsilon^{ij}$<br>Proper/inertial frame<br>Metric tensor: $\eta^{ij}$<br>Jacobian determinant: $J = 1$<br>$\sigma^{ij}$ of first order | Use of small deformation $\epsilon^{\mu\nu}$<br>Variational form function of $\epsilon^{\mu\nu}$<br>Proper/inertial frame<br>Metric tensor: $\eta^{\mu\nu}$<br>Jacobian determinant: $J = 1$<br>$T_{\sigma}^{\mu\nu}$ of first order |
| (Without external source of heat/temperature) | ▪ 3 degrees of freedom ($dep_i$) | ▪ 4 degrees of freedom ($dep_\mu$, $\theta$) |
| (With external source of heat/temperature) | ▪ 4 degrees of freedom ($dep_i$, $\Delta\theta$) | ▪ 4 degrees of freedom ($dep_\mu$, $\theta$) |
| Large deformations theory | Use of large deformation $E^{ij}/e^{ij}$<br>Variational form function of $E^{ij}/e^{ij}$<br>Proper/inertial frame<br>Metric tensor: $\eta^{ij}$<br>Jacobian determinant: $J \neq 1$<br>$\sigma^{ij}$ of first order | Use of large deformation $E^{\mu\nu}/e^{\mu\nu}$<br>Variational form function of $E^{\mu\nu}/e^{\mu\nu}$<br>Proper frame ($\Gamma^{\mu}_{\kappa\lambda} \neq 0$)<br>Metric tensor: $\hat{g}^{\mu\nu}$<br>Jacobian determinant: $J \neq 1$<br>$T_{\sigma}^{\mu\nu}$ of second order |
| (Without external source of heat/temperature) | ▪ 3 degrees of freedom ($dep_i$) | ▪ 4 degrees of freedom ($dep_\mu$, $\theta$) |
| (With external source of heat/temperature) | ▪ 4 degrees of freedom ($dep_i$, $\Delta\theta$) | ▪ 4 degrees of freedom ($dep_\mu$, $\theta$) |

**Tab. 14:** Summary on the difference of Newtonian and spacetime modeling using small and large deformations theories

In this manuscript, the Newtonian modeling of some behaviors for small and large deformations was conducted (sections 4.2.2, 4.2.3, 4.2.4 and 4.2.6) in order to be a reference of comparison for the spacetime modeling. In section 5.8 and Appendix B, many cases are considered in order to test the spacetime thermo-hyperelastic model for small deformations using spacetime numerical simulations. Test cases include numerical simulations of the spacetime thermo-hyperelastic behavior using a Hooke-like model::

- For a beam under traction load (linear load) for the case when thermal expansion is null (see section 5.8)
- For a beam under bending load for the case when thermal expansion is null (see Appendix B)
- For a beam under pure thermal constraints for the cases when thermal expansion is null and not null (see Appendix B)
- For a beam traction (sinusoidal load) for the case when thermal expansion is not null (see Appendix B)

Simulations are done under the assumptions of spacetime modeling for small deformations (see sections 5.5 and 5.5.4).

## 5.8 Test case: Numerical simulation of the spacetime thermo-hyperelastic behavior using a Hooke-like model: beam under traction load

In this section, we describe a test case applied on spacetime model and compared to the results obtained using a Newtonian model as a step of validation for a specific loading. The problem is the same as the one described in section 4.2.5.1 except that here the numerical resolution is performed in the spacetime domain.

Let us consider that the beam has the behavior of a Hooke-like model. We will investigate this model in case of (thermo-)hyperelasticity (the weak integral form is given in Eq. 5.86), consequently we assume that the yield stress of the material is not reached. We will simulate a traction problem using small strain (Eq. 4.2).

The model is constrained by:

- $\forall y \in \partial\omega_1, \forall t,\ f_{SC1} = dep(x = 0, y, t) = (0, 0)$ on the clamped boundary of the beam.
- $\forall y \in \partial\omega_2, \forall t,\ f_{SC2} = dep(x = L, y, t) = (\chi(t), 0, t) = (0.1\,t, 0)$ on the right boundary of the beam.
- $\forall x, \forall y,\ f_{TC1} = dep(x, y, t = 0) = (0, 0)$ represents the initial condition on the displacement.
- $\forall x, \forall y,\ f_{TC2} = \theta(x, y, t = 0) = \theta_0 = 0\,°C$ represents the initial condition on the temperature ($\theta_0$ is the initial temperature considered as reference temperature).

The parameters for the numerical simulation are the same as in section 4.2.5.3 (cf. table 11). The numerical simulation is done for $\alpha = 0$, hereby the traction is expected to be isothermal.

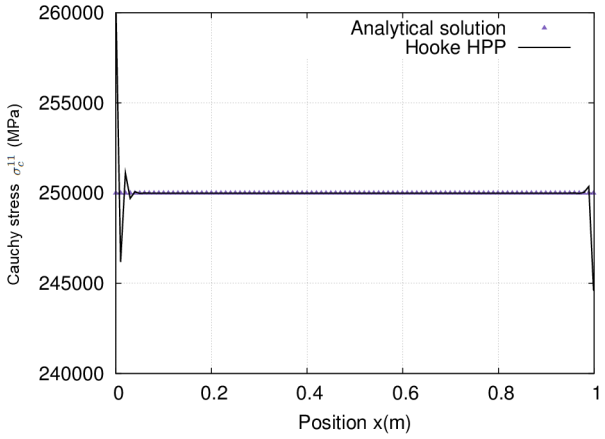


**Fig. 41:** Evolution of $\sigma_c^{11}(x, y, t)$ obtained from analytical solution and spacetime simulation as function of the space in the $x$-direction at $y = W/2$ and $t = t_{max}$.

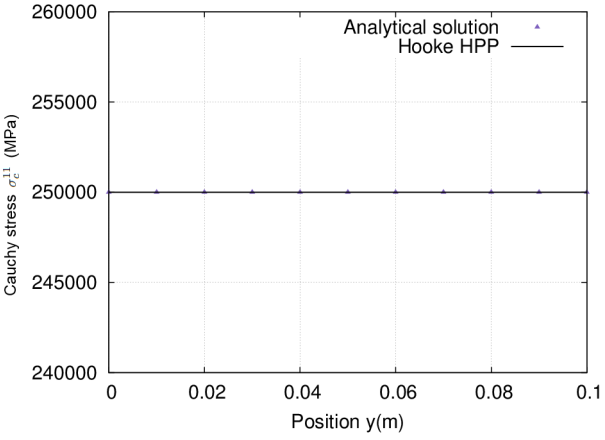


**Fig. 42:** Evolution of $\sigma_c^{11}(x, y, t)$ obtained from analytical solution and spacetime simulation as function of the space in the $y$-direction at $x = L/2$ and $t = t_{max}$.

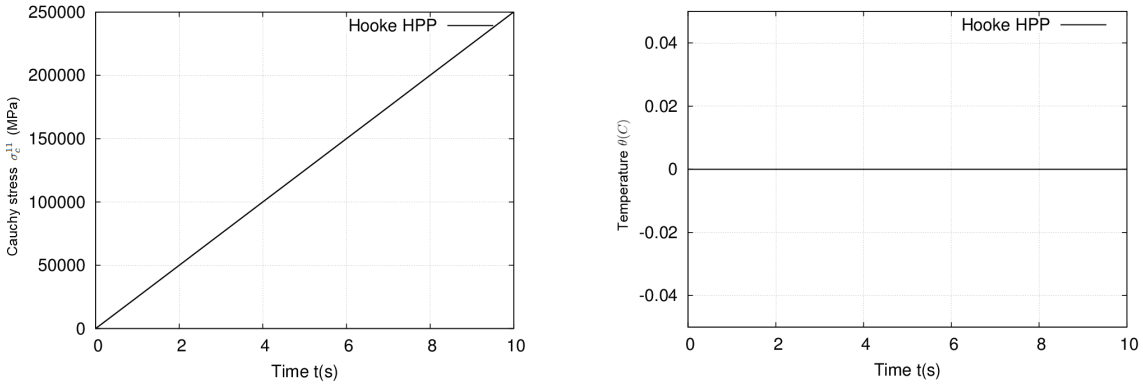


**Fig. 43:** On the left: Evolution of $\sigma_c^{11}(x, y, t)$ obtained from spacetime simulation as function of the time at $x = L/2$ and $y = W/2$. On the right: Evolution of $\theta(x, y, t)$ obtained from spacetime simulation as function of the time at $x = L/2$ and $y = W/2$.

The error and percentage of error on $\sigma_c^{11}$ are respectively around $556.4\,MPa$ and $0.0038\,\%$, which are mainly deriving form border effects (clearly seen in Fig. 41). More test cases can be found in appendix B

## 5.9 Application: the modeling of a bimetallic element behavior

### 5.9.1 Description of the problem

We consider the case of a bimetallic element of 2 layers of equal width having different materials (1 and 2) as represented in Figure 44. For simplification, the two materials are considered to have identical mechanical properties but different thermal expansion coefficients. We suppose that the bimetallic element is clamped at one end and simply supported at the other such that its displacement in the $y$-direction is blocked.

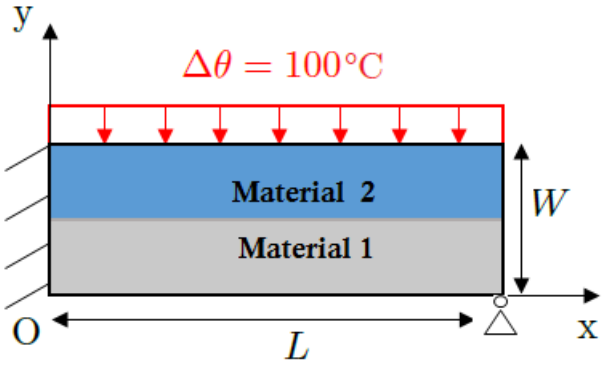


**Fig. 44:** Bimetallic element subjected to temperature

This case is studied under some assumptions [Timoshenko,1925]:

- Material coefficients remain constant during heating. Thus, the difference in the coefficients of expansion remain constant.
- Friction at the supports can be neglected.

- Thickness $H$ of the element is taken equal to unity.
- Cross-sections of the element originally plane and perpendicular to the axis remain plane during bending and become perpendicular to the curved axis of the element.

For these conditions, the analytical solution of the problem leads to the maximum bending moment expression at the clamped end:

This leads to the maximum bending stress [Timoshenko,1925]:

$$\sigma_c^{11}{}_{(max)} = \frac{9}{8} E(\alpha_2 - \alpha_1)\Delta\theta \tag{5.91}$$

### 5.9.2 Boundary conditions, weak integral form of the problem for the Newtonian thermo-hyperelastic model and parameters of the numerical simulation of the bending behavior

The model is constrained by:

- $\forall y \in \partial\omega_1, \forall t,\ f_{SC1} = dep(x = 0, y) = (0, 0)$ on the clamped boundary of the bimetallic element.
- $\forall y \in \partial\omega_2, \forall t,\ f_{SC2} = dep(x = L, y) = (x, 0)$ on the right boundary of the bimetallic element to block the displacement at the boundary along the $x$-direction.
- $\forall x \in \partial\omega_3, \forall t,\ f_{SC3} = \Delta\theta(x, y = W) = 100°C$ on the upper boundary of the bimetallic element.
- $f_{TC1} = dep(x, y, t = 0) = (0, 0)$ represents the initial condition of the displacement on the time boundary $\omega_{t=0}$ defined at $t = 0$.
- $f_{TC2} = \Delta\theta(x, y, t = 0) = 0°C$ represents the initial condition of the temperature on the time boundary $\omega_{t=0}$ defined at $t = 0$.

We will investigate this model in case of thermoelasticity (the weak integral form is given in Eq. 4.29). We will simulate a bending problem using small strain (Eq. 4.2).

### 5.9.3 Boundary conditions, weak integral form of the problem for the spacetime thermo-hyperelastic model of the numerical simulation of the bending behavior

The model is constrained by:

- $\forall y \in \partial\omega_1, \forall t,\ f_{SC1} = dep(x = 0, y, t) = (0, 0)$ on the clamped boundary of the bimetallic element.
- $\forall y \in \partial\omega_2, \forall t,\ f_{SC2} = dep(x = L, y, t) = (x, 0)$ on the right boundary of the bimetallic element to block the displacement of the end along the $x$-direction.
- $\forall x \in \partial\omega_3, \forall t,\ f_{SC} = \theta(x, y = W, t) = 100°C + \theta_0$ on the upper boundary of the bimetallic element.
- $f_{TC1} = dep(x, y, t = 0) = (0, 0)$ represents the initial condition of the displacement on the time boundary $\omega_{t=0}$ defined at $t = 0$.
- $f_{TC2} = \theta(x, y, t = 0) = \theta_0 = 20°C$ represents the initial condition of the temperature on the time boundary $\omega_{t=0}$ defined at $t = 0$.

For the thermo-hyperelastic model, Eq. 5.90 with the definition of small deformation (Eq. 4.2) represents the weak integral form using small strain.

### 5.9.4 Numerical simulation of the bimetallic element behavior using Newtonian and spacetime thermo-hyperelastic models using FEniCS project

As follows are the input parameters of the numerical simulation of the Hooke-like model subjected to bending:

| | Parameter | Value |
|---|---|---|
| Geometry (beam) | Length | $L = 0.2\ (m)$ |
| | Width | $W = 0.02\ (m)$ |
| | Thickness | $H = 0.0001\ (m)$ |
| Material 1 and 2 | Young's modulus | $E = 220000\ (MPa)$ |
| | Poisson coefficient | $\nu = 0.315$ (adim) |
| | Density | $\widetilde{\rho_c} = 8950\ (kg/m^3)$ |
| | Thermal expansion of material 1 | $\alpha_1 = 1.3 \times 10^{-6}\ (K^{-1})$ |
| | Thermal expansion of material 2 | $\alpha_2 = 13.5 \times 10^{-6}\ (K^{-1})$ |
| | Thermal conductivity | $\lambda = 91\ (w.m^{-1}.K^{-1})$ |
| | Specific heat capacity at constant 3D volume | $\mathcal{C}_{m\omega} = 460\ (J.kg^{-1}.K^{-1})$ |
| | Width of material 1 in the bimetallic element | $h_1 = W/2$ |
| | Width of material 2 in the bimetallic element | $h_2 = W/2$ |
| Mesh and time stepping | Number of nodes through the $x$-direction of space | $N_x = 100$ (adim) |
| | Number of nodes through the $y$-direction of space | $N_y = 50$ (adim) |
| | Number of loading steps | $N_{step} = 6$ (adim) |
| Thermal load | Time of application of temperature | $t_{max} = 500\ (s)$ |

**Tab. 15:** Parameters of the numerical simulation for the beam subjected to bending

Below are the results of the stress and displacement obtained from Newtonian and spacetime numerical simulations:

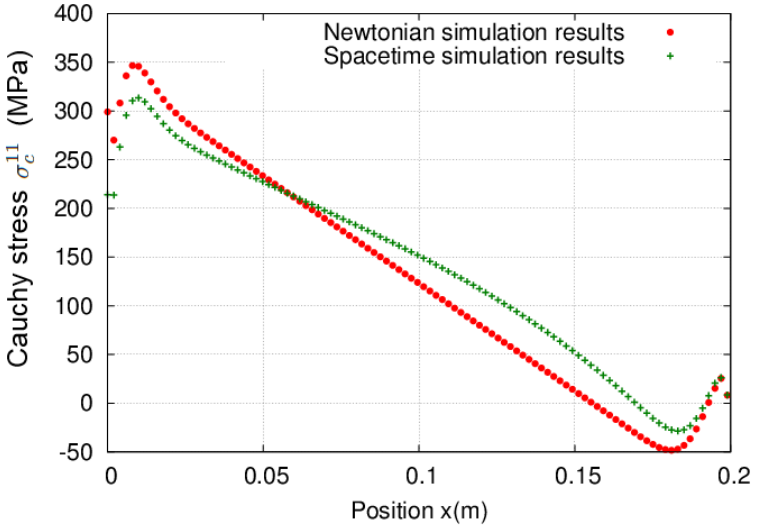


**Fig. 45:** Evolution of $\sigma_c^{11}(x, y, t)$ obtained from Newtonian and spacetime simulations as function of the space in the $x$-direction at $y = 0$ and $t = t_{max}$.

These values can be compared to the analytical solution of stress obtained from Eq. 5.91. For the parameters of table 15, the maximum value of Cauchy stress using the analytical solution is $\sigma_c^{11}{}_{(max)} = 301.95\,MPa$. The relative error resulting from the Newtonian simulation is 12.7 % and that resulting from the spacetime simulation is 3.5 %. Graphs nearly superimpose since the resulting deformations are small. The observed differences may derive from the difference between the meshing in a 2D domain and a 2D+1

domain. In addition, the variation of stress at a cross section is as expected [Timoshenko,1925]: maximums are at the boundaries. Border effects are also seen; even in simulations using a finer mesh at the borders.

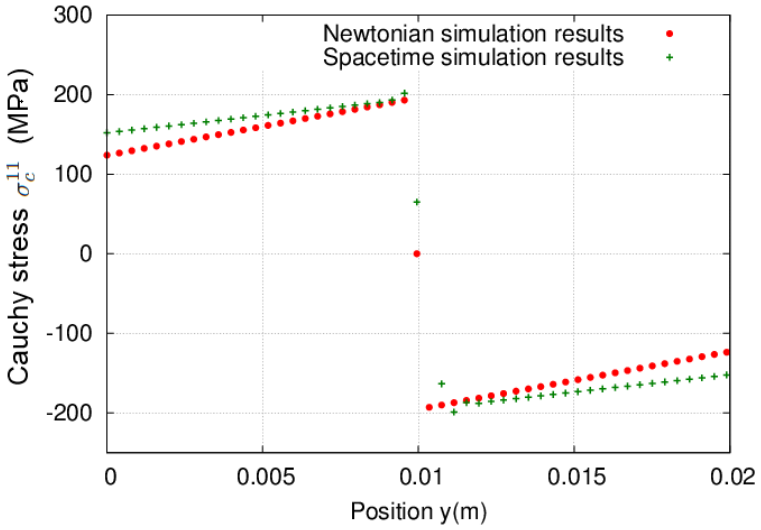


**Fig. 46:** Evolution of $\sigma_c^{11}(x, y, t)$ obtained from Newtonian and spacetime simulations as function of the space in the $y$-direction at $x = L/2$ and $t = t_{max}$.

The resulting displacements show that small deformations are occuring. The displacement along the $x$-direction resulting from the Newtonian and spacetime simulations nearly superimpose. However, a relative error of maximum 27% is noted for the displacement along the $y$-direction. It may also derive from the difference between the meshing in a 2D domain and a 2D+1 domain.

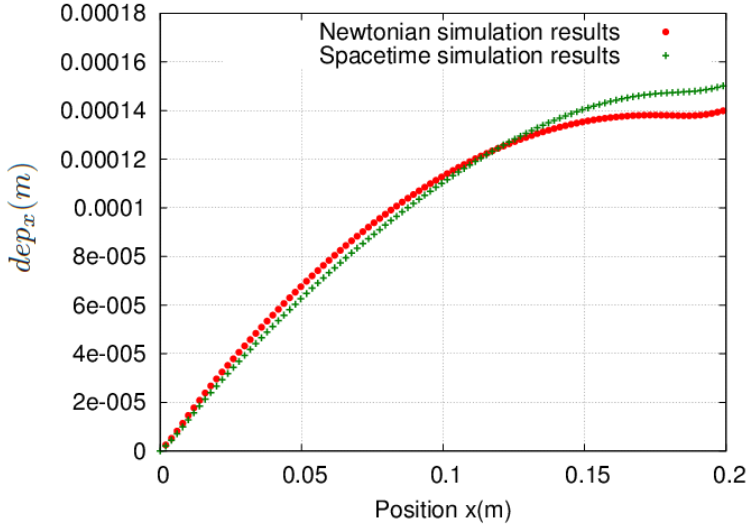


**Fig. 47:** Evolution of $dep_x$ obtained from Newtonian and spacetime simulations as function of the space in the $x$-direction at $y = 0$ and $t = t_{max}$.

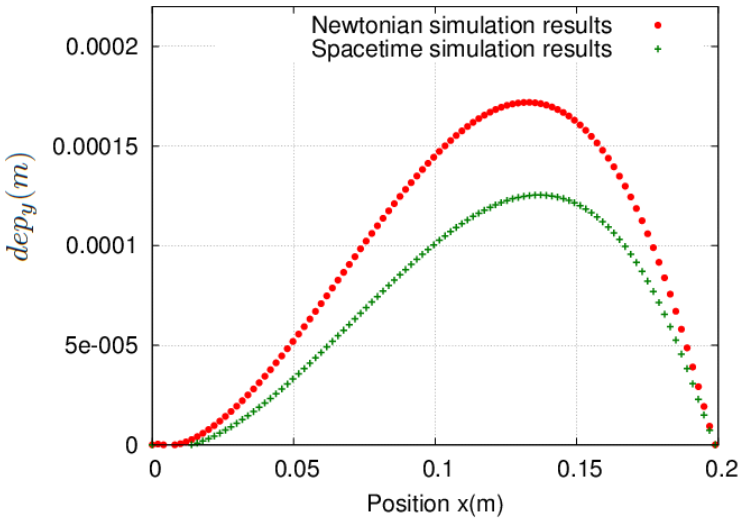


**Fig. 48:** Evolution of $dep_y$ obtained from Newtonian and spacetime simulations as function of the space in the $x$-direction at $y = 0$ and $t = t_{max}$.

Then the influence of one material property is tested. The aim is to verify that the model varies accordingly. Results from spacetime numerical simulations for different values of Young's modulus are illustrated. The percentage of error with respect to the correponding analytical solutions are 3.8, 3.8, 3.4, 3.5 % for respectively $E = 55000$, 110000, 165000, 220000 $MPa$.

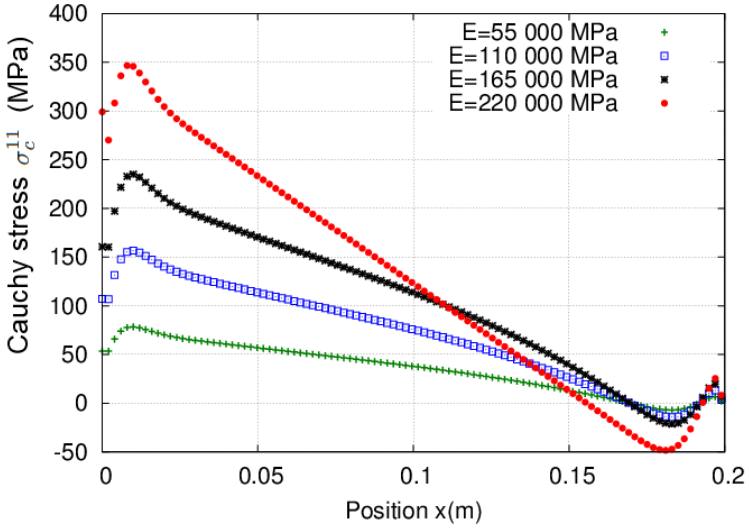


**Fig. 49:** Evolution of $\sigma_c^{11}(x, y, t)$ obtained from spacetime simulations as function of the space in the $x$-direction at $y = 0$ and $t = t_{max}$ for different materials.

## 5.10 Application on the tube bending process

As a perspective, we propose the study of a forming process to illustrate results of the two approaches. The tube bending process is considered for the comparison. As follows, we describe the purpose of modeling

the tube bending process. Due to the complexity of spacetime simulations for large deformation our study is not yet completed. The modeling of this process and results obtained from Newtonian simulations (for small and large deformations) and spacetime simulations (for small deformations) are thus summed up in appendix C.

Many techniques could lead to tube deformation. One important type of tube forming is the tube bending process. Over the last decade, technologies of tube bending were a center of interest since they are important in many industries such as aerospace, automotive and HVAC systems e.g. forming of large-diameter thin-walled Ti–6Al–4V tubes used in light-weight and high-performance components [Zhijun et al.,2017].

Research aimed at improving the process and reducing the manufacturing defects in order to obtain high quality end-products with lower costs and shortened production times. Some of the defects encountered are wrinkling, spring back, breakage and ovalisation [Koseoglu and Parlak,2012]. The geometry of the material such as the bending radius and the tube thickness as well as the friction factor between dies and the tube are factors that affect the productions of these defects. These difficulties for example faced the developement of waveguides having severe requirements on the tolerance as they are used aircraft and missile applications in which high speeds and power are used. One way to overcome these difficulties is by modeling the tube bending process in the most representative way possible. This requires a good understanding of the bending phenomena. To do so, we begin by the study of the bending phenomena in the Newtonian space. This requires a thermomechanical coupling and an assessment using the plastic deformation theory [Tang,2000, Koseoglu and Parlak,2012].

We then propose in this manuscript, a study of the process using a spacetime model since we believe that the modeling and numerical aspects covered by this model is advantageous compared to the Newtonian models. We will limit the spacetime modeling to the study of the thermo-hyperelastic behaviors in small deformations which opens horizons for later studies covering the springback computation and plasticity modeling in large deformations.

Moreover, numerical simulations using FEniCS project are possible for 3D problems without any special programming. Under the assumption of invariant bending on the thickness of the beam and planar stress state, for the Newtonian models, a 2D beam geometry can be studied instead of a 3D beam geometry. These models will be compared to spacetime models with a 2D+1D beam geometry (2D for the space and 1D for the time), which is possible using FEniCS project.

The effect of the bending machine parts including; wiper die, mandrel, booster and supporter die is explained in the appendix C in order to identify the model parameters and the boundary conditions. Then, by applying these requirements to the suggested behavior models, it will be possible to have a prediction on the stress inside the tube. This could be used in sizing the bending system and in identifying the changes necessary to avoid defects.

Note that our aim is to model a cold bending process, consequently we assume that no external heat is applied to the model. Thus, we limit the modeling to cover the mechanical behavior in the Newtonian case. However, keeping the same assumption, spacetime modeling involves a degree of freedom on the variation of temperature thus the modeling will cover the thermomechanical behavior.

In appendix C, we first describe the components of this forming process, we then investigate the parameters necessary for its modeling. In this manuscript, the bending tube process is studied by modeling the (thermo-)mechanical behavior of a 2D beam geometry subjected to a bending load expressed using Dirichlet conditions. First, the Newtonian mechanical model is illustrated using the weak forms of elastic, hyperelastic and elasto-plastic which are then implemented in FEniCS project in addition to the parameters and the boundary conditions corresponding to the bending process (see Fig. 50). Then, the spacetime model is sought. Parameters for the simulations of Newtonian and spacetime models are the same. Results show the compatibility of Newtonian and spacetime models for small deformations. Border effects are also seen. Finner meshing on borders may improve the precision of the constant value of Von mises stress investigated along the tube geometry.

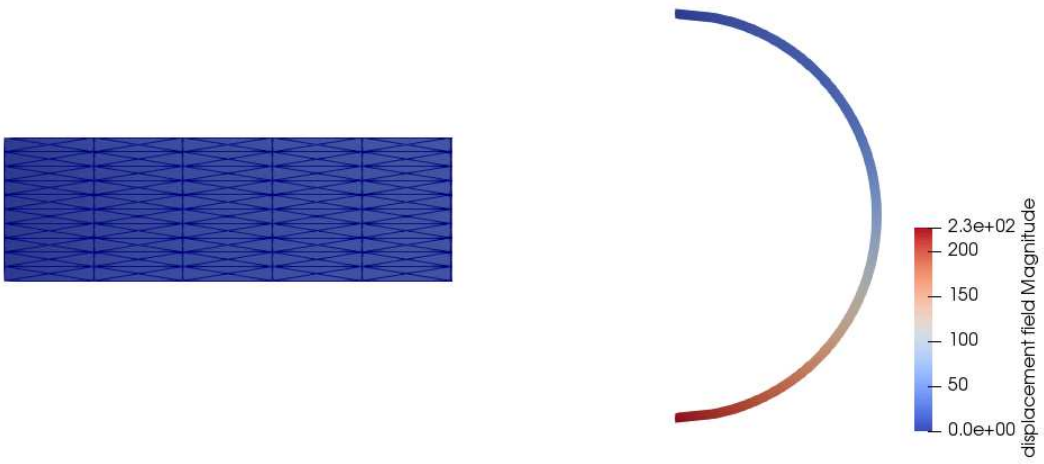


**Fig. 50:** On the left: A sample of the mesh used for the simulation of the tube bending problem using a Newtonian hyperelastic model for small deformations. On the right: The displacement field magnitude in $mm$ resulting from the simulation of the tube bending problem using a Newtonian hyperelastic model for small deformations.

## 5.11 Conclusions

In this chapter, the aim was to define the methodology enabling the spacetime thermomechanical modeling for small and large deformations using a thermodynamical approach. As previously mentionned, this guarantees obtaining thermomechanical models respecting the covariance and causality principles while being compatible with the laws of thermodynamics.

First, the covariant forms of laws of thermodynamics taking into account the mechanical behavior were first investigated using the definition of the energy-momentum tensor (section 5.3).This enables writing these laws in different frames. The classical laws of thermodynamics can be obtained using the spacetime laws written in an inertial frame at the non-relativistic limit.

Second, the spacetime thermo-hyperelastic behaviors of a general model then of a specific reversible model (section 5.5) were obtained under the assumptions of: strong coupling between thermal and mechanical behaviors, isotropic behavior of materials and respect of balance laws (molecules number, momentum and energy, internal energy and entropy). Moreover, to obtain correct behavior models, it is also required to use the spatial projector (introduced in section 2.2.4) when deriving the spacetime stress tensor contribution using the invariants. The obtained model was investigated in the case of (section 5.5.3):

- small deformations and finite temperature variation. At the non-relativistic limit, compared to the Newtonian thermo-hyperelastic model, this model shows additional terms related to the evolution of temperature and its impact on the mechanical behavior due to the thermomechanical coupling.
- small deformations and small temperature variation. At the non-relativistic limit, this model converges to the Newtonian thermo-hyperelastic model.
- for large transformations. At the non-relativistic limit, this model shows additional terms related to the evolution of temperature and large deformations and their impact on the mechanical behavior due to the thermomechanical coupling.

Note that, the benefits of the use of the spacetime approach come essentially from the use of the Lie derivative, because this derivative of the strain tensor reveals the deformation rate. Moreover, the use of spacetime framework includes naturally the time derivative part to build the non-autonomous Lie derivative.

The expression of the spacetime thermo-hyperelastic model in the proper frame is used to write the variational forms which enabled their implementation to simulate the model (section 5.6). We chose to validate in this manuscript the spacetime model obtained under the assumptions of small deformations

and small temperature variation as a first step of verification. Results of the simulations of the 2D and 2D+1D models under simple traction and bending loads, shows the compatibility of the Newtonian and the spacetime results. Slight numerical errors may appear due to the difference of mesh construction between the two models which leads to border effects.

The Newtonian and spacetime modeling of the thermomechanical behavior, for respectively small and large deformations, are compared in section 5.7.

One important result of the modeling is that a spacetime thermomechanical model has 4 degrees of freedom (including the displacement and temperature) even if the external source of heat and temperature are null. Moreover, for small deformations, the proper and inertial frame are indiscernible for Newtonian and spacetime modeling. However, for large deformations, they are. The spacetime modeling enables us to write covariant models. When written in a proper frame, these models show additional terms compared to the corresponding Newtonian models and which are not taken into account in a Newtonian approach. Since this proposed approach is able to model material behavior for small and large deformations, it has various applications in the industry. In this chapter, the spacetime thermo-hyperelastic model was used to study the behavior of a bimetallic element (section 5.9). Results of stress and displacement obtained from Newtonian and spacetime simulations superimpose since the resulting deformations are small.

Moreover, we proposed an approach for modeling the behavior of a tube bending system including the corresponding boundary conditions as a mean to improve this process (section 5.10). In appendix C, we propose the modeling of such a behavior in spacetime. However, the numerical resolution was limited under the assumption of considering small deformations because of the complexity of a numercial simulation for large deformations which was not completely tested and validated.

# 6 Conclusions and perspectives

## 6.1 Conclusions

This research aimed to study the thermomechanical behavior of materials for large deformations. The main interest of this investigation is to find models that help to overcome the difficulties faced in the development of forming processes to reduce their cost and time. The methodology used offers to build thermomechanical models respecting the laws of thermodynamics, the causality principle and the covariance principle. Based on a quantitative and qualitative analysis, it can be concluded that the thermodynamical relativistic approach used in this manuscript enables obtaining spacetime models that cover large deformations and are, at the same time, compatible with the classical behavior models at the Newtonian limit. The results indicate that even though spacetime models need the development of distinctive methods to be obtained, they can solve the problems faced in Newtonian mechanics. These latter can be summarized by: the causality of thermal signals, obtaining models independent of the frame and the modeling of dissipative mechanical behaviors.

In order to write models in the spacetime framework, spacetime operators and variables were first defined and discussed. The use of covariant derivatives in such a framework guarantees obtaining covariant spacetime thermomechanical models. In the first part of the manuscript, the aim was to obtain covariant models covering the thermal conduction behavior in materials. The covariant forms of thermodynamics laws were obtained by relativization of the classical laws, by generalizing their variables into spacetime, without taking the mechanical behavior into account.

The spacetime heat conduction models were then investigated. Spacetime Fourier's model was obtained using two methods: the direct relativization of Fourier's model of heat conduction and a spacetime thermodynamical approach. The obtained models are covariant, thermodynamically compatible with the linear classical irreversible thermodynamics (CIT), however do not respect the causality principle. Moreover, spacetime Cattaneo's model which takes into consideration the relaxation time was obtained using: the direct relativization of Cattaneo's model of heat conduction and the complexification of the spacetime Fourier's model of heat conduction from CIT. The obtained models are covariant, thermodynamically compatible with the extended irreversible thermodynamics (EIT) and respect the causality principle (see table 6). The main added value of these last two models compared to Newtonian models is their covariant character. Additional terms also appear in the spacetime models in comparison with Newtonian models. At the non-relativistic limit, in an inertial proper frame, in which we choose to do the numerical simulations in the first part of the manuscript, these terms vanish.

The variational forms of the spacetime heat conduction models are then written in the inertial proper frame in order to be simulated using FEniCS project. Validation tests were conducted on 2D+1D Fourier's and Cattaneo's models (2 dimensions dedicated to the space and 1 dimension to the time). Results show that the spacetime thermal models obtained have a consistent behavior with respect to mesh refinement and change of material parameters. Spacetime thermal behaviors are also compared to the Newtonian thermal behaviors (integrated on a 2D domain). Results show a compatibility between the two modes of resolution. However, the spacetime finite element method is more expensive in terms of CPU time than the one of the classical approach. For a simulation using Fourier's model, the CPU time needed for the spacetime model is about 5 times the CPU time needed for the Newtonian model for a meshing respectively stepping $N_t = 160$ over time. It is also shown that the spacetime Fourier's model can be used in predicting the heat conduction phenomenon occurring in a cooling fin, which can be useful in the mechanical dimensioning and design of fins when the development of a model is required.

The spacetime thermal model was then used to model self-heating occurring during fatigue tests. The aim is to test the advantages of this model in predicting the resulting temperature of such a phenomenon

especially when the thermal dissipation is variable through time. An innovative methodology is developed: it consists of using experimental data to compute the time parameter characterizing the heat transfer perpendicular to the direction of heat conduction flux $\tau_{ND}$ and the normalized heat source $f_r$ via Newtonian thermal models and injecting them in the spacetime models. Its use shows that spacetime models are able to predict the temperature variation resulting from self-heating during the fatigue test. Various methods can be used for the parameters ($\tau_{ND}$, $f_r$) identification step using the Newtonian models. These methods can be classified as 0D, 1D and 2D methods. To apply the 0D method, the maps of surface temperature obtained at each time step by the IR camera are subjected to temperature averaging through the width and length. To apply the 1D method, the maps of surface temperature are subjected to temperature averaging through the width only. However, to apply the 2D method, the maps of surface temperature are directly used in the computation of thermal dissipation. Using these methods, the self-heating parameters identification is possible in different ways. The 0D method can be used together with the calculation of $\tau_{0D}$ and global optimization of $f_r$ (method A), or with the simultaneous and global optimization of $\tau_{0D}$ and $f_r$ (method B), or with the global optimization of $\tau_{0D}$ and local calculation of $f_r$ (method C). Moreover, the 1D method can be used with the parameters identification by simultaneous global optimization of $\tau_{1D}$ and local calculation of $f_r$ (method D).

The four Newtonian methods described lead to different values for $\tau_{ND}, N = 0, 1$ and $f_r$. For the case studied in this manuscript, the time parameter obtained by the optimization process, used in methods B and C, has a value of $72.73\,s$ approximately two times smaller than the direct calculation by use of its definition $123\,s$, as used in method A. The latter is strongly dependent on the choice for the numerical value of the natural convection coefficient $h$ with a significant uncertainty. For the heat source term, values for methods A to C are in the range of $0.34825\,°C.s^{-1}$ to $0.51\,°C.s^{-1}$ (for long times). Its evolution with time tends to a constant value, which strongly depends on the type of 0D method used. The use of method D increased the accuracy on the values of the parameters since the space variations of $f_r(y,t)$, which are directly related to the stress amplitude variations in the sample with the length ($y$-direction), are taken into account. For a time parameter $\tau_{1D} = 43\,s$, the heat source term is a function of space and time, reaching a maximum at $f_r(y = 30\,mm, t_f = 226.366\,s) = 1.2\,°C.s^{-1}$.
A study of uncertainty is also done based on relative uncertainty on the physical properties and measurement errors related to the camera features. The relative uncertainty on the time parameter value is estimated to $25.5\,\%$ because of the difficulty of its identification as seen for the different methods. The relative uncertainty on the intrinsic dissipation varies for different methods: for method C (0D) it is estimated to vary between 0 and $23.5\,\%$, however, for method D (1D) it is estimated to vary between 0 and $4.43\,\%$ since the diffusivity is taken into account.

Spacetime Fourier's model of heat conduction is then used for the numerical simulation using the parameters previously identified and boundary conditions reproducing the fatigue test conditions. This use is especially advantageous when the intrinsic dissipation is a function of time in the aim of increasing the precision on its value. A quantitative study between the spacetime simulation results and the experimental data shows their compatibility and that the use of method D increases the accuracy because of the significant effect of diffusivity in the self-heating phenomenon. Fully space averaged values of temperature from simulations show good agreement with experimental averaged values resulting from the use of 0D methods as well, whatever the identification method is. These can also be relevantly used for quick simulations requiring only average values on space. They enable obtaining the temporal dynamics of the self-heating phenomenon.

The spacetime modeling introduced in the manuscript can then be used as a reliable approach in modeling the self-heating phenomenon. It is justified by the convergence of experimental results and simulation results using different methods. The hypothesis taken into account in building the spacetime model are the only constraints on the model. There is no limit on the loading frequency nor the value of variation of temperature. The material properties are assumed to be constants in this model. Thus, the model

can be further developed by adding their variation, which can be caused by the variation of temperature, in function of time. The spacetime model enables a more precise computation of dissipation in function of time since the time derivative used is covariant. The suggested methodology helps predicting the temperature resulting from the self-heating phenomenon independently of the number of fatigue cycles causing it.

Briefly, the results in this part of the manuscript show that the spacetime modeling and numerical resolution guarantees the covariance of thermal calculations, which is important for the coupling with mechanical behaviors studied in the second part. However, the precision on the variation of temperature is not improved in case the time is in the macroscopic scale; the results of spacetime and Newtonian models superimpose. The main benefit of such a modeling is to be used in the formulation of spacetime thermomechanical models.

In the second part of the manuscript, the aim was to obtain covariant models covering the thermomechanical behavior of materials. Newtonian models of the elastic, thermoelastic, hyperelastic and elasto-plastic behaviors were reviewed for small and large deformations in order to have reference behaviors to compare with the spacetime thermomechanical models proposed later. Moreover, the elastic, hyperelastic and plastic models were illustrated. A traction respectively bending load was applied to Newtonian elastic respectively hyperelastic and plastic models using a Dirichlet boundary condition on a beam geometry. The evolution of the Cauchy stress tensor in the $x$-direction in function of time shows that the model using Green-Lagrange strain has different elastic, hyperelastic and plastic behaviors than the ones using small strain and Euler-Almansi strain.

Then the thermodynamical approach taking into account the stress contribution and thermomechanical couplings was used to build the spacetime models. Covariant laws of thermodynamics were first formulated. Small and large deformations obey to these laws whatever the frame is. These laws are then used to model the thermomechanical behavior. The covariant derivative was replaced by the Lie derivative where possible. This choice is related to the existence of derived terms multiplied by the spacetime velocity field. The resulting models are covariant as per the requirements in this manuscript. Some assumptions were taken into consideration: the strong coupling between thermal and mechanical behaviors (coupling between the deformation and the variation of temperature which is proportional to the thermal expansion), the isotropic behavior of materials and the respect of balance laws. The specific free energy used is an additive decomposition of three effects: the thermal effect, the stress effect and the thermomechanical coupling effect. These effects are expressed in function of independent projected invariants $\underline{I}_I$ and $\underline{I}_{II}$. These latter should correspond respectively to the deformation of volume (including the effect of thermomechanical coupling) and deformation of surface of the material continuum. They are written using spatial projectors. The use of covariant derivatives and the spatial projector in the modeling, enables the obtention of additional terms in comparison to Newtonian equivalent models. The spacetime thermo-hyperelastic model was written under these assumptions for a general model then for a specific reversible model. The projected invariants are thus chosen by generalizing the invariants of Newtonian Hookean-like models. We chose: $\underline{I}_I = \underline{e}_{\mu\nu}\underline{g}^{\mu\nu} = \underline{e}_{\mu\nu}g^{\mu\nu} = e_{\mu\nu}\underline{g}^{\mu\nu}$ and $\underline{I}_{II} = \underline{e}_{\mu\nu}\underline{e}^{\mu\nu} = \underline{e}_{\mu\nu}e^{\mu\nu} = e_{\mu\nu}\underline{e}^{\mu\nu}$.

The obtained model for a specific reversible model was then investigated for different cases:

- For small deformations and finite temperature variation: this model, at the non-relativistic limit, was compared to the Newtonian thermo-hyperelastic model. It shows additional terms related to the evolution of temperature and its impact on the mechanical behavior due to the thermomechanical coupling.
- For small deformations and small temperature variation: this model, at the non-relativistic limit, converges to the Newtonian thermo-hyperelastic model (see section 5.5.3.2).
- For large transformations: this model, at the non-relativistic limit, shows additional terms related to the evolution of temperature and large deformations and their impact on the mechanical behavior due to the thermomechanical coupling.

The corresponding variational form for the specific reversible model was formulated and implemented for numerical simulation in FEniCS project. Validation tests are conducted: The thermo-hyperelastic behavior of a beam subjected to different load applications such as traction and bending resulting from thermal and mechanical loads, is studied. The evolution of displacement, temperature and Cauchy stress are investigated. Results of validation tests show that using non-relativistic computation conditions (but using equations valid for all loading velocities), the spacetime (2D+1) and Newtonian (2D) models (for which the time is discretized) have the same behavior for small deformations and finite temperature variation. This means that results of spacetime models converge to the results of classical behavior models, which fulfills the requirements. In section B.4, the validation test reproduces the self-heating problem: a cyclic mechanical load is applied and the resulting temperature variation is computed. This enables further developments of the method investigated in chapter 3 in order to take into account the thermomechanical couplings.

The spacetime thermo-hyperelastic model was then used to simulate the behavior of a bimetallic element. Results of stress obtained from spacetime simulations superimpose with results obtained from Newtonian simulations since only small deformations are considered. The modeling of the tube bending process was also proposed in this study. Only the modeling of the thermo-hyperelastic behavior using small deformations could be justified in this manuscript. This is the first step towards a realistic modeling of the process which requires the use of large deformations. The results obtained can be used as a reference to evaluate the behavior obtained using spacetime models for large deformations and to estimate the added value of such a modeling.

The main difference between the modeling using small and large deformations is the that variational forms are consequently function of different variables e.g. small and large strains. The Jacobian determinant is also different: it is equal to 1 for small deformations and not equal to 1 for large deformations. The stress is of first order for both in the Newtonian modeling but of second order using large deformations in spacetime. Moreover, it is shown that the thermomechanical modeling in spacetime implies 4 degrees of freedom of the model (including the displacement and temperature) even if the external source of heat and temperature are null. This guarantees the conservation of internal energy in spacetime and is an important difference with the Newtonian classical modeling. The spacetime framework also enables writing thermomechanical models in the proper frame (for which Christoffel symbols are not null) as well as in the inertial frame independently, since they derive from covariant models. This is an important contribution in the large deformations modeling where these two frames are clearly different.

To sum up, the methodology used for writing covariant thermomechanical models in this manuscript enables the obtaining of models respecting the causality principle and the laws of thermodynamics. We then, through this approach, propose the possibility to resolve problems faced while modeling thermal problems [Straugham,2011, Auriault,2017, Cattaneo,1958, Christov,2009, Osborne,1950, Vernotte,1961, Tavernier,1962, Chapman and Cowling,1970] and mechanical problems [Valanis,1970, Lubliner,1984, Prasolov,1997, Wiechert,1893, Zener,1948, Oldroyd,1950, Wineman,2009, Mooney,1940, Rivlin,1948, Rivlin and Saunders,1951, Ogden,1984, Boyce and Arruda,2000, Steinmann et al.,2012]. This brings the spacetime modeling in continuum mechanics as an important topic to explore and develop. Moreover, this research clearly illustrates the modeling of thermomechanical behavior of materials for large deformations in a spacetime domain, but it also raises the question of the completeness of the assumptions taken into consideration and their implementation for the spacetime simulations.

## 6.2 Perspectives

The modeling and simulation of spacetime thermomechanical material behaviors were discussed in this manuscript. The spacetime modeling covered small and large deformations. However, only the numerical results of the spacetime simulation for small deformations are given in this manuscript for the considered

applications (tube bending and behavior of bimetallic element). This is because the integration of large deformations in a spacetime numerical simulation is complex and requires further checking to be compatible with the theoretical challenges. Thus, further calculations concerning the spacetime simulation for large deformations should be done. This latter step is important to better understand the implications of the results of the spacetime modeling. Hence, future studies could address the spacetime simulation of applications for large deformations and estimate the added value of this formalism in critical cases. Moreover, the spacetime thermo-hyperelastic model was specifically studied. This behavior covers a limited type of thermomechanical modeling. In order to cover the forming processes modeling, in which the material is deformed permanently, the plasticity should also modeled in the spacetime framework.

In addition to that, the method proposed in this manuscript for building spacetime models can be used to develop any type of material behavior in spacetime. It is useful since it systematically guarantees the covariance, the causality and the thermodynamical compatibility of the obtained material models. It is especially interesting to be developed is the case of rate-dependent models e.g. when viscoelasticity and viscoplasticity behaviors occur [Wineman,2009, Bertram,2012]. The Lie derivative introduced in this manuscript can particularly be advantageous in such cases. The generality of this formalism opens the discussion on the possible value of its use in modeling different types of materials (homogeneous, isotropic, anisotropic...) and even composite materials facing challenges in predicting the dynamic mechanical behavior e.g. the sliding wear, the ageing of linen reinforced composites subjected to temperature.

Throughout this manuscript, many phenomena occurring during mechanical applications were also modeled. Some phenomena can be further studied in the spacetime formalism in order to obtain a more realistic modeling. We proposed in chapter 3 the spacetime modeling of the self-heating phenomenon occurring during fatigue tests. The heat dissipation resulting from this transformation was used to model the phenomenon in spacetime without explicitly modeling the thermomechanical coupling. The modeling the thermomechanical coupling can be done at each cycle using the spacetime thermomechanical model developed in the second part of the manuscript and which may give a more accurate modeling. A load similar to the one used in section B.4 can be added to the model in order to apply the thermoelastic source of dissipation. Then, another thermomechanical coupling source due to internal state variable evolution (such as plasticity) can also be possibly used. The amount of contribution of these sources can consequently be deduced. Furthermore, the parameters identification (i.e. identification of time parameter characterizing the heat transfer perpendicular to the direction of heat conduction flux $\tau_{ND}$ and the normalized heat source $f_r$) was suggested in the Newtonian formalism using four different methods. One possible way to improve the model can be by developing spacetime methods for the identification step.

We also proposed, in chapter 5, the modeling of the tube bending process which should require, for more realistic predictions, the assumptions of large deformations but also of the dissipative behavior (plasticity, friction for the contact). Many critical phenomena (ovalisation, elastic spring-back...) also interfere in the modeling of such a process. In this manuscript (Appendix C), the Newtonian elasto-plastic model was studied to reproduce the reality of the process. For spacetime modeling, at first approximation, the thermo-hyperelastic behavior was only taken into account. The Newtonian and spacetime thermo-hyperelastic models representing this process were developed. For simulation, these two models were compared in a resolution considering small deformations only. The numerical simulation taking into account large deformations is to be studied in future works. The implementation of Christoffel symbols should be particularly tested. A study of convergence for the meshing of the suggested geometry can also be conducted. The general modeling and simulation of plasticity in spacetime for this particular application is also to be done: the variational forms for plasticity in spacetime should be developed.

Despite the advantages of using a formalism guaranteeing the covariance, causality and thermodynamical compatibility of models, an additional time of computation or the need of a bigger computational capacity can be encountered (as proved for the spacetime thermal models). This is why it will be important to specify the necessity and advantages of use of the spacetime formalism for each case of study. Its use for

modeling large transformations is useful for developing existing models but should hence be coupled with a profitability study. If the cost of the modeling and the computational complexity can be made affordable for the processes facing challenges, the use of a spacetime formalism will be prioritized.

Eventually, the simulations of validation tests and thermomechanical applications were all conducted for 0D/1D/2D Newtonian models and 0D+1D/1D+1D/2D+1D spacetime models since the tool used for simulation (FEniCS project) enables the implementation of 3 dimensions finite elements for resolution. Simulations using a higher-order finite elements solver which enables the spacetime meshing of 3D+1D spacetime models would be more accurate for models in some applications e.g. where symmetry is not applicable. Firedrake is an example of a solver that may be used for this cause by extruding meshes hence "allowing users to construct many finite element spaces beyond those supported by existing software packages" [McRae et al.,2016].

# 7 Résumé en français

## 7.1 Introduction

Les procédés de fabrication dans l'industrie sont divers, on distingue par exemple: l'obtention par enlèvement de matière, les techniques par fabrication additive, la fonderie... C'est un secteur en développement perpétuel. En particulier, les procédés de mise en forme envisagent des défis pour optimiser la qualité et le prix des pièces fabriquées. Ces défis peuvent être potentiellement résolus par le biais de la simulation numérique. Un des verrous pour la modélisation des procédés de mise en forme est la modélisation du comportement des matériaux en grandes déformations [Panicaud et al.,2015].

Plusieurs contributions dans ce domaine adoptent un point de vue géométrique pour la mécanique des matériaux en grandes transformations. C'est ce que nous proposons également de faire. La base du point de vue adopté dans cette étude est de formuler des lois physiques dont la forme se conserve en changeant de référentiels [Wang,2016]. Adopter un point de vue géométrique est réalisé en examinant l'action du groupe des changements de référentiels sur les équations de la physique. On s'assure donc que la physique reste la même quel que soit le référentiel, ce qui conduit à postuler la covariance des équations. On parle alors de relativité ou de théories relativistes en physique. Comme conséquence de l'application du principe de covariance, les théories de la relativité décrivent des phénomènes dans un domaine d'espace et de temps simultanément.

En plus, les lois de comportement dissipatives, nécessaires à la modélisation des procédés de mise en forme, devront être compatibles avec le second principe de la thermodynamique, qui prend en général la forme de l'inéquation de Clausius-Duhem. Afin de proposer des lois de dissipation covariantes plastiques ou visqueuses, il faudra donc proposer une formulation covariante de cette inéquation de Clausius-Duhem [Lamoureux-Brousse,1989]. Cette étude a donc pour but de trouver des modèles représentatifs et applicables aux procédés de mise en forme qui nous intéressent, incluant également les phénomènes thermiques, d'où la nécessité de prendre en compte certains couplages thermomécaniques. La modélisation du comportement comprend donc des phénomènes thermiques qui posent dans l'approche Newtonienne (dite 3D) comme dans l'approche espace-temps (dite 4D) le problème de causalité. Par exemple, la loi de propagation de chaleur par conduction selon Fourier suppose une propagation instantanée de la chaleur. Ceci ouvre la discussion sur la possibilité de résoudre ce problème par différentes approches, en 3D à l'aide de modèles plus élaborés, mais aussi en 4D à l'aide des théories relativistes de la dissipation.

De façon générale, l'objectif de ce travail est donc d'obtenir le comportement thermomécanique dans un cadre relativiste, à partir des principales grandeurs cinématiques et physiques. Le comportement thermomécanique attendu devrait alors assurer les notions de covariance et de causalité, souvent violées dans les cadres thermodynamiques Newtoniens [Christov and Jordan,2005, Fichera,1992]. Les modèles devront pouvoir présenter le moins d'approximation possibles pour pouvoir être applicables en grandes déformations et en grandes vitesses de déformations (néanmoins non-relativistes pour les vitesses des procédés qui nous intéressent, ce qui les rend comparables aux modèles 3D.

## 7.2 Démarche proposée

La démarche proposée pour les modélisations et les simulations souhaitées se résume à la construction d'une approche thermodynamique espace-temps dans laquelle on développe la modélisation thermique et mécanique de procédés de mise en forme. Le but final étant la simulation thermo-mécanique, la plus représentative possible de ces procédés, dans un domaine espace-temps.

Les détails de la démarche que nous envisageons dans le cadre de ce projet sont décrits ci-dessous:

- La description d'un formalisme espace-temps garantissant la covariance des lois physiques.

- La généralisation des lois de la thermodynamique dans un formalisme espace-temps en partant des lois Newtoniennes (conservation de l'énergie interne, du moment et de l'énergie totale). Ceci aboutit aussi et notamment à une écriture covariante de l'inéquation de Clausius-Duhem.
- La formulation espace-temps de modèles de conduction thermique et des modèles thermomécaniques en s'appuyant sur différentes méthodes, notamment l'approche thermodynamique espace-temps précédemment construite.
- La construction des formes variationnelles espace-temps de ces modèles afin de d'effectuer la simulation numérique de problèmes multi-physiques.
- La simulation numérique des modèles espace-temps via le logiciel FEniCS project.
- L'utilisation des modèles espace-temps pour la modélisation d'applications d'ingénierie, de caractérisation de matériaux et de procédés de mise en forme (modélisation de la conduction thermique dans une ailette refroidissante, modélisation de l'autoéchauffement, modélisation du procédé de flexion de tube et du comportement de bilame).
- Comparaison des résultats obtenus par les approches Newtonienne et relativiste afin de valider la dernière à la limite Newtonienne.

## 7.3 Modélisation thermique du comportement des matériaux

### 7.3.1 Etude bibliographique sur la modélisation thermique en 3D et en espace-temps

L'aspect thermique dans la modélisation du comportement d'un matériau est une partie essentielle dans la plupart des applications [Lamoureux-Brousse,1989]. La première partie de ce manuscrit vise à modéliser le comportement de conduction thermique. Plusieurs modèles Newtoniens existent dans la littérature [Fourier,1988, Cattaneo,1958, Tavernier,1962, Osborne,1950, Vernotte,1961, Battaglia,2007] (section 1.5). Cependant, il a été identifié que tous les modèles ne remplissent pas toutes les exigences pour une modélisation précise.

Les difficultés rencontrées en thermomécanique Newtonienne (section 1.6) peuvent être résumées par: certains des modèles trouvés dans la littérature ne respectent pas le principe de causalité [Fourier,1988] et certains ne sont pas covariants [Cattaneo,1958, Tavernier,1962, Osborne,1950, Vernotte,1961] (voir tableau 16). Puisque ces deux principes sont nécessaires pour un modèle de conduction thermique, ainsi que la prise en compte correctement de l'irréversibilité pour les grandes transformations, un formalisme thermodynamique spatio-temporel garantissant la covariance des modèles est nécessaire (section 1.7).

| Propriétés/Modèles | Fourier | Cattaneo | Osborne | Vernotte |
|---|---|---|---|---|
| Vérifie le principe de covariance dans le sens 3D | Oui | Non | Non | Non |
| Vérifie le principe de causalité | Non | Oui | Oui | Oui |
| Compatibilité thermodynamique | Oui | NA | NA | NA |

**Tab. 16:** Liste des différents modèles Newtoniens trouvés dans la littérture et de leurs propriétés (NA = non applicable)

Quelques modèles relativistes de conduction thermique existent déjà dans la littérature [Eckart,1940, Carter,1988, Landau and Lifshitz,1975, Israel and Stewart,1979a, Israel and Stewart,1979b] (section 1.8). Les modèles relativistes issus de CIT ne respectent pas le principe de causalité [Eckart,1940]. D'autres issus de l'EIT respectent ce principe [Israel and Stewart,1979a, Carter,1988] mais le prix à payer est de trouver des coefficients de correction du second ordre pour les sources d'entropie (voir tableau 17). De plus, les conditions de stabilité dans ces modèles sont plutôt artificielles. Les modèles relativistes existants ne répondant pas systématiquement à toutes les exigences, des investigations complémentaires sur les modèles spatio-temporels sont nécessaires.

| Propriétés/Modèles | Eckart | Landau and Lifshitz | Israel and Stewart | Carter |
|---|---|---|---|---|
| Vérifie le principe de covariance | Oui | Oui | Oui | Oui |
| Vérifie le principe de causalité | Non | Non | Oui | Oui |
| Compatibilité thermodynamique | Oui | Oui | Oui | Oui |

**Tab. 17:** Liste des différents modèles relativistes trouvés dans la littérture et de leurs propriétés

Notre objectif est de développer un cadre qui garantit la covariance des modèles de conduction thermique, respecte le principe de causalité et pourrait en même temps être dérivé de la thermodynamique irréversible classique. Ce cadre est construit dans un domaine euclidien de l'espace-temps sans gravitation.

Ce cadre nous permet de construire des modèles de conduction de chaleur spatio-temporels utilisables pour des applications d'ingénierie (voir chapitre 2). L'auto-échauffement est l'un des phénomènes modélisables (section 1.9). Il se produit au cours de divers processus, en particulier les tests de fatigue. Des études Newtoniennes de l'auto-échauffement se trouvent dans [Chrysochoos et al.,2009, Boulanger et al.,2004, Lemaitre and Chaboche,1990, La Rosa and Risitano,2000, Galtier,1993, Poncelet et al.,2011, Munier,2012]. La dissipation qui en résulte permet d'étudier la limite de fatigue. Nous modélisons ce phénomène au chapitre 3 pour prouver la possibilité d'utiliser les modèles de chaleur spatio-temporels obtenus au chapitre 2 pour représenter des techniques d'analyse et de caractérisation des matériaux et pour améliorer la résolution numérique d'un tel phénomène.

### 7.3.2 La modélisation thermique en espace-temps dans ce manuscrit

Nous avons d'abord étudié la modélisation d'un comportement thermique en utilisant une approche thermodynamique. L'originalité vient de l'utilisation systématique d'un formalisme d'espace-temps pour assurer l'indifférence au changement de référentiels, tant pour les modèles physiques que pour les schémas de résolution numérique. En utilisant la conservation de l'énergie interne écrite dans l'espace-temps et la variation du flux d'entropie, la forme covariante de l'inégalité de Clausius-Duhem est proposée.

L'évolution thermique pure en cas de conduction thermique est spécifiquement étudiée. Les équivalents spatio-temporels des équations de Fourier et de Cattaneo ont été soit obtenus par la généralisation de l'espace-temps des équations Newtoniennes, soit déduits de la forme covariante de l'inégalité de Clausius-Duhem. En assumant l'absence des couplages thermomécaniques dissipatifs, deux types de modèles ont été obtenus à partir de ces différentes méthodes. C'est à noter qu'une méthodologie particulière n'impliquant que le cadre CIT a également été proposée pour obtenir le modèle de Cattaneo dans le domaine de l'espace-temps, en utilisant la transformée de Laplace et la complexification. Elle peut être facilement généralisée pour obtenir d'autres modèles conduisant à une dérivée espace/temps du troisième ordre (ou plus) de la température dans l'équation de la chaleur. Différents modèles covariants généralisants le modèle Newtonien de Cattaneo peuvent ainsi être obtenus à partir d'un cadre CIT sans avoir besoin d'utiliser un cadre EIT. De tels termes restent à être étudié d'un point de vue numérique. Quel que soit le référentiel, le modèle spatio-temporel de Fourier peut être exprimé par (section 2.3):

$$q^{\mu} = \frac{\lambda}{c}\Pi^{\mu\nu}\nabla_{\nu}\theta = \frac{\lambda}{c}(g^{\mu\nu} - u^{\mu}u^{\nu})\nabla_{\nu}\theta \tag{7.1}$$

où $q^{\mu}$ est le flux de chaleur spatio-temporel, $\lambda$ est la conductivité thermique, $c$ est la célérité de la lumière, $\Pi^{\mu\nu}$ est le projecteur spatial, $\nabla_{\nu}$ est la dérivée covariante, $\theta$ est la température, $g^{\mu\nu}$ est la métrique spatio-temporelle et $u^{\mu}$ est la vitesse spatio-temporelle. Quel que soit le référentiel, le modèle spatio-temporel de Cattaneo peut être exprimé par(section 2.4):

$$q^{\mu} - \tau c u^{\nu}\nabla_{\nu}q^{\mu} = \frac{\lambda}{c}(g^{\mu\nu} - u^{\mu}u^{\nu})\left(\nabla_{\nu}\theta - \tau_1 c u^{\kappa}\nabla_{\kappa}(\nabla_{\nu}\theta)\right) \tag{7.2}$$

où $\tau$ et $\tau_1$ sont les temps de relaxation.

Comme dans sa forme Newtonienne, le modèle de Cattaneo en espace-temps contient des termes de relaxation qui expriment le caractère non-instantané de conduction de la chaleur dans le corps. L'existence de ces termes conduit par conséquent à surmonter les problèmes de causalité rencontrés dans certains autres modèles thermiques, qui supposent une propagation de chaleur à une vitesse infinie. Par conséquent, ce formalisme de l'espace-temps atteint son objectif en créant des modèles de conduction de chaleur spatio-temporels covariants et en respectant simultanément le principe de causalité.

### 7.3.3 Formes variationelles du problème thermique

Une fois que les modèles thermiques à utiliser ont été identifiés, on a choisi d'écrire le problème variationnel des modèles de Fourier et de Cattaneo dans un formalisme espace-temps. Ce problème est dans ce muscrit écrit dans le référentiel inertiel et intégré sur un hypervolume (volume spatial $\times$*durée*).

Le problème variationnel correspondant à un modèle de Fourier dans un repère inertiel dans des conditions aux limites de Dirichlet est :

$$W(\theta,\theta^*) = \int_\Omega \theta^* \frac{\partial\theta}{\partial t}\,\mathrm{d}H_\Omega + \int_\Omega a\frac{\partial\theta^*}{\partial x^j}\frac{\partial\theta}{\partial x_j}\,\mathrm{d}H_\Omega - \int_\Omega \theta^* f_r\,\mathrm{d}H_\Omega = 0, \forall\theta^* \tag{7.3}$$

$\theta$, étant la température d'essai. $\theta^*$, étant la température test. $\Omega$, étant le domaine d'intégration espace-temps. $a$, étant la diffusivité du milieu.

Pour écrire les conditions aux limites, on définit: $\partial\Omega^j = \partial\omega \cup t$ comme étant la limite spatiale du domaine et $\partial\Omega^4 = \omega \cup \partial t$ comme étant la limite temporelle du domaine, $\omega$ étant le domaine d'intégration spatial (3D).

Le problème variationnel correspondant à un modèle de Cattaneo dans un repère inertiel et dans des conditions aux limites de Dirichlet est :

$$W(\theta,\theta^*) = \int_\Omega \theta^* \frac{\partial\theta}{\partial t}\,\mathrm{d}H_\Omega + \int_\Omega a\frac{\partial\theta^*}{\partial x^j}\frac{\partial\theta}{\partial x_j}\,\mathrm{d}H_\Omega - \int_\Omega \tau\frac{\partial\theta^*}{\partial t}\frac{\partial\theta}{\partial t}\,\mathrm{d}H_\Omega - \int_\Omega \theta^* f_r\,\mathrm{d}H_\Omega = 0, \forall\theta^* \tag{7.4}$$

Les conditions aux limites des deux formes variationnelles sont ainsi divisées en conditions sur l'espace et conditions sur le temps. Le premier type peut être exprimé par: $\theta(x^\mu \in \partial\Omega^j) = f_{SC}(x^\mu \in \partial\Omega^j)$, $f_{SC}$ étant la fonction représentant les conditions limites sur l'espace. Le second type peut être exprimé par: $\theta(x^\mu \in \partial\Omega^4) = f_{TC}(x^\mu \in \partial\Omega^4)$, $f_{TC}$ étant la fonction représentant les conditions limites sur le temps initial. La seule condition temporelle sur la température est au temps initial puisque la température au temps final est calculée par le modèle de conduction thermique.

Les formes variationnelles correspondant aux deux modèles dans un repère inertiel dans des conditions aux limites de Neumann-Dirirchlet sont aussi formulées dans la section 2.6. Des simulations numériques avec FEniCS ont également été effectuées pour illustrer cette approche. Pour les problèmes thermiques purs, les formes intégrales faibles en espace-temps proposées pour les modèles de conduction thermique (Eqs. 2.52, 2.53, 2.55 et 2.56) diffèrent de celles des modèles Newtoniens (Eq. 2.57) uniquement par le domaine d'intégration. Dans les premières, le temps est une dimension du domaine de l'intégration. Cependant dans les secondes c'est un paramètre et il est généralement discrétisé à l'aide d'une méthode explicite par une différence décentrée amont pour la dérivée temporelle de premier ordre et une différence centrée pour la dérivée temporelle de second ordre (si nécessaire pour le modèle de Cattaneo). La condition initiale sur le temps discrétisé (modèle Newtonien) est dans ce cas équivalente à une condition aux limites pour l'intégration spatio-temporelle (modèle relativiste).

Les modèles numériques spatio-temporels ont été comparés aux modèles Newtoniens de Fourier et Cattaneo. Les résultats montrent une compatibilité entre les deux (Figure 51). La juxtaposition des graphes des modèles espace-temps (courbe rouge) et Newtonien (courbe verte) avec le temps discrétisé pour chacun des modèles justifie cette validation. La figure ci-dessous montre cette comparaison pour un modèle de Fourier.

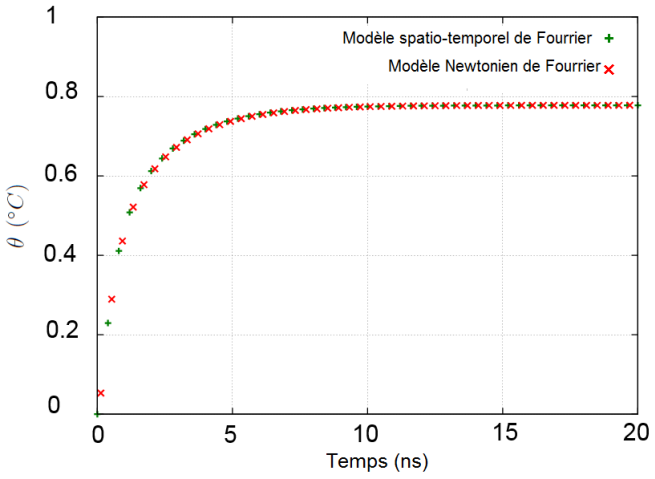


**Fig. 51:** Evolution de la temperature en fonction du temps à la position $x$ pour les modèles de Fourier spatio-temporel (courbe verte) et Fourier 3D avec le temps discrétisé (courbe rouge), en supposant que $f_r = 0$.

Cependant, la méthode des éléments finis en espace-temps a un temps de calcul d'ordre supérieur (second ordre) par rapport à celui nécessaire pour l'approche classique. De plus, l'influence du domaine de intégration, du maillage et des paramètres du matériau ont été étudiées pour des modèles 1D + 1D. Ainsi, des simulations montrant la comparaison entre les modèles de Fourier et de Cattaneo dans un formalisme espace-temps dans les mêmes conditions ont été faites. La figure 52 montre l'évolution de la température en un point d'un modèle 1D+1D au cours du temps. Les résultats montrent qu'à partir d'un certain temps le modèle de Cattaneo (courbe verte) est en retard par rapport au modèle de Fourier (courbe rouge) ce qui est logique vu le temps de relaxation introduit dans ce dernier. Ceci permet finalement d'assurer simultanément la covariance et la causalité.

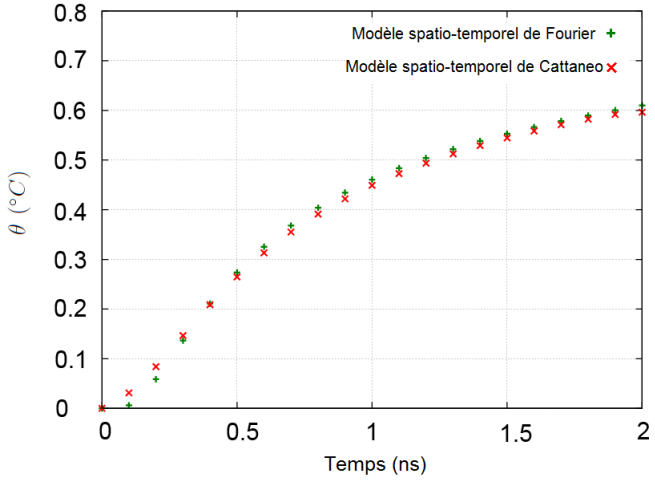


**Fig. 52:** Evolution de la temperature en fonction du temps à une position $x$ pour les modèles de Fourier (courbe verte) et de Cattaneo (courbe rouge) dans un formalisme espace-temps.

Le modèle spatio-temporel de Fourier a été ensuite utilisé pour résoudre un problème de conduction thermique dans une ailette de refroidissement. Les résultats montrent que ce modèle est capable de prédire la conduction de chaleur dans cette application particulière.

L'utilisation d'un formalisme d'espace-temps semble avoir moins d'intérêt dans le cas d'un corps immobile subissant la conduction thermique en termes de temps de calcul. Cependant, ce cas particulier est considéré comme un cas limite du cas de corps subissant simultanément des transferts de chaleur par conduction et des grandes déformations mécaniques, comme dans un procédé de mise en forme. Ce dernier cas est approfondi dans la deuxième partie du manuscrit (chapitres 4 et 5).

### 7.3.4 Etude bibliographique sur l'autoéchauffement

Le phénomène d'autoéchauffement est également étudié à l'aide des modèles thermiques spatio-temporels. Il est présenté dans nombreux ouvrages et articles [Boulanger et al.,2004, Chrysochoos and Louche,2000]. Comme son nom l'indique, ce phénomène implique une variation de température du corps soumis à une transformation mécanique (souvent cyclique), sans apport de chaleur de l'extérieur. Il se produit au cours de nombreux processus de mise en forme et dans de nombreux tests mécaniques, par exemple les essais de fatigue. Au cours de ces tests, une quantité variable d'énergie mécanique est convertie en chaleur via un comportement inélastique. La chaleur peut être mesurée à l'aide de différents dispositifs expérimentaux: par un calorimètre [Shenogin et al.,2002], par des thermocouples [Zehnder et al.,1998], ou par des capteurs IR [Chrysochoos and Louche,2000]. Selon les études réalisées, ces mesures donnent des résultats sensiblement similaires.

De nos jours, la "fatigue à très grand nombre de cycles" (VHCF) devient de plus en plus un sujet d'intérêt. La raison principale revient à l'intérêt donné aux nombreux composants utilisés dans les industries aéronautiques, ferroviaires et automobiles qui doivent avoir une durée de vie en fatigue supérieure au mégacycle. Cela correspond au VHCF ou au régime de fatigue gigacylique. Les recherches se concentrent sur la dissipation résultante qui est une source de chaleur en volume associée à des processus irréversibles induits par des mécanismes de déformation et une diffusion de chaleur.

Une approche prometteuse pour étudier la dissipation repose sur l'utilisation de la thermographie infrarouge (IR) quantitative et de l'extensométrie optique. Ces outils visent à évaluer l'énergie dissipée associée au chargement cyclique. Spécifiquement, les caméras infrarouges peuvent être utilisées pour enregistrer simultanément les champs correspondant aux variations de température et aux déplacements dans le plan sur la partie testée de l'échantillon. De plus, les performances des caméras infrarouges ont été considérablement améliorées avec la découverte des capteurs infrarouges. De nos jours, ces caméras fournissent une résolution spatiale fine et un faible bruit thermique. En conséquence, plusieurs approches expérimentales basées sur des mesures de température via des techniques IR quantitatives ont récemment été adoptées pour estimer cette transformation énergétique. En effet, la dissipation peut être déduite des champs de données thermiques en estimant les opérateurs différentiels partiels de l'équation de diffusion de la chaleur [Boulanger et al.,2004]. Un certain nombre de formulations simplifiées, utilisant différentes hypothèses, peuvent être utilisées pour les évaluations de cette dissipation.

La première consiste à considérer que le champ de température varie très peu dans l'épaisseur de l'éprouvette. Cette hypothèse permet de passer d'un problème 3D à un problème 2D. Elle permet de travailler avec les champs de température en surface de l'éprouvette tels que ceux fournis par un dispositif de thermographie IR, en supposant que cette température de surface est représentative de la température moyennée suivant l'épaisseur. Afin d'alléger les calculs, des approches dites 1D puis 0D ont aussi été étudiées (Figure 54). Ces dernières sont moins contraignantes au niveau des temps de traitement des essais mais elles donnent des résultats moins précis.

### 7.3.5 La méthodologie pour l'étude d'autoéchauffement en espace-temps

Afin de modéliser le phénomène d'auto-échauffement dans un domaine spatio-temporel, de nombreuses étapes sont nécessaires:

- Etude des paramètres du test de fatigue qui comprend l'analyse des données expérimentales et l'identification des paramètres du modèle Newtonien (section 3.3). La dissipation thermique exprimée en Eq. 2.35, est un paramètre important à calculer. Sur la base des études précédentes [Favier et al.,2016, Chrysochoos et al.,2009, Boulanger et al.,2004], Plusieurs méthodes d'identification sont développées afin de réduire les erreurs probables de cette étape.
- Injection de la dissipation thermique résultante dans un modèle de chaleur spatio-temporel représentant le phénomène d'auto-échauffement. Les conditions aux limites sont étudiées afin de reproduire les conditions du test de fatigue fournissant les données expérimentales (section 3.5.1.1).
- Simulation numérique du problème variationnel spatio-temporel du modèle. L'évolution de la température dans un domaine spatio-temporel est alors obtenue (section 3.5).
- Comparaison entre l'évolution de la température survenant lors de l'auto-échauffement obtenue à partir de résultats expérimentaux et celle obtenue par une approche spatio-temporelle (résultats de la simulation du modèle de chaleur spatio-temporelle, voir section 3.5.2).

Cette dernière étape a pour but de valider le modèle spatio-temporel en montrant sa capacité à reproduire le phénomène d'auto-échauffement et par conséquent valider le modèle de conduction thermique spatio-temporelle utilisée ainsi que la méthode et le cadre proposés pour le construire.

### 7.3.6 Le cas expérimental d'autoéchauffement étudié

Dans ce manuscrit, l'autoéchauffement survenant durant le test de fatigue est étudié en se basant sur des données expérimentales.

L'éprouvette de fatigue est mince et plate en forme de sablier (Fig. 53). Les essais de fatigue ont été réalisés à une fréquence de 20 $kHz$ à l'aide d'un appareil de fatigue par ultrasons au Laboratoire de mécanique énergétique et d'électromagnétisme (LEME) de l'Université Paris-Nanterre. Le chargement cyclique est une contrainte imposée à 221 $MPa$ et à un rapport de charge de $R = -1$. Aucun dispositif de refroidissement (débit d'air ou de gaz) n'est utilisé pendant les essais. L'éprouvette étudiée est en acier C65 fréquemment utilisé dans la fabrication de pièces. Le tableau 18 montre les propriétés thermophysiques de l'acier considéré.

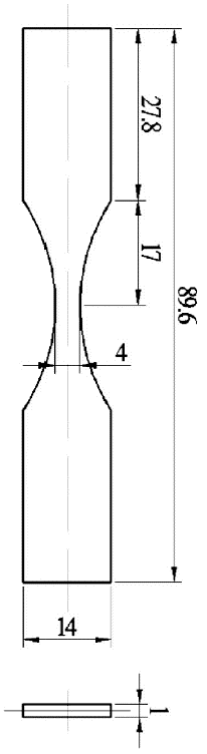


**Fig. 53:** La géométrie et les dimensions de l'échantillon en mm.

| Variable | Valeur |
|---|---|
| Densité $\widetilde{\rho_c}$ | $7800\, kg.m^{-3}$ |
| Chaleur massique $\mathcal{C}_{m\omega}$ | $473\, J.kg^{-1}.K^{-1}$ |
| Conductivité thermique $\lambda$ | $50.2\ W.m^{-1}.K^{-1}$ |
| Diffusivité thermique $a = \dfrac{\lambda}{\widetilde{\rho_c}\mathcal{C}_{m\omega}}$ | $13.6 \times 10^{-6}\ m^2.s^{-1}$ |

**Tab. 18:** Propriétés thermophysiques de l'acier C65 [ASM,1998]

L'échantillon est soumis à une convection naturelle avec son environnement (ayant un coefficient de transfert de chaleur convectif $h$ et étant à température ambiante $\theta_0$). Il est également soumis à une conduction thermique avec un mors en titane, sur laquelle l'éprouvette est serrée lors des essais à l'aide d'une petite pièce d'acier. La température du mors reste assez proche de la température ambiante pendant le test.

La machine de fatigue piézoélectrique utilisée pour effectuer les essais de fatigue est conçue selon [Bathias and Paris,2005]. Le système de fatigue vibratoire est constitué de plusieurs éléments. Le premier est le générateur qui peut atteindre une puissance de 2 $kW$ et dont la fréquence est accordée entre 19,5 $kHz$ et 20,5 $kHz$. Il génère un signal sinusoïdal au convertisseur, qui produit des vibrations. La fonction de ce dernier est de transformer les vibrations électriques en vibrations mécaniques. De plus, un amplificateur appelé «booster» augmente ou diminue (1,5 fois) le déplacement du convertisseur. Enfin, une borne constituée d'une partie cylindrique suivie d'une section profilée en forme de cône complète l'équipement. L'amplitude de déplacement du système (convertisseur et booster) étant limitée, le cône permet d'augmenter l'amplitude vibratoire de l'éprouvette pour atteindre la contrainte requise. L'échantillon est vissé sur la borne et son extrémité inférieure est sans contrainte. Un étalonnage de la configuration est nécessaire pour définir la contrainte requise. Il consiste à trouver une relation linéaire existant entre la tension de commande et l'amplitude de déplacement de la limite cône /éprouvette. Cette dernière est mesurée par un capteur laser.

La détection par thermographie a été réalisée à l'aide d'une caméra infrarouge FLIR A325sc. Il s'agit d'une caméra à base de microbolomètres avec un détecteur à 320 ×240 et une résolution thermique (différence de température équivalente au bruit) de 0,1 $^oC$. C'est la moyenne utilisée pour mesurer la température de surface de l'échantillon à différents intervalles de temps $t$. Pendant les tests, l'axe de l'objectif de la caméra a été maintenu fixe et perpendiculaire à la surface de l'échantillon. La résolution spatiale adoptée nous permet d'observer la partie centrale de la jauge de l'échantillon. La fréquence d'images de la caméra infrarouge est de 3,75 images par seconde (c'est-à-dire que la fréquence d'échantillonnage est de $f_{IR} = 3,75\ Hz$).

Les images fournies par la caméra entre $t_i = 0\ s$ et $t_f = 3\ min\ 46,366\ s$ sont traitées afin de calculer la dissipation et l'évolution de la température pendant cet intervalle de temps correspondant à $\approx 4510^5$ cycles pour illustrer la méthodologie. Il faut noter que $t_i$ et $t_f$ sont choisis de telle manière qu'une grande variation temporelle de température puisse être observée. A chaque pas de temps, une cartographie 2D est obtenue par thermographie.

### 7.3.7 La modélisation Newtonienne du cas d'autoéchauffement étudié

On commence par le calcul Newtonien de la dissipation intrinsèque. L'équation de diffusion de chaleur selon ces différentes approches se réduit selon l'approximation considérée à:

*Dans l'approche 2D:*

$$\frac{\partial \bar{\theta_d}(x,y,t)}{\partial t} + \frac{\bar{\theta_d}(x,y,t)}{\tau_{2D}(y)} - a\left(\frac{\partial^2 \bar{\theta_d}(x,y,t)}{\partial x^2} + \frac{\partial^2 \bar{\theta_d}(x,y,t)}{\partial y^2}\right) = \frac{\bar{d_1}(x,y,t)}{\widetilde{\rho_c}\mathcal{C}_{m\omega}} \tag{7.5}$$

où: $\bar{\theta_d} = \bar{\theta} - \theta_0$ est la différence entre la temperature moyennée sur une dimension d'espace et la température ambiante. La moyenne est notée par une "barre" et est effectuée dans ce cas sur l'épaisseur (la direction $z$). $\tau_{2D}$ est le paramètre de temps qui caractérise l'échange de chaleur perpendiculaire à la direction du flux de conduction de chaleur. Notons que ce temps peut être fonction de la direction de longueur $y$. Ceci revient à la variation de l'épaisseur de l'échantillon en fonction de la longueur. Dans ce cas, il caractérise l'échange de chaleur dans la direction $z$. $\dfrac{\bar{d_1}(x,y,t)}{\widetilde{\rho_c}\mathcal{C}_{m\omega}}$ est la moyenne sur l'épaisseur du terme de dissipation intrinsèque.

*Dans l'approche 1D:*

$$\frac{\partial \bar{\bar{\theta}}_d(y,t)}{\partial t} + \frac{\bar{\bar{\theta}}_d(y,t)}{\tau_{1D}(y)} - a\left(\frac{\partial^2 \bar{\bar{\theta}}_d(y,t)}{\partial y^2}\right) = \frac{\bar{\bar{d}}_1(y,t)}{\widetilde{\rho_c}\mathcal{C}_{m\omega}} \tag{7.6}$$

où: $\bar{\bar{\theta}}_d = \bar{\bar{\theta}} - \theta_0$ est la différence entre la temperature moyennée sur deux dimensions d'espace et la température ambiante. La moyenne est notée par une "double barre" et est effectuée dans ce cas sur l'épaisseur et la largeur (les directions $z$ et $x$). $\tau_{1D}$ est le paramètre de temps qui caractérise l'échange de chaleur perpendiculaire à la direction du flux de conduction de chaleur. Dans ce cas, il caractérise l'échange de chaleur dans les directions $z$ et $x$. $\dfrac{\bar{\bar{d}}_1(y,t)}{\widetilde{\rho_c}\mathcal{C}_{m\omega}}$ est la moyenne sur l'épaisseur et la largeur du terme de dissipation intrinsèque. La méthode 1D nécessite moins de temps de traitement des tests de fatigue que celui nécessaire pour la méthode 2D tout en donnant des résultats moins précis.

*Dans l'approche 0D:*

$$\frac{\partial \bar{\bar{\bar{\theta}}}_d(t)}{\partial t} + \frac{\bar{\bar{\bar{\theta}}}_d(t)}{\tau_{0D}} = \frac{\bar{\bar{\bar{d}}}_1(t)}{\widetilde{\rho_c}\mathcal{C}_{m\omega}} \tag{7.7}$$

où: $\bar{\bar{\bar{\theta}}}_d = \bar{\bar{\bar{\theta}}} - \theta_0$ est la différence entre la temperature moyennée sur trois dimensions d'espace et la température ambiante. La moyenne est notée par une "triple barre" et est effectuée dans ce cas sur l'épaisseur, la largeur et la longueur de l'échantillon (les directions $z$, $x$ et $y$). $\dfrac{\bar{\bar{\bar{d}}}_1(t)}{\widetilde{\rho_c}\mathcal{C}_{m\omega}}$ est la moyenne sur l'épaisseur, la largeur et la longueur du terme de dissipation intrinsèque. $\tau_{0D}$ est le paramètre de temps qui caractérise l'échange de chaleur perpendiculaire à la direction du flux de conduction de chaleur. Dans ce cas, il caractérise l'échange de chaleur dans toutes les directions spatiales.

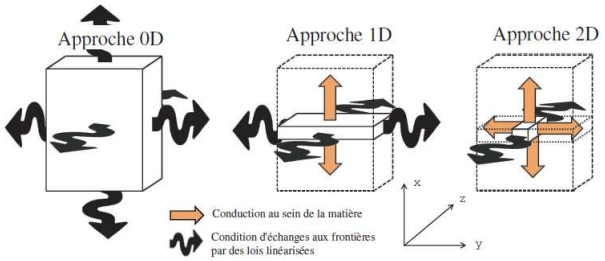


**Fig. 54:** Schéma montrant la différence entre les approches 0D, 1D et 2D.

### 7.3.8 La modélisation spatio-temporelle du cas d'autoéchauffement étudié

Pour calculer les variations de température dans un domaine d'espace-temps, nous avons besoin de l'identification du terme de dissipation intrinsèque et du paramètre de temps. De nombreuses méthodes sont possibles pour calculer ces paramètres. Nous avons étudié différentes méthodes d'identification notamment pour la dissipation intrinsèque et du temps caractéristique, soit par calcul direct avec l'équation de chaleur Newtonienne, soit par optimisation d'une solution analytique dans des cas spécifiques (méthodes A à D, section 3.3.4). Les valeurs obtenues en fonction du temps et/ou de l'espace sont cohérentes avec la bibliographie du matériau étudié (acier C65). Les différentes méthodes présentent de légères divergences.

Le terme de source de chaleur est à peu près indépendant du temps lorsqu'il est moyenné sur l'espace. Sa variation avec l'espace a également été obtenue en considérant la méthode 1D. Une telle méthode fournit plus d'informations. Cependant, sa variation est difficile à analyser en termes de mécanismes matériels. La tendance est directement liée au chargement mécanique conduisant à l'auto-échauffement de la géométrie de l'éprouvette, en raison de la variation de contrainte sur sa longueur. En effet, la géométrie de l'éprouvette en forme de sablier conduit à la variation de contrainte donc à la variation de température sur la longueur, puisqu'une charge de fatigue constante est appliquée sur des surfaces de l'éprouvette variant le long de la longueur.

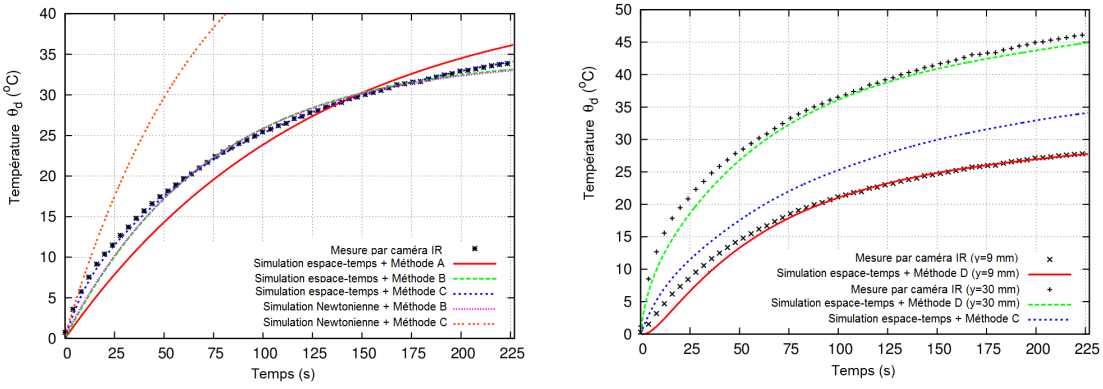


**Fig. 55:** A gauche: a) Evolution de $\bar{\bar{\theta}}_d(t)$ obtenue des mesures expérimentales et des simulations numériques en espace-temps, en fonction du temps. A droite: b) Evolution de $\bar{\bar{\theta}}_d(t)$ obtenue des mesures expérimentales et de la simulation numérique en espace-temps basée sur la méthode D, en fonction du temps.

Nous avons également proposé des formes variationnelles spatio-temporelles directement adaptées à la modélisation de l'auto-échauffement. Les simulations d'espace-temps qui en résultent à partir du modèle obtenu donnent les variations de température dans l'espace et le temps, en utilisant un environnement de programmation approprié. La méthode 1D+1D est ainsi choisie pour l'application à l'auto-échauffement.

Des simulations du modèle d'espace-temps ont été comparées aux mesures de données expérimentales. Les résultats montrent une bonne concordance avec de légères différences dérivant de l'inertie thermique et / ou de l'approximation du lissage des données expérimentales (en particulier $f_r$). La concordance est correcte lors de la comparaison des valeurs moyennes de température dans l'espace, quelle que soit la méthode d'identification. Cela signifie que les valeurs moyennes des paramètres identifiés avec un modèle moins précis que celui utilisé pour la simulation sont pertinentes pour obtenir des simulations fiables, précises et rapides.

La prise en compte de la dépendance spatiale de la dissipation, grâce à l'utilisation de la diffusivité thermique dans l'étape d'identification, est également nécessaire pour une description correcte des variations de température sur la longueur de l'échantillon, à condition que les conditions aux limites spatiales soient suffisamment réalistes. Des résultats plus précis pourraient être obtenus en complexifiant l'étape d'identification. L'effet de la diffusivité thermique sur les simulations 1D + 1D a également été directement étudié et montre une forte influence sur les résultats lorsque l'on considère la variation spatiale de la température et du terme de la source de chaleur.

L'accord entre la simulation et les résultats expérimentaux conduit à admettre la modélisation de l'espace-temps introduite dans le manuscrit comme une approche pratique pour décrire le phénomène d'auto-échauffement en particulier lorsque les paramètres dépendent du temps. L'étude détaillée de l'auto-échauffement induit par la fatigue gigacylique, dans ce manuscrit, en est un exemple concret. Une plus grande précision pourrait être obtenue en modélisant le comportement mécanique et en ajoutant explicitement les couplages thermomécaniques qui sont étudiés dans la deuxième partie du manuscrit. Des recherches supplémentaires pourraient être menées afin de fournir une approche spatio-temporelle complète dans la modélisation de l'auto-échauffement en proposant une méthode spatio-temporelle pour l'étape d'identification des paramètres.

## 7.4 Modélisation thermomécanique du comportement des matériaux

### 7.4.1 L'étude bibligraphique sur la modélisation thermomécanique du comportement des matériaux

Dans cette deuxième partie du manuscrit, la modélisation thermomécanique des grandes déformations a été revue. La non-linéarité des modèles mécaniques a été introduite par l'utilisation des déformations de Green-Lagrange et d'Euler-Almansi (section 4.2.1). La déformation Newtonienne de Green-Lagrange est définie par:

$$E_{ij} = \frac{1}{2}(C_{ij} - I_{ij}) \tag{7.8}$$

$C_{ij}$ étant le tenseur de Cauchy-Green droit définit par:

$$C_{ij} = F_i^a F_j^b I_{ab} \tag{7.9}$$

où $F_j^i$ et $F_j'^i$ sont respectivement le gradient de déformation et son inverse.

La déformation Newtonienne d'Euler-Almansi est définie par:

$$e_{ij} = \frac{1}{2}(I_{ij} - b_{ij}) \tag{7.10}$$

$b_{ij}$ étant l'inverse du tenseur de Cauchy-Green gauche définit par:

$$b_{ij} = F_i'^a F_j'^b I_{ab} \tag{7.11}$$

En utilisant ces définitions et la loi d'équilibre mécanique (Eq. 4.14), les modèles Newtoniens élastiques, thermoélastiques, hyperlastiques et élasto-plastiques et les formes intégrales faibles correspondantes pour les petites puis grandes déformations (sections 4.2.2 , 4.2.3, 4.2.4 et 4.2.6) ont été construits pour des milieux continus dans le cas de matériaux isotropes homogènes. Les couplages thermomécaniques n'ont été pris en compte que pour les modèles thermoélastiques. Des descriptions lagrangiennes et eulériennes

ont été utilisées pour des modèles de grandes déformations utilisant respectivement les déformations de Green-Lagrange et d'Euler-Almansi.

Les formes faibles de ces modèles ont ensuite été déduites en multipliant les modèles par des fonctions de test arbitraires et en les intégrant sur le domaine 3D. Cette étape est utile pour comparer les modèles Newtoniens à différents modèles d'espace-temps qui sont développés au chapitre 5.

Deux exemples illustrent les modèles Newtoniens examinés. Dans le premier exemple, des modèles élastiques et hyperélastiques ont été étudiés (section 4.2.5). Le problème consistait à appliquer une charge de traction en utilisant une condition aux limites de Dirichlet sur une géométrie de poutre. L'évolution du tenseur de contraintes de Cauchy $\sigma_c^{11}$ dans la direction $x$ en fonction du temps montre que le modèle utilisant la déformation de Green-Lagrange a des comportements élastiques et hyperélastiques différents tandis que les autres modèles (utilisant une petite déformation et la déformation d'Euler-Almansi) ont les mêmes comportements élastiques et hyperélastiques.

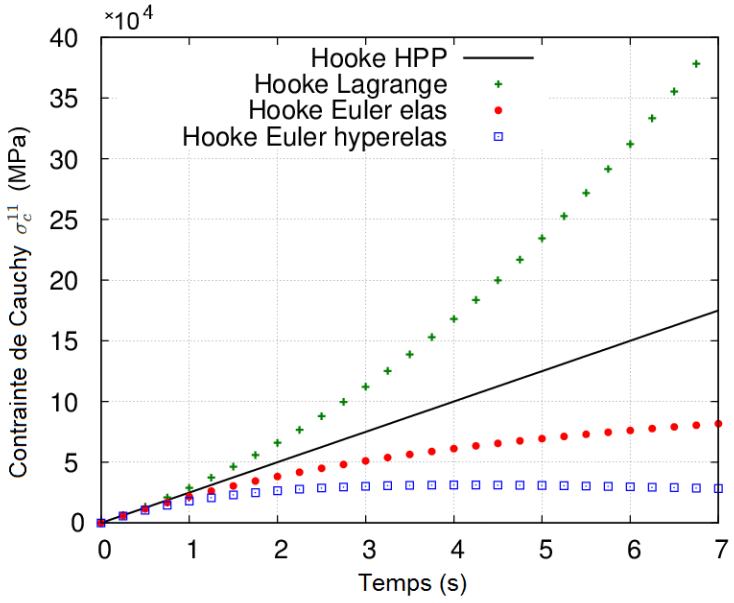


**Fig. 56:** Variation de $\sigma_c^{11}$ en fonction du temps pour une poutre en traction pour différents modèles élastiques et hyperélastiques Newtoniens pour un temps allant de 0 à $7s$.

Dans le deuxième exemple, le comportement plastique a été observé: la même géométrie, la même charge et les mêmes conditions aux limites que dans l'exemple précédent ont été appliquées (section 4.2.7). Les résultats de l'évolution de $\sigma_c^{11}$ en fonction du temps montrent que le modèle plastique utilisant la déformation de Green-Lagrange a une évolution de $\sigma_c^{11}(t)$ différente de celle utilisant utilisant une petite déformation et la déformation d'Euler-Almansi due à son comportement élastique différent.

Ces exemples aident à visualiser le comportement de différents modèles en utilisant différentes définitions de déformation et donnent ainsi quelques comportements attendus de ces modèles mécaniques.

De plus, la modélisation mécanique Newtonienne présente des difficultés qui sont principalement: la non-linéarité des modèles (par exemple les modèles plastiques) et la nécessité de respecter l'objectivité matérielle des modèles. L'utilisation d'une approche thermodynamique construite dans un formalisme d'espace-temps (comme celle introduite dans la partie 1 du manuscrit) semble pouvoir réduire ces problèmes. Davantage d'outils d'espace-temps nécessaires à la modélisation mécanique dans un formalisme d'espace-temps ont été introduits dans cette deuxième partie par ex. le gradient de déformation spatio-temporel, les tenseurs de déformation spatio-temporels, la dérivée de Lie, le taux de déformation... Dans la section 4.6,

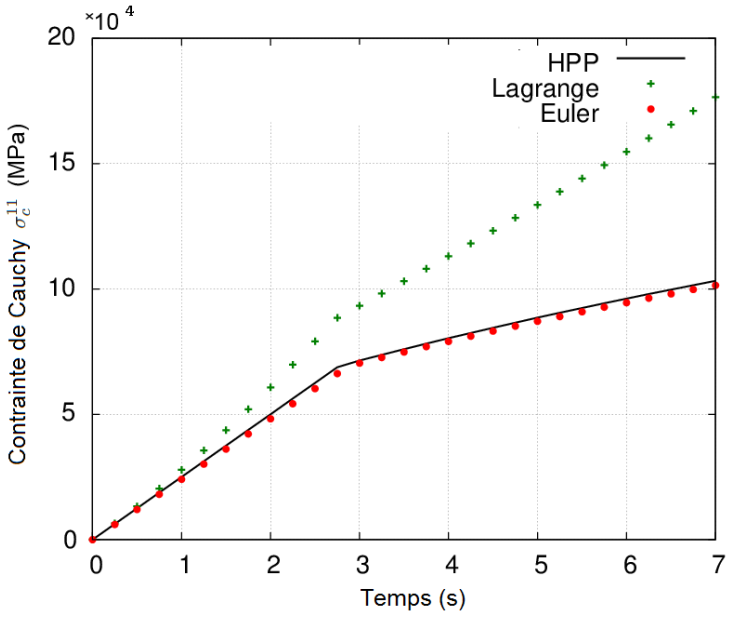


**Fig. 57:** Variation de $\sigma_c^{11}$ en fonction du temps pour un poutre en traction pour différents modèles élasto-plastiques Newtoniens.

un exemple illustre les termes supplémentaires résultant de l'application du principe de covariance sur les transformations et en particulier dans le cas d'un tenseur du second ordre.

Des auteurs ont proposés différents modèles mécaniques spatio-temporels, tels que des expansions spatio-temporelles du modèle de Hooke prenant en compte les non-linéarités provenants de la cinématique/géométrie. Dans [Rouhaud et al.,2013] et [Panicaud et al.,2015], des modèles spatio-temporels thermoélastiques, thermo-hyperélastiques et hypoélastiques ont déjà été obtenus en utilisant différentes méthodes telles que la relativisation directe des modèles Newtoniens, l'approche thermodynamique, en utilisant la théorie de la représentation ... Cependant, dans [Rouhaud et al.,2013] et [Panicaud et al.,2015], les modèles covariants ont été obtenus sous des hypothèses qui limitent leur utilisation. En outre, dans certains modèles, les opérateurs de dérivation de Lie et de projection n'ont pas été utilisés dans la méthodologie, ce qui nécessite un développement plus poussé des modèles obtenus.

De plus, Wang [Wang,2016] (section 4.7.4) a étudié les modèles élastiques et élastoplastiques anisotropes spatio-temporels. Cette étude s'est limitée à la modélisation mécanique, ainsi la modélisation du comportement thermique du matériau et le couplage thermomécanique ont été négligés dans les modèles résultants. De plus, seule la projection spatiale des modèles d'espace-temps a été utilisée pour la simulation numérique et a été comparée aux modèles mécaniques Newtoniens. Cela limite la capacité d'étudier l'impact d'une approche spatio-temporelle sur les modèles mécaniques d'un point de vue numérique puisque la résolution numérique du problème est quasiment Newtonienne. Ainsi, les avantages d'une résolution numérique de l'espace-temps: utilisation de dérivées covariantes, métrique d'espace-temps, expression du tenseur énergie-impulsion d'espace-temps ... ne sont pas appliqués.

Dans ce qui suit, nous proposons une méthodologie thermodynamique spatio-temporelle conduisant à des modèles spatio-temporels qui prennent en compte le couplage thermomécanique. Cette méthodologie respecte le principe de covariance et l'utilisation de dérivées covariantes. Elle respecte également l'utilisation des opérateurs de projection dans le développement de modèles d'espace-temps. La forme faible du problème sera ensuite implémentée pour la simulation sans projection spatiale en utilisant le projet FEniCS qui permet une résolution numérique spatio-temporelle. Les résultats obtenus à partir des modèles d'espace-temps seront ensuite comparés aux résultats obtenus à partir des modèles Newtoniens correspondants.

### 7.4.2 La modélisation thermomécanique en espace-temps dans ce manuscrit

Dans l'objectif de définir la méthodologie permettant la modélisation thermomécanique spatio-temporelle des petites et grandes déformations, l'approche thermodynamique spatio-temporelle est étudiée. Comme mentionné précédemment, cela garantit l'obtention de modèles thermomécaniques respectant les principes de covariance et de causalité tout en étant compatibles avec les lois de la thermodynamique. Pour la causalité, c'est le fait d'obtenir des équations hyperboliques qui le garantira à la toute fin.

Dans un premier temps, les formes covariantes des lois de la thermodynamique prenant en compte le comportement mécanique ont été étudiées en utilisant la définition du tenseur impulsion-énergie (section 5.3), ce qui permet d'écrire ces lois dans différents cadres. Ci-dessous sont les lois de conservation covariantes du nombre molécules, de l'impulsion-énergie, de l'énergie interne et de l'entropie.

#### 7.4.2.1 La conservation du nombre de molécules

Nous supposons que les molécules ne peuvent pas être créées ou détruites, ce qui conduit à la loi de conservation du nombre de molécules. Nous considérons à nouveau l'espace-temps global domaine du matériau de l'hypervolume $\mathcal{D}$ ayant la frontière $\partial\mathcal{D}$. Nous introduisons le flux de molécules $n^\mu$ qui vérifie:

$$\forall x^\mu \in \mathcal{D}, \nabla_\mu n^\mu = 0 \tag{7.12}$$

Des problèmes surviennent lors de la définition de la vitesse spatio-temporelle de ce flux de molécules. Dans le contexte général de la physique relativiste, ce flux de molécules peut être défini comme:

$$n^\mu = n u^\mu + \nu^\mu \tag{7.13}$$

$n$ étant la densité des molécules (par unité de volume) dans le référentiel propre et la vitesse spatio-temporelle $\nu^\mu$ représente le courant de diffusion des molécules. En cas de dissipation non thermomécanique, deux hypothèses peuvent être adoptées: elles ont été proposées par [Eckart,1940] et par [Landau and Lifshitz,1975]. Différents auteurs ont tenté de fusionner ces deux approches [Schellstede et al.,2014, Israel,1989]. Dans ce manuscrit, puisque de telles dissipations ne sont pas considérées, le terme de diffusion est choisi tel que $\nu^\mu = 0$. Par conséquent, la loi de conservation des molécules dans $\mathcal{D}$ conduit finalement à:

$$\forall x^\mu \in \mathcal{D}, \nabla_\mu (\widetilde{\rho}_c u^\mu) = 0 \tag{7.14}$$

Eq. 7.14 correspond à l'équilibre de la masse au repos par unité de le volume. Dans la limite non relativiste, cela conduirait à l'équation de continuité classique.

#### 7.4.2.2 La conservation de l'impulsion-énergie

L'équilibre de l'impulsion-énergie dans un domaine spatio-temporel peut être obtenu à partir de la définition du tenseur impulsion-énergie. Dans un référentiel quelconque, elle peut être écrite localement:

$$\forall x^\mu \in \mathcal{D}, \nabla_\nu T^{\mu\nu} = 0 \tag{7.15}$$

$$\Leftrightarrow \forall x^\mu \in \mathcal{D}, \nabla_\nu T^{\mu\nu}_{\mathcal{U}} + \nabla_\nu T^{\mu\nu}_{q} + \nabla_\nu T^{\mu\nu}_{\sigma} = 0 \tag{7.16}$$

Eq. 5.1 et Eq. 5.6 donnent:

$$\forall x^\mu \in \mathcal{D}, \nabla_\nu (T^{\mu\nu}_{\mathcal{U}} + T^{\mu\nu}_{q} + T^{\mu\nu}_{\sigma}) = 0 \tag{7.17}$$

$$\Leftrightarrow \forall x^\mu \in \mathcal{D}, \nabla_\nu \left( \widetilde{\rho}_c c^2 \left(1 + \frac{e_{int}}{c^2}\right) u^\mu u^\nu + \frac{\lambda}{c} (\Pi^{\mu\kappa} u^\nu + \Pi^{\nu\kappa} u^\mu) \partial_\kappa \theta + T^{\mu\nu}_{\sigma} \right) = 0 \tag{7.18}$$

Les expressions de $e_{int}(\theta, dep^\mu)$ et $T^{\mu\nu}_{\sigma}(\theta, dep^\mu, g^{\mu\nu})$ peuvent ensuite être injectées dans Eq. 7.18:

$$\nabla_\nu \left( \widetilde{\rho}_c c^2 \left( 1 + \frac{e_{int}(\theta, dep^\mu)}{c^2} \right) u^\mu u^\nu + \frac{\lambda}{c} (\Pi^{\mu\kappa} u^\nu + \Pi^{\nu\kappa} u^\mu) \partial_\kappa \theta + T_\sigma^{\mu\nu}(\theta, dep^\mu, g^{\mu\nu}) \right) = 0 \tag{7.19}$$

Les expressions de $e_{int}$ et $T_\sigma^{\mu\nu}$ doivent ensuite être déterminées et sont reliées.

#### 7.4.2.3 La conservation de l'énergie interne

Il est utile de calculer le bilan du tenseur impulsion-énergie suivant la direction de la vitesse spatio-temporelle pour obtenir l'équilibre de l'énergie interne du système. Avec le projecteur de temps (voir section 2.2.4), il conduit localement à:

$$\forall x^\mu \in \mathcal{D}, u_\mu \nabla_\nu T^{\mu\nu} = 0 \tag{7.20}$$

Dans le but de développer l'Eq. 7.20, on utilise :

$$u_\mu \nabla_\nu T^{\mu\nu} = \nabla_\nu (u_\mu T^{\mu\nu}) - T^{\mu\nu} \nabla_\nu u_\mu = 0 \tag{7.21}$$

En utilisant: $\nabla_\nu (u_\mu T_\sigma^{\mu\nu}) = 0$ car $u_\mu T_\sigma^{\mu\nu} = 0$ (par construction en projettant $T^{\mu\nu}$, voir section 2.2.8 [Wang,2016]) et $u_\mu T_q^{\mu\nu} = q^\nu$ obtenu en utilisant Eq. 2.21:

$$\begin{aligned} u_\mu T_q^{\mu\nu} &= u_\mu q^\nu u^\mu + u_\mu q^\mu u^\nu \\ &= q^\nu + (\delta_\alpha^\mu - u^\mu u_\alpha) u_\mu T^{\alpha\beta} u_\beta u^\nu = q^\nu \end{aligned} \tag{7.22}$$

On obtient:

$$\nabla_\nu (u_\mu T^{\mu\nu}) = \nabla_\nu (\tilde{\rho_c} (c^2 + e_{int}) u^\nu) + \nabla_\nu q^\nu \tag{7.23}$$

Puis, en utilisant $u_\mu u^\mu = 1$, on déduit que: $u^\mu \nabla_\nu u_\mu = u_\mu \nabla_\nu u^\mu = 0$. Par conséquent:

$$T^{\mu\nu} \nabla_\nu u_\mu = q^\mu u^\nu \nabla_\nu u_\mu + T_\sigma^{\mu\nu} \nabla_\nu u_\mu \tag{7.24}$$

Eqs. 7.23 and 7.24 lead to:

$$u_\mu \nabla_\nu T^{\mu\nu} = \nabla_\nu (\tilde{\rho_c} (c^2 + e) u^\nu) + \nabla_\nu q^\nu - q^\mu u^\nu \nabla_\nu u_\mu - T_\sigma^{\mu\nu} \nabla_\nu u_\mu \tag{7.25}$$

Si $T^{\mu\nu}$ est symétrique, alors comme par définition (Eq. 2.23), $T_\sigma^{\mu\nu}$ est métrique. En utilisant le taux de déformation $d^{\mu\nu}$, Eq. 7.25 donne:

$$u_\mu \nabla_\nu T^{\mu\nu} = \nabla_\nu (\tilde{\rho_c} (c^2 + e_{int}) u^\nu) + \nabla_\nu q^\nu - q^\mu u^\nu \nabla_\nu u_\mu - T_\sigma^{\mu\nu} d_{\mu\nu} = 0 \tag{7.26}$$

On en déduit la loi de conservation de l'énergie interne:

$$\nabla_\nu (\tilde{\rho_c} (c^2 + e_{int}) u^\nu) + \nabla_\nu q^\nu - q^\mu u^\nu \nabla_\nu u_\mu = T_\sigma^{\mu\nu} d_{\mu\nu} \tag{7.27}$$

Dans le cas de comportement adiabatique et puisque $u^\mu u^\nu d_{\mu\nu} = 0$ ($\underline{d}_{\mu\nu} = d_{\mu\nu}$), la loi de conservation d'énergie interne peut être écrite comme une fonction du tenseur impulsion-énergie:

$$\forall x^\mu \in \mathcal{D}, \nabla_\nu (\tilde{\rho_c} (c^2 + e_{int}) u^\nu) = T^{\mu\nu} d_{\mu\nu} \tag{7.28}$$

#### 7.4.2.4 L'inégalité de Clausius-Duhem

Comme en mécanique newtonienne, il est possible d'exprimer localement le second principe de thermodynamique par construction de l'inégalité Clausius-Duhem généralisée en espace-temps. Par conséquent:

$$\forall x^\mu \in \mathcal{D}, \theta \nabla_\nu S^\nu - u_\mu \nabla_\nu T^{\mu\nu} = \frac{\Phi}{c} \geq 0 \tag{7.29}$$

$$\Rightarrow \forall x^\mu \in \mathcal{D}, \theta \nabla_\nu (\widetilde{\rho}_c \eta_c u^\nu) + \nabla_\nu (\frac{q^\mu}{\theta}) - \nabla_\nu (\rho_c c^2 u^\nu)$$

$$-\nabla_\nu (q^\nu) + q^\mu u^\nu \nabla_\nu (u_\mu) + T^{\mu\nu} d_{\mu\nu} = \frac{\Phi}{c} \geq 0$$

$$\widetilde{\rho}_c \theta u^\mu \nabla_\mu \eta_c - \widetilde{\rho}_c u^\mu \nabla_\mu e_{int} - \frac{1}{\theta} q^\mu \nabla_\mu \theta + q_\nu u^\mu \nabla_\mu u^\nu + T_\sigma^{\mu\nu} d_{\mu\nu} \geq 0 \tag{7.30}$$

Dans cette inégalité, les termes sont respectivement liés à l'évolution d'entropie, l'évolution de l'énergie interne, les dissipations thermiques (dont une partie est couplée à la mécanique avec le terme $u^\mu \nabla_\mu u^\nu$) et la puissance mécanique interne $T_\sigma^{\mu\nu} d_{\mu\nu}$.

En introduisant l'énergie libre spécifique: $\psi = e_{int} - \theta \eta_c$, l'inégalité précédente est équivalente à:

$$-\widetilde{\rho}_c (u^\mu \nabla_\mu \psi + \eta_c u^\mu \nabla_\mu \theta) \quad - \quad q^\mu \left( \frac{1}{\theta} \nabla_\mu \theta - u^\nu \nabla_\nu u_\mu \right) + T_\sigma^{\mu\nu} d_{\mu\nu} = \frac{\Phi}{c} \geq 0 \tag{7.31}$$

Les lois classiques de la thermodynamique peuvent être obtenues en utilisant les lois de l'espace-temps écrites dans un référentiel inertiel à la limite non relativiste.

Ensuite, les comportements thermo-hyperélastiques spatio-temporels d'un modèle général puis d'un modèle réversible spécifique (section 5.5) ont été obtenus sous les hypothèses suivantes:

- couplage fort entre les comportements thermiques et mécaniques
- comportement isotrope des matériaux à l'échelle macroscopique. Le comportement isotrope nécessite au moins 2 paramètres de matériau indépendants (par exemple les coefficients de Lamé) [Wang,2016]. Par conséquent, le comportement choisi est également indépendant de la rotation dans l'espace-temps, par conséquent invariant à la translation galiléenne à la limite non-relativiste. Cette symétrie complète est supposée dans ce qui suit.

En plus, le modèle doit statisfaire:

- La loi de conservation du nombre de molécules (Eq. 7.12), de l'implusion-énergie (Eq. 7.16), de l'énergie inetrne (Eq. 5.15), de l'entropie (Eq. 5.27) et l'inégalité de Clausius-Duhem (Eq. 7.30).
- $T_\sigma^{\mu\nu} u_\mu = 0$ pour respecter la construction de $T^{\mu\nu}$.
- La symétrie de $T^{\mu\nu}$ and $T_\sigma^{\mu\nu}$.
- $T_\sigma^{\mu\nu}$ est une fonction de l'énergie libre spécifique $\Psi$ qui dépend de quantités projetées sur l'espace au moins pour sa partie mécanique.

On propose la forme suivante de $\Psi$:

$$\Psi = \Psi_\theta(\mathcal{C}_{mP}, \theta) + \Psi_\sigma(\Lambda/\widetilde{\rho}_c, \mu/\widetilde{\rho}_c, \underline{I}_I, \underline{I}_{II}) + \Psi_{\theta,\sigma}(\kappa\alpha/\widetilde{\rho}_c, \Delta\theta, \underline{I}_I) + \Psi_0 \tag{7.32}$$

$\mathcal{C}_{mP}$ étant la chaleur massique à pression constante, $\Lambda/\widetilde{\rho}_c$ et $\mu/\widetilde{\rho}_c$ sont les coefficients de Lamé spécifique (par unité de masse). $\kappa\alpha/\widetilde{\rho}_c$ est le coefficient spécifique de couplage relié au module de compression $\kappa = \Lambda + 2\mu/3$ et au coefficient d'expansion thermique $\alpha$ .

Ces 3 coefficients sont censés être indépendants de la température. $\underline{I}_I$ et $\underline{I}_{II}$ sont les invariants projetés du tenseur de déformation. Le couplage thermomécanique est exprimé par $\Psi_{\theta,\sigma}$ dans lequel $\Delta\theta = \theta - \theta_0$ est la variation de température provoquée par le comportement thermoélastique et mesurée par rapport à une température de référence $\theta_0$. Ce choix est une forme générale de l'énergie libre spécifique $\Psi$ dépendant des invariants.

Il est également nécessaire d'utiliser le projecteur spatial en construisant les modèles de comportement (présenté dans la section 2.2.4) surtout lors de la dérivation du tenseur de contrainte d'espace-temps à l'aide des invariants.

### 7.4.3 Application en utilisant une énergie libre spécifique basée sur des invariants projetés

En utilisant Eq. 7.31, le comportement réversible peut être exprimé par:

$$-\widetilde{\rho}_c(\eta_c\mathcal{L}_u(\theta)+\mathcal{L}_u(\Psi_\theta))-\widetilde{\rho}_c\mathcal{L}_u(\Psi_\sigma)-\widetilde{\rho}_c\mathcal{L}_u(\Psi_{\theta,\sigma})-q^\mu\left(\frac{1}{\theta}\nabla_\mu\theta-u^\nu\nabla_\nu u_\mu\right)+T^{\mu\nu}_\sigma d_{\mu\nu}=0 \tag{7.33}$$

$$\begin{aligned}\Leftrightarrow\ \widetilde{\rho}_c\left(\eta_c\mathcal{L}_u(\theta)+\frac{\partial\Psi_\theta}{\partial\mathcal{C}_{mP}}\mathcal{L}_u(\mathcal{C}_{mP})+\frac{\partial\Psi_\theta}{\partial\theta}\mathcal{L}_u(\theta)\right)\ &+\\ \widetilde{\rho}_c\left(\frac{\partial\Psi_\sigma}{\partial(\Lambda/\widetilde{\rho}_c)}\mathcal{L}_u(\Lambda/\widetilde{\rho}_c)+\frac{\partial\Psi_\sigma}{\partial(\mu/\widetilde{\rho}_c)}\mathcal{L}_u(\mu/\widetilde{\rho}_c)+\frac{\partial\Psi_{\theta,\sigma}}{\partial(\kappa\alpha/\widetilde{\rho}_c)}\mathcal{L}_u(\kappa\alpha/\widetilde{\rho}_c)+\frac{\partial\Psi_{\theta,\sigma}}{\partial\Delta\theta}\mathcal{L}_u(\Delta\theta)\right)\ &+\\ \widetilde{\rho}_c\left(\frac{\partial\Psi_\sigma}{\partial\underline{I}_I}\mathcal{L}_u(\underline{I}_I)+\frac{\partial\Psi_{\theta,\sigma}}{\partial\underline{I}_I}\mathcal{L}_u(\underline{I}_I)+\frac{\partial\Psi_\sigma}{\partial\underline{I}_{II}}\mathcal{L}_u(\underline{I}_{II})\right)+q^\mu\left(\frac{1}{\theta}\nabla_\mu\theta-u^\nu\nabla_\nu u_\mu\right)\ &=\\ T^{\mu\nu}_\sigma d_{\mu\nu}\end{aligned} \tag{7.34}$$

L'énergie libre spécifique est exprimée en Eq. 7.32 comme une décomposition additive de trois effets. Les deux invariants doivent correspondre physiquement respectivement à la déformation du volume et à la déformation de surface du milieu matériel [Farhat et al.,1991, Nayfeh and Nemat-Nasser,1971]:

$$\Psi_\sigma = \frac{\Lambda}{\widetilde{\rho}_c}\frac{\underline{I}_I^{\mathfrak{n}_1}}{\mathfrak{n}_1}+\frac{\mu}{\widetilde{\rho}_c}\frac{\underline{I}_{II}^{\mathfrak{n}_2}}{\mathfrak{n}_2} \tag{7.35}$$

$$\Psi_{\theta,\sigma} = -\frac{3\kappa\alpha}{\widetilde{\rho}_c}\Delta\theta\underline{I}_I \tag{7.36}$$

où $\mathfrak{n}_1$ et $\mathfrak{n}_2$ sont les exposants des lois de puissance ($\in\mathbb{N}^{+*}$). Les invariants sont censés être indépendants pour obtenir un découplage des effets mécaniques, et ils seront exprimés en fonction du tenseur de déformation $\boldsymbol{e}$ et/ou du tenseur métrique $\boldsymbol{g}$. Suivant les Eqs. 4.54 à 4.55, les dérivées de Lie de ces invariants sont des fonctions linéaires du tenseur du taux de déformation $\boldsymbol{d}$, comme il sera illustré plus loin. Nous pouvons ensuite calculer les différents termes de l'Eq. 7.34 avec:

$$\frac{\partial\Psi_\sigma}{\partial(\Lambda/\widetilde{\rho}_c)} = \frac{\underline{I}_I^{\mathfrak{n}_1}}{\mathfrak{n}_1} \tag{7.37}$$

$$\mathcal{L}_u(\Lambda/\widetilde{\rho}_c) = \frac{\Lambda}{\widetilde{\rho}_c}\underline{g}^{\mu\nu}d_{\mu\nu} \tag{7.38}$$

$$\frac{\partial\Psi_\sigma}{\partial(\mu/\widetilde{\rho}_c)} = \frac{\underline{I}_{II}^{\mathfrak{n}_2}}{\mathfrak{n}_2} \tag{7.39}$$

$$\mathcal{L}_u(\mu/\widetilde{\rho}_c) = \frac{\mu}{\widetilde{\rho}_c}\underline{g}^{\mu\nu}d_{\mu\nu} \tag{7.40}$$

$$\frac{\partial\Psi_{\theta,\sigma}}{\partial(\kappa\alpha/\widetilde{\rho}_c)} = -3\Delta\theta\underline{I}_I \tag{7.41}$$

$$\mathcal{L}_u(\kappa\alpha/\widetilde{\rho}_c) = \frac{\kappa\alpha}{\widetilde{\rho}_c}\underline{g}^{\mu\nu}d_{\mu\nu} \tag{7.42}$$

$$\frac{\partial\Psi_\sigma}{\partial\underline{I}_I}+\frac{\partial\Psi_{\theta,\sigma}}{\partial\underline{I}_I} = \frac{\Lambda}{\widetilde{\rho}_c}\underline{I}_I^{\mathfrak{n}_1-1}-\frac{3\kappa\alpha}{\widetilde{\rho}_c}\Delta\theta \tag{7.43}$$

$$\mathcal{L}_u(\underline{I}_I) = A^{\mu\nu}_I d_{\mu\nu} \tag{7.44}$$

$$\frac{\partial\Psi_\sigma}{\partial\underline{I}_{II}} = \frac{\mu}{\widetilde{\rho}_c}\underline{I}_{II}^{\mathfrak{n}_2-1} \tag{7.45}$$

$$\mathcal{L}_u(\underline{I}_{II}) = A^{\mu\nu}_{II}d_{\mu\nu} \tag{7.46}$$

$$\mathcal{L}_u(\Delta\theta) = \mathcal{L}_u(\theta)-\mathcal{L}_u(\theta_0)=\mathcal{L}_u(\theta) \tag{7.47}$$

$$\mathcal{L}_u(\mathcal{C}_{mP}) = 0 \tag{7.48}$$

où $A_I^{\mu\nu}$ et $A_{II}^{\mu\nu}$ sont les fonctions tensorielles qui doivent être explicitées. A noter que la dérivée de Lie d'une densité scalaire et constante est nulle $W = 0$. En utilisant les Eqs. 7.37 à 7.48 in Eq. 7.34, il est possible d'écrire:

$$\widetilde{\rho}_c\left(\eta\mathcal{L}_u(\theta)+\tfrac{\partial\Psi_\theta}{\partial\theta}\mathcal{L}_u(\theta)\right)+\widetilde{\rho}_c\left(\tfrac{\underline{I}_I^{\mathfrak{n}_1}}{\mathfrak{n}_1}\tfrac{\Lambda}{\widetilde{\rho}_c}\underline{g}^{\mu\nu}d_{\mu\nu}+\tfrac{\underline{I}_{II}^{\mathfrak{n}_2}}{\mathfrak{n}_2}\tfrac{\mu}{\widetilde{\rho}_c}\underline{g}^{\mu\nu}d_{\mu\nu}-3\Delta\theta\underline{I}_I\tfrac{\kappa\alpha}{\widetilde{\rho}_c}\underline{g}^{\mu\nu}d_{\mu\nu}-3\tfrac{\kappa\alpha}{\widetilde{\rho}_c}\underline{I}_I\mathcal{L}_u(\theta)\right)$$
$$+\quad\widetilde{\rho}_c\left((\tfrac{\Lambda}{\widetilde{\rho}_c}\underline{I}_I^{\mathfrak{n}_1-1}-\tfrac{3\kappa\alpha}{\widetilde{\rho}_c}\Delta\theta)A_I^{\mu\nu}d_{\mu\nu}+\tfrac{\mu}{\widetilde{\rho}_c}\underline{I}_{II}^{\mathfrak{n}_2-1}A_{II}^{\mu\nu}d_{\mu\nu}\right)-q^\mu\left(\frac{1}{\theta}\nabla_\mu\theta-u^\nu\nabla_\nu u_\mu\right)=T_\sigma^{\mu\nu}d_{\mu\nu}\quad(7.49)$$

En considérant des transformations indépendantes et réversibles, nous obtenons simultanément:

$$\forall\mathcal{L}_u(\theta),\eta_c \;=\; -\frac{\partial\Psi_\theta}{\partial\theta}+3\frac{\kappa\alpha}{\widetilde{\rho}_c}\underline{I}_I \quad(7.50)$$

$$\forall\theta,q^\mu\left(\frac{1}{\theta}\nabla_\mu\theta-u^\nu\nabla_\nu u_\mu\right) \;\geq\; 0 \quad(7.51)$$

$$\begin{aligned}\forall d_{\mu\nu},T_\sigma^{\mu\nu} &= \frac{\underline{I}_I^{\mathfrak{n}_1}}{\mathfrak{n}_1}\Lambda\underline{g}^{\mu\nu}+\frac{\underline{I}_{II}^{\mathfrak{n}_2}}{\mathfrak{n}_2}\mu\underline{g}^{\mu\nu}-3\Delta\theta\underline{I}_I\kappa\alpha\underline{g}^{\mu\nu}\\ &+ \left((\Lambda\underline{I}_I^{\mathfrak{n}_1-1}-3\kappa\alpha\Delta\theta)A_I^{\mu\nu}+\mu\underline{I}_{II}^{\mathfrak{n}_2-1}A_{II}^{\mu\nu}\right)^{Sym}\end{aligned}\quad(7.52)$$

Comme prévu, cette équation est symétrique et le choix de $\underline{I}_I^{\mathfrak{n}_1-1}$ doit respecter $T_\sigma^{\mu\nu}u_\mu=0$

### 7.4.4 Comportement thermo-hyperélastique spatio-temporel d'un modèle réversible spécifique

Dans ce modèle, des projecteurs spatiaux permettent de définir l'énergie libre spécifique. Les invariants projetés sont choisis en généralisant les invariants des modèles de type hookéen [Ugural and Fenster,2003]. Le premier invariant projeté est donné par:

$$\underline{I}_I \;=\; \underline{e}_{\mu\nu}\underline{g}^{\mu\nu}=\underline{e}_{\mu\nu}g^{\mu\nu}=e_{\mu\nu}\underline{g}^{\mu\nu} \quad(7.53)$$

cela conduit alors à:

$$\mathcal{L}_u(\underline{I}_I) \;=\; A_I^{\mu\nu}d_{\mu\nu}=(\underline{g}^{\mu\nu}-2\underline{e}^{\mu\nu})d_{\mu\nu} \quad(7.54)$$

Le deuxième invariant projeté est:

$$\underline{I}_{II} \;=\; \underline{e}_{\mu\nu}\underline{e}^{\mu\nu}=\underline{e}_{\mu\nu}e^{\mu\nu}=e_{\mu\nu}\underline{e}^{\mu\nu} \quad(7.55)$$

cela conduit alors à:

$$\mathcal{L}_u(\underline{I}_{II}) \;=\; A_{II}^{\mu\nu}d_{\mu\nu}=(2\underline{e}^{\mu\nu}-2\underline{e}^{\mu}{}_{\beta}\underline{e}^{\beta\nu}-2\underline{e}^{\mu\beta}\underline{e}_{\beta}{}^{\nu})d_{\mu\nu} \quad(7.56)$$

En supposant une forme quadratique pour l'énergie libre spécifique, suivant le choix de ces invariants, cela conduit à $\mathfrak{n}_1=2$ et $\mathfrak{n}_2=1$. En utilisant Eqs. 7.53 à 7.56 et 7.52, la courbe contrainte-déformation peut alors être obtenue:

$$\begin{aligned}T_\sigma^{\mu\nu} &= \frac{(e_{\alpha\beta}\underline{g}^{\alpha\beta})^2}{2}\Lambda\underline{g}^{\mu\nu}+(\underline{e}_{\alpha\beta}\underline{e}^{\alpha\beta})\mu\underline{g}^{\mu\nu}+\Lambda(e_{\alpha\beta}\underline{g}^{\alpha\beta})(\underline{g}^{\mu\nu}-2\underline{e}^{\mu\nu})\\ &+ 2\mu\underline{e}^{\mu\nu}-4\mu\left(\underline{e}^{\mu}{}_{\beta}\underline{e}^{\beta\nu}\right)^{Sym}-3\kappa\alpha\Delta\theta(e_{\alpha\beta}\underline{g}^{\alpha\beta})\underline{g}^{\mu\nu}-3\kappa\alpha\Delta\theta(\underline{g}^{\mu\nu}-2\underline{e}^{\mu\nu})\end{aligned}\quad(7.57)$$

$$\begin{aligned}&= \Lambda(e_{\alpha\beta}\underline{g}^{\alpha\beta})\left(\underline{g}^{\mu\nu}+\frac{1}{2}(e_{\alpha\beta}\underline{g}^{\alpha\beta})\underline{g}^{\mu\nu}-2\underline{e}^{\mu\nu}\right)\\ &+ 2\mu\left(\underline{e}^{\mu\nu}+\frac{1}{2}(e_{\alpha\beta}\underline{e}^{\alpha\beta})\underline{g}^{\mu\nu}-2\left(\underline{e}^{\mu}{}_{\beta}\underline{e}^{\beta\nu}\right)^{Sym}\right)\\ &- 3\kappa\alpha\Delta\theta\left((e_{\alpha\beta}\underline{g}^{\alpha\beta})\underline{g}^{\mu\nu}+\underline{g}^{\mu\nu}-2\underline{e}^{\mu\nu}\right)\end{aligned}\quad(7.58)$$

Comme prévu, cette expression est symétrique puisque le projecteur spatial conserve la propriété de symétrie. De plus, Eq. 7.58 vérifie $T_\sigma^{\mu\nu}u_\mu = 0$. Les termes non linéaires dans l'Eq. 7.52 correspondent aux termes de la dérivée de Lie pouvant être liés à la dérivée par rapport aux paramètres du matériau et aux composantes du tenseur métrique. En utilisant $\Psi_\sigma(\Lambda/\widetilde{\rho}_c, \mu/\widetilde{\rho}_c, \underline{e}_{\mu\nu}, \underline{g}^{\mu\nu})$ et $\Psi_{\theta,\sigma}(\kappa\alpha/\widetilde{\rho}_c, \Delta\theta, \underline{e}_{\mu\nu}, \underline{g}^{\mu\nu})$ au lieu de $\Psi_\sigma(\Lambda/\widetilde{\rho}_c, \mu/\widetilde{\rho}_c, \underline{I}_I, \underline{I}_{II})$ et $\Psi_{\theta,\sigma}(\kappa\alpha/\widetilde{\rho}_c, \Delta\theta, \underline{I}_I)$, nous obtiendrions exactement le même modèle de comportement. Comme prévu, Eq. 7.58 conduit à l'absence de contrainte spatio-temporelle pour $\underline{e}^{\alpha\beta} = 0$, $\Delta\theta = 0$.

Dans ce qui suit, le modèle obtenu a été étudié dans pour différents cas de déformation et de température.

#### 7.4.4.1 Pour les petites déformations et les variations finies de température

On suppose que les déformations sont petites ($\forall\mu,\nu, e^{\mu\nu} \ll 1 \Leftrightarrow ||e|| \ll 1$) et la variation de température est finie, alors Eq. 7.58 conduit à:

$$\begin{aligned} T_\sigma^{\mu\nu} &= (\Lambda - 3\kappa\alpha\Delta\theta)(e_\alpha{}^\beta(\delta^\alpha{}_\beta - u^\alpha u_\beta))(g^{\mu\nu} - u^\mu u^\nu) \\ &+ 2(\mu + 3\kappa\alpha\Delta\theta)e^{\alpha\beta}(\delta^\mu{}_\alpha - u^\mu u_\alpha)(\delta^\nu{}_\beta - u^\nu u_\beta) \\ &- 3\kappa\alpha\Delta\theta(g^{\mu\nu} - u^\mu u^\nu) \end{aligned} \tag{7.59}$$

L'Eq. 7.59 montre que $e^{\alpha\beta} = 0$ ou $e^{\alpha\beta} = \mathcal{N}u^\alpha u^\beta$, avec $\mathcal{N} \in \mathbb{R}^*$ et $\Delta\theta = 0$ conduisent à l'absence de contrainte spatio-temporelle. Dans un référentiel inertiel, Eq. 7.59 conduit à:

$$\begin{aligned} T_\sigma^{\mu\nu} &= (\Lambda - 3\kappa\alpha\Delta\theta)(e_\alpha{}^\beta(\delta^\alpha{}_\beta - \gamma^2 v^\alpha v_\beta/c^2))(\eta^{\mu\nu} - \gamma^2 v^\mu v^\nu/c^2) \\ &+ 2(\mu + 3\kappa\alpha\Delta\theta)e^{\alpha\beta}(\delta^\mu{}_\alpha - \gamma^2 v^\mu v_\alpha/c^2)(\delta^\nu{}_\beta - \gamma^2 v^\nu v_\beta/c^2) \\ &- 3\kappa\alpha\Delta\theta(\eta^{\mu\nu} - \gamma^2 v^\mu v^\nu/c^2) \end{aligned} \tag{7.60}$$

où $e^{\mu\nu} = \frac{1}{2}(\eta^{\mu\nu} - b^{\mu\nu})$ déduit de l'Eq. 4.45. A la limite non-relativiste, ça conduit à:

$$T_\sigma^{\mu\nu} \approx (\Lambda - 3\kappa\alpha\Delta\theta)(e_\alpha{}^\beta\delta^\alpha{}_\beta)\eta^{\mu\nu} + 2(\mu + 3\kappa\alpha\Delta\theta)e^{\mu\nu} - 3\kappa\alpha\Delta\theta\eta^{\mu\nu} \tag{7.61}$$

$$\approx (\Lambda - 3\kappa\alpha\Delta\theta)(e_a{}^b\delta^a{}_b)\eta^{\mu\nu} + 2(\mu + 3\kappa\alpha\Delta\theta)e^{\mu\nu} - 3\kappa\alpha\Delta\theta\eta^{\mu\nu} \tag{7.62}$$

En l'absence de couplage thermomécanique, Eq. 7.62 conduit à un modèle de type Hookéen pour les petites déformations en thermoélasticité, tout en supposant que $e_4{}^4 \approx 0$ si la vitesse de chargement est non relativiste, de sorte que seules les composantes spatiales restent dans la trace de $e^{\mu\nu}$.

Dans un référentiel propre, où $\hat{u}^\mu = (0,0,0,1)$, Eq. 7.59 mène aux composantes spatiales:

$$\begin{aligned} \hat{T}_\sigma^{ij} &= J(\Lambda - 3\kappa\alpha\Delta\theta)(\hat{e}_a{}^b\delta^a{}_b + \hat{e}_4{}^4 - \hat{e}_4{}^\beta\hat{u}_\beta)\hat{g}^{ij} + 2J(\mu + 3\kappa\alpha\Delta\theta)\hat{e}^{ij} \\ &- 3J\kappa\alpha\Delta\theta\hat{g}^{ij} \end{aligned} \tag{7.63}$$

où $\hat{e}^{\mu\nu} = \frac{1}{2}(\hat{g}^{\mu\nu} - \hat{b}^{\mu\nu}) = \frac{1}{2}(\hat{g}^{\mu\nu} - \hat{g}^{\mu\alpha}\hat{g}^{\nu\beta}\eta_{\alpha\beta})$ à partir de l'Eq. 4.45. Puisque $\Lambda$ et $\mu$ sont des densités scalaires, le determinant $J$ doit être introduit et pour les petites déformations $J \approx 1$. Ce qui mène au modèle classique de Hooke pour les petites déformations (Eq. 4.25), avec des nouveaux termes couplant la déformation et la variation finie de température $-3\kappa\alpha\Delta\theta(\hat{e}_a{}^b\delta^a{}_b)\hat{g}^{ij} + 6\kappa\alpha\Delta\theta\hat{e}^{ij}$ et le terme $\hat{e}_4{}^4 - \hat{e}_4{}^\beta\hat{u}_\beta$ qui est strictement nul quand le référentiel propre et locallement inertiel ($\hat{g}^{\mu\nu} = \eta^{\mu\nu}$ leading to $\hat{u}_\mu = (0,0,0,1)$). Dans le référentiel propre mais non-inertiel, ce terme peut être négligé si et seulement si la vitesse de chargement est non-relativiste [Panicaud et al.,2014]. Pour les composantes temporelles:

$$\begin{aligned} \hat{T}_\sigma^{i4} &= J(\Lambda - 3\kappa\alpha\Delta\theta)(\hat{e}_a{}^b\delta^a{}_b + \hat{e}_4{}^4 - \hat{e}_4{}^\beta\hat{u}_\beta)\hat{g}^{i4} + 2J(\mu + 3\kappa\alpha\Delta\theta)\hat{e}^{i\beta}(\delta^4{}_\beta - \hat{u}_\beta) \\ &- 3J\kappa\alpha\Delta\theta\hat{g}^{i4} \end{aligned} \tag{7.64}$$

et

$$\begin{aligned} \hat{T}_\sigma^{44} &= J(\Lambda - 3\kappa\alpha\Delta\theta)(\hat{e}_a{}^b\delta^a{}_b + \hat{e}_4{}^4 - \hat{e}_4{}^\beta\hat{u}_\beta)(\hat{g}^{44} - 1) \\ &+ 2J(\mu + 3\kappa\alpha\Delta\theta)\hat{e}^{\alpha\beta}(\delta^4{}_\alpha - \hat{u}_\alpha)(\delta^4{}_\beta - \hat{u}_\beta) \\ &- 3J\kappa\alpha\Delta\theta(\hat{g}^{44} - 1) \end{aligned} \tag{7.65}$$

L'Eq. 7.65 est nulle si et seulement si le référentiel propre est aussi inertiel ($\hat{g}^{\mu\nu} = \eta^{\mu\nu}$ menant à $\hat{u}_\mu = (0,0,0,1)$). Pour les autres référentiels, certains termes apparaissent pour les composantes de temps et peuvent être considérées très petites, comme par exemple dans le référentiel propre, si la vitesse de chargement est non relativiste. Dans ce référentiel, en raison du choix du tenseur de déformation, Eq. 7.63 est nulle pour $\hat{e}^{\alpha\beta} = 0$, uniquement si l'hypothèse supplémentaire $\Delta\theta = 0$ est prise en compte. L'utilisation du projecteur dans l'énergie libre spécifique assure la modélisation des contributions spatiales pour les expressions de contrainte et de déformation pour le référentiel propre si la vitesse de chargement est très petite.

#### 7.4.4.2 Pour les petites déformations et les petites variations de température

On suppose que les déformations et la variation de température sont petites ($\forall \mu, \nu, e^{\mu\nu} \ll 1 \Leftrightarrow ||e|| \ll 1$ et $\Delta\theta \ll \theta_0$, tel que $\Delta\theta e^{\mu\nu} \to 0$, alors Eq. 7.59 conduit à:

$$\begin{aligned} T_\sigma^{\mu\nu} &= \Lambda(e_\alpha{}^\beta(\delta^\alpha{}_\beta - u^\alpha u_\beta))(g^{\mu\nu} - u^\mu u^\nu) \\ &+ 2\mu e^{\alpha\beta}(\delta^\mu{}_\alpha - u^\mu u_\alpha)(\delta^\nu{}_\beta - u^\nu u_\beta) \\ &- 3\kappa\alpha\Delta\theta(g^{\mu\nu} - u^\mu u^\nu) \end{aligned} \tag{7.66}$$

Eq. 7.66 montre que $e^{\alpha\beta} = 0$, $\Delta\theta = 0$ sauf que $e^{\alpha\beta} = \mathcal{N} u^\alpha u^\beta$, $\Delta\theta = 0$, où $\mathcal{N} \in \mathbb{R}^*$ ce qui conduit à l'absence de contrainte spatio-temporelle. Dans un référentiel inertiel, Eq. 7.66 conduit à:

$$\begin{aligned} T_\sigma^{\mu\nu} &= \Lambda(e_\alpha{}^\beta(\delta^\alpha{}_\beta - \gamma^2 v^\alpha v_\beta/c^2))(\eta^{\mu\nu} - \gamma^2 v^\mu v^\nu/c^2) \\ &+ 2\mu e^{\alpha\beta}(\delta^\mu{}_\alpha - \gamma^2 v^\mu v_\alpha/c^2)(\delta^\nu{}_\beta - \gamma^2 v^\nu v_\beta/c^2) \\ &- 3\kappa\alpha\Delta\theta(\eta^{\mu\nu} - \gamma^2 v^\mu v^\nu/c^2) \end{aligned} \tag{7.67}$$

où $e^{\mu\nu} = \frac{1}{2}(\eta^{\mu\nu} - b^{\mu\nu})$ est déduit de l'Eq. 4.45. A la limite non-relativiste, cela conduit à:

$$T_\sigma^{\mu\nu} \approx \Lambda(e_\alpha{}^\beta \delta^\alpha{}_\beta)\eta^{\mu\nu} + 2\mu e^{\mu\nu} - 3\kappa\alpha\Delta\theta\eta^{\mu\nu} \tag{7.68}$$

$$\approx \Lambda(e_a{}^b \delta^a{}_b)\eta^{\mu\nu} + 2\mu e^{\mu\nu} - 3\kappa\alpha\Delta\theta\eta^{\mu\nu} \tag{7.69}$$

Eq. 7.69 conduit au modèle classique de Hooke pour les petites déformations en élasticité couplé à de petites variation de température, tout en supposant que $e_4{}^4 \approx 0$ si la vitesse de chargement est non relativiste, de sorte que seules les composantes spatiales restent dans la trace de $e^{\mu\nu}$.

Dans un référentiel propre, où $\hat{u}^\mu = (0,0,0,1)$, Eq. 7.66 mène aux composantes spatiales:

$$\begin{aligned} \hat{T}_\sigma^{ij} &= J\Lambda(\hat{e}_a{}^b \delta^a{}_b + \hat{e}_4{}^4 - \hat{e}_4{}^\beta \hat{u}_\beta)\hat{g}^{ij} + 2J\mu\hat{e}^{ij} \\ &- 3J\kappa\alpha\Delta\theta\hat{g}^{ij} \end{aligned} \tag{7.70}$$

où $\hat{e}^{\mu\nu} = \frac{1}{2}(\hat{g}^{\mu\nu} - \hat{b}^{\mu\nu}) = \frac{1}{2}(\hat{g}^{\mu\nu} - \hat{g}^{\mu\alpha}\hat{g}^{\nu\beta}\eta_{\alpha\beta})$ à partir de l'Eq. 4.45. Puisque $\Lambda$ et $\mu$ sont des densités scalaires, le determinant $J$ doit être introduit et pour les petites déformations $J \approx 1$. Ceci mène au modèle classique de Hooke pour les petites déformations couplé au petites variations de température, en addition d'un nouveau terme $\hat{e}_4{}^4 - \hat{e}_4{}^\beta \hat{u}_\beta$ qui est strictement nul si le référentiel propre est localement inertiel aussi ($\hat{g}^{\mu\nu} = \eta^{\mu\nu}$ ce qui mène à $\hat{u}_\mu = (0,0,0,1)$). Dans un référentiel propre mais non-inertiel, ce terme peut être considéré comme négligeable si et seulement si la vitesse de chargement est non-relativiste [Panicaud et al.,2014]. Pour les composantes temporelles:

$$\begin{aligned} \hat{T}_\sigma^{i4} &= J\Lambda(\hat{e}_a{}^b \delta^a{}_b + \hat{e}_4{}^4 - \hat{e}_4{}^\beta \hat{u}_\beta)\hat{g}^{i4} + 2J\mu\hat{e}^{i\beta}(\delta^4{}_\beta - \hat{u}_\beta) \\ &- 3J\kappa\alpha\Delta\theta\hat{g}^{i4} \end{aligned} \tag{7.71}$$

and

$$\begin{aligned} \hat{T}_\sigma^{44} &= J\Lambda(\hat{e}_a{}^b \delta^a{}_b + \hat{e}_4{}^4 - \hat{e}_4{}^\beta \hat{u}_\beta)(\hat{g}^{44} - 1) \\ &+ 2J\mu\hat{e}^{\alpha\beta}(\delta^4{}_\alpha - \hat{u}_\alpha)(\delta^4{}_\beta - \hat{u}_\beta) \\ &- 3J\kappa\alpha\Delta\theta(\hat{g}^{44} - 1) \end{aligned} \tag{7.72}$$

Comme annoncé précédemment, ces deux expressions sont nulles si et seulement si le référentiel propre est aussi inertiel ($\hat{g}^{\mu\nu} = \eta^{\mu\nu}$ ce qui mène à $\hat{u}_\mu = (0,0,0,1)$). Pour d'autres référentiels, certains termes qui peuvent être considérés comme très petits apparaissent en plus dans les composantes temporelles. C'est le cas pour le référentiel propre par exemple, si la vitesse de chargement n'est pas relativiste.

Dans le référentiel propre, et à cause du choix du tenseur de déformation, les composantes du tenseur de contrainte calculé par l'Eq. 7.70 sont nulles pour $\hat{e}^{\alpha\beta} = 0$, puisque $\Delta\theta$ est petite. En revanche, cette condition est équivalente à l'hypothèse que le référentiel propre est inertiel aussi. Par conséquence, et à l'aide de la définition de la déformation choisie, on déduit: $\hat{e}_{\mu\nu} = \frac{1}{2}(\hat{g}_{\mu\nu} - \hat{b}_{\mu\nu})$ qui est équivalent à $\hat{b}_{\mu\nu} = \hat{g}_{\mu\nu} - 2\hat{e}_{\mu\nu}$. La définition de $\boldsymbol{b}$ ce qui mène à $\hat{b}_{\mu\nu} = \eta_{\mu\nu}$. De plus, si le référentiel propre est inertiel alors $\hat{g}_{\mu\nu} = \eta_{\mu\nu}$, thus $\hat{b}_{\mu\nu} = \hat{g}_{\mu\nu}$. Par conséquence, $\hat{g}_{\mu\nu} = \eta_{\mu\nu}$ est équivalent à avoir $\hat{e}_{\mu\nu} = 0$. Les trois dernières équations sont des expressions équivalentes qui mènent à déduire que si le référentiel propre est inertiel, les composantes du tenseur de déformation élastique sont nulles et donc les composantes du tenseur de contraintes sont nulles aussi pour le modèle hyperélastique considéré. Réciproquement, la déformation spatio-temporelle dans la configuration non déformée qui est nécessairement inertielle est nulle.

#### 7.4.4.3 Pour les grandes transformations (grandes déformations et variations finies de température)

Pour les petites déformations, aucune différence n'est prévue entre l'approche espace-temps à la limite non relativiste et l'approche Newtonienne classique d'un point de vue de modélisation. Il est maintenant intéressant d'étudier les expressions obtenues pour les grandes déformations et les variations finies de température..

A partir de l'Eq. 7.58 exprimée dans un référentiel propre, les composantes spatiales du modèle s'écrivent:

$$\begin{aligned}
\hat{T}^{ij}_\sigma/J &= (\Lambda - 3\kappa\alpha\Delta\theta)(\hat{e}_{\alpha\beta}(\hat{g}^{\alpha\beta} - \hat{u}^\alpha\hat{u}^\beta))\hat{g}^{ij} + 2(\mu + 3\kappa\alpha\Delta\theta)\hat{e}^{ij} \\
&\quad + \frac{1}{2}\Lambda(\hat{e}_{\alpha\beta}(\hat{g}^{\alpha\beta} - \hat{u}^\alpha\hat{u}^\beta))^2\hat{g}^{ij} + \mu(\hat{e}_{\kappa\lambda}(\hat{g}^{\kappa\alpha} - \hat{u}^\kappa\hat{u}^\alpha)(\hat{g}^{\lambda\beta} - \hat{u}^\lambda\hat{u}^\beta)\hat{e}_{\alpha\beta})\hat{g}^{ij} \\
&\quad - 2\Lambda(\hat{e}_{\alpha\beta}(\hat{g}^{\alpha\beta} - \hat{u}^\alpha\hat{u}^\beta))\hat{e}^{ij} - 4\mu(\hat{e}^{i\alpha}\hat{e}_\alpha{}^j - \hat{e}^{i\alpha}\hat{e}_4{}^j\hat{u}_\alpha)^{Sym} \\
&\quad - 3\kappa\alpha\Delta\theta\hat{g}^{ij} \qquad (7.73) \\
&= (\Lambda - 3\kappa\alpha\Delta\theta)(\hat{e}_a{}^b\delta^a{}_b + \hat{e}_4{}^4 - \hat{e}_4{}^\beta\hat{u}_\beta)\hat{g}^{ij} + 2(\mu + 3\kappa\alpha\Delta\theta)\hat{e}^{ij} \\
&\quad + \frac{1}{2}\Lambda(\hat{e}_a{}^b\delta^a{}_b + \hat{e}_4{}^4 - \hat{e}_4{}^\beta\hat{u}_\beta)^2\hat{g}^{ij} + \mu(\hat{e}^{\alpha\beta}\hat{e}_{\alpha\beta} - \hat{e}^\alpha{}_4\hat{e}_{\alpha 4} - \hat{e}_\alpha{}^4\hat{e}_{4\beta} + \\
&\quad + \hat{e}_{44}\hat{e}_{44})\hat{g}^{ij} - 2\Lambda(\hat{e}_a{}^b\delta^a{}_b + \hat{e}_4{}^4 - \hat{e}_4{}^\beta\hat{u}_\beta)\hat{e}^{ij} \\
&\quad - 4\mu(\hat{e}^{ia}\hat{e}_a{}^j + \hat{e}^{i4}\hat{e}_4{}^j - \hat{e}^{ia}\hat{e}_4{}^j\hat{u}_a - \hat{e}^{i4}\hat{e}_4{}^j\hat{u}_4)^{Sym} \\
&\quad - 3\kappa\alpha\Delta\theta\hat{g}^{ij} \qquad (7.74) \\
&\approx (\Lambda - 3\kappa\alpha\Delta\theta)(\hat{e}_a{}^b\delta^a{}_b)\hat{g}^{ij} + 2(\mu + 3\kappa\alpha\Delta\theta)\hat{e}^{ij} + \frac{1}{2}\Lambda(\hat{e}_a{}^b\delta^a{}_b)^2\hat{g}^{ij} + \mu(\hat{e}^{\alpha\beta}\hat{e}_{\alpha\beta})\hat{g}^{ij} \\
&\quad - 2\Lambda(\hat{e}_a{}^b\delta^a{}_b)\hat{e}^{ij} - 4\mu(\hat{e}^{ia}\hat{e}_a{}^j)^{Sym} - 3\kappa\alpha\Delta\theta\hat{g}^{ij} \qquad (7.75)
\end{aligned}$$

L'Eq. 7.75 est obtenue en considérant que la vitesse de chargement est non-relativiste. Dans cette équation 4 termes non-linéaires correspondent à l'expansion du modèle Hookéen pour les grandes déformations. De plus, les termes supplémentaires (linéaires en la déformation) $-3\kappa\alpha\Delta\theta(\hat{e}_a{}^b\delta^a{}_b)\hat{g}^{ij}$ et $6\kappa\alpha\Delta\theta\hat{e}^{ij}$ correspondent à l'expansion causée par la variation finie de la température par rapport au modèle Hookéen. L'effet résultant de ces termes dépend de la valeur de la déformation. Pour les grandes déformations, la valeur de ces termes est importante par rapport à la valeur du dernier terme de l'Eq. 7.75. Par conséquent, en comparant au modèle Newtonien Hookéen thermoélastique (Eq. 4.25), six termes dépendant de trois paramètres du matériau sont ajoutés au modèle spatio-temporel comme résultat de l'utilisation de l'hypothèse de grandes transformations. Au cas où la transformation est isotherme $\Delta\theta = 0$, l'Eq. 7.75 peut être comparée à l'expression du modèle Hookéen Newtonien élastique (Eq. 4.15). Quatre termes quadratiques dépendant de deux paramètres du matériau sont ajoutés au modèle comme résultat de l'utilisation de l'hypothèse des grandes transformations.

#### 7.4.4.4 La dérivée de Lie

Notons que les avantages de l'utilisation de l'approche spatio-temporelle proviennent essentiellement de l'utilisation de la dérivée de Lie, car cette dérivée du tenseur de déformation donne le taux de déformation. De plus, l'utilisation du cadre de l'espace-temps inclut naturellement la partie dérivée du temps. Le résultat de cette dérivée est indépendant du référentiel et de la superposition de mouvements de corps rigides. Par conséquent, on parle d'une dérivée objective [Rouhaud et al.,2013].

Les expressions explicites de la dérivée de Lie par rapport à la vitesse spatio-temporelle $\boldsymbol{u}$ (définie à la section 2.2.2) d'une densité scalaire $\mathcal{S}$ et des composantes covariantes respectivement contravariantes d'une densité de second ordre $\boldsymbol{\mathcal{T}}$ ayant un poids de densité tensorielle $W$ [Schouten,1954] sont:

$$\mathcal{L}_u(\mathcal{S}) = u^\lambda \frac{\partial \mathcal{S}}{\partial x^\lambda} + W\mathcal{S}\frac{\partial u^\lambda}{\partial x^\lambda} \tag{7.76a}$$

$$\mathcal{L}_u(\mathcal{T}_{\mu\nu}) = u^\lambda \frac{\partial \mathcal{T}_{\mu\nu}}{\partial x^\lambda} + \mathcal{T}_{\lambda\nu}\frac{\partial u^\lambda}{\partial x^\mu} + \mathcal{T}_{\mu\lambda}\frac{\partial u^\lambda}{\partial x^\nu} + W\mathcal{T}_{\mu\nu}\frac{\partial u^\lambda}{\partial x^\lambda} \tag{7.76b}$$

$$\mathcal{L}_u(\mathcal{T}^{\mu\nu}) = u^\lambda \frac{\partial \mathcal{T}^{\mu\nu}}{\partial x^\lambda} - \mathcal{T}^{\lambda\nu}\frac{\partial u^\mu}{\partial x^\lambda} - \mathcal{T}^{\mu\lambda}\frac{\partial u^\nu}{\partial x^\lambda} + W\mathcal{T}^{\mu\nu}\frac{\partial u^\lambda}{\partial x^\lambda}. \tag{7.76c}$$

La dérivée de Lie est intrinsèque car la dérivée du champ tensoriel est prise le long d'un champ vectoriel physique: la vitesse. Cet opérateur pourrait être interprété comme une entité lagrangienne (car il est défini pour une particule de matière), et il est calculé dans un formalisme eulérien (puisqu'il est défini à un événement donné de l'espace-temps). De plus, la dérivée de Lie obéit à la règle de Leibnitz [Protter,1985] et à la règle de la chaîne [Rodriguez and Lopez Fernandez,2010].

Notons qu'en particulier la dérivée de Lie du tenseur métrique $\mathbf{g}$ n'est pas nulle, sauf si le mouvement est isométrique. C'est la raison pour laquelle les formules sont différentes pour les composantes contravariants et covariants.

### 7.4.5 Les formes variationnelles du problème thermomécanique

L'expression du modèle thermo-hyperélastique spatio-temporel dans le cadre approprié est utilisée pour écrire les formes variationnelles qui ont permis leur implémentation pour simuler ensuite numériquement le modèle (section 5.6).

Eq. 7.15 représente l'équation d'équilibre local du tenseur impulsion-énergie spatio-temporel. La forme variationnelle faible du problème thermomécanique est obtenue en multipliant cette équation par une fonction de test $r^*_\mu$ combinant le champ de température virtuel $\theta^*$ et le champ de déplacement virtuel $dep^*_\mu$ tel que:

$$r^*_\mu = \begin{pmatrix} \theta^* \\ dep^*_\mu \end{pmatrix} \tag{7.77}$$

Ensuite, l'équation résultante est intégrée sur l'hypervolume spatio-temporel $\mathrm{d}H_\Omega$.

$$\mathcal{W}(r_\mu, r^*_\mu) = \int_\Omega r^*_\mu \nabla_\nu T^{\mu\nu}\, dH_\Omega = 0, \forall r^*_\mu \tag{7.78}$$

$r_\mu$ étant la fonction d'essai définie par:

$$r_\mu = \begin{pmatrix} \theta \\ dep_\mu \end{pmatrix} \tag{7.79}$$

L'Eq. 5.83 est ensuite développée:

$$\mathcal{W}(r_\mu, r^*_\mu) = \int_\Omega \left(\nabla_\nu (T^{\mu\nu}\, r^*_\mu) - T^{\mu\nu}\nabla_\nu r^*_\mu\right)\, dH_\Omega = 0, \forall r^*_\mu \tag{7.80}$$

En utilisant le théorème de Green-Ostrogradski, Eq. 7.80 peut être écrite:

$$\mathcal{W}(r_\mu, r_\mu^*) = \int_\Omega T^{\mu\nu}\,\nabla_\nu r_\mu^*\,dH_\Omega - \int_{\partial\Omega} T^{\mu\nu}\,r_\mu^* n_\nu\,\mathrm{d}S_\Omega = 0, \forall r_\mu^* \tag{7.81}$$

$n_\nu$ étant le vecteur normal à la hypersurface d'intégration $\mathrm{d}S_\Omega$.
Les conditions aux limites du problème sont résumées dans le tableau 19.

| Type de conditions aux limites | Variable | Limite | Condition | Fonctions représentant les conditions aux limites |
|---|---|---|---|---|
| Conditions aux limites de Dirichlet | $dep_\mu$ | $\partial\Omega_{dep_\mu}$ | $\partial\Omega_{dep_\mu} \cup \partial\Omega_{T_M} = \partial\Omega$<br>$\partial\Omega_{dep_\mu} \cap \partial\Omega_{T_M} = \varnothing$ | $f_{SC}(x^\mu \in \partial\Omega_{dep_\mu}) = dep_\mu(x^\mu \in \partial\Omega_{dep_\mu})$<br>$f_{TC}(x^\mu \in \partial\Omega_{dep_\mu}) = dep_\mu(x^\mu \in \partial\Omega_{dep_\mu})$ |
| | $\theta$ | $\partial\Omega_\theta$ | - | $f_{SC}(x^\mu \in \partial\Omega_\theta) = \theta(x^\mu \in \partial\Omega_\theta)$<br>$f_{TC}(x^\mu \in \partial\Omega_\theta) = \theta(x^\mu \in \partial\Omega_\theta)$ |
| Conditions aux limites de Neumann | $T_M$ | $\partial\Omega_{T_M}$ | $\partial\Omega_{dep_\mu} \cup \partial\Omega_{T_M} = \partial\Omega$<br>$\partial\Omega_{dep_\mu} \cap \partial\Omega_{T_M} = \varnothing$ | $f_{SC}(x^\mu \in \partial\Omega_{T_M}) = T_M(x^\mu \in \partial\Omega_{T_M})$<br>$f_{TC}(x^\mu \in \partial\Omega_{T_M}) = T_M(x^\mu \in \partial\Omega_{T_M})$ |

**Tab. 19:** Conditions aux limites pour un modèle thermomécanique spatio-temporel.

**Développements spécifiques pour la résolution numérique:**

Afin de procéder à la simulation numérique du modèle thermo-hyperélastique à l'aide du logiciel FEniCS project, nous devons déterminer les formes intégrales faibles correspondants aux comportements simulés et les conditions aux limites correspondantes.

Pour implémenter la forme intégrale faible obtenue dans la section 5.6, Eq. 7.78 est développée:

$$\mathcal{W}(r_\mu, r_\mu^*) = \int_\Omega r_\mu^* \nabla_\nu (T_{\mathcal{U}}^{\mu\nu} + T_q^{\mu\nu} + T_\sigma^{\mu\nu})\,dH_\Omega \quad = \quad 0, \forall r_\mu^* \tag{7.82}$$

Le premier terme de l'Eq. 7.82 peut être exprimé par:

$$\begin{aligned}
\int_\Omega r_\mu^* \nabla_\nu T_{\mathcal{U}}^{\mu\nu}\,dH_\Omega &= \int_\Omega r_\mu^* \nabla_\nu (\tilde{\rho_c}(c^2 + e_{int}) u^\mu u^\nu)\,dH_\Omega \\
&= \int_\Omega r_\mu^* \nabla_\nu (\tilde{\rho_c} e_{int} u^\mu u^\nu)\,dH_\Omega \\
&= \int_\Omega (\tilde{\rho_c} e_{int} u^\mu u^\nu)\,\nabla_\nu r_\mu^*\,dH_\Omega - \int_{\partial\Omega} (\tilde{\rho_c} e_{int} u^\mu u^\nu)\,r_\mu^* n_\nu\,\mathrm{d}S_\Omega
\end{aligned} \tag{7.83}$$

En utilisant le théorème de Green-Ostrogradski, Eq. 7.82 s'écrit:

$$\begin{aligned}
\mathcal{W}(r_\mu, r_\mu^*) &= \int_\Omega (\tilde{\rho_c} e_{int} u^\mu u^\nu)\,\nabla_\nu r_\mu^*\,dH_\Omega - \int_{\partial\Omega} (\tilde{\rho_c} e_{int} u^\mu u^\nu)\,r_\mu^* n_\nu\,\mathrm{d}S_\Omega \\
&+ \int_\Omega (T_q^{\mu\nu} + T_\sigma^{\mu\nu})\,\nabla_\nu r_\mu^*\,dH_\Omega - \int_{\partial\Omega} (T_q^{\mu\nu} + T_\sigma^{\mu\nu})\,r_\mu^* n_\nu\,\mathrm{d}S_\Omega \\
&= 0, \forall r_\mu^*
\end{aligned} \tag{7.84}$$

Puis le problème thermomécanique est écrit pour un référentiel propre convenant à l'étude des comportements des matériaux (voir section 1.3.3) et dans lequel $\hat{u}^\mu = (0,0,0,1)$. Dans un référentiel propre, Eq. 7.84 s'écrit:

$$\begin{aligned}\mathcal{W}(r_\mu, r_\mu^*) &= \int_\Omega (\tilde{\rho_c} e_{int})\, \nabla_4 r_4^*\, dH_\Omega - \int_{\partial\Omega} (\tilde{\rho_c} e_{int})\, r_4^* \hat{n}_4\, \mathrm{d}S_\Omega \\ &+ \int_\Omega (\hat{T}_q^{\mu\nu} + \hat{T}_\sigma^{\mu\nu})\, \nabla_\nu r_\mu^*\, dH_\Omega - \int_{\partial\Omega} (\hat{T}_q^{\mu\nu} + \hat{T}_\sigma^{\mu\nu})\, r_\mu^* \hat{n}_\nu\, \mathrm{d}S_\Omega \\ &= 0, \forall r_\mu^* \end{aligned} \tag{7.85}$$

Dans le cas d'un référentiel propre et inertiel, en supposant une relation linéaire entre l'énergie spécifique $e_{int}$ d'une part et la température $\theta$ avec le coefficient $\mathcal{C}_{m\omega}$ $(J.kg^{-1}.K^{-1})$ d'autre part, et en l'absence de $\hat{T}_\sigma^{\mu\nu}$ et du couplage thermomécanique (la fonction $r_{\ mu}$ sera réduite à $r_4 = \theta$), Eq. 7.85 peut s'écrire:

$$\begin{aligned}\mathcal{W}(r_\mu, r_\mu^*) &= \int_\Omega \left( (\tilde{\rho_c} \mathcal{C}_{m\omega} \theta)\, \nabla_4 r_4^* + \hat{T}_q^{4\nu}\, \nabla_\nu r_4^* \right)\, dH_\Omega \\ &- \int_{\partial\Omega} \left( \hat{T}_q^{4\nu}\, r_4^* \hat{n}_\nu + \tilde{\rho_c} \mathcal{C}_{m\omega} \theta\, r_4^* \hat{n}_4 \right)\, \mathrm{d}S_\Omega = 0, \forall r_\mu^* \end{aligned}$$

En plus, dans ce référentiel particulier, $\hat{q}^4 = 0$. D'où Eq. 7.86 s'écrit:

$$\begin{aligned}\mathcal{W}(r_\mu, r_\mu^*) &= \int_\Omega \left( (\tilde{\rho_c} \mathcal{C}_{m\omega} \theta)\, \nabla_4 r_4^* + q^i u^4\, \nabla_i r_4^* \right)\, dH_\Omega \\ &- \int_{\partial\Omega} \left( q^i u^4\, r_4^* \hat{n}_i + \tilde{\rho_c} \mathcal{C}_{m\omega} \theta\, r_4^* \hat{n}_4 \right)\, \mathrm{d}S_\Omega = 0, \forall r_\mu^* \end{aligned}$$

En divisant Eq. 7.86 par $\dfrac{\tilde{\rho_c} \mathcal{C}_{m\omega}}{c}$ et en remplaçant $q^i = \dfrac{\lambda}{c} I^{ij} \nabla_j \theta$, on obtient:

$$\mathcal{W}(\theta, \theta^*) = \int_\Omega \left( \theta\, \frac{\partial \theta^*}{\partial t} + a I^{ij}\, \frac{\partial \theta}{\partial x^j}\, \frac{\partial \theta^*}{\partial x^i} \right)\, dH_\Omega - \int_{\partial\Omega} \left( \theta^*\, \frac{c\, q^i}{\widetilde{\rho_c} \mathcal{C}_{m\omega}} n_i + c\theta\, \theta^* \hat{n}_4 \right)\, \mathrm{d}S_\Omega = 0, \forall r_\mu^*$$

De plus, $-\int_{\partial\Omega} c\theta\, \theta^* \hat{n}_4\, \mathrm{d}S_\Omega = -\int_\Omega c \dfrac{\partial(\theta\, \theta^*)}{c \partial t}\, dH_\Omega = -\displaystyle\int_\Omega \theta^* \frac{\theta}{\partial t}\, dH_\Omega - \int_{\partial\Omega} \theta \frac{\theta^*}{\partial t}\, dH_\Omega$. Eq. 7.86 peut alors s'écrire:

$$\mathcal{W}(\theta, \theta^*) = \int_\Omega \left( \theta^*\, \frac{\partial \theta}{\partial t} + a I^{ij}\, \frac{\partial \theta}{\partial x^j}\, \frac{\partial \theta^*}{\partial x^i} \right)\, dH_\Omega - \int_{\partial\Omega_q} \theta^*\, \frac{c\, q^i}{\widetilde{\rho_c} \mathcal{C}_{m\omega}} n_i\, \mathrm{d}S_\Omega = 0, \forall r_\mu^*$$

Par conséquence, la forme intégrale faible spatio-temporelle du problème de conduction thermique pour un modèle de Fourier est de nouveau obtenue (section 2.6.3.2). Eq. 7.86 est réduite à Eq. 2.53 avec $f_r = 0$ et $q_{ext}^i = q^i$.

Nous avons choisi de valider dans ce manuscrit le modèle de l'espace-temps obtenu sous les hypothèses de petites déformations et de faibles variations de température dans une première étape de vérification. Les résultats des simulations des modèles 2D et 2D+1D sous de simples charges de traction et de flexion, montrent la compatibilité des résultats Newtoniens et spatio-temporels. De légères erreurs numériques peuvent apparaître en raison de la différence de construction du maillage entre les deux modèles ce qui conduit à des effets de bords différents.

Les modélisations Newtonienne et spatio-temporelle du comportement thermomécanique, pour respectivement les petites et grandes déformations, sont comparées dans la section 5.7. Le tableau 20 résume cette comparaison.

| | **Modélisation Newtonieene** | **Modélisation en espace-temps** |
|---|---|---|
| Hypothèse des petites déformations | Définition de petite déformation $\epsilon^{ij}$<br>Forme variationnelle en fonction de $\epsilon^{ij}$<br>Référentiel propre/inertiel<br>Le tenseur métrique: $\eta^{ij}$<br>Le Jacobien: $J = 1$<br>$\sigma^{ij}$ d'ordre 1 | Définition de petite déformation $\epsilon^{\mu\nu}$<br>Forme variationnelle en fonction de $\epsilon^{\mu\nu}$<br>Référentiel propre/inertiel<br>Le tenseur métrique: $\eta^{\mu\nu}$<br>Le Jacobien: $J = 1$<br>$T_{\sigma}^{\mu\nu}$ d'ordre 1 |
| (Sans chaleur/température) | ▪ 3 degrés de liberté ($dep_i$) | ▪ degrés de liberté ($dep_\mu$, $\theta$) |
| (Avec chaleur/température) | ▪ 4 degrés de liberté ($dep_i$, $\Delta\theta$) | ▪ 4 degrés de liberté ($dep_\mu$, $\theta$) |
| Hypothèse des grandes déformations | Définition de grande déformation $E^{ij}/e^{ij}$<br>Forme variationnelle en fonction de $E^{ij}/e^{ij}$<br>Référentiel propre/inertiel<br>Le tenseur métrique: $\eta^{ij}$<br>Le Jacobien: $J \neq 1$<br>$\sigma^{ij}$ d'ordre 1 | Définition de grande déformation $E^{\mu\nu}/e^{\mu\nu}$<br>Forme variationnelle en fonction de $E^{\mu\nu}/e^{\mu\nu}$<br>Référentiel propre ($\Gamma^{\mu}_{\kappa\lambda} \neq 0$)<br>Le tenseur métrique: $\hat{g}^{\mu\nu}$<br>Le Jacobien: $J \neq 1$<br>$T_{\sigma}^{\mu\nu}$ d'ordre 2 |
| (Sans chaleur/température) | ▪ 3 degrés de liberté ($dep_i$) | ▪ 4 degrés de liberté ($dep_\mu$, $\theta$) |
| (Avec chaleur/température) | ▪ 4 degrés de liberté ($dep_i$, $\Delta\theta$) | ▪ 4 degrés de liberté ($dep_\mu$, $\theta$) |

**Tab. 20:** Résumé des différences/similitudes entre la modélisation Newtonienne et la modélisation en espace-temps sous les hypothèses des petites et des grandes déformations sans/avec apport extérieur de chaleur/température.

Un résultat important de la modélisation est qu'un modèle thermomécanique spatio-temporel a 4 degrés de liberté (y compris le déplacement et la température) même si la source externe de chaleur et de température est nulle. De plus, pour les petites déformations, les modèles Newtoniens et spatio-temporels sont indiscernables, notamment dans les référentiels propres ou inertiels. Cependant, pour de grandes déformations, ils présentent des différences significatives. La modélisation de l'espace-temps nous permet d'écrire des modèles covariants. Ces modèles présentent des termes supplémentaires par rapport aux modèles Newtoniens. Puisque cette approche proposée est capable de modéliser le comportement des matériaux pour des petites et grandes déformations, elle pourra être appliquée à des applications industrielles telles que les procédés de mise en forme. Dans ce manuscrit, le modèle thermo-hyperélastique spatio-temporel a été utilisé pour étudier le comportement d'un élément bimétallique (section 5.9). La comparaison des résultats de contraintes obtenues par les simulations spatio-temporelles sont superposées à celles obtenues par les simulations Newtoniennes puisque les déformations sont petites.

De plus, nous avons proposé une approche pour modéliser le comportement d'un système de flexion de tube avec les conditions aux limites correspondantes comme moyen d'améliorer ce processus (section 5.10). En annexe C, nous proposons la modélisation d'un tel comportement dans l'espace-temps. Cependant, la résolution numérique était limitée à l'hypothèse des petites déformations en raison de la complexité d'une simulation numérique pour les grandes déformations qui n'a pas été complètement testée et validée. Les résultats des simulations numériques Newtoniennes et spatio-temporelles sont compatibles en petites déformations.

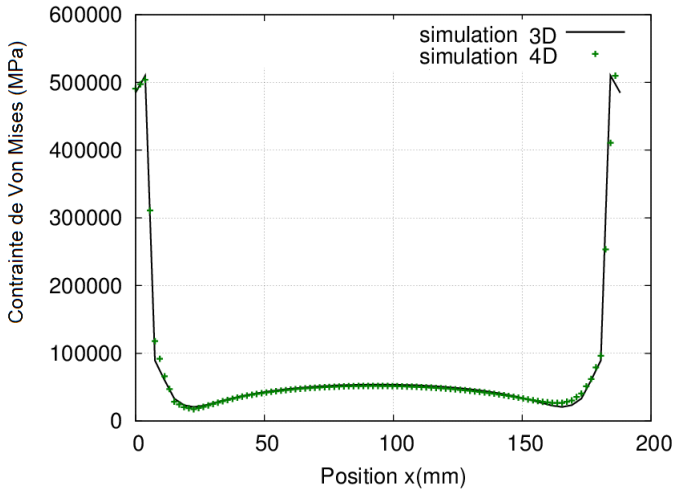


**Fig. 58:** Evolution de la contrainte de Von Mises stress tout au mong du tube fléchi pour des modèles de comportement hyperélastiques Newtonien et spatio-temporel en petites déformations.

## 7.5 Conclusions et perspectives

Le comportement thermomécanique des matériaux en grandes déformations est étudié dans cette thèse dans le but de surmonter les difficultés rencontrées lors des développements des procédés de fabrication. Ces développements sont principalement faits pour minimiser le prix et le temps de fabrication des procédés. Nous proposons dans ce manuscrit une méthodologie permettant de construire des modèles thermomécanique respectant à la fois les lois de la thermodynamique, le principe de causalité et le principe de covariance. D'après une analyse quantitative et qualitative, nous pouvons conclure que l'approche thermodynamique spatio-temporel (en espace-temps) proposée permet d'obtenir des modèles thermomécaniques spatio-temporels qui couvrent le spectre des grandes déformations et en même temps convergent vers les modèles de comportement classiques à la limite Newtonienne. Malgré le fait que les modèles spatio-temporels sont obtenus par une méthode complexe, leur utilisation reste importante vu les avantages qu'ils offrent dans la résolution des problèmes envisagés en mécanique Newtonienne: l'absence de causalité des signaux thermiques, la dépendance des modèles obtenus des référentiels dans lesquels ils sont conçus, la difficulté de modéliser les comportements mécaniques à caractère dissipatif... Pour obtenir les modèles spatio-temporels, les opérateurs et les variables utilisés dans l'espace-temps sont introduits et discutés. Les dérivées covariantes dans ce domaine garantissent l'obtention de modèles thermomécaniques spatio-temporels covariants.

Dans la première partie du manuscrit, le but était d'obtenir des modèles covariants du comportement thermique des matériaux en conduction. La forme covariante des lois de thermodynamiques sont premièrement formulées par relativisation des lois de thermodynamique sans prendre en compte l'effet du comportement mécanique.

Les modèles spatio-temporels de conduction thermique sont ensuite recherchés. Le modèle spatio-temporel de Fourier est obtenu par deux méthodes: la relativisation directe du modèle Newtonien de Fourier et une approche thermodynamique relativiste. Les modèles spatio-temporels obtenus sont covariants et compatibles avec les lois de la thermodynamique irréversible classique. Par contre, ces modèles ne respectent pas le pricipe de causalité ce qui conduit à développer le modèle spatio-temporel de Cattaneo dans lequel le temps de relaxation thermique est pris en compte. Ce modèle est obtenu par deux méthodes: la relativisation directe du modèle Newtonien de Cattaneo et la complexification du modèle de Fourier. Les modèles spatio-temporels obtenus sont covariants (en différence du modèle Newtonien de Cattaneo), compatibles avec les lois de la thermodynamique irreversible étendue et respectent le pricipe de causalité.

Les formes variationnelles des modèles spatio-temporels de conduction thermique sont ensuite formulées dans un référentiel inertiel propre dans le but d'effectuer des simulations numériques via le logiciel FEniCS

project. Des tests de validation sont faits pour les modèles 2D+1D de Fourier et de Cattaneo respectivement. Les réultats montrent que les modèles spatio-temporels ont un comportement cohérent vis-à-vis du raffinement du maillage et du changement des paramètres du matériau. Le comportement des modèles spatio-temporels est aussi comparé au comportement des modèles Newtoniens correspondants. Les résultats montrent une compatibilité entre les deux modes de résolution. Cependant, la méthode des éléments finis de l'espace-temps est plus coûteuse en termes de temps de calcul que celle de l'approche Newtonienne classique.

Nous montrons également dans cette première partie que le modèle spatio-temporel de Fourier peut être utilisé pour prédire le phénomène de conduction thermique se produisant dans une ailette de refroidissement, ce qui peut être utile dans le dimensionnement mécanique.

Le modèle spatio-temporel de Fourier a ensuite été utilisé pour modéliser l'auto-échauffement survenant lors des essais de fatigue. Une méthodologie innovante est développée: elle consiste à utiliser des données expérimentales pour calculer le temps de relaxation d'auto-échauffement $\tau_{ND}$ et la source volumique de chaleur $f_r$ via un modèle thermique Newtonien et de les injecter dans le modèle spatio-temporel.

Son utilisation montre que les modèles relativistes sont capables de prédire la variation de température résultant de l'auto-échauffement lors du test de fatigue. Différentes méthodes peuvent être utilisées pour l'étape d'identification des paramètres ($\tau_{ND}$, $f_r$): la méthode 0D peut être utilisée par soit le calcul analytique de $\tau_{0D}$ et l'optimisation globale de $f_r$ ( méthode A), soit avec l'optimisation globale simultanée de $\tau_{0D}$ et $f_r$ (méthode B), soit avec l'optimisation globale de $\tau_{0D}$ et calcul local de $f_r$ (méthode C). De plus, la méthode 1D peut être utilisée avec l'identification des paramètres par optimisation globale simultanée de $\tau_{0D}$ et calcul local de $f_r$ (méthode D). Une étude quantitative entre les résultats de la simulation en l'espace-temps et les données expérimentales montre leur compatibilité et que l'utilisation de la méthode D augmente la précision sur les résultats, compte tenu de l'impact considérable de la diffusivité dans le phénomène d'auto-échauffement. Les résultats de cette partie du manuscrit montrent que la modélisation et la résolution en l'espace-temps garantissent la covariance des modèles thermiques qui est importante pour le couplage avec les comportements mécaniques. Cependant, la précision sur la variation de température en espace-temps n'est pas améliorée dans le cas où le temps est à l'échelle macroscopique ($\geq 1\mu s$).

Dans la seconde partie du manuscrit, l'objectif était d'obtenir des modèles covariants du comportement thermomécanique des matériaux. Des modèles Newtoniens des comportements élastiques, thermoélastiques, hyperélastiques et élastoplastiques ont été revus pour les petites et grandes déformations afin d'avoir des comportements de référence à comparer avec les modèles thermomécaniques spatio-temporels proposés ultérieurement.

L'approche thermodynamique prenant en compte la contribution des contraintes et les couplages thermomécaniques est utilisée pour construire les modèles dans le domaine d'espace-temps. Les lois covariantes de la thermodynamique ont d'abord été formulées. Les petites et grandes déformations obéissent à ces lois quel que soit le référentiel. Ces lois sont ensuite utilisées pour modéliser le comportement thermomécanique. Les modèles résultants sont covariants. L'utilisation de dérivées covariantes et du projecteur spatial dans la modélisation, permet d'obtenir des termes supplémentaires par rapport aux modèles équivalents Newtoniens. Certaines hypothèses ont été prises en compte: le couplage fort entre les comportements thermiques et mécaniques, le comportement isotrope des matériaux et le respect des lois d'équilibre thermodynamique. Le modèle thermo-hyperélastique spatio-temporel a été formulé sous ces hypothèses. La forme variationnelle correspondante a été formulée et mise en œuvre pour la simulation numérique dans le projet FEniCS.

Des tests de validation ont été menés. Les résultats montrent qu'à la limite non relativiste les modèles spatio-temporels et Newtoniens ont le même comportement pour les petites déformations. Cela signifie que les résultats de l'utilisation de modèles d'espace-temps convergent vers les résultats de l'utilisation de modèles de comportement classiques. Le modèle thermo-hyperélastique spatio-temporel a ensuite été utilisé pour simuler le comportement d'un élément bimétallique.

En résumé, la méthodologie décrite dans ce manuscrit permet d'écrire des modèles thermomécaniques covariants respectant le principe de causalité et les lois de la thermodynamique. Nous proposons, via cette approche, la possibilité de résoudre les problèmes rencontrés lors de la modélisation des problèmes thermiques [Straugham,2011, Auriault,2017, Cattaneo,1958, Christov,2009, Osborne,1950,

Vernotte,1961, Tavernier,1962, Chapman and Cowling,1970] et mécaniques [Valanis,1970, Lubliner,1984, Prasolov,1997, Wiechert,1893, Zener,1948, Oldroyd,1950, Wineman,2009, Mooney,1940, Rivlin,1948, Rivlin and Saunders,1951, Ogden,1984, Boyce and Arruda,2000, Steinmann et al.,2012].

Cela fait de la modélisation spatio-temporelle un sujet important à explorer et à développer. Par ailleurs, cette étude illustre bien la modélisation du comportement thermomécanique des matériaux pour de grandes déformations dans un domaine spatio-temporel, mais elle pose également la question de l'exhaustivité des hypothèses prises en compte et de leur mise en œuvre pour les simulations spatio-temporelles. C'est pourquoi les cas simulés dans cette étude sont limités à de petites déformations dans l'espace-temps.

Pour mieux comprendre les implications de ces résultats, de futures études pourraient aborder la simulation spatio-temporelle des applications pour les grandes déformations et estimer la valeur ajoutée de ce formalisme dans les cas critiques.

Nous avons également proposé dans le chapitre 5, la modélisation du processus de flexion des tubes qui inclut la modélisation des grandes déformations mais aussi du comportement dissipatif et de nombreux phénomènes critiques (ovalisation, retour élastique...). Dans ce manuscrit (Annexe C), le modèle élasto-plastique Newtonien a été étudié pour reproduire la réalité du processus. Pour la modélisation spatio-temporelle, sur une première estimation, uniquement le comportement hyperélastique a été pris en compte. Les modèles hyperélastiques Newtoniens et spatio-temporels représentant ce processus ont été écrits sous une forme variationnelle puis implémentés dans un script pour la résolution à l'aide de FEniCS project. Pour la simulation, ces deux modèles ont été comparés dans une résolution ne prenant en compte que les petites déformations. La simulation numérique prenant en compte les grandes déformations reste à étudier dans les prochaines recherches, ainsi que la modélisation générale et la simulation de la plasticité dans l'espace-temps.

# A Application of Newtonian elastic models for bending

As follows, we list the parameters and results of the numerical simulation of the Newtonian elastic behavior using a Hooke-like model for a beam under bending load.

## A.1 Description of the problem

Let us consider a beam geometry fixed at its left boundary and subjected to a bending load applied in the form of imposed displacement varying with time and space at the upper boundary $y = W$ (see Fig. 59). The expression of the displacement imposed in the $y$-direction is:

$$dep_y(t) = \frac{-T_M x^2}{24EIL}(x^2 - 4xL + 6L^2)\frac{t}{t_{max}} \tag{A.1}$$

where:

- $T_M$ is the equivalent linear load that has to be applied on the upper boundary of dimension $L$ to obtain an equivalent displacement constraint $dep_y(t)$, $T_M = 1.67 \times 10^{-5}\, kN.m^{-1}$ for this example
- $E$, $I$ are respectively the Young's modulus and second moment of area
- $t$ is the time varying between 0 and $t_{max}$. $t_{max}$ is the time at which the maximum loading is applied.

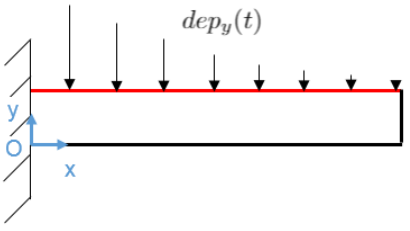


**Fig. 59:** Beam subjected to bending load.

Let us consider that the beam has the behavior of a Hooke-like model. We will investigate this model in case of elastacity (the weak integral form is given in Eq. 4.22), consequently we assume that the yield stress of the material is not reached. We will simulate a bending problem using small strain tensor (Eq. 4.2).

The model is constrained by:

- $\forall y \in \partial\omega_1, \forall t,\ f_{SC1} = dep(x = 0, y) = (0, 0)$ represents the clamped end.
- $\forall x \in \partial\omega_2, \forall t,\ f_{SC2} = dep(x, y = W) = (0, \frac{-T_M x^2}{24EIL}(x^2 - 4xL + 6L^2)\frac{t}{t_{max}})$ represents the displacement imposed on the upper boundary of the beam.

## A.2 Parameters for the numerical simulation

As follows are the input parameters of the numerical simulation of the Hooke-like model subjected to bending:

| | Parameter | Value |
|---|---|---|
| Geometry (beam) | Length | $L = 1\ (m)$ |
| | Width | $W = 0.01\ (m)$ |
| | Thickness | $H = 0.01\ (m)$ |
| Material | Young's modulus | $E = 250000\ (MPa)$ |
| | Poisson coefficient | $\nu = 0.$ (adim) |
| | Density | $\widetilde{\rho_c} = 7850\ (kg/m^3)$ |
| | Thermal expansion | $\alpha = 0\ (K^{-1})$ |
| | Thermal conductivity | $\lambda = 500000\ (w.m^{-1}.K^{-1})$ |
| | Specific heat capacity at 3D volume | $\mathcal{C}_{m\omega} = 520\ (J.kg^{-1}.K^{-1})$ |
| Mesh and time stepping | Number of nodes through the $x$-direction of space | $N_x = 210$ (adim) |
| | Number of nodes through the $y$-direction of space | $N_y = 10$ (adim) |
| | Number of loading steps | $N_{step} = 6$ (adim) |
| Loading | Time at which the maximum loading is applied | $t_{max} = 1\ (s)$ |
| | Volume force vector | $f_M = (0, 0)\ (N)$ |
| | Surface force vector | $T_M = (0, 0)\ (N)$ |

**Tab. 21:** Parameters of the numerical simulation for the beam subjected to bending

## A.3 Results of the simulation

The evolution of $\sigma_c^{11}$ along the $x$-direction at $y = W$ and $t = t_{max}$ is illustrated in Fig. 60. For verification, results are compared to the analytical solution deriving from the classical beam theory [Timoshenko,1953]:

$$\sigma_c^{11}(x, y, t)_{(sol)} = \left| \frac{W}{2I}(-T_M L x + 0.5 T_M L x^2 + 0.5 T_M L^2) \frac{t}{t_{max}} \right|_{y=W,\, t=t_{max}} . \tag{A.2}$$

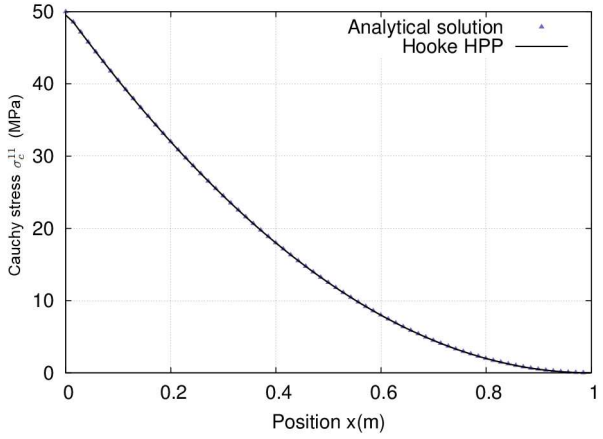


**Fig. 60:** Evolution of $\sigma_c^{11}(x, y, t)$ obtained from analytical solution ($\sigma_c^{11} = E\chi(t_{max})$ and Newtonian simulation as function of the space in the $x$-direction at $y = W$ and $t = t_{max}$.

The evolution of $\sigma_c^{11}$ along the $y$-direction at $x = L/2$ and $t = t_{max}$ is illustrated in Fig. 61. Results are compared to the analytical solution deriving from the classical beam theory [Timoshenko,1953]:

$$\sigma_c^{11}(x, y, t)_{(sol)} = \left| \frac{W}{2I}(-T_M L x + 0.5 T_M L x^2 + 0.5 T_M L^2)\,(y - W/2) \frac{t}{t_{max}} \right|_{x=L/2,\, t=t_{max}} \tag{A.3}$$

where $0 \leq y \leq W$.

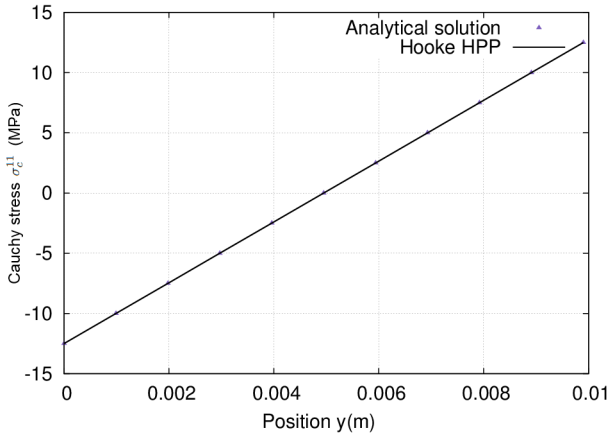


**Fig. 61:** Evolution of $\sigma_c^{11}(x, y, t)$ obtained from analytical solution ($\sigma_c^{11} = E\chi(t_{max})$ and Newtonian simulation as function of the space in the $y$-direction at $x = L/2$ and $t = t_{max}$.

The linear character of variation of $\sigma_c^{11}$ along the $y$-direction is guaranteed in the numerical simulation. Graphs obtained from analytical solutions and Newtonian simulations superimpose.

The evolution of $\sigma_c^{11}$ in function of the loading time at $x = L/2$ and $y = W$ is illustrated in Fig. 62. $\sigma_c^{11}$ vary linearly with time at this space position. This corresponds to the linear variation of the applied displacement in time through the stretch that varies linearly with time.

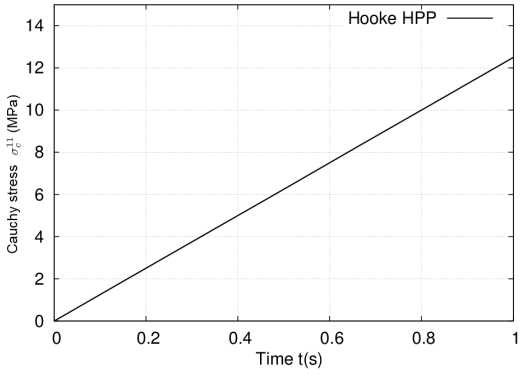


**Fig. 62:** Evolution of $\sigma_c^{11}(x, y, t)$ obtained from Newtonian simulation as function of the time at $x = L/2$ and $y = W$.

The error and percentage of error on $\sigma_c^{11}$ obtained of the numerical solution compared to the analytical solution are respectively around $0.0014\,MPa$ and $0.001\,\%$.

# B Applications of spacetime thermo-hyperelastic models

## B.1 Numerical simulation of the spacetime thermo-hyperelastic behavior using a Hooke-like model: beam under bending load

The problem is the same as the one described in section A.1 except that here the numerical resolution is in the spacetime domain. The thermal expansion is also considered to be null in order to test the decoupled mechanical problem.

Let us consider that the beam has the behavior of a Hooke-like model. We will investigate this model in case of hyperelasticity (the weak integral form is given in Eq. 5.86), consequently we assume that the yield stress of the material is not reached (besides the deformations are considered small). We will simulate a bending problem using small strain (Eq. 4.2).

The model is constrained by:

- $\forall y \in \partial\omega_1, \forall t,\ f_{SC1} = dep(x = 0, y, t) = (0, 0)$ represents the clamped end.
- $\forall x \in \partial\omega_2, \forall t,\ f_{SC2} = dep(x, y = W, t) = (0, \frac{-T_M x^2}{24EIL}(x^2 - 4xL + 6L^2)\frac{t}{t_{max}})$ represents the displacement imposed on the upper boundary of the beam.
- $\forall x, \forall y,\ f_{TC1} = dep(x, y, t = 0) = (0, 0)$ represents the initial condition on the displacement.
- $\forall x, \forall y,\ f_{TC2} = \theta(x, y, t = 0) = \theta_0 = 0\,°C$ represents the initial condition on the temperature ($\theta_0$ is the initial temperature considered as reference temperature).

The parameters for the numerical simulation are the same as in section A.2.

## B.2 Results of the simulation

The evolution of $\sigma_c^{11}$ along the $x$-direction at $y = W$ and $t = t_{max}$ is illustrated in Fig. 63. For verification, results are compared to the analytical solution (Eq. A.2) deriving from the classical beam theory [Timoshenko,1953].

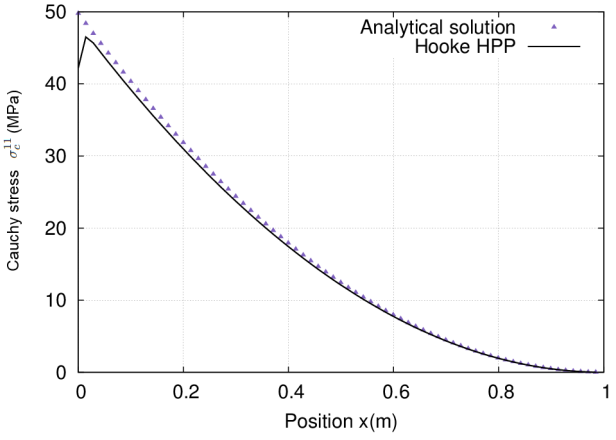


**Fig. 63:** Evolution of $\sigma_c^{11}(x, y, t)$ obtained from analytical solution and spacetime simulation as function of the space in the $x$-direction at $y = W$ and $t = t_{max}$.

The error and percentage of error on $\sigma_c^{11}$ obtained of the numerical solution compared to the analytical solution are respectively around $0.309\,MPa$ and $0.416\,\%$, which are acceptable differences mainly deriving form border effects. This can be observed by comparing the evolution of $\sigma_c^{11}$ along the $x$-direction at $y = W$

for different time values $t = t_{max}/6$, $t_{max}/2$, $5 * t_{max}/6$, $t_{max}$ (Fig. 64). Borders effects are limited at small positions $x$ for small times $t$.

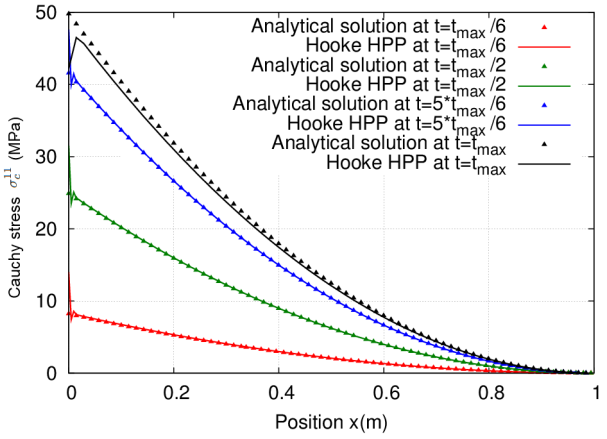


**Fig. 64:** Evolution of $\sigma_c^{11}(x, y, t)$ obtained from analytical solution and spacetime simulation as function of the space in the $x$-direction at $y = W$ and respectively $t = t_{max}/6$, $t_{max}/2$, $5 * t_{max}/6$, $t_{max}$.

The evolution of $\sigma_c^{11}$ along the $y$-direction at $x = L/2$ and $t = t_{max}$ is illustrated in Fig. 65. Results are compared to the analytical solution (Eq. A.3) deriving from the classical beam theory [Timoshenko,1953].

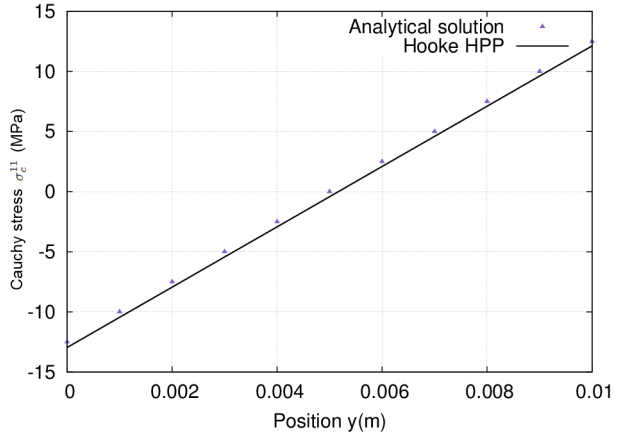


**Fig. 65:** Evolution of $\sigma_c^{11}(x, y, t)$ obtained from analytical solution and spacetime simulation as function of the space in the $y$-direction at $x = L/2$ and $t = t_{max}$.Note that the origin in the $y$-direction is the lower boundary of the beam.

The linear character of variation of $\sigma_c^{11}$ along the $y$-direction is guaranteed in the numerical simulation. However, a slight difference between results is observed: this can be related to the choice of meshing along this direction and the border effects earlier discussed (Fig. 64).

The evolution of $\sigma_c^{11}$ and $\Delta\theta$ along the $t$-direction at $x = L/2$ and $y = W$ are illustrated in Figs. 66 a) and b). $\sigma_c^{11}$ vary linearly with time at this space position except at the upper boundary (loss of linearity on the boundary). This corresponds to the linear variation of the applied displacement in time. $\Delta\theta$ is constant and null since the load applied to the beam is purely mechanical ($\alpha = 0$) and the deformations are small.

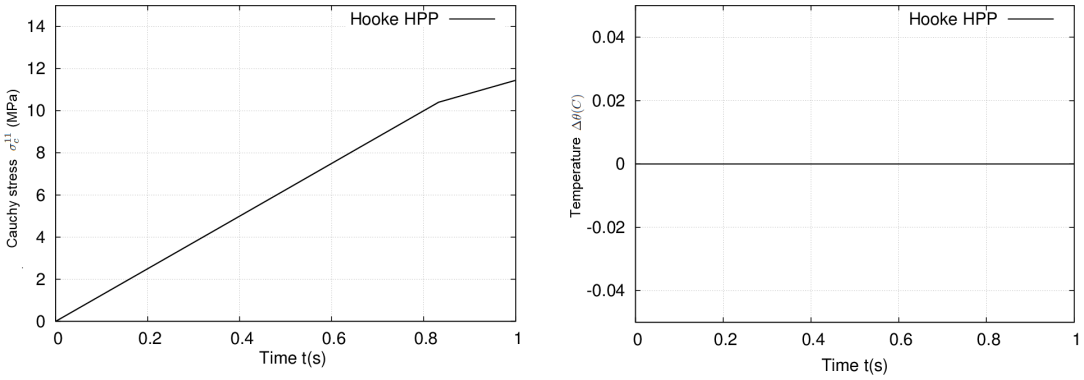


**Fig. 66:** On the left: Evolution of $\sigma_c^{11}(x, y, t)$ obtained from spacetime simulation as function of the time at $x = L/2$ and $y = W$. On the right: Evolution of $\Delta\theta(x, y, t)$ obtained from spacetime simulation as function of the time at $x = L/2$ and $y = W$.

## B.3 Testing of the spacetime thermo-hyperelastic model under pure thermal constraints

### B.3.1 Case when thermal expansion is null

The parameters of the numerical simulation are the same as in table 21. No mechanical displacement is applied to the beam but a thermal variation is applied to the right boundary.

Then the model is constrained by:

- $\forall y \in \partial\omega_1, \forall t,\ f_{SC1} = dep(x = 0, y, t) = (0, 0)$ represents the clamped end.
- $\forall x \in \partial\omega_2, \forall t,\ f_{SC2} = \theta(x, y = W, t) = 100\,t + \theta_0$, where $\theta_0$ is the initial temperature (considered as reference temperature). $f_{SC2}$ represents the applied temperature on the upper boundary of the beam.
- $\forall x, \forall y,\ f_{TC1} = dep(x, y, t = 0) = (0, 0)$ represents the initial condition on the displacement.
- $\forall x, \forall y,\ f_{TC2} = \theta(x, y, t = 0) = \theta_0 = 0\,°C$ represents the initial condition on the temperature.

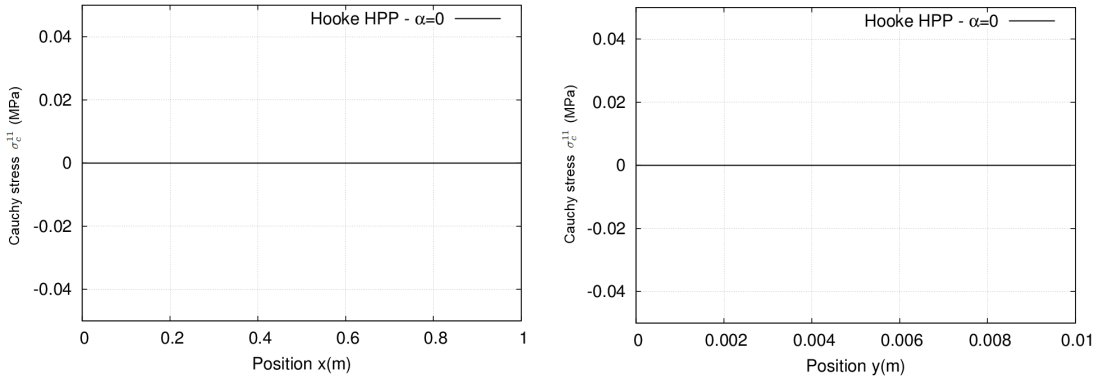


**Fig. 67:** On the left: Evolution of $\sigma_c^{11}(x, y, t)$ obtained from spacetime simulation as function of the space in the $x$-direction at $y = W/2$ and $t = t_{max}$. On the right: Evolution of $\sigma_c^{11}(x, y, t)$ obtained from spacetime simulation as function of the space in the $y$-direction at $x = L/2$ and $t = t_{max}$.

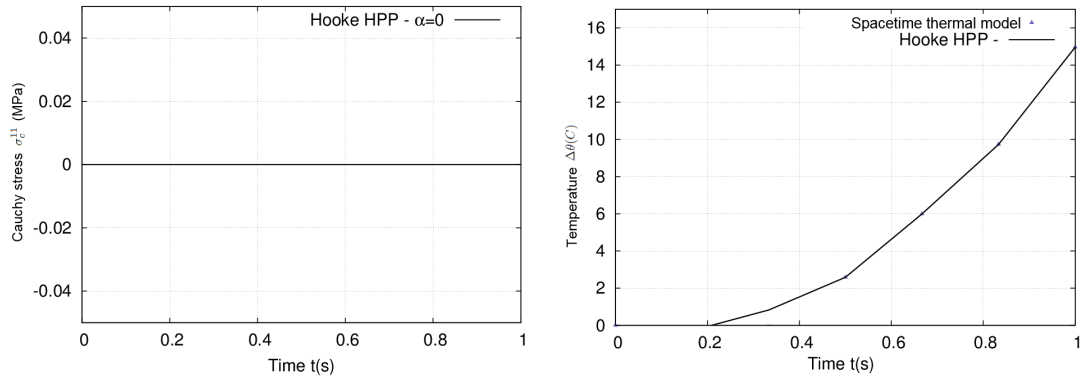


**Fig. 68:** On the left: Evolution of $\sigma_c^{11}(x, y, t)$ obtained from spacetime simulation as function of the time at $x = L/2$ and $y = W/2$. On the right: Evolution of $\Delta\theta(x, y, t)$ obtained from spacetime simulation of the purely thermal model (Eq. 2.52) and spacetime simulation as function of the time at $x = L/2$ and $y = W/2$.

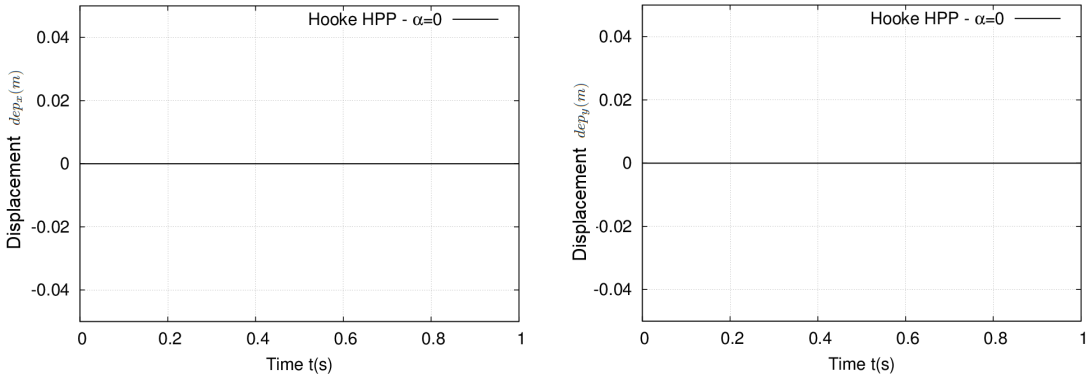


**Fig. 69:** On the left: Evolution of $dep_x(x, y, t)$ obtained from spacetime simulation as function of the time at $x = L/2$ and $y = W/2$. On the right: Evolution of $dep_y(x, y, t)$ obtained from spacetime simulation as function of the time at $x = L/2$ and $y = W/2$.

As expected, the components of stress and displacement are null since the thermal expansion is null. The problem is purely thermal.

### B.3.2 Case when thermal expansion is not null

The parameters of the numerical simulation are the same as in table 21 except that the thermal expansion is not null ($\alpha = 13 \times 10^{-6}\, K^{-1}$) . No mechanical displacement is applied to the beam but a thermal variation is applied to the right boundary. Then the model is constrained by the same boundary conditions mentioned in section B.3.1.

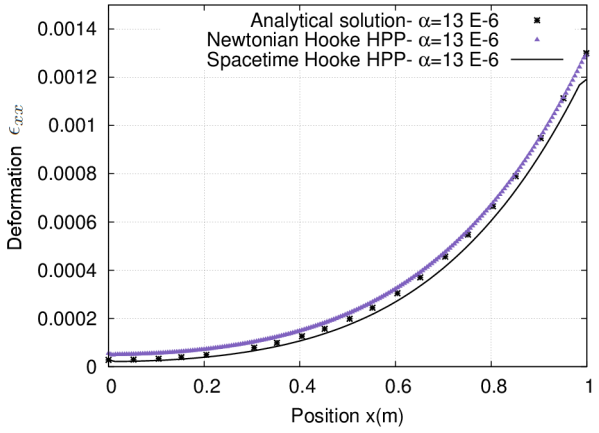


**Fig. 70:** Evolution of the thermal strain $\epsilon_{xx}$ obtained from analytical solution ($\epsilon_{xx} = \alpha\Delta\theta$), Newtonian simulation (using Eq. 4.28)and spacetime simulation (using Eq. 5.86) as function of the space in the $x$-direction at $y = W/2$ and $t = t_{max}$. bote that the exponential variation of thermal strain is a result of the exponential variation of temperature as function of the time.

The first component of stress due to thermal expansion is investigated:

$$\sigma^{11}_{TH}(x, y, t) = -\kappa\Delta\theta g^{11} \tag{B.1}$$

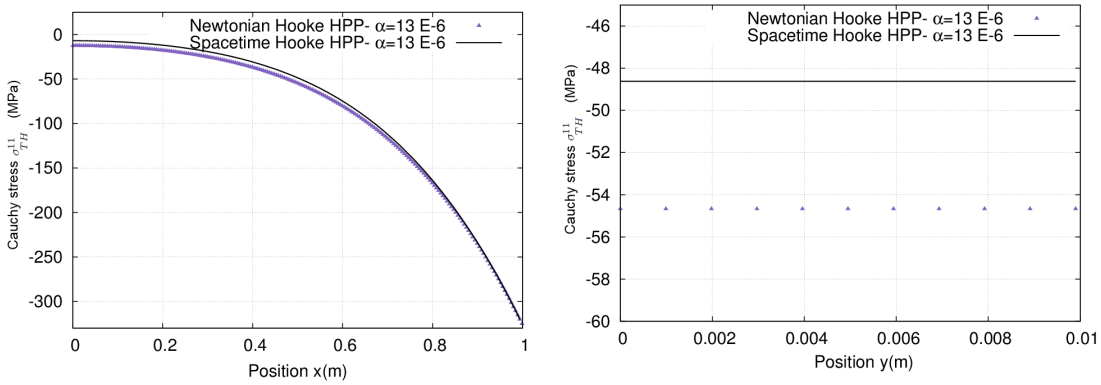


**Fig. 71:** On the left: Evolution of $\sigma^{11}_{TH}(x, y, t)$ obtained from Newtonian and spacetime simulations as function of the space in the $x$-direction at $y = W/2$ and $t = t_{max}$. On the right: Evolution of $\sigma^{11}_{TH}(x, y, t)$ obtained from Newtonian and spacetime simulations as function of the space in the $y$-direction at $x = L/2$ and $t = t_{max}$.

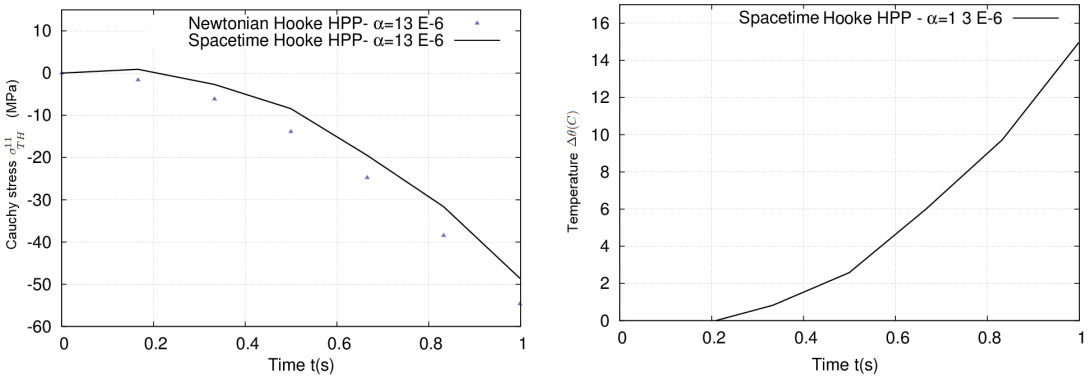


**Fig. 72:** On the left: Evolution of $\sigma_{TH}^{11}(x,y,t)$ obtained from Newtonian and spacetime simulations as function of the time at $x = L/2$ and $y = W/2$. On the right: Evolution of $\Delta\theta(x,y,t)$ obtained from Newtonian and spacetime simulations as function of the time at $x = L/2$ and $y = W/2$. Note that the analytical result is closer to the spacetime solution $(\sigma_{TH}^{11}(x = 0.5, y, t = t_{max}) = -\kappa\Delta\theta g^{11} = -3.25 * 14.95 = -48.58\, MPa)$. The error on $\sigma_{TH}^{11}(x,y,t)$ between the Newtonian and spacetime approaches is $7.22\%$

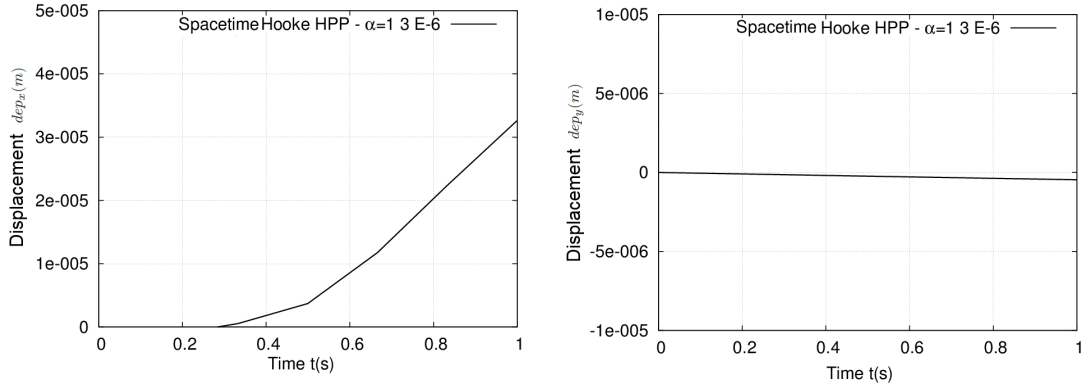


**Fig. 73:** On the left: Evolution of $dep_x(x,y,t)$ obtained from spacetime simulation as function of the time at $x = L/2$ and $y = W/2$. On the right: Evolution of $dep_y(x,y,t)$ obtained from spacetime simulation as function of the time at $x = L/2$ and $y = W/2$.

## B.4 Testing of the spacetime thermo-hyperelastic model under pure mechanical constraints (sinusoidal load)

The parameters of the numerical simulation are the same as in table 21 except that the thermal expansion is not null ($\alpha = 13 \times 10^{-6}\, K^{-1}$) . No thermal load is applied to the beam but a displacement (sinusoidal in time) is applied to the right boundary.

Then the model is constrained by:

- $\forall y \in \partial\omega_1, \forall t,\ f_{SC1} = dep(x = 0, y, t) = (0, 0)$ represents the clamped end.
- $\forall y \in \partial\omega_2, \forall t,\ f_{SC2} = dep(x = L, y, t) = (sin(\frac{\pi}{4}\, t), 0)$.
- $\forall x, \forall y,\ f_{TC1} = dep(x, y, t = 0) = (0, 0)$ represents the initial condition on the displacement.
- $\forall x, \forall y,\ f_{TC2} = \theta(x, y, t = 0) = \theta_0 = 293\,°C$ represents the initial condition on the temperature ($\theta_0$ is the initial temperature considered as reference temperature).

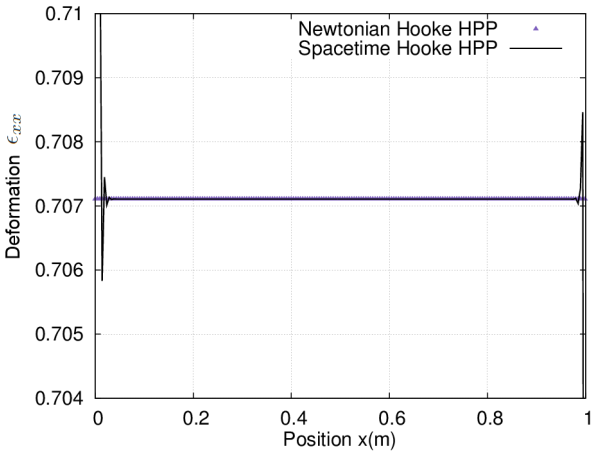


**Fig. 74:** Evolution of the total strain $\epsilon_{xx}$ obtained Newtonian simulation and spacetime simulation as function of the space in the $x$-direction at $y = W/2$ and $t = t_{max}$. We note the presence of oscillations of the value of deformation near the borders which can be related to border effects.

The first component of stress due to thermal expansion $\sigma^{11}_{TH}(x, y, t)$ is investigated.

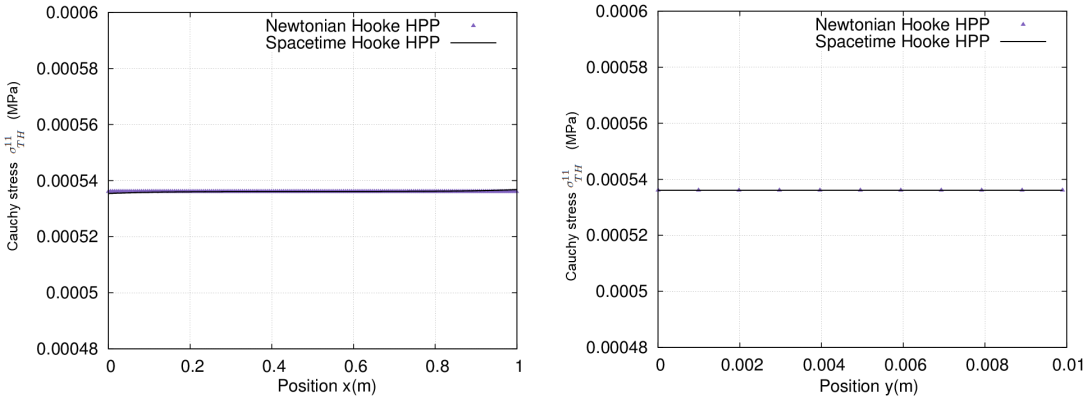


**Fig. 75:** On the left: Evolution of $\sigma^{11}_{TH}(x, y, t)$ obtained from Newtonian and spacetime simulations as function of the space in the $x$-direction at $y = W/2$ and $t = t_{max}$. On the right: Evolution of $\sigma^{11}_{TH}(x, y, t)$ obtained from spacetime simulation as function of the space in the $y$-direction at $x = L/2$ and $t = t_{max}$.

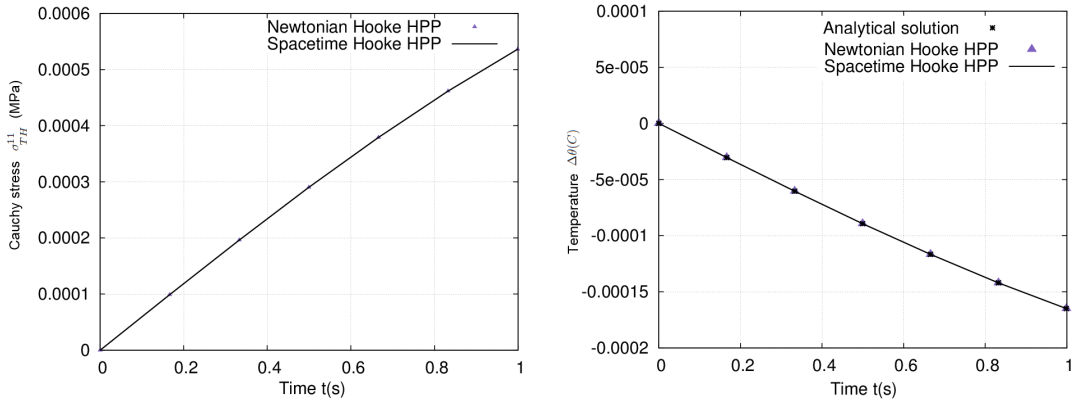


**Fig. 76:** On the left: Evolution of $\sigma^{11}_{TH}(x, y, t)$ obtained from Newtonian and spacetime simulation as function of the time at $x = L/2$ and $y = W/2$. On the right: Evolution of $\Delta\theta(x, y, t)$ obtained from the analytical solution, Newtonian and spacetime simulation as function of the time at $x = L/2$ and $y = W/2$. This result is compatible with the analytical solution: $ln(\theta) = ln(\theta_0) - \frac{3\alpha}{\widetilde{\rho_c} c_{m,\omega}} tr(\epsilon)$. At $t_{max}$, the analytical solution gives: $\Delta\theta = 293 - 292.999835 = -1.64 \times 10^{-4} K$.

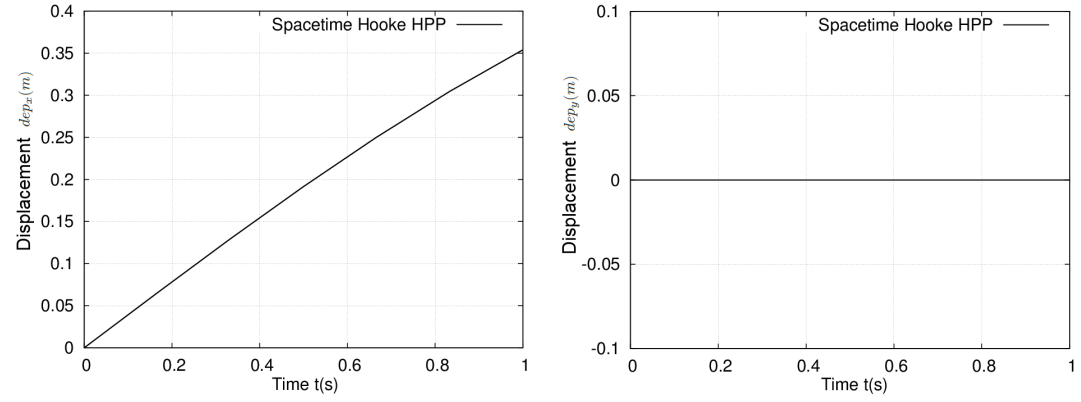


**Fig. 77:** On the left: Evolution of $dep_x(x, y, t)$ obtained from spacetime simulation as function of the time at $x = L/2$ and $y = W/2$. On the right: Evolution of $dep_y(x, y, t)$ obtained from spacetime simulation as function of the time at $x = L/2$ and $y = W/2$.

We further observed this model's behavior for a time period $t_{max} = 8s$ corresponding to one period of the sine. We increase the number of loading steps for this purpose to $N_{step} = 18$ in order to have a better precision on time. The sinusoidal character of the displacement imposed leads to a sinusoidal variation of $\sigma^{11}_{TH}(x, y, t)$, $\Delta\theta(x, y, t)$ and $dep_x(x, y, t)$. We note that the variation of $dep_x(x, y, t)$ and $\sigma^{11}_{TH}(x, y, t)$ are in phase in time, while $\Delta\theta(x, y, t)$ is phase shifted of $\pi$ because of the negative sign of Eq. B.1.

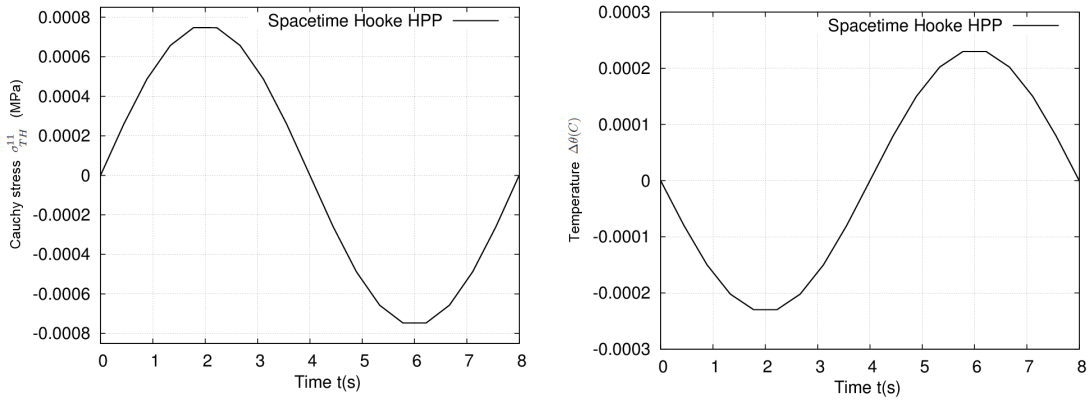


**Fig. 78:** On the left: Evolution of $\sigma^{11}_{TH}(x, y, t)$ obtained spacetime simulation as function of the time at $x = L/2$ and $y = W/2$. On the right: Evolution of $\Delta\theta(x, y, t)$ obtained from spacetime simulation as function of the time at $x = L/2$ and $y = W/2$.

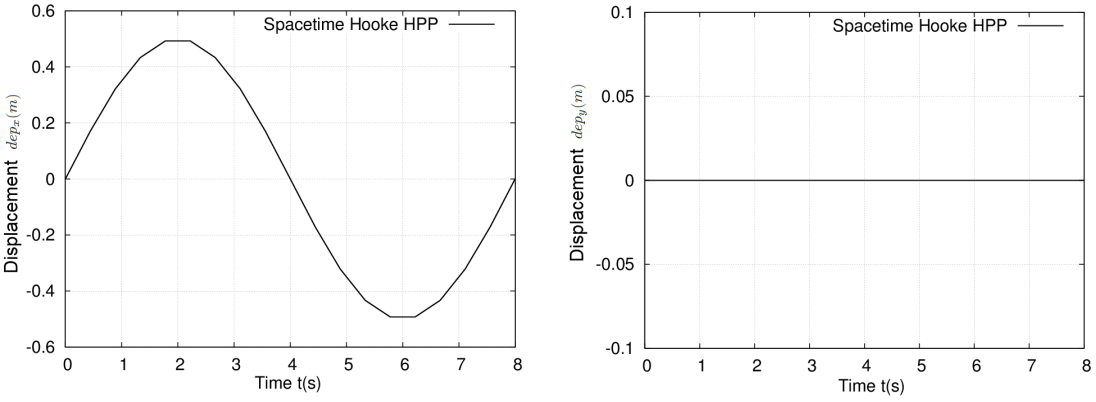


**Fig. 79:** On the left: Evolution of $dep_x(x, y, t)$ obtained from spacetime simulation as function of the time at $x = L/2$ and $y = W/2$. On the right: Evolution of $dep_y(x, y, t)$ obtained from spacetime simulation as function of the time at $x = L/2$ and $y = W/2$.

# C On the modeling of the tube bending process

## C.1 Components of the bending system

As discussed in section 5.10, the components of the bending system determine the boundary conditions of the model. This is why in this section the role of the components is described. Among the bending methods, we choose to describe the rotary draw bending [Tingley,2001]. Five main parts can be differentiated in this type of machinery. The first three components are necessary to make the bend: the bend die, the clamp die and the pressure die (Fig. 80). The bend die is the tool to make a specific radius of bend. The clamp die's function is to ensure that the tube is clamped on the bend die. It is consequently a helping component to the bend die. It moves in and out to allow the feeding of the tube. The pressure die also called the support presses the tube against the bend die through the process of bending. Hence, it moves with the tube as it is formed.

The other two are used in some cases where there is a probability of wrinkling or section collapse [Johansson,2011]. These are the mandrel and the wiper (Fig. 80).

When the radius of the bend is relatively small and/or the wall of the tube is relatively thin, the wiper die is used to prevent wrinkles and a ball mandrel supports the inner radius of bend thus preventing the flattening and the wrinkling of the tube. The mandrel is a fixed component. The balls are used to prevent the collapse of the tube after leaving the mandrel. We note that booster can be also placed: its function is to apply an assist-pressure to both sides of the tube which helps pushing the tubing material through the point of bend. Consequently, it helps the bending process. Figure 80 illustrates the different parts of the rotary bending machine.

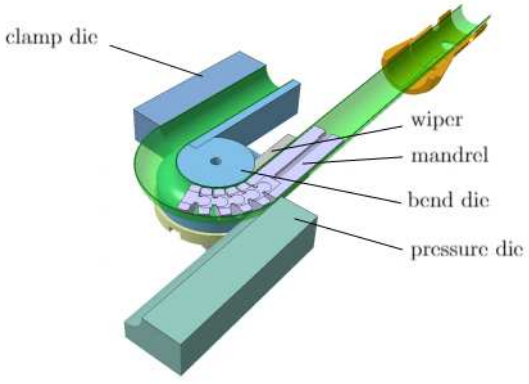


**Fig. 80:** Components of a tube draw bender [Johansson,2011]

## C.2 Description of the problem for Newtonian elastic and hyperelastic models

We first look to model the elastic and hyperelastic behaviors of a beam subjected to rotary bending consequently we assume that the yield stress of the material is not reached. For this purpose, let us consider a beam geometry clamped at its left boundary and subjected to bending loads applied to its upper, lower and right boundaries in the form of imposed displacement.

The imposed displacement is chosen such that the final geometry of the beam is semi-circular and clamped to the bend die.

Let us consider that the beam has the behavior of a Hooke-like model. We will investigate this model in case of elasticity (Eq. 4.21) and hyperelasticity (Eq. 4.34). We assume that in these simulations the material

yield strength is not reached. Then for each case, we will simulate bending using small strain (Eq. 4.2), Green-Lagrange strain (Eq. 4.5) and Euler-Almansi strain (4.8).

These models will be compared to spacetime thermo-hyperelastic models.

## C.3 Boundary conditions corresponding to the tube bending system

The model corresponds to a 2D beam subjected to four Dirichlet boundary conditions (Figure 81):

- The left boundary $\Gamma_1$ is clamped
- The lower boundary $\Gamma_2$ is subjected to a displacement corresponding to the bent profile of the beam $\Gamma_2'$. It represents the contact between the bend die and the lower boundary and it specifies the bend radius.
- The upper boundary $\Gamma_3$ is subjected to a displacement corresponding to the bent profile of the beam $\Gamma_3'$. It represents the pressure that the pressure die applies on the upper boundary.
- The right boundary $\Gamma_4$ is subjected to a displacement corresponding to the bent profile of the beam $\Gamma_4'$. It represents the effect of the clamped die which keeps the beam against the bend die.
- At the initial time, the displacement is null for every point of the beam

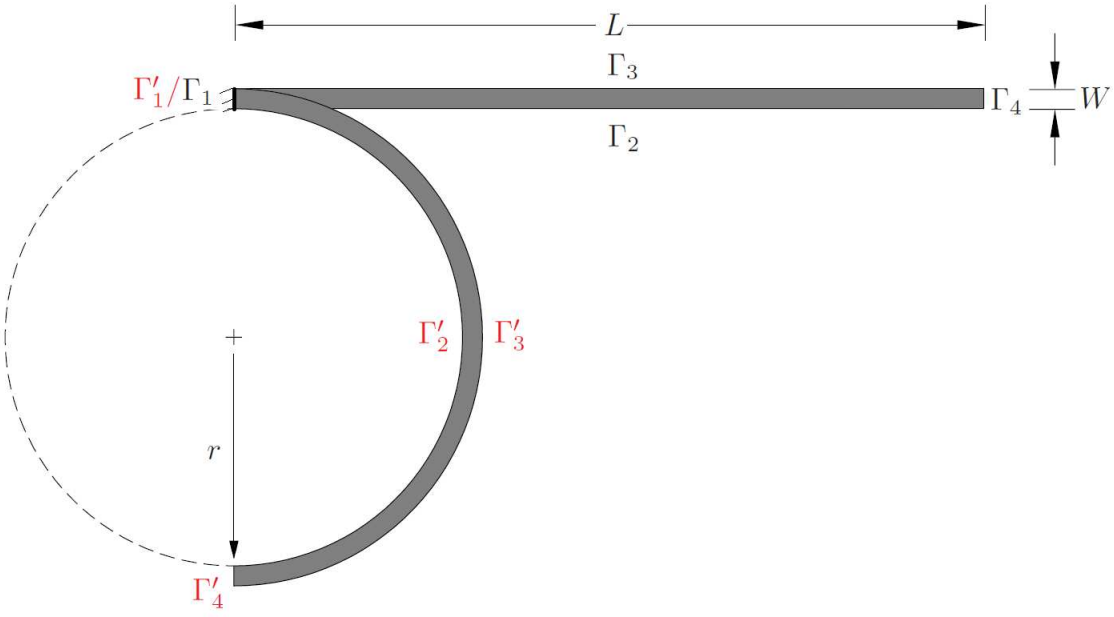


**Fig. 81:** Initial and final configurations of the bent beam

In order to find the values of the increment of displacement $\Delta dep(z^1, z^2, t)$ applied at each boundary, the following methodology, illustrated in the case of the lower boundary, is used:

1. Let $R$ be the frame corresponding to the initial configuration and $R'$ the frame corresponding to the final configuration (bent beam). Let $[z^1, z^2]$ be the spatial components in $(R)$ at a time $t$. And let $[z'^1, z'^2]$ be the spatial components in $(R')$ at a time $t$.
2. In the final configuration, the lower boundary $\Gamma_2$ describes a semicircle of equation: $\left(z'^1\right)^2 + \left(z'^2 - r\right)^2 = r^2$, where $r$ is the bend radius equal to $\dfrac{L}{\pi}$ so that the perimeter of the semicircle is equal to the length of the beam.

3. Then $z'^1$, $z'^2$ are expressed in function of $z^1$, $z^2$ respectively. For the lower boundary, $z'^1$ and $z^1$ are related by the equation of an ellipse centered at $(L/2, 0)$ with width $L/2$ and height $r$: $\frac{(z^1 - L/2)^2}{(L/2)^2} + \frac{\left(z'^1\right)^2}{r^2} = 1$. This leads to: $z'^1 = r\sqrt{1 - \frac{(z^1 - L/2)^2}{(L/2)^2}}$. Moreover, for the lower boundary, $z'^2$ and $z^2$ are related by a linear relationship: $z'^2 = \frac{-2\,r}{L} z^2$.
4. Then the imposed displacement can be calculated for each boundary using: $\forall t,\ dep(z^1, z^2) = \big((z'^1 - z^1)t, (z'^2 - z^2)t\big)$.
   For the lower boundary, $\forall t,\ dep(z^1, z^2 = 0) = \left((r\sqrt{1 - \frac{(z^1 - L/2)^2}{(L/2)^2}} - z^1)t, (\frac{-2\,r}{L} z^2)t\right)$

The same methodology is applied to determine the imposed increment of displacement on the upper boundary $\Gamma_3$: The equations obtained for the lower boundary remain valid, however in this case $r$ is replaced by $(r + W)$ where $W$ is the width of the beam. Concerning the right boundary $\Gamma_4$: $z'^1 = 0$ and $z'^2 = -2\,r - z^2$. This leads to $dep(z^1 = L, z^2) = (-L, -2r - 2z^2)$.

The boundary conditions for this problem can be written: $f_{SC}(z^i \in \partial\Omega) = dep(z^i \in \partial\Omega, t)$, where $f_{SC}$ is the function representing the space boundary conditions.

Consequently, all the models are constrained by:

- $\forall z^2, \forall t,\ f_{SC1} = dep(z^1 = 0, z^2) = (0, 0)$ on $\Gamma_1$.
- $\forall z^1, \forall t,\ f_{SC2} = dep(z^1, z^2 = 0) = \left((r\sqrt{1 - \frac{(z^1 - L/2)^2}{(L/2)^2}} - z^1)t, (\frac{-2\,r}{L} z^2)t\right)$ on $\Gamma_2$.
- $\forall z^1, \forall t,\ f_{SC3} = dep(z^1, z^2 = W) = \left(((r + W)\sqrt{1 - \frac{(z^1 - L/2)^2}{(L/2)^2}} - z^1)t, (\frac{-2\,(r + W)}{L} z^2)t\right)$ on $\Gamma_3$.
- $\forall z^2, \forall t,\ f_{SC4} = dep(z^1 = L, z^2) = \big(-Lt, (-2r - 2z^2)t\big)$ on $\Gamma_4$.

## C.4 Weak integral form of the problem for Newtonian elastic and hyperelastic models and parameters of the numerical simulation of the bending behavior

In order to implement this example for simulation using FEniCS project, we need to determine the weak integral forms related to the behaviors simulated and the corresponding boundary conditions. Eqs. 4.22, 4.23 and 4.24 represent the weak integrals forms of elastic models using respectively small strain, Green-Lagrange strain and Euler-Almansi strain.

Eq. 4.34 represents the weak integral form together with Eq. 4.35, where the $strain^{ij}$ tensor is respectively replaced with the corresponding type of strain (Eqs. 4.2,4.5 and 4.8) to obtain hyperelastic models using respectively small strain, Green-Lagrange strain and Euler-Almansi strain.

In this manuscript, we will consider the case of a mild steel beam subjected to bending for numerical simulations. As follows are the input parameters of the numerical simulation of the Hooke-like model subjected to bending:

| | Parameter | Value |
|---|---|---|
| Geometry (beam) | Length | $L = 188\ (mm)$ |
| | Width | $W = 3\ (mm)$ |
| | Thickness | $H = 3\ (mm)$ |
| Material (Mild steel) | Young's modulus | $E = 200000\ (MPa)$ |
| | Poisson coefficient | $\nu = 0.303$ (adim) |
| | Density | $\widetilde{\rho_c} = 7850E^{-9}\ (kg/mm^3)$ |
| Mesh and time stepping | Number of nodes through the $z^1$-direction of space | $N_1 = 100$ (adim) |
| | Number of nodes through the $z^2$-direction of space | $N_2 = 10$ (adim) |
| | Number of loading steps | $N_{step} = 1$ (adim) |
| Loading | Time at which the maximum loading is applied | $t_{max} = 1\ (s)$ |
| | Volume force vector | $f = (0, 0)\ (N)$ |
| | Surface force vector | $T = (0, 0)\ (N)$ |

**Tab. 22:** Parameters of the numerical simulation for the beam subjected to bending

## C.5 Numerical simulation of the bending behavior using Newtonian elastic and hyperelastic models using FEniCS project

Fig. 82 shows the result of evolution of $\sigma_{VM}$ at the upper boundary of the beam, as a function of space for Newtonian elastic models (function of small deformation, Green-Lagrange large deformation and Euler-Almansi large deformation) and the hyperelastic model space for Newtonian elastic models (function of small deformation and Green-Lagrange large deformation).

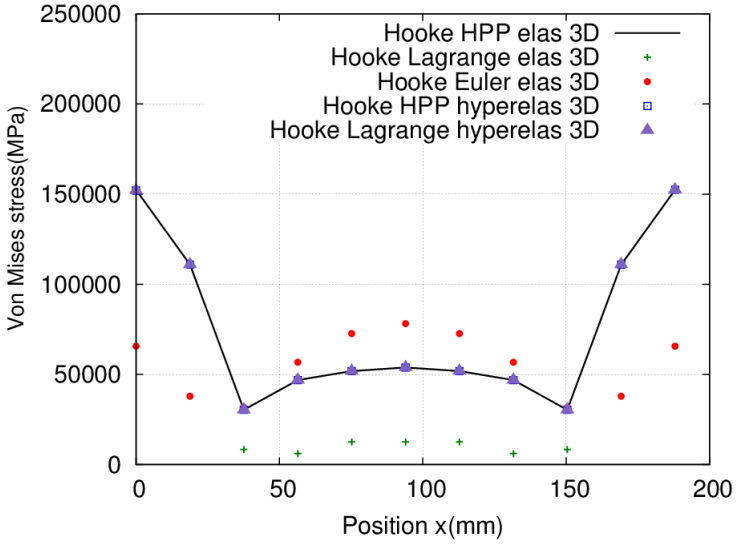


**Fig. 82:** The variation of $\sigma_{VM}$ as a function of space for a bended beam for different Newtonian elastic and hyperelastic models examined.

We notice that $\sigma_{VM}$ is nearly constant along the upper boundary of the beam. This a satisfying result since the bending moment along the beam is expected to be constant, hence a constant stress is expected along the beam. We also notice the existence of a border effect near the left and right boundary. This may be improved by a mesh refinement near the borders (see section C.6).

For Newtonian elastic and hyperelastic models using small deformation $\sigma_{VM}$ is around $53814\,MPa$. For Newtonian elastic and hyperelastic models using Euler-Almansi large deformation it is around $78131\,MPa$. For the Newtonian elastic model using Green-Lagrange large deformation, it is around $12539\,MPa$. For the Newtonian hyperelastic model using Green-Lagrange large deformation, it is around $12539,3\,MPa$.

We remind that at this stage, the yield stress is not taken into consideration which explains the large values of stress obtained. These results will serve to value the use of a spacetime approach comparing to the use of Newtonian approach.

## C.6 Numerical simulation of the bending behavior using the Newtonian elasto-plastic model: description of the problem, weak integral form and boundary conditions

Even though the spacetime modeling will be limited to the study of the elastic behavior in small deformations, we will study the Newtonian elasto-plastic model of the tube bending process to illustrate the reality of process.

In order to implement this example for simulation using FEniCS project, we need to determine the weak integral forms related to the behaviors simulated and the corresponding boundary conditions.

Eq. 4.40 represents the weak integral form, where the $strain^{ij}$ tensor is replaced respectively with the small strain and Euler-Almansi strain (Eqs. 4.2 and 4.8).

The boundary conditions for this problem can be written: $f_{SC}(z^i \in \partial\Omega) = \Delta dep(z^i \in \partial\Omega, t)$, where $f_{SC}$ is the function representing the space boundary conditions.

Consequently, all the models are constrained by:

- $\forall z^2, \forall t,\ f_{SC1} = \Delta dep(z^1 = 0, z^2) = (0,0)$ on $\Gamma_1$.
- $\forall z^1, \forall t,\ f_{SC2} = \Delta dep(z^1, z^2 = 0) = (r\sqrt{1 - \frac{(z^1 - L/2)^2}{(L/2)^2}} - z^1, \frac{-2\,r}{L}z^2)$ on $\Gamma_2$.
- $\forall z^1, \forall t,\ f_{SC3} = \Delta dep(z^1, z^2 = W) = \left((r+W)\sqrt{1 - \frac{(z^1 - L/2)^2}{(L/2)^2}} - z^1, \frac{-2\,(r+W)}{L}z^2\right)$ on $\Gamma_3$.
- $\forall z^2, \forall t,\ f_{SC4} = \Delta dep(z^1 = L, z^2) = (-L, -2r - 2z^2)$ on $\Gamma_4$.

The same parameters of geometry, mesh, time stepping, volume and surface force vectors mentioned in section C.4 are used for the numerical simulation of the model. However, the material has an elasto-plastic behavior with linear isotropic hardening characterized by: a yield stress $\sigma_0 = 370\,MPa$ and a hardening modulus $H = 200\,MPa$.

Fig. 83 shows the evolution of the von Mises stress $\sigma_{VM}$ at the upper boundary of the beam, as a function of space for Newtonian plastic models (function of small deformation and Euler-Almansi large deformation) at $t_{max}$.

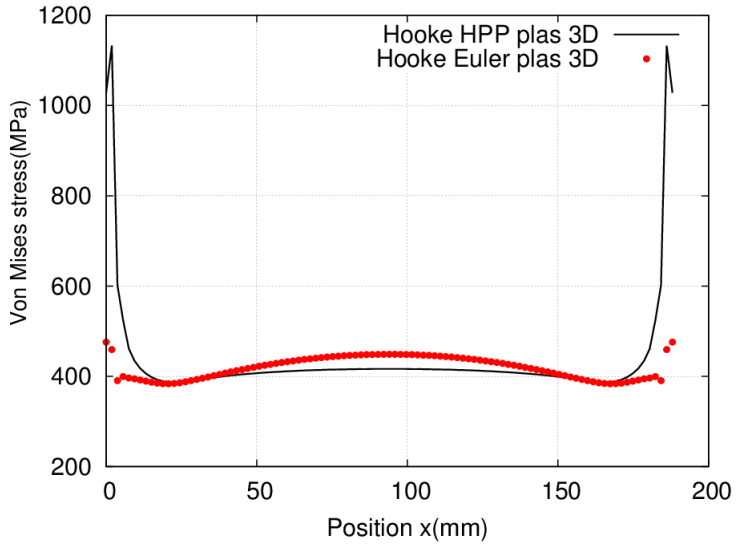


**Fig. 83:** The variation of $\sigma_{VM}$ at $t_{max}$ as a function of space at the upper boundary of a beam subjected to bending for different Newtonian plastic models examined.

Fig. 84 shows the evolution of equivalent plastic strain $PEEQ = \sqrt{\frac{4}{3}e^{ij}e_{ij}}$ [Chen and Han,1988], where $e^{ij}$ is the deviatoric part of $strain_P^{ij}$ at the upper boundary of the beam, as a function of space for Newtonian plastic models (function of small deformation and Euler-Almansi large deformation) at $t_{max}$.

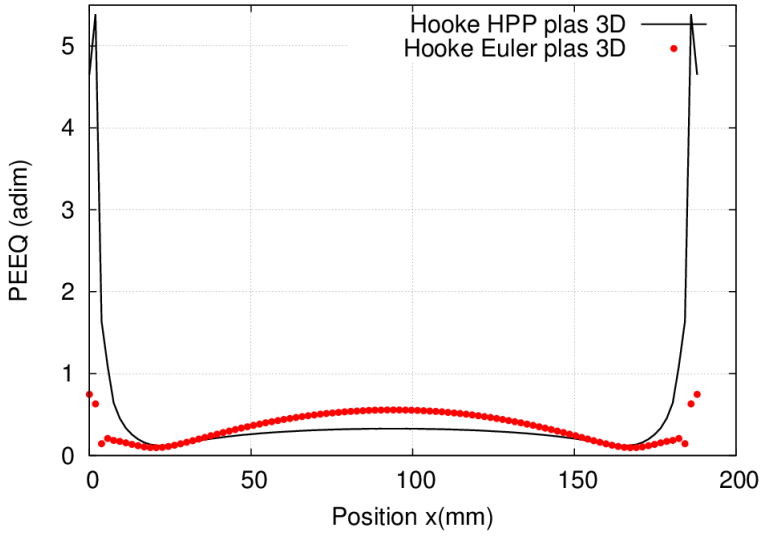


**Fig. 84:** The variation of $PEEQ$ at $t_{max}$ as a function of space at the upper boundary of a beam subjected to bending for different Newtonian plastic models examined.

As deduced in section C.5, $\sigma_{VM}$ and $PEEQ$ are nearly constant along the upper boundary of the beam. They are respectively around $416MPa$ and 0.33 for the model using small strain.

The resulting Von Mises stress is inferior to the tensile strength ($450MPa$) of the considered material. As mentionned before, constant $\sigma_{VM}$ and $PEEQ$ are satisfying results since the bending moment along the

beam is expected to be constant, hence a constant stress is expected along the beam. We also notice the existence of a border effect near the left and right boundary. This may be improved by a mesh refinement near the borders. In the following, a mesh refinement is applied 5 times on a distance $L/20$ near the borders. Results are as follows.

Fig. 85 shows the evolution of the von Mises stress $\sigma_{VM}$ after mesh refinement at the upper boundary of the beam, as a function of space for Newtonian plastic models (function of small deformation and Euler-Almansi large deformation) at $t_{max}$.

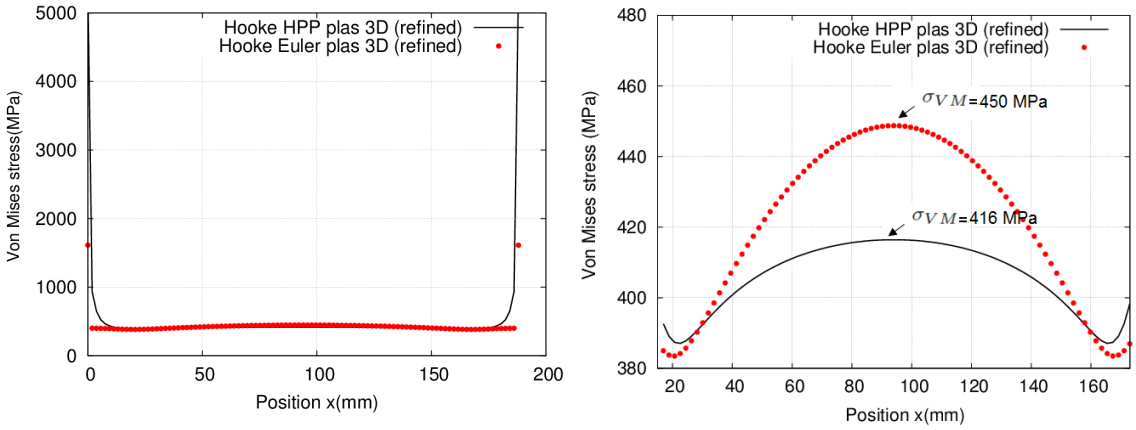


**Fig. 85:** On the left: The variation of $\sigma_{VM}$ at $t_{max}$ as a function of space after mesh refinement at the upper boundary of a beam subjected to bending for different Newtonian plastic models examined. On the right: The variation of $\sigma_{VM}$ at $t_{max}$ as a function of space after mesh refinement at the upper boundary for $15\,mm \leq x \leq 175\,mm$ of a beam subjected to bending for different Newtonian plastic models examined.

Fig. 86 shows the evolution of equivalent plastic strain $PEEQ$ after mesh refinement, at the upper boundary of the beam, as a function of space for Newtonian plastic models (function of small deformation and Euler-Almansi large deformation) at $t_{max}$.

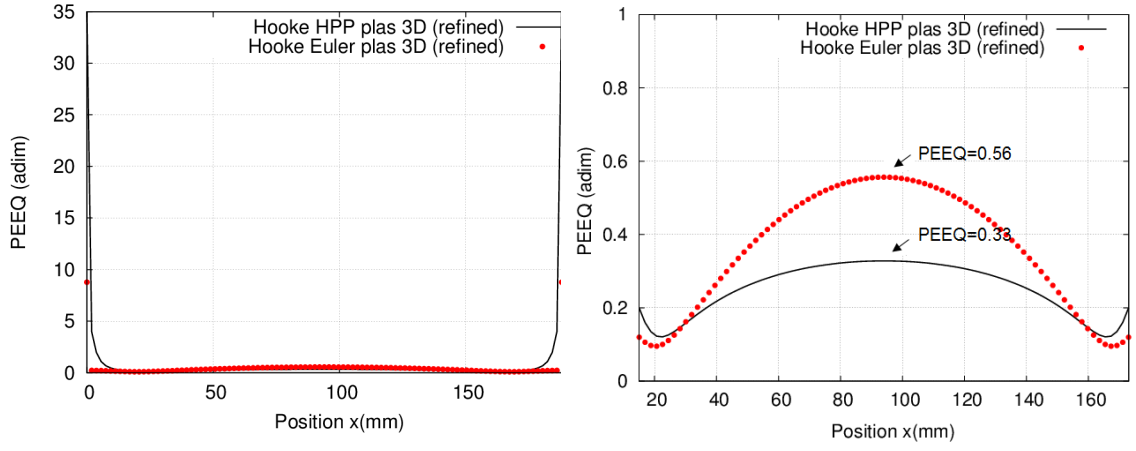


**Fig. 86:** On the left: The variation of $PEEQ$ at $t_{max}$ as a function of space after mesh refinement at the upper boundary of a beam subjected to bending for different Newtonian plastic models examined.. On the right: The variation of $PEEQ$ at $t_{max}$ as a function of space after mesh refinement at the upper boundary for $15\,mm \leq x \leq 175\,mm$ of a beam subjected to bending for different Newtonian plastic models examined.

Results show that the border effect is reduced and the constant tendency of the variables is more clear starting an offset of $+\epsilon$ from the borders.

## C.7 Numerical simulation of the bending behavior using spacetime thermo-hyperelastic model using FEniCS project

For the thermo-hyperelastic model, Eq. 5.90 represents the weak integral form using small strain tensor.

The spacetime elastic model is constrained by:

- $\forall z^2, \forall t,\ f_{SC1} = dep(z^1 = 0, z^2, t) = (0, 0)$ which represents the constraint on the space boundary $\Gamma_1$ of the beam (Fig. 81).
- $\forall z^1, \forall t,\ f_{SC2} = dep(z^1, z^2 = 0, t) = \left((r\sqrt{1 - \frac{(z^1 - L/2)^2}{(L/2)^2}} - z^1)t, (\frac{-2\,r}{L}z^2)t\right)$ which represents the constraint on the space boundary $\Gamma_2$ of the beam (Fig. 81).
- $\forall z^1, \forall t,\ f_{SC3} = dep(z^1, z^2 = W, t) = \left(((r+W)\sqrt{1 - \frac{(z^1 - L/2)^2}{(L/2)^2}} - z^1)t, (\frac{-2\,(r+W)}{L}z^2)t\right)$ which represents the constraint on the space boundary $\Gamma_3$ of the beam (Fig. 81).
- $\forall z^2, \forall t,\ f_{SC4} = dep(z^1 = L, z^2, t) = \big(-Lt, (-2r - 2z^2)t\big)$ which represents the constraint on the space boundary $\Gamma_4$ of the beam (Fig. 81).
- $\forall z^1, \forall z^2,\ f_{TC1} = dep(z^1, z^2, t = 0) = (0, 0)$ which represents the initial condition of the displacement on the time boundary $\Gamma_{t=0}$ defined at $t = 0$.
- $\forall z^1, \forall z^2,\ f_{TC2} = \theta(z^1, z^2, t = 0) = 0\,°C$ which represents the initial condition of the temperature on the time boundary $\Gamma_{t=0}$ defined at $t = 0$.

Parameters for the simulations of spacetime models are the same as the parameters selected for simulations of Newtonian models (see table 22).

Results show the compatibility of Newtonian and spacetime models for small deformations. Border effects are also seen. Finner meshing on borders may improve the precision of the constant value of Von mises stress investigated along the tube geometry.

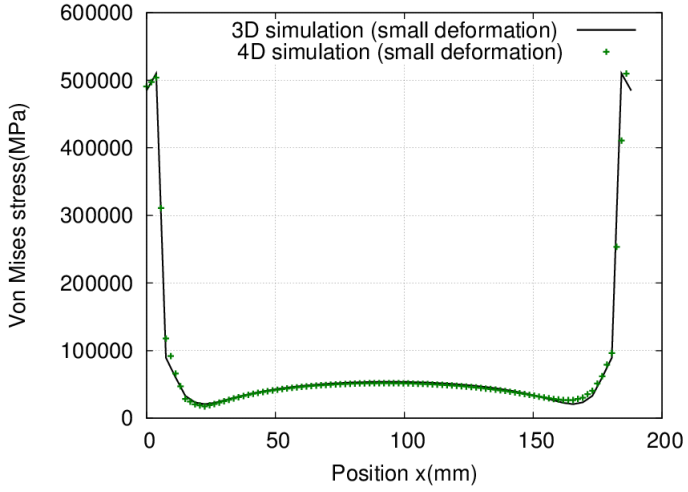


**Fig. 87:** Evolution of the Von Mises stress along the bended beam for the Newtonian and spacetime hyperelastic model using small deformation.

# References


[Ablat and Qattawi,2017] Ablat MA, Qattawi A (2017) Numerical simulation of sheet metal forming: a review. *The International Journal of Advanced Manufacturing Technology* 89.

[Altemeyer et al.,2016] Altmeyer G, Panicaud B, Rouhaud E, Wang M, Roos A, Kerner R (2016) Viscoelasticity behavior for finite deformations, using a consistent hypoelastic model based on Rivlin materials. *Cont. Mech. and Thermod.* 28:1741–1758.

[ASM,1998] ASM international (1998) *Metals handbook desk edition*. Davis JR.

[Augier,2012] Augier D (2012) *Coordonnées, variétés et espaces courbes*. augier.david.free.fr/notes/coord.pdf.

[Auriault,2017] Auriault J-L (2017) The paradox of fourier heat equation: A theoretical refutation. *International Journal of Engineering Science* 118:82-88.

[Badreddine,2006] Badreddine H (2006) *Elastoplasticité anisotrope endommageable en grandes déformations : aspects théoriques, numériques et applications*, PhD thesis in Systèmes mécaniques et matériaux. Troyes: Université de Technologie de Troyes. Available on: http://www.theses.fr/2006TROY0005

[Banabic,2010] Banabic D (2010) *Sheet Metal Forming Processes: Constitutive Modelling and Numerical Simulation*. Springer, New York.

[Bathias and Paris,2005] Bathias C, Paris PC (2005) *Gigacycle Fatigue in Mechanical Practice*. CRC press, New York.

[Battaglia,2007] Battaglia J-L (2007) *Transferts thermiques dans les procédés de mise en forme des matériaux*. Lavoisier éditions, Paris.

[Bechir et al.,2006] Bechir H, Chevalier L, Chaouche M, Boufala K (2006) Hyperelastic constitutive model for rubber-like materials based on the first seth strain measures invariant. *European Journal of Mechanics–A/Solids* 25:110-124.

[Beig and Schmidt,2005] Beig R, Schmidt BG (2005) Relativistic elastostatics: I. Bodies in rigid rotation. *Class. Quantum Grav.* 22:2249-2268.

[Belinfante and Garrison,1962] Belinfante FJ, Garrison JC (1962) On the Uniqueness of Fock's Harmonic Coordinate Systems in the Presence of Static, Spherically Symmetric Source., *Phys. Rev.* 125:1124-1130.

[Belouaggadia et al.,2015] Belouaggadia N, Abid NC, Brun R, *Eléments fondamentaux des transferts thermiques*. Cépaduès éditions, Toulouse.

[Belytschko et al.,2006] Belytschko T, Liu WK, Moran B, Elkhodary K (2006) *Nonlinear Finite Elements for Continua and Structures*, 2nd edn. John Wiley  Sons Ltd., New York.

[Benaarbia et al.,2014] Benaarbia A, Chrysochoos A, Robert G (2014) Influence of relative humidity and loading frequency on the PA6.6 cyclic thermomechanical behavior: Part I. mechanical and thermal aspects. *Polym. Test.* 40:290–298.

[Benaarbia et al.,2016] Benaarbia A, Chrysochoos A, Robert G (2016) Thermomechanical analysis of the onset of strain concentration zones in wet polyamide 6.6 subjected to cyclic loading. *Mechanics of Materials* 99:9–25.

[Bernard,2019] Bernard G (2019) La transformation de Lorentz, le temps et l'espace. Généralisation du facteur gamma en fonction de la direction du mouvement caché dans les horloges, *Congrès Général de la Société Française de Physique*. https://hal.archives-ouvertes.fr/hal-02068970. Accessed 27 Jan 2020.

[Berthel,2007] Berthel B (2007) Dissipation field measurements accompanying the high cycle fatigue of steel by infrared thermography (in French). Thesis, University of Montpellier II.

[Bertram,2012] Bertram A (2012) *Elasticity and Plasticity of Large Deformations*, 3rd edn. Springer, Berlin.

[Besson et al.,2009] Besson J, Cailletaud G, Forest S (2009) *Non-Linear Mechanics of Materials*. Springer, Netherlands.

[Blanche,2015] Blanche A, Chrysochoos A, Ranc N, Favier V (2015) Dissipation assessments during dynamic very high cycle fatigue tests. *Experimental Mechanics* 55:699-709.

[Boehler,1978] Boehler JP (1978) Anisotropic constitutive equations for continuous media. *J Mec* 17(2):153–190.

[Bonet and Wood,2008] Bonet J, Wood RD (2008) *Nonlinear continuum mechanics for finite element analysis*, 2nd edn. Cambridge university press, New York.

[Bonnet,2014] Bonnet, M. (2014) *The finite element method in solid mechanics*. McGraw Hill Education, New York.

[Boratav,1991] Boratav M, Kerner R (1991) *Relativité*, Ellipses, Paris.

[Boratav and Kerner,1991] Boratav M, Kerner R (1991) *Relativité*, Ellipses, Paris.

[Borja,2013] Borja RI (2013) *Plasticity*, Springer-Verlag, Berlin.

[Both et al.,2016] Both S, Czél B, Fülöp T, Gróf GY, Gyenis A, Kovács R, Ván P and Verhás J (2016) Deviation from the Fourier law in room-temperature heat pulse experiments. *Journal of Non-Equilibrium Thermodynamics* 41(1):41-48.

[Boukamel,2006] Boukamel A (2006) *Modélisation mécaniques et numériques des matériaux et structures en élastomères*, PhD thesis. Aix-Marseille: Université de la Méditerranée - Aix-Marseille II, 152p. Available on: https://tel.archives-ouvertes.fr/tel-00517997

[Boulanger et al.,2004] Boulanger T, Chrysochoos A, Mabru C, Galtier A (2004) Calorimetric analysis of dissipative and thermoelastic effects associated with the fatigue behavior of steels. *Int J Fatigue* 26:221-229.

[Boyce and Arruda,2000] Boyce MC, Arruda EM (2000) Constitutive models of rubber elasticity: a review. *Rubber Chemistry and Technology* 73:504-523.

[Bressan,1963] Bressan A (1963) Cinematica dei sistemi continui in relativita generale. *Annali di matematica pura ed applicata* 61(1):99-148.

[Bressan,1978] Bressan A (1978) *Relativistic Theories of Materials*. Springer-Verlag, Berlin.

[Britannica,2011] The Editors of Encyclopaedia Britannica (2011) *Euclidean space*. https://www.britannica.com/science/Euclidean-space. Accessed 27 Jan 2020.

[Broer,2019] Broer A. *Introduction à la théorie de la représentation* (2019) Département de mathématiques et de statistique, Université de Montréal, Montréal.

[Bruhns and Meyers,1998] Bruhns OT, Meyers A (1998) Direct relationship between the lagrangean logarithmic strain and the lagrangean stretching and the lagrangean Kirchhoff stress. *Mechanics research Communications* 25(1):59-67.

[Brunet,2009] Brunet M (2009) *Analyse non linéaire des matériaux et des structure*. Institut national des sciences appliquées de Lyon, Lyon.

[Buckingham,1914] Buckingham E (1914) On physically similar systems. Illustrations of the use of dimensional equations. *Physical Review* 4(4):345–376.

[Carter,1988] Carter B (1988) Conductivity with Causality in Relativistic Hydrodynamics - the Regular Solution to Eckart's Problem. *International Conference on Gravitation and Cosmology* 58-65.

[Cattaneo,1958] Cattaneo C (1958) Sur une forme de l'équation de la chaleur éliminant le paradoxe d'une propagation instantanée. *Comptes Rendus de l'Académie des Sciences* 247:431-433.

[Cazaud,1948] Cazaud R (1948) *La fatigue des métaux*. Dunod, Paris.

[Cengel,2008] Cengel Y (2008) *Introduction to thermodynamics and heat transfer*. McGraw-Hill, New York.

[Chapman and Cowling,1970] Chapman S, Cowling TG (1970) *The Mathematical Theory of Non-Uniform Gases*, 3rd edn. Cambridge University Press, Cambridge.

[Charnock,2017] Charnock T (2017) *Advanced Gravity*. http://www2.iap.fr/users/charnock/notes/advancedgravity.pdf. Accessed 27 Jan 2020

[Chen and Han,1988] Chen WF, Han DJ (1988) *Plasticity for Structural Engineers*. Springer-Verlag, New York.

[Christov,2009] Christov CI (2009) On frame-indifferent formulation of the Maxwell-Cattaneo model of finite-speed heat conduction. *Mechanics Research Communications* 36:481-486.

[Christov and Jordan,2005] Christov CI, Jordan PM (2005) Heat conduction paradox involving second sound propagation in moving media. *Phys. Rev. Lett.* 94(15):154301.

[Chrysochoos et al.,2009] Chrysochoos A, Wattrisse B, Muracciole JM, El Kaim Y (2009) Fields of stored energy associated with localized necking of steel. *Journal of Mechanics of Materials and Structures* 4(2):245-262.

[Chrysochoos and Louche,2000] Chrysochoos A, Louche H (2000) An infrared picture processing to analyse the calorific effects accompanying strain localisation. *Int. J. Eng. Sci.* 38(16):1759-1788.

[Clément and Martin,2016] Clément F, Martin V (2016) *The Lax-Milgram Theorem. A detailed proof to be formalized in Coq*. https://arxiv.org/pdf/1607.03618.pdf. Accessed 14 Dec 2019.

[Colmez,2009] Colmez P (2009) *Éléments d'analyse et d'algèbre (et de théorie des nombres)*. Éditions de l'École Polytechnique, Paris.

[Conner,2013] Conner M (2013) Characterization of heat transfer coefficient uncertainty in support of high temperature probe measurement technology. Masters thesis, University of Tennessee- Knoxville. https://trace.tennessee.edu/utk_gradthes/2600/.

[Cowles,1996] Cowles BA (1996) High cycle fatigue in aircraft gas turbines - an industry perspective. *International Journal of Fracture* 80:147-163.

[Coxeter,1961] Coxeter HSM (1961) *Introduction to Geometry*. Wiley, New York.

[Day,1997] Day WA (1997) On rates of propagation of heat according to fourier theory. *Quarterly of Applied Mathematics* 55(1):127–138.

[Debard,2011] Debard Y (2011) Méthode des éléments finis: thermique, Université du Mans Master Modélisation Numérique et Réalité Virtuelle. http://iut.univ-lemans.fr/ydlogi/index.html. Accessed 14 Dec 2019.

[De Saxce and Vallée,2016] De Saxce G, Vallée C (2016) *Galilean Mechanics and Thermodynamics of Continua*. John Wiley & Sons, New Jersey.

[De Souza Neto et al.,2011] De Souza Neto EA, Peric D, Owen DRJ (2011) *Computational methods for plasticity: theory and applications*. John Wiley Sons, New Jersey.

[Dogui,1989] Dogui A (1989) *Plasticité anisotrope en grandes déformations*, PhD thesis. Lyon: Université Claude Bernard-Lyon I. Available on: https://tel.archives-ouvertes.fr/tel-00848713.

[Dogui and Sidoroff,1985] Dogui A, Sidoroff F (1985) Kinematic hardening in large elastoplastic strain. *Engineering fracture mechanics* 21:685-695.

[Doudard et al.,2009] Doudard C, Calloch S, Hild F, Roux S (2009) Identification of heat source fields from infra-red thermography: Determination of 'self-heating' in a dual-phase steel by using a dog bone sample. *Mechanics of Materials* 42:55-62.

[Eckart,1940] Eckart C (1940) The thermodynamics of irreversible processes. iii. relativistic theory of the simple fluid. *Phys. Rev.* 58(10):919-924.

[Edelen,1967] Edelen DG (1967) Lorentz invariance, momentum-energy tensors and the mhd problem. *International Journal of Engineering Science* 5(3):235–250.

[Einstein,1920] Einstein A (1920) *Relativity: The Special and General Theory*. Henry Holt and company, New York.

[Ekoue et al.,2013] Ekoue F, Fouache Plantamp G, Zajdman E (2013) Maxwell-Cattaneo Regularization of Heat Equation. World Academy of Science, Engineering and Technology. *International Journal of Physical and Mathematical Sciences* 7(5):772-776.

[Eringen,1962] Eringen AC (1962) *Nonlinear Theory of Continuous Media*. McGraw-Hill, New York.

[Eshraghi et al.,2013] Eshraghi A, Papoulia KD, Jahed H (2013) Eulerian framework for inelasticity based on Jaumann rate and a hyperelastic constitutive relation - Part I: Rate-form hyperelasticity. *Journal of Applied Mechanics* 80:1-11.

[Farhat et al.,1991] Farhat C, Park KC, Dubois-Pelerin Y (1991) An unconditionally stable staggered algorithm for transient finite element analysis of coupled thermoelastic problems. *Computer Methods in Applied Mechanics and Engineering* 85(3):349-365.

[Favier et al.,2016] Favier V, Blanche A, Wang C, Lam Phung N, Ranc N, Wagner D, Bathias C, Chrysochoos A, Mughrabi H (2016) Very high cycle fatigue for single phase ductile materials: Comparison between $\alpha$-iron, copper and $\alpha$-brass polycrystals. *International Journal of Fatigue* 93:326–338.

[Fer,1970] Fer F (1970) *Thermodynamique macroscopique*, tomes 1 et 2. Gordon & Breach, London.

[Fichera,1992] Fichera G (1992) Is the fourier theory of heat propagation paradoxical? *Int. Rendiconti del Circolo Matematico di Palermo* 2(41):5-28.

[Fourier,1988] Fourier J (1988) *Théorie analytique de la chaleur*, Editions Jacques Gabay, Paris.

[Frémond,2006] Frémond M (2006) *The Clausius-Duhem Inequality, an Interesting and Productive Inequality. In: Nonsmooth Mechanics and Analysis. Advances in Mechanics and Mathematics*, vol. 12. Springer, Boston.

[Frewer,2009] Frewer M (2009) More clarity on the concept of material frameindifference in classical continuum mechanics. *Acta Mechanica* 202(1-4):213–246.

[Galántai,2000] Galántai A (2000) The theory of Newton's method. *Journal of Computational and Applied Mathematics* 124:25–44.

[Galtier,1993] Galtier A (1993) *Contribution à l'étude de l'endommagement des aciers sous sollicitations uni ou multi-axiales*, PhD thesis. Paris: École Nationale Sup. d'Arts et Métiers. Available on: http://www.theses.fr/1993ENAM0008

[Gao et al.,2014] Gao H, Ma X, Qi N, Berry C, Griffith BE, Luo X (2014) A finite strain nonlinear human mitral valve model with fluid-structure interaction. *Int J Numer Method Biomed Eng*. 30:1597–613.

[Garrigues,2007] Garrigues J (2007) *Fondements de la Mécanique des Milieux Continous*. Lavoisier, Hermès Science Pulications, Paris.

[Germain,1973] Germain P (1973) La méthode des puissances virtuelles en mécanique des milieux continus. *J. Mécanique* 12:236-274.

[Germain,1983] Germain P, Nguyen QS, Suquet P (1983) Continuum thermomechanics. *J Appl Mech-Trans Asme* 50:1010–20.

[Gondran and Gondran,2014] Gondran M, Gondran A (2014) *« Chapitre 10. Les interprétations de la relativité », Mécanique quantique. Et si Einstein et de Broglie avaient aussi raison ?*. Editions Matériologiques, Paris.

[Gray,1997] Gray A (1997) *Euclidean Spaces in Modern Differential Geometry of Curves and Surfaces with Mathematica*, 2nd edn. CRC Press:2-5, Boca Raton, FL.

[Green and Naghdi,1965] Green AE, Naghdi PM (1965) A general theory of an elastic-plastic continuum. *Archive for Rational Mechanics and Analysis* 18:251-281.

[Groover,2010] Groover, M. (2010) *Fundamentals of modern manufacturing*, 4th edn. John Wiley  Sons, New Jersey.

[Grot and Eringen,1966a] Grot RA, Eringen A (1966) Relativistic continuum mechanics part I - mechanics and thermodynamics. *International Journal of Engineering Science* 4(6):611-638.

[Grot and Eringen,1966b] Grot RA, Eringen AC (1966) Relativistic continuum mechanics: Part II - electromagnetic interactions with matter. *International Journal of Engineering Science* 4:639-670

[Guillemet and Bardon,2000] Guillemet P, Bardon J-P (2000) Conduction de la chaleur aux temps courts: les limites spatio-temporelles des modèles parabolique et hyperbolique. *Int.J. Therm. Sci.* 39: 968-982.

[Guo et al.,2015] Guo Q, Guo X, Fan J, Syed R, Wu C (2015) An energy method for rapid evaluation of high-cycle fatigue parameters based on intrinsic dissipation. *International Journal of Fatigue* 80:136–144.

[Gurtin,1982] Gurtin ME (1982) *An introduction to continuum mechanics*, Vol. 158. Academic press, Cambridge.

[Havas,1964] Havas P (1964) Four-dimensional formulations of newtonian mechanics and their relation to the special and the general theory of relativity. *Reviews of Modern Physics* 36(4):938.

[Hayward,1999] Hayward SA (1999) *Relativistic 13 thermodynamics*. Yukawa Institute for Theoretical Physics, Kyoto University, Kyoto.

[Hehl,2012] Hehl WF (2012) *Gauge Theory of Gravity and Spacetime*, eprint:1204.3672, https://arxiv.org/pdf/1204.3672.pdf. Accessed 18 Feb 2020.

[Hossain and Steinmann,2013] Hossain M, Steinmann P (2013) More hyperelastic models for rubber-like materials: Consistent tangent operator and comparative study. *Journal of the Mechanical Behaviour of Materials* 22(1-2):27-50.

[Israel,1987] Israel W (1987) Covariant fluid mechanics and thermodynamics: an introduction. *Lectures delivered at CIME Session on Relativistic Fluid Dynamics*.

[Israel,1989] Israel W, Anile A, Choquet-Bruhat Y (1989) *Covariant fluid mechanics and thermodynamics: An introduction to Relativistic Fluid Dynamics*, Springer, Berlin.

[Israel and Stewart,1979a] Israel W, Stewart JM (1979) On transient relativistic thermodynamics and kinetic theory II. *Royal Society of London Proceedings Series A* 365:43-52.

[Israel and Stewart,1979b] Israel W, Stewart JM (1979) Transient relativistic thermodynamics and kinetic theory. *Annals of Physics* 118:341-372.

[Jaeger,2014] Jaeger G, What in the (quantum) world is macroscopic? *American Journal of Physics* 82(9):896–905.

[Jaumann,1911] Jaumann G (1911) Geschlosssenes system physikalischer und chemischer differentialgesetze. *Akad. Wiss. Wien Sitzber*. 385-530

[JCGM,1995] Joint Committee for Guides in Metrology (JCGM) (1995) *Guide pour l'Expression de l'Incertitude de Mesure*. ISO 07-020.

[Johansson,2011] Johansson J (2011) *Automated Computer Systems for Manufacturability Analyses and Tooling Design*. Thesis, Chalmer University of Technology, Gothenburg. 82p. Available on: https://pdfs.semanticscholar.org.

[Joseph and Preziosi,1989] Joseph D, Preziosi L (1989) Heat waves. *Rev. Mod. Phys.* 61(1):41.

[Jou et al.,1988] Jou D, Casas-Vázquez J,Lebon G (1988) Extended irreversible thermodynamics. *Reports on Progress in Physics* 51(8):1105.

[Katunin,2017] Katunin A (2017) Domination of self-heating effect during fatigue of polymeric composites. *Procedia Structural Integrity* 5:93-98.

[Kerner,2014] Kerner R (2014) *Relativité*, Ellipses, Paris.

[Khajehsaeid,2013] Khajehsaeid H, Arghavani J, Naghdabadi R (2013) A hyperelastic constitutive model for rubber-like materials. *European Journal of Mechanics-A/Solids* 38:144-151.

[Kijowski and Magli,1997] Kijowski J, Magli G (1997) Unconstrained variational principle and canonical structure for relativistic elasticity. *Reports on mathematical physics* 39:99-112.

[Knudsen and Hjorth,1995] Knudsen M, Hjorth P (1995) *Elements of Newtonian Mechanics*. Springer-Verlag Berlin Heidelberg, Berlin.

[Kobayashi and Nomizu,1996] Kobayashi S, Nomizu K (1996) *Foundations of Differential Geometry*, Vol. 1. Wiley-Interscience, New Jersey.

[Koseoglu and Parlak,2012] Koseoglu S, Parlak H (2012) *Capacity calculator for rotary draw tube bending*, Degree Project. Sweden: Linnaeus University, School of Engineering, 23p. Available on: http://www.lnu.se.

[Kostädt and Liu,2000] Kostädt P, Liu M, On the causality and stability of the relativistic diffusion equation, *Physical Reviews D* 62:023003.

[Kovács and Ván,2015] Kovács R, Ván P (2015) Generalized heat conduction in heat pulse experiments. *Int. J. Heat Mass Trans.* 83:613-620.

[Krapez et al.,1999] Krapez JC, Pacou D, Bertin C (1999) Application of lock-in thermography to a rapid evaluation of the fatigue limit in metals, Ed. E. Grinzato et Al. *5th AITA, Int. Workshop on Advanced Infrared Techn. and Appl., Venezia* 379–385.

[Kurt,1985] Kurt, L. (1985) *Handbook of Metal Forming*. McGraw-Hill, Inc., New York.

[Lagrée,2010] Lagrée P-Y (2010) *Coefficient d'échange, Ailettes*. http://www.lmm.jussieu.fr.

[Lai et al.,2010] Lai D, Rubin W, Krempl E (2010) *Introduction to Continuum Mechanics*, 4th edn. Butterworth-Heinemann, Oxford.

[Lamoureux-Brousse,1989] Lamoureux-Brousse L (1989) Infinitesimal deformations of finite conjugacies in non-linear classical or general relativistic theory of elasticity. *Physica D* 35:203-219.

[Landau and Lifshitz,1966] Landau LD and Lifshitz EM (1966) *Fluid Mechanics*, 3rd edn. Pergamon Press, London.

[Landau and Lifshitz,1971] Landau LD, Lifshitz EM (1971) *The classical theory of fields*, 3th edn. Pergamon press, Oxford.

[Landau and Lifshitz,1975] Landau LD, Lifshitz EM (1975) *The Classical Theory of Fields*, 4th edn. Elsevier, Amsterdam.

[Landau and Lifshitz,1976] Landau LD, Lifshitz EM (1976) *Mechanics: volume 1 of course of theoretical physics*, 3th edn. Butterworth-Heinemann, Oxford.

[Landau and Lifshitz,1982] Landau LD, Lifshitz EM (1982) *Physique théorique*, 4th edn. Éditions Mir, Moscou.

[Langtangen and Logg,2017] Langtangen HP, Logg A (2017). *Solving PDEs in Python, The FEniCS Tutorial I*. Springer Open.

[La Rosa and Risitano,2000] La Rosa G, Risitano A (2000) Thermographic methodology for rapid determination of the fatigue limit of materials and mechanical components. *International Journal of Fatigue* 22:65–73.

[[Lehr,1926] Lehr E (1926) Die dauerfestigkeit, ihre bedeutung für die praxis und ihre kurzfristige ermittlung mittels neuartiger prüfmaschinen. *Glasers Annalen* 1184:109–114.

[Lejeunes,2014] Lejeunes S (2014) *Grandes Déformations : Comportement des Matériaux*, École d'ingénieur. France. ffcel-01104172v1f. Accessed 18 Feb 2020.

[Lemaitre and Chaboche,1990] Lemaitre J, Chaboche JL (1990) *Mechanics of solid materials*. Cambridge University Press, Cambridge.

[Lichnerowicz,1994] Lichnerowicz A (1994) *Magnetohydrodynamics: waves and shock waves in curved spacetime*, vol. 14. Springer, Netherlands.

[Liu,2004] Liu I (2004) On euclidean objectivity and the principle of material frame indifference. *Continuum Mechanics and Thermodynamics* 16:177–183.

[Liu et al.,2017] Liu W, Saanouni K, Forest S, Hu P (2017) The Micromorphic Approach to Generalized Heat Equations. *Journal of Non-Equilibrium Thermodynamics* 42(4):327-357.

[López-Monsalvo,2011] López-Monsalvo CS (2011) *Covariant Thermodynamics and Relativity*,University of Southampton, Faculty of Social and Human Sciences, School of Mathematics.

[Louck and Galbraith,1976] Louck JD, Galbraith HW (1976) Eckart vectors, Eckart frames, and polyatomic molecules. *Reviews of Modern Physics* 48(1):69.

[Lubarda,2002] Lubarda VA (2002) *Elastoplasticity Theory*. CRC Press, Florida.

[Lubliner,1984] Lubliner J (1984) A maximum-dissipation principle in generalized plasticity. *Acta Mechanica* 52(3-4):225-237.

[Luong,1998] Luong MP (1998) Fatigue limit evaluation of metals using an infrared thermographic technique. *Mechanics of Materials* 28:155–163.

[Makowski,2009] Makowski D (2009) Analyse d'incertitude, analyse de sensibilité. Objectifs et principales étapes. Ecole chercheur Analyse de sensibilité et exploration de modèles, Giens. https://reseau-mexico.fr/sites/default/files/pr2_MakowskiECanalyseSensibilite.pdf. Accessed 09 Mar 2020.

[Mandel,1983] Mandel J (1983) Sur la definition de la vitesse de deformation elastique en grande transformation elasto-plastique. *International Journal of Solids and Structures* 19(7):573–578.

[Maquin and Pierron,2009] Maquin F, Pierron F (2009) Heat dissipation measurements in low stress cyclic loading of metallic materials: from internal friction to micro-plasticity. *Mech Mater* 41:928–942.

[Mareau,2007] Mareau C (2007) *Modélisation micromécanique de l'échauffement et de la microplasticité des aciers sous sollicitation cyclique*, PhD thesis. Metz: ENSAM. Available on: https://www.theses.fr/2007ENAM0037

[Mariano,2017] Mariano PM (2017) Finite-speed heat propagation as a consequence of microstructural changes. *Continuum Mech. Thermodyn* 29:1241-1248.

[Marleau,2017] Marleau L (2017) *Introduction à la physique des particules*. Université Laval, Quebec.

[Marsden and Hughes,1994] Marsden JE, Hughes TJ (1994) *Mathematical foundations of elasticity*. Courier Corporation, Massachusetts.

[Maugin,1971a] Maugin G (1971) Champ des déformations d'un milieu continu dans l'espace-temps de minkowski. *CR Acad. Sci. Paris A* 273:65–68.

[Maugin,1971b] Maugin G (1971) Un modèle viscoélastique en relativité générale. *CR Acad. Sci Paris A* 272:1482-1484.

[Maugin,1973] Maugin G (1973) Sur les notions de fluide visqueux, de solide élastique et de conduction de la chaleur en relativité. *CR Acad. Sci. Paris A* 276:1027-1030.

[Maxwell,1867] Maxwell JC (1867) On the dynamical theory of gases, *Phil. Trans. Roy. Soc. Lond. Series I* 157.

[McRae et al.,2016] McRae A, Bercea GT, Mitchell L, Ham D, Cotter C (2016) Automated generation and symbolic manipulation of tensor product finite elements. *SIAM Journal on Scientific Computing* 38(5):S25–S47.

[Moller,1972] Moller C (1972) *The Theory of Relativity*. Clarendon, Oxford.

[Mooney,1940] Mooney M (1940) A theory of large elastic deformation. *Journal of Applied Physics* 11:582-592.

[Moore and Kommers,1921] Moore HF, Kommers JB (1921) Fatigue of metals under repeated stress. *Chem. Met. Eng.* 25:1141–1144.

[Muhr,2005] Muhr AH (2005) Modeling the stress–strain behavior of rubber. *Rubber Chemistry and Technology* 78(3):391–425.

[Muller,1969] Muller I (1969) Toward Relativistic Thermodynamics. *Arch. Rat. Mech. Anal.* 34:259-282.

[Muller,1985] Muller I (1985) *Thermodynamics*, Pitman Publishing Limited, London.

[Muller,2008] Muller I (2008) Extended Thermodynamics: a Theory of Symmetric Hyperbolic Field Equations. *Entropy* 10:477-492.

[Müller and Ruggeri,1998] Müller I, Ruggeri T (1998) *Rational Extended Thermodynamics*, vol. 37, 2nd edn. Springer Verlag, New York.

[Munier,2012] Munier R (2012) *Etude de la fatigue des aciers laminés à partir de l'auto-échauffement sous sollicitation cyclique: essais, observations, modélisation et influence d'une pré-déformation plastique*. PhD thesis, University of Bretagne occidentale - Brest. https://tel.archives-ouvertes.fr/tel-00717932.

[Murdoch,1983] Murdoch AI (1983) On Material Frame-Indifference, Intrinsic Spin, and Certain Constitutive Relations Motivated by the Kinetic Theory of Gases. *Archive for Rational Mechanics and Analysis* 83:185-194.

[Muschik and Borzeszkowski,2014] Muschik W, Borzeszkowski H-H (2014) Exploitation of the dissipation inequality in general relativistic continuum thermodynamics. *Archive of Applied Mechanics* 84:1517-1531.

[Muschik and Borzeszkowski,2015] Muschik W, Borzeszkowski HH V (2015) Entropy Production and Equilibrium Conditions of General-Covariant Spin Systems. *Entropy* 17:8325-8340.

[Muschik and Restuccia,2008] Muschik W, Restuccia L (2008) Systematic remarks on objectivity and frame-indifference, liquid crystal theory as an example. *Archive of Applied Mechanics* 78:837-854.

[Nakagawa and Sasa,2019] Nakagawa N, Sasa S (2019) Thermodynamics for Heat Conduction Systems, *J Stat Phys* 177:825–888.

[Narasimhan,1999] Narasimhan TN (1999) Fourier's heat conduction equation: history, influence, and connections. *Reviews of Geophysics* 37(1):151-172.

[Nayfeh and Nemat-Nasser,1971] Nayfeh A, Nemat-Nasser S (1971) Thermoelastic waves in solids with thermal relaxation. *Acta Mech.* 12(1-2):5369.

[Nemat-Nasser,1974] Nemat-Nasser S (1974) General variational principles in nonlinear and linear elasticity with applications. *Mechanics today* 1:214–261.

[Nemat-Nasser,1979] Nemat-Nasser S (1979) Decomposition of strain measures and their rates in finite deformation elastoplasticity. *International Journal of Solids and Structures* 15(2):155–166.

[Nemat-Nasser,2004] Nemat-Nasser S (2004) *Plastic: A Treatise on Finite Deformation of Heterogeneous Inelastic Materials*. Cambridge university press, Cambridge.

[Nicholson and Lin,1996] Nicholson DW, Lin B (1996) Theory of thermohyperelasticity for near-incompressible elastomers. *Acta Mechanica* 116:15–28.

[Ogawa et al.,2001] Ogawa M, Mukai K, Fukui T, Baba T (2001) The development of a thermal diffusivity reference material using alumina. *Meas. Sci. Technol.*, 12:2058-2063.

[Ogden,1984] Ogden RW (1984) *Non-linear elastic deformations*. Dover Publications, New York.

[Oldroyd,1950] Oldroyd JG (1950) On the Formulation of Rheological Equations of state. *Proceedings of the Royal Society Lond. A* 200:523-541.

[Oliveira and Fernandes,2019] Oliveira M, Fernandes J (2019) Modelling and Simulation of Sheet Metal Forming Processes. *Metals- Open Access Metallurgy Journal* 9(12):1356.

[O'Neill,1966] O'Neill B (1966) *Elementary Differential Geometry*. Academic Press, San Diego, CA.

[Onsager,1931] Onsager L (1931) Reciprocal Relations in Irreversible Processes. *I. Physical Review* 37:405-426.

[Osborne,1950] Osborne JG (1950) Propagation of Second Sound Below 1 K. *Low Temp. Phys. NBS(US) Circular* 519:139.

[Ottinger,1998] Ottinger HC (1998) On the structural compatibility of a general formalism for nonequilibrium dynamics with special relativity. *Physica A: Statistical Mechanics and its Applications* 259:24-42.

[Oudin,2008] Oudin H (2008) *Méthode des éléments finis*. https://cel.archives-ouvertes.fr/cel-00341772v3. Accessed 14 Dec 2019.

[Panicaud et al.,2014] Panicaud B, Rouhaud E (2014) A frame-indifferent model for a thermo-elastic material beyond the three-dimensional Eulerian and Lagrangian descriptions. *Continuum Mechanics and Thermodynamics* 26:79-93.

[Panicaud et al.,2015] Panicaud B, Rouhaud E, Altmeyer G, Wang M, Kerner R, Roos A, et al. (2015) Consistent hypoelastic behavior using the four-dimensional formalism of differential geometry. *Acta Mechanica* 227(3):651–675.

[Papon and Leblond,2005] Papon P, Leblond J (2005) *Thermodynamique des états de la matière 193*. Hermann, Paris.

[Poncelet et al.,2011] Poncelet M, Witz JF, Pron H, Wattrisse B (2011) A study of IRFPA camera measurement errors: radiometric artefacts. *Quantitative InfraRed Thermography Journal* 8 (2):165-186.

[Pourasghar and Chen,2019] Pourasghar A, Chen Z (2019) Dual-phase-lag heat conduction in FG carbon nanotube reinforced polymer composites. *Physica B: Condensed Matter* 564(1):147-156.

[Prasolov,1997] Prasolov P Ph (1997) A strain-based relaxation theory of plasticity for anisotropic metals. *Acta Mechanica* 122:65–74.

[Prigogine,1980] Prigogine I (1980) *From being to becoming: time and complexity in the physical sciences*, W. H. Freeman, New York.

[Prost-Domasky et al.,1997] Prost-Domasky SA, Szabo BA, Zahalak GI (1997) Large deformation analysis of non-linear elastic fluids. *Computers and Structures* 64(5-6):1281-1290.

[Protter,1985] Protter MH (1985) Morrey CB, Jr. *Intermediate Calculus*, 2nd edn. Springer, New York.

[Prucha,2003] Prucha T (2003) Metal Mold Processes – Gravity and Low Pressure Technology, *Proceedings from the AFS International Conference on Structural Aluminum Casting, Orlando*.

[Pu et al.,2019] Pu X, Petit J, Darbord-Ranc I, Wagner D (2019) Thermal response of iron and C-Mn steels with different ferrite/pearlite phase fraction under ultrasonic fatigue loading. *Materials Science and Engineering A* 749:96-105.

[Reif,1965] Reif F, *Fundamentals of Statistical and Thermal Physics*, International student edn. McGraw-Hill, Boston

[Rivlin,1948] Rivlin RS (1948) Large elastic deformations of isotropic materials. IV. Further developments of the general theory. *Philosophical Transactions of the Royal Society of London. Series A* 241:379-397.

[Rivlin and Saunders,1951] Rivlin RS, Saunders DW (1951) Large elastic deformations of isotropic materials VII. Experiments on the deformation of rubber. *Philosophical Transactions of the Royal Society of London. Series A* 243:251-288.

[Rodriguez and Lopez Fernandez,2010] Rodriguez OH, Lopez Fernandez JM (2010) A semiotic reflection on the didactics of the Chain rule. *The Mathematics Enthusiast* 7(2):article 10.

[Romano et al.,2014] Romano G, Barretta R, Diaco M (2014) The Geometry of Nonlinear Elasticity. *Acta Mech.* 225(11):3199-3235.

[Romano et al.,2018] Romano G, Barretta R, Diaco M (2018) A geometric rationale for invariance, covariance and constitutive relations. *Continuum Mechanics and Thermodynamics* 30:175-194.

[Romano and Barretta,2011] Romano G, Barretta R (2011) Covariant hypo-elasticity. *European Journal of Mechanics A/Solids* 30:1012-1023.

[Rouhaud et al.,2013] Rouhaud E, Panicaud E, Kerner R (2013) Canonical frame-indifferent transport operators with the four-dimensional formalism of differential geometry. *Computational Materials Science* 77:120-130.

[Rougée,1997] Rougée P (1997) *Mécanique des grandes transformations*. Springer-Verlag, Berlin Heidelberg.

[Ruben,2010] Ruben PM (2010) *Study of the fatigue strength in the gigacycle regime of metallic alloys used in aeronautics and off-shore industries*, PhD thesis. Paris: Arts et Métiers ParisTech, 263p.[consultée le 8 Septembre 2010]. Available on: https://www.theses.fr/2010ENAM0027.

[Saanouni,2012] Saanouni K (2012) *Damage Mechanics in metal forming. Advanced modeling and numerical simulation*. ISTE/Wiley, London.

[Schellstede et al.,2014] Schellstede G, Von Borzeszkowski H-H, Chrobok T, Muschik W (2014) The relation between relativistic and non-relativistic continuum thermodynamics. *General Relativity and Gravitation* 46(1):1640.

[Schouten,1954] Schouten JA (1954) *Ricci-calculus: An Introduction to Tensor Analysis and Its Geometrical Applications*, Springer-Verlag, Berlin.

[Semay and Silvestre-Brac,2007] Semay C, Silvestre-Brac B (2007) *Introduction au calcul tensoriel, Applications à la physique*. Dunod, Malakoff.

[Shenogin et al.,2002] Shenogin SV, Hohne v, Oleinik EF (2002) Thermodynamics of the pre-yield deformation behavior of glassy polymers: measurements with new deformation calorimeter. *Thermochim. Acta* 391(1-2):13-23.

[Sidoroff] Sidoroff F (1973) The geometrical concept of intermediate configuration and elasticplastic finite strain. *Arch. Mech.* 25(2):299-308.

[Soffel and Langhans,2013] Soffel M, Langhans R (2013) *Space-Time Reference Systems*. Springer-Verlag Berlin Heidelberg, Berlin.

[Speziale and Galbraith,1987] Speziale CG, Galbraith HW (1987) Comments on the "material frame-indifference" controversy. *Physical Review A* 36(9):4522.

[Steinmann et al.,2012] Steinmann P, Hossain M, Possart G (2012) Hyperelastic models for rubber-like materials: Consistent tangent operators and suitability for Treloar's data. *Archive of Applied Mechanics* 82(9):1183-1217.

[Stewart,1977] Stewart JM (1977) On transient relativistic thermodynamics and kinetic theory. *Royal Society of London Proceedings Series A* 357:59-75.

[Stover and Eric,2020] Stover C, Eric W (2020) *Euclidean space*. http://mathworld.wolfram.com/EuclideanSpace.html. Accessed 27 Jan 2020.

[Straugham,2011] Straugham B (2011) *Heat Waves*. Springer, New York.

[Stromeyer,1914] Stromeyer CE (1914) The determination of fatigue limits under alternting stress conditions. *Proc. Roy. Soc. London,A* 90:411–425.

[Stump and Plotkowski,2019] Stump B, Plotkowski A (2019) An adaptive integration scheme for heat conduction in additive manufacturing. *Applied Mathematical modeling* 75:787-805.

[Taillet et al.,2009] Taillet R, Villain L, Febvre P (2009) *Dictionnaire de physique*, 2nd edn. De Boeck, Louvain-la-Neuve.

[Talpaert,2000] Talpaert Y (2000) *Differential geometry with applications to mechanics and physics*. CRC Press, Florida.

[Tang,2000] Tang NC (2000) Plastic deformation analysis in tube bending. *International Journal of Pressure Vessels and Piping* 77:751-759.

[Tavernier,1962] Tavernier J (1962) Sur l'équation de Conduction de la Chaleur [The Equation of Heat Conduction]. *Comptes Rendus de l'Academie des Sciences [Proceedings of the Academy of Sciences]* 254:69-71.

[Terentev,2004] Terentev VF (2004) On the problem of the fatigue limit on metallic materials. *Metal Science and Heat Treatment* 46:244-249.

[Thurston,1997] Thurston V (1997) *Three-dimensional geometry and topology*, Vol. 1. JPrinceton Mathematical Series 35. Princeton university press, New Jersey.

[Timoshenko,1925] Timoshenko S (1925) *Analysis of bi-metal thermostat*, Scientific paper 178, Westinghouse research laboratory, East Pittsburgh, PA.

[Timoshenko,1953] Timoshenko S (1953) *History of Strength of Materials*, McGraw-Hill, New York.

[Tingley,2001] Tingley W (2001) *The Rotary-Draw Tube-Bending Guide. Bend Tooling*. Inc. Grand Rapids, Michigan.

[Tolman,1930] Tolman RC: On the use of the entropy principle in general relativity. *Physical Review* 35:896.

[Truesdell,1966] Truesdell C (1966) *The elements of continuum mechanics*. Springer- Verlag, Berlin.

[Truesdell and Noll,2003] Truesdell C, Noll W (2003) *The Non-Linear Field Theories of Mechanics*, 3rd edn. Springer, Berlin.

[Tsallis et al.,1995] Tsallis C, Levy SV, Souza AM, Maynard R (1995) Statistical-mechanical foundation of the ubiquity of Lévy distributions in nature. *Physical Review Letters* 75:3589.

[Tzou,2014] Tzou D (2014) *Macro-to microscale heat transfer: the lagging behavior*, 2nd edn. John Wiley and Sons, Chichester, West Sussex.

[Ugural and Fenster,2003] Ugural AC, Fenster SK (2003) *Advanced Strength and Applied Elasticity*, 4th edn. Prentice-Hall, New Jersey.

[Valanis,1970] Valanis KC (1970) On the thermodynamic foundation of classical plasticity. *Acta Mechanica* 9(3/4):278-291.

[Vallée,1981] Vallée C (1981) Relativistic thermodynamics of continua. *International Journal of Engineering Science* 19:589-601.

[Ván et al.,2013] Ván P, Czél B, Fulop T, Grof GY, Gyenis Á, Verhás J (2013) Experimental aspects of heat conduction beyond Fourier. *Proceedings of the 12th Joint European Thermodynamics Conference Brescia*:519-524.

[Ván,2016] Ván P (2016) Theories and heat pulse experiments of non-Fourier heat conduction. *Comm. Appl. Ind. Math.* 7(2):150-166.

[Ván et al.,2016] Ván P, Ciancio V and Restuccia L (2016) Generalized Galilean transformations of tensors and cotensors with application to general fluid motion. *Atti Accademia Peloritana dei Pericolanti* 97:A25-16.

[Ván et al.,2017] Ván P, Berezovski A, Fülöp T, Gróf GY, Kovács R, Lovas Á, Verhás J (2017) Guyer-Krumhansl-type heat conduction at room temperature. *EPL* 118:50005.

[Ván and Biró,2012] Ván P, Biró TS (2012) First order and generic stable relativistic dissipative hydrodynamics. *Physics Letters B* 709(1-2):106-110.

[Vaschy,1892] Vaschy A (1892) Sur les lois de similitude en physique. *Annales Télégraphiques* 19:25–28.

[Venturi,2009] Venturi D (2009) Convective derivatives and reynolds transport in curvilinear time-dependent coordinates. *Journal of Physics A: Mathematical and Theoretical* 42(12):125-203.

[Vernotte,1961] Vernotte P (1961) Quelques complications possibles dans les phénomènes de conduction thermique. *Comptes Rendus Hebdomadaires de Séance de l'Académie des Sciences, Paris* 252:2190–2191.

[Vitokhin and Ivanova,2017] Vitokhin EY, Ivanova E (2017) Dispersion relations for the hyperbolic thermal conductivity, thermoelasticity and thermoviscoelasticity. *Continuum Mech. Thermodyn.* 29:1219-1240.

[Wagner et al.,2009] Wagner D, Ranc N, Bathias C, Paris PC (2009) Fatigue crack initiation detection by an infrared thermography method. *Fatigue and Fracture of Engineering Materials and Structures* 33(1):12-21.

[Wang,2016] Wang M (2016) *A covariant 4D formalism to establish constitutive models : from thermodynamics to numerical applications*, PhD thesis. Troyes: Université de Technologie de Troyes, 2016, 212p. Available on: http://www.theses.fr/2016TROY0025

[Weinberg,1972] Weinberg S (1972) *Gravitation and cosmology: principles and applications of the general theory of relativity*, vol. 1. Wiley, New York.

[Welter,1937] Welter G (1937) Essais d'endurance par traction et compression. *Wiadomoveci Instytutu Metalurgii i Metaloznawstwa* 4:30–39.

[Wiechert,1893] Wiechert E (1893) Gesetze der elastischen Nachwirkung für constante Temperatur. *Annalen der Physik.* 286.

[Wineman,2009] Wineman A (2009) Nonlinear viscoelastic solids-a review. *Mathematics and Mechanics of Solids* 14:300-366.

[Wohler,1867] Wöhler A (1867) Wöhler's experiments on the strength of metals. *Engineering* 4:160-161.

[Xiao et al.,1999] Xiao H, Bruhns OT, Meyers A (1999) A natural generalization of hypoelasticity and Eulerian rate type formulation of hyperelasticity. *Journal of Elasticity* 56:59-93.

[Yavari et al.,2006] Yavari A, Marsden JE, Ortiz M (2006) On spatial and material covariant balance laws in elasticity. *Journal of Mathematical Physics* 47:1-53.

[Yavari and Marsden,2012] Yavari A, Marsden JE (2012) Covariantization of nonlinear elasticity. *Z. Angew. Math. Phys.* 63:921-927.

[Yavari and Ozakin,2008] Yavari A, Ozakin A (2008) Covariance in linearized elasticity. *Z. Angew. Math. Phys.* 59:1081-1110.

[Zehnder et al.,1998] Zehnder AT, Babinsky E, Palmer T (1998) Hybrid method for determining the fraction of plastic work converted to heat. *Exp. Mech.* 38(4):295-302.

[Zener,1948] Zener CM (1948) *Elasticity and anelasticity of metals*. University of Chicago Press, Chicago.

[Zhang et al.,2011] Zhang ZM, Bright TJ, Peterson GP (2011) Reexamination of the Statistical Derivations of Fourier's Law and Cattaneo's Equation. *Nanoscale and Microscale Thermophysical Engineering* 15(4):220-228.

[Zhijun et al.,2017] Zhijun, T, Heng, L, Jun, M, Heng, Y, Chao, L, Guangjun, L (2017) FE modeling of a complete warm-bending process for optimal design of heating stages for the forming of large-diameter thin-walled Ti–6Al–4V tubes. *Manufacturing Rev.* 4:8.

[Zubarev,1974] Zubarev DN (1974) *Nonequilibrium Statistical Thermodynamics*. Consultants Bureau, New York.

# Roula AL NAHAS

## Doctorat : Matériaux, Mécanique, Optique, Nanotechnologie

Année 2021


## Un formalisme espace-temps pour les applications thermomécaniques


La modélisation du comportement thermomécanique des grandes déformations est un sujet de recherche de grand intérêt. L'objectivité des modèles est mise en question. Cette étude évalue l'approche de modélisation en espace-temps comme un moyen de construire des modèles thermomécaniques respectant à la fois les principes de covariance et de causalité ainsi que les lois de la thermodynamique. Plusieurs modèles sont proposés dans le cadre de l'espace-temps et ensuite comparés aux modèles existants : la conduction thermique et le comportement thermo-hyperélastique des matériaux sont discutés. Des simulations numériques ont ensuite été réalisées. La comparaison des modèles relativistes avec les modèles Newtoniens classiques faite à la limite non relativiste montre la compatibilité de leurs résultats. Des applications dans le but de la modélisation de la conduction thermique dans les ailettes de refroidissement, l'auto-échauffement survenant lors des essais de fatigue et le comportement d'un bilame montrent que l'utilisation de l'approche relativiste permet de prédire les comportements des matériaux. Nous suggérons également l'utilisation de cette approche pour modéliser le processus de flexion des tubes, des résultats préliminaires sont donnés en annexe. Étant donné que cette approche s'avère avantageuse pour les applications proposées, il serait intéressant que des recherches supplémentaires couvrent différents comportements des matériaux, comme la plasticité à titre d'exemple.



Mots clés : objectivité – métaux, fatigue – relativité (physique) – physique, modèles mathématiques – thermodynamique – élastoplasticité – éléments finis, méthode des – déformations (mécanique) – thermoélasticité.


## On the Use of a Spacetime Formalism for Thermomechanical Applications


In order to optimize the forming processes, modeling the thermomecanical behavior for large deformations is particularly interesting. Objectivity of the models is questioned. This study investigates the spacetime approach as a mean to build thermomechanical models respecting the covariance and causality principles as well as the laws of thermodynamics. Several models are proposed in the spacetime framework and next compared to existing models: heat conduction and the thermo-hyperelastic behavior are discussed. The spacetime numerical resolution is also tested: the variational forms corresponding to thermal and thermomechanical problems were developed. The study of material behavior is possible using these forms written in the proper frame. Numerical simulations implementing these forms in the software FEniCS project were then conducted in order to validate test cases of the spacetime models. Comparison of the spacetime models with the classical Newtonian models at the non-relativistic limit shows the compatibility of their results. Applications aiming to model the heat conduction in cooling fins, the self-heating occurring during fatigue tests and the behavior of a bimetallic element show that the use of the spacetime approach enable predicting material behaviors while guaranteeing objectivity of the models. We also suggest the use of this approach to model the tube bending process, preliminary results requiring more investigation are given in the appendix.



Keywords: objectivity – metals, fatigue – relativity (physics) – thermodynamics – elastoplasticity – finite element method – deformations (mechanics) – thermoelasticity.



**Thèse réalisée en partenariat entre :**

Grand Est ALSACE CHAMPAGNE-ARDENNE LORRAINE — l'Europe s'engage en Champagne-Ardenne avec le FEDER — Union Européenne Fonds Européen de Développement Régional — utt Université de Technologie Troyes

**Ecole Doctorale** "Sciences pour l'Ingénieur"